# PHASE CHANGE MATERIAL OPTIMIZED FOR INTEGRATION WITH DOMESTIC HEAT PUMP.

**by**

**Bashir Oladele Jimoh**

A thesis submitted in partial fulfilment of the requirements for the degree of Doctor of Philosophy

University of Warwick, School of Engineering.

May 2018

## Table of Contents

## List of Figures

**List of Tables**

**Acknowledgements**

I would like to appreciate my supervisor, Dr Stan Shire for his unstinting encouragement, excellent supervision, endless guidance patience, understanding and support throughout this research. I would like to extend my gratitude the STET team, Prof Bob Critoph, Dr Roger Thorpe, Dr Roger Moss, Dr Steve, Dr Angeles Riveros. Dr Muyiwa Oyinlola, Yemi Jegede and Dr Hassan also helped me out with the provision of the thermocouple and coriolis flow meter used I want to also appreciate the support of the workshop team of the School of Engineering, especially Joel Whittle, who helped with the fabrication of the two rigs and several jobs done in the workshop.

I am truly grateful to my family, the Jimoh's (my Parents) and the Ilesanmi for the huge financial sacrifice/investment made towards this degree, words cannot express my gratitude. I would also appreciate Mrs Eniiwaju Etomi and all the members of HGZ, Coventry. Other family members and friends, too numerous to mention, I am deeply grateful. Thanks to Dr Festus, Egwolo and their two Princesses for giving me a home to stay during the final lap of my Ph.D. journey.

To my Queen (Dr (Mrs) Modupe Jimoh and three wonderful Princes; Imole, Ola and Ife; thank you for your understanding, patience, support and motivation. I appreciate your continuous tolerance, unconditional love, encouragement and support. Without you all, I would have struggled to complete this thesis. You are simply the best. Above all, I am indebted to the King of Kings, God almighty for the grace, wisdom, understanding and knowledge and good health to complete this degree.

Only God made this all possible, He deserves all the praise and glory

"All things are possible to him that believes"

## Declaration

I declare that the work in this thesis has been composed by me and no portion of the work has been submitted in support of an application for another degree or qualification of this or any other university or other institute of learning. The work has been my own except where indicated and all quotations have been distinguished by quotations marks and the sources of information have been acknowledged.

Parts of this thesis have been published by the author. These publications are mentioned in the next section.

## Contributions to Knowledge

**Peer Reviewed conference proceedings.**

1. Jimoh, B.O. and Shire, G.S.F. (2013) Experimental investigation of thermal behaviour of PCM in a thermal store, The 13th UK Heat Transfer Conference (UKHTC), Imperial College, London, UK.
2. Jimoh, B.O., Shire, G.S.F. (2017) Experimental investigation on the behaviour of PCM in a Serpentine thermal store rig. The 15th UK Heat Transfer Conference (UKHTC), Brunel University, London, UK.

**Abstract**

The purpose or objective of this research was to study the behaviour of a thermal store for integration with a heat pump. Two different types of heat exchanger, plate heat exchanger (PHE) and serpentine heat exchanger (SHE), were designed and modular units built in the workshop at the University of Warwick. Both heat exchangers were used to study the effect of the mass flow rate, inlet heat transfer fluid temperature, thickness of phase change material (PCM), thermal properties of the PCM etc. on the behaviour of the thermal energy storage (TES). The PCMs selected for this research had phase change temperatures in the range of 50°C-60°C. Thermophysical properties of four different PCMs were determined in the laboratory. PCMs including RT 52, RT 58, Climsel C58 and a eutectic mix of magnesium hexahydrate and ammonium nitrate that are suitable for use with heat pumps were studied using the differential scanning calorimeter (DSC) and hot disk to determine their thermal behaviour when compared to manufactures' data.

The modular units were charged and discharged at different inlet heat transfer fluid temperatures. The PHE experiment was carried out using both RT 52 and RT 58, while the SHE experiments were carried out using RT 52 only. The heat transfer fluid used in the experiments was water. The PHE was made from polypropylene sheet (a polymer material), with channels that carry the water in and out of the store. The SHE was based on a shell and tube concept, designed and used as a thermal store.

A MATLAB model was developed based on the enthalpy method using finite difference to study and compare the temperature profile, charge rate and energy stored in the PHE using the thermal properties of RT 52 or RT58 as PCMs suitable for this thermal energy storage application. The MATLAB model was validated for both the charge process and discharge process, with the inlet HTF temperature from the experiment. Experimental results from the SHE experiment are presented for RT 52.

The charge rate and energy stored during charging and discharging processes were analysed for different thicknesses of PCM around each PHE module. Results showed that the greater the PCM thickness, the higher the amount of energy stored in the PHE module and the slower it is for the module to charge or discharge. The model was used to evaluate the performance for when the store was fully charged and half charged and the results presented. To increase the capacity of the store for effective use with a domestic heat pump for a specified period of charging during off-peak tariff periods, a thermal store design using 30mm PCM thickness is proposed. With this PCM thickness, a 32kWh thermal store would require about twenty polypropylene sheets. Twenty-two (22) polypropylene sheets arranged in parallel could be charged at 8.89kW, allowing the store to work in conjunction with an 8kW heat pump. This type of PHE storage module could be installed in suitable locations in the home, such as beneath kitchen cabinets or within ceiling voids, which would accommodate the dimensions of the plate heat exchanger. The sheet capacity and number of sheets required for a store of 32kWh was determined for six different PCM thickness using RT 52.

A plot of sheet charge rate or store charge rate against the reciprocal of the thickness was produced that can be used to determine the thickness or charge rate is presented. This enables the required store characteristics (PCM thickness and number of sheets) to be determined quickly and easily from the plot or fitted equation.

## Nomenclature

### Symbols

| | |
|---|---|
| A | Area ($m^2$) |
| a | Height of rectangular channel (m) |
| b | Width of rectangular channel (m) |
| B | Total thermal resistance ($m^2K/W$) |
| C | Carbon |
| $C_p$ | Specific heat capacity (J. $kg^{-1}$. $K^{-1}$) |
| d | Diameter (m) |
| $D_h$ | Hydraulic Diameter (m) |
| dx | Distance step in HTF flow direction(m) |
| dy | Distance step in PCM (m) |
| E | Energy (J) |
| f | Friction factor |
| H | Hydrogen |
| H | Enthalpy (J/kg) |
| h | heat transfer coefficient ($W/m^2K$) |
| L, $h_{sf}$ | Latent heat of PCM (J/kg) |
| i | Current time step |
| k | Thermal conductivity (W/mK.) |
| Lx | Length of PP sheet (m) |
| m | mass (kg) |
| $\dot{m}$ | Mass flow rate (kg/s) |
| N | Number of sheet. |
| $n$ | Number of samples |
| numx | Number of elements in flow direction |
| numy | Number of element in y-direction. |
| Nu | Nusselt Number |

| | |
|---|---|
| Pr | Prandtl Number |
| P | Perimeter (m) |
| Q | Quantity of heat store or released (J) |
| $Q_T$ | Sheet capacity (MJ) |
| $\dot{Q}_s$ | Sheet charge rate (W) |
| $\dot{Q}$ | Rate of heat transfer (W) |
| $\dot{Q}$ | Charge rate, discharge rate (W) |
| $\dot{q}$ | Heat flux ($Wm^{-2}$) |
| r | Radius(m) |
| $r_{TPS}$ | Radius of TPS sensor (m) |
| R | Thermal resistance ($m^2K/W$) |
| Re | Reynolds number |
| RN | North resistance ($m^2K/W$) |
| RS | South resistance ($m^2K/W$) |
| RW | West resistance ($m^2K/W$) |
| RE | East resistance ($m^2K/W$) |
| T | Temperature (K) |
| TN | North temperature (K) |
| TS | South temperature (K) |
| TW | West temperature (K) |
| TE | East temperature (K) |
| $\Delta T$ | Change (difference) in temperature (K) |
| t | Time (seconds) |
| $t_{PCM}$ | Thickness of PCM (m) |
| $T_{ct}$ | Total characteristic time |
| U | Overall heat transfer coefficient ($W/m^2K$) |
| v | Velocity (m/s) |

| | |
|---|---|
| $\dot{V}$ | Volumetric flow rate ($m^3/s$) |
| X | Liquid fraction |
| x | x-direction(horizontal) (m) |
| $x_i$ | Measured value |
| $\overline{X}$ | Mean |
| y | y-direction(vertical) (m) |

**Greek symbols**

| | |
|---|---|
| $\alpha$ | Thermal diffusivity ($m^2/s$) |
| $\rho$ | Density ($kg/m^3$) |
| $\mu$ | Dynamic viscosity ($Ns/m^2$) |
| $\sigma_m$ | Standard deviation mean |
| $\sigma$ | Standard deviation |
| $\nabla$ | Laplacian Operator |

**Abbreviations**

| | |
|---|---|
| ABS | Acrylonitrile Butadiene Styrene |
| ASHRAE | American Society for Heating Refrigeration and Air-conditioning Engineers. |
| CCHH | Calcium chloride hexahydrate. |
| CFD | Computational fluid dynamics. |
| CNF | Carbon nano-fibres |
| CSP | Concentrating Solar Power |
| DSC | Differential Scanning Calorimeter |
| GNF | Graphite nano-fibres |
| HTF | Heat Transfer Fluid |
| IPF | Ice packing factor |
| LHS | Latent Heat Storage |

| | |
|---|---|
| LHTES | Latent Heat Thermal Energy Storage |
| MSDS | Material safety data sheet |
| PCM | Phase Change Material |
| PHE | Plate Heat Exchanger |
| PIR | Polyisocyanurate |
| PP | Polypropylene |
| PVC | Polyvinyl Chloride |
| RTD | Resistance Temperature Detectors |
| SHE | Serpentine Heat Exchanger |
| SSDH | Sodium sulphate decahydrate |
| TC | Thermocouple |
| TES | Thermal Energy Storage |
| TPS | Transient plane source |
| USB | Universal Serial Bus |

**Subscripts**

| | |
|---|---|
| AN | Analytical |
| c | Cross-section |
| cond | Conduction |
| conv | Convection |
| element | Element |
| f | Fluid |
| F | Final |
| h | Hydraulic |
| htf | Heat transfer fluid |
| ini | Initial |
| l | Liquid |
| liquid | Liquid |
| MO | Model |

| | |
|---|---|
| m,n | Nodal positions in numerical solution |
| melt | Melt |
| no | Number of carbon atoms |
| OUTPUT | Output |
| p | PCM |
| pcm | PCM |
| s | Solid |
| S | Sheet |
| solid | Solid |
| T | Total |
| w | polypropylene wall |
| wall | Wall |

# 1 Introduction

## 1.1 Background

A Thermal energy store is a means of storing and releasing renewable heat till it is required. It could be used for heating, cooling or power generation. Thermal energy storage is useful in cases where the electricity cost is high during peak periods; costs can be reduced by using thermal energy storage: charging the unit during off-peak periods when electricity is cheaper and recovering the energy when the unit discharges at times of higher energy costs. Several countries utilise this technology to shift the peak load to off-peak periods. There are various forms of thermal energy storage process, namely thermo-chemical storage, latent heat storage and sensible heat storage. Latent heat storage is used to store thermal energy through change of phase when a material is charged or discharged. The material used for this purpose is called Phase Change Material (PCM). PCMs possess a unique property of high storage density at small temperature change. For this research, attention will be centered on the Latent heat thermal energy storage (LHTES).

Most of the world's energy comes from fossil fuels, but due to their harmful environment effect on the atmosphere, there is a demand for renewable energy sources. A latent heat thermal energy system is useful because it provides high capacity storage with the use of PCMs. Various researchers have carried out experiment and numerical analysis using this type of thermal energy storage.

The project is based on designing thermal stores using a plate heat exchanger and a shell and tube exchanger embedded with PCM. The work is divided into two phases of experiment using existing hardware in the laboratory. The first phase involves the use of measuring devices; differential scanning calorimeter and hot disk to determine the suitable phase change material for optimal thermal efficiency and a heat transfer simulation model in MATLAB (Conduction only). The second phase entails a detailed heat/mass transfer program and builds a lab scale heat source, sink and store.

The thermo physical properties of the phase change material, type of store geometry and numerical model used are key factors that determine the thermal efficiency of a thermal energy system and its optimisation. Cylindrical geometries are the most commonly used geometry for commercial heat exchanger. This is because of their

capability to achieve a huge efficiency in a small volume. Various researchers use this geometry for LHTES, occupying the tube or shell with PCM. This research looks at using both a plate heat exchanger concept using polypropylene material and shell and tube geometry concept (serpentine heat exchanger) to investigate the thermal behaviour of a thermal store.

### 1.1.1 Aim and Objectives of the Study

The project looks at feasibility of compact heat storage materials (using PCM in this case) as an effective means to alleviate strain on the electricity grid from increasing load from heat pumps. An advantage of plate and serpentine heat exchanger compared to others, is a greater ratio of phase change material (PCM) to water within the thermal store, thus reducing volume and at the same time, improving heat transfer. The purpose of this project is to develop a low weight and easy to install thermal storage system with effective heat transfer.

Knowing the energy performance, degradation of performance over time, cost, and flexibility to enable load shifting over a range of hours would be of great benefit to this retrofit application.

The objectives of this study are to:

1. Investigate the optimum phase change material that would improve heat transfer and storage capacity, whilst reducing volume within the thermal store using a plate heat exchanger (polymer extrusion).
2. Experimentally investigate the thermal behaviour of a thermal store using a plate heat exchanger design (Polymer extrusion) and a shell and tube heat exchanger geometry concept. The idea is to ascertain that both exchanger design concepts for thermal energy storage can be efficient and beneficial.
3. Contribute to the body of knowledge of utilizing the properties of PCM to balance load on the electricity grid in a thermal energy storage system in domestic heat pumps.
4. Develop a heat transfer model that optimizes the temperature time relationship and amount of energy that could be absorbed and released from the PCM in a thermal store.

### 1.1.2 Thesis Outline

The outline of this thesis consists of twelve chapters with **Chapter 1** as an introduction to thermal energy storage and the theory on which it is based. Each chapter has a summary of the content in that chapter. **Chapter 2** comprises of the literature review which looks at past and current research with regards to LHTES**. Chapter 3** comprises of the description of PCM and its properties. The differences between subcooling and hysteresis in PCMs are compared. Heat transfer in PCMs is discussed and various numerical methods used to solve heat transfer problems in PCMs**. Chapter 4** focuses on the thermal behaviour of PCMs and how the differential scanning calorimeter (DSC) and hot disk devices are used to determine the PCM thermal properties. Also different PCMs used in the research were investigated and data obtained was compared with manufacturers' data. **Chapter 5,** discusses the results obtained from the experimental analysis done in Chapter 4. It also highlights the concern of sub cooling present in some PCMs, thus comparing the advantage of using organic and inorganic PCM as probable PCMs for this research. **Chapter 6** focuses on one of the heat exchanger designs: the plate heat exchanger used for this research. Two heat exchangers were used for this research: a plate heat exchanger and a serpentine heat exchange based on a shell and tube concept. The experimental setup of the PHE is explained in detail as well as the materials and apparatus used. The charging and discharge process is discussed. The chapter also looks at the statistical analysis done and uncertainty in the experiment. **Chapter 7** discusses the design and experimental setup of the thermal store using a serpentine heat exchanger (SHE), which is the second heat exchanger used in this research. Charging and discharging process are explained in detail**. Chapter 8** comprises of the experimental results for the PHE using two different PCMs; RT52 and RT 58. The latter is the first PCM used to commence the research before replacing with RT 52. **Chapter 9** deals with the experimental results for the SHE. Discussions on the thermal behaviour of the thermal store when such parameters as flow rate, inlet HTF temperature are varied are discussed in detail. **Chapter 10** discusses the model of the PCM for the plate heat exchanger thermal store**. Chapter 11** deals with the conclusion and further work associated with the research**. Chapter 12** comprises of the references of all sources used in the research**.**

**The appendix** consists of figures and other relevant information; references are made to them within the thesis**.**

## 1.2 Thermal Energy Storage (TES)

Thermal energy stores utilizing phase change material are widely accepted and various researches carried out on how heat transfer can be enhanced. Based on the plans to reduce the emission of greenhouse gases, of which most of the carbon emissions can be linked to burning of fossil fuels, the need of latent heat thermal energy storage (LHTES) cannot be overemphasised .The built environment emits about 30-40% of carbon emissions in the UK (Whiffen and Riffat (2012)). Domestic heating and hot water systems consume about 50% of the energy required in a building during the cold season. In the UK homes, heat pumps are regarded as a proven energy efficient space device (Huang and Hewitt (2011). The advantage of high energy storage density per unit volume that thermal energy storage provides using PCM has been keenly studied over the last three decades. The benefits of using PCM storage system as a component of a heating system are in areas of; reduction of energy cost, peak energy saving, reduction in equipment size and enhanced system operation (ASHRAE (2003). Photovoltaic and solar are expensive when compared to fossil fuel, however the sustainability of the energy source and its impact on the environment cannot be overlooked, thus thermal storage provides a safer and cheaper benefits (Nallusamy (2016).

Thermal energy storage system prolongs the life time of the heat pump by reducing the start and stop times of the heat pump; and reduces demand on the electricity grid by utilising PCMs ability to absorb and release heat during change of phase.

TES is needed when the energy available does not coincide in time or meet up with the process demand. This is due to discrepancy between supply of energy and demand. TES is essential for energy efficiency (Nallusamy (2016).

The application of latent heat storage energy systems improves thermal efficiency in buildings and also balances load on the electricity grid. In domestic buildings it can be used to reduce electricity cost by utilising the electricity reduction tariff plans (economy 7, economy 10 etc.) from providers, when working with domestic heat pumps. The thermal store could be charged during off peak periods and the heat recovered during peak periods. It is important that the charge cycle is completed during the off peak period and the operation of the heat pump and efficiency of the

thermal storage system plays a vital role in achieving this. Economy 7 provides cheaper electricity rate for seven hours, mostly at night (12a.m to 7a.m). This is dependent on the energy providers, for the time for off peak periods could vary. Considering Economy 10 tariff, it provides ten hours of cheap electricity at three different periods during the day. Table 1:1 shows the difference between the Economy 7 and 10 tariffs.

Table 1:1: Difference between Economy 7 and Economy 10 tariff.

| Economy 7 | Economy 10 |
|---|---|
| 7 hours of cheap electricity | 10 hours of cheaper electricity |
| Off peak periods at night | Off peak periods at three different times during the day;<br>3 hours off peak-- afternoon<br>2 hours off peak-- evening<br>5 hours off peak-- night |
| Higher cost during the day and evening (peak periods). | Higher cost outside the off peak time periods |

Charging time for the thermal energy storage is based on off peak electricity using Economy 7(E7) or economy 10 (E10) tariff, where it is possible to charge the thermal store during off peak period. Off peak period for economy 7(E7) is seven hours (between 1a.m to 8a.m) and for economy 10(E10), ten hours off peak (between 1pm to 4pm; 8pm to 10pm and 12 a.m. to 5a.m). These times do vary, depending on the energy provider and region within the United Kingdom. In this research, the design of the thermal store was based on utilizing the periods to charge and discharge the thermal store. Charging of the thermal store was done to absorb the heat and discharging of the thermal store, to recover the heat when required. The thermal store works in conjunction with a heat pump. The thermal store is charged with the aid of the heat pump during off peak periods, when the electricity tariff is cheap. The advantage of a heat pump working with a thermal energy storage helps to prevent continuous cycle (on/off or start/stop) action termed as short cycling, when the demand for heat is low.

Leonhardt C (2009) carried out simulation, using plate heat exchanger to design a LHTES and warm water storage (buffer storage) incorporated with a heat pump system. A paraffin with melting temperature of 47°C and latent heat of 180kJ/kg was used. It was discovered that the LHTES improves the performance of the heat pump when compared to the use of the warm water storage. Also the LHTES reduces the on and off sequence of the heat pump during operation.

The analysis of this research is based on the plan to take advantage of the off-peak electricity using economy 7(7 hours). Based on active occupancy, a period of four hours was chosen for the design of the PCM store. The design was based on using a 8kW heat pump with four hours off peak electricity tariff. This gives a total capacity of 32kWh (8kW x 4hrs). During the charging mode, the store was charged at an inlet HTF temperature (60-70°C) to completely melt the PCM and in the process latent heat was stored. The inlet HTF temperature was carefully chosen for this LHTES, taking into consideration the concern of the growth of Legionella bacteria in storage tanks. To prevent growth of Legionella bacteria, the temperature of the hot water tank is kept at 60°C (HSE Publications (2013) . The store can be charged during the off peak period when the heat pump is switched on. During the discharge mode, the heat pump is switched off during peak periods. The store is discharged at 40°C by the action of the HTF flowing through the PCM thermal store. Water Temperature of a typical shower for domestic use is 40°C (Lawrence and Bull (1976).

For example, Moreno et al. (2014) carried out experiments using two different PCMs; S10 and S46, which stored cold and heat respectively. The PCMs were in encapsulated plastic slabs (FlatICE) with a dimension of 500 mm × 250 mm × 32 mm. The PCM slabs are arranged in two columns of six (6) slabs with a slab spacing of 1cm. The slab spacing acts as the HTF channel. The experiment comprised two TES tanks coupled with a heat pump (4.2kW for cooling and 5.2kW for heating) to simulate summer conditions to cool a small house (2.4mx2.4mx2.4m). The slab spacing provides a short conduction length between the HTF, PCM and the plastic for effective heat transfer. During the charging mode, the hot tank was charged with hot HTF(55-58°C) from the heat pump and cool HTF(2-5°C) from the evaporator to the cold tank during the off peak period . During the discharge mode, the heat pump is switched off during evening peak periods with the energy demand coming from the cold tank.

Huang et al. (2004) stated that there have been no detailed investigations into the modification resulting from using PCM for thermal storage system for heat pump application, however some research has been done to improve heat transfer and rapid charging of the system. Huang et al. (2004) investigated the performance of thermal regulation by PCM for building integrated photovoltaics. The experiment and simulation results showed how heat transfer (conduction and natural convection) of the melting process in the thermal storage unit was enhanced by fins in contact with the PCM. Understanding the thermo physical properties of the PCM and design of the thermal store are essential in taking advantage of off peak electricity tariffs as an avenue to reducing heat pump operation costs for the consumer and utility company. Heat energy can be stored as sensible or latent heat; this is discussed in detail in the sub-sections below.

### 1.2.1 Sensible heat

Sensible heat is the heat that causes change in temperature in a body. It could be defined as the storage of thermal energy by raising the temperature of a medium (solid or liquid). Mathematically, the amount of thermal energy stored in the form of sensible heat can be expressed as in Equation 1.1 and Equation 1.2.

$$Q = m.\mathrm{C_p}.\Delta T \qquad 1.1$$

$$Q = \int_{T_{ini}}^{T_F} m.C_p.\mathrm{d}T \qquad 1.2$$

Q is the amount of thermal energy stored or released in the form of sensible heat (Joules), m is the mass of the material (kg), $T_{ini}$, $T_F$ are the initial and final temperature respectively. $C_p$ is the specific heat capacity of the material (J/kg K).

It is evident that the amount of thermal energy stored in this form depends on the specific heat, mass and difference in temperature. The relationship between temperature and amount of heat stored is described in Figure 1:1.

Sensible heat storage is the most common thermal energy storage. Examples of sensible heat storage are solids such as stones and bricks or liquids such as water or

oil. Domestic water heating in most homes is based on the sensible heat storage principle. Water is regarded as one of the best materials to be used to store energy in the form of sensible heat for it has a high specific heat capacity when compared to others. Table 1:2 shows other materials used for sensible heat storage. The difference between sensible and latent heat storage is highlighted in Table 1:3.

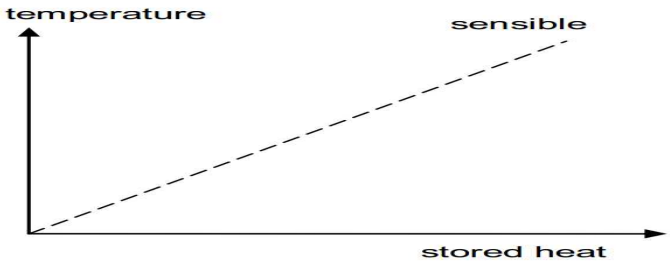


Figure 1:1 Plot showing relationship between sensible heat and temperature.

Table 1:2: Properties of some materials used for sensible heat storage.Sharma et al. (2009)

| Medium | Fluid type | Temperature range (°C) | Density (kg/m$^3$) | Specific heat (J/kg K) |
|---|---|---|---|---|
| Rock | | 20 | 2560 | 879 |
| Brick | | 20 | 1600 | 840 |
| Concrete | | 20 | 1900–2300 | 880 |
| Water | | 0–100 | 1000 | 4190 |
| Caloriea HT43 | Oil | 12–260 | 867 | 2200 |
| Engine oil | Oil | Up to 160 | 888 | 1880 |
| Ethanol | Organic liquid | Up to 78 | 790 | 2400 |
| Proponal | Organic liquid | Up to 97 | 800 | 2500 |
| Butanol | Organic liquid | Up to 118 | 809 | 2400 |
| Isotunaol | Organic liquid | Up to 100 | 808 | 3000 |
| Isopentanol | Organic liquid | Up to 148 | 831 | 2200 |
| Octane | Organic liquid | Up to 126 | 704 | 2400 |

Table 1:3: Comparison of thermal energy storage form.Gang Li (2016)

| | Sensible | Latent |
|---|---|---|
| Medium of storage | Water, soil, pebble, gravel | Organic, Inorganic PCM |
| Advantage | Cheap, simple | High storage density, isothermal temperature |
| Disadvantage | Low energy density, | Corrosion, sub-cooling, toxicity |
| Current status | Large scale demonstration plants. Hot water tanks, Electric storage heaters and Thermal mass of buildings. | Laboratory-scale prototypes & early stage commercialisation.PCM plasterboards(KNAUF), heat battery (SUNAMP), Ice store system(Viessman) |

### 1.2.2 Latent heat

Latent heat is the heat that causes the change of state of a body or object without any change in temperature. Latent heat storage makes use of the latent heat of the material to store thermal energy. It is the heat absorbed or heat released during change of phase; from solid to liquid phase or vice-versa. Latent heat is also termed 'hidden heat'. This is the latent heat of fusion, measured in Joules per kilogram (J/kg). This is a vital property of any PCM, which determines the effectiveness of its use for energy storage. The amount of thermal energy stored in the form of latent heat is expressed as in Equation 1.3.

$$Q = m.L \qquad 1.3$$

Q is the amount of thermal energy stored or released in the form of latent heat (Joules), m is the mass of the material (kg), and L is the latent heat of fusion or vaporisation of the material (J/kg). Water is regarded as the best known PCM and has been used for cold storage for centuries.

Heat can be stored in the form of latent heat of vaporisation or latent of fusion; measured in Joules/kilogram. For the case of PCMs, we are concerned with the latter. Figure 1:2 shows the relationship between sensible and latent heat with regards to stored heat.

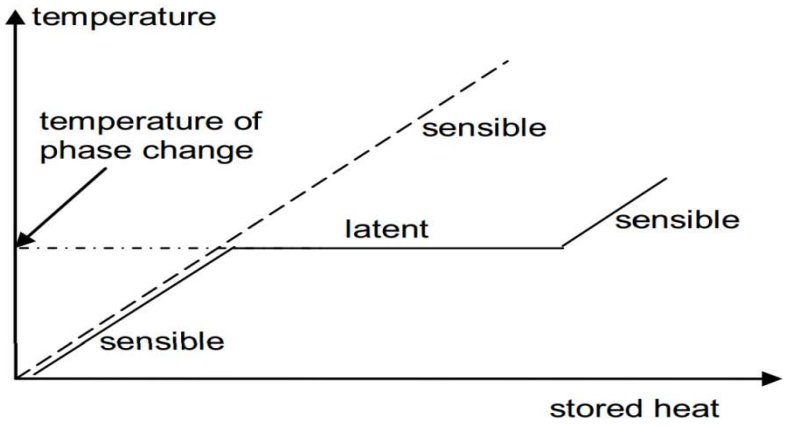


Figure 1:2 Relationships between the latent and sensible heat.Mehling and Cabeza (2008)

Table 1:4 shows the storage densities (MJ/ $m^3$) of different types of thermal energy storage. It shows the storage density of latent heat thermal storage is higher when compared to the sensible storage.

Table 1:4: Storage densities of different energy storage. Mehling and Cabeza (2008)

| Energy Storage | $MJ/m^3$ | kJ/kg | Comment |
|---|---|---|---|
| **Sensible Heat** | | | |
| Granite | 50 | 17 | dT=20°C |
| Water | 84 | 84 | dT=20°C |
| **Latent Heat** | | | |
| Water | 306 | 330 | Melting temp 0°C |
| Paraffin | 180 | 200 | Melting temp 5-130°C |
| Salt Hydrates | 300 | 200 | Melting temp 5-130°C |
| Salts | 600-1500 | 300-700 | Melting temp 300-800°C |

### 1.2.3 Application of TES

Thermal energy storage (TES) has application in diverse fields. It can be used as a means of storing energy in concentrating solar power (CSP) due to its ability to make available continuous operation for the entire period. It can increase output of the CSP plant and increase value of energy sold as studied by Mao (2016). TES can also be integrated in buildings, clothing, industrial applications, domestic application etc. Pielichowska and Pielichowski (2014) explained that these storage systems are either passive or active storage systems. The passive systems are unmanaged and are used to regulate temperature without active control. An active system requires some form of subsidiary system for control to determine when heat is put into a store or taken out of it. D.A (1989) mentioned that PCMs have been used for thermal storage in buildings from 1980; they are used in the interior components of building materials. It is also used for safety; temperature maintenance in rooms with computers or electrical appliances.

Saman et al. (2005) mentioned that with regards to space heating and cooling of buildings; increasing cost of fossil fuels and environmental concerns emanating from pollution from carbon dioxide has made thermal energy storage relevant. Building temperature and energy can be controlled by PCMs as they absorb and release heat

based on environmental conditions. Aigbotsua (2011) carried out research on thermal energy storage incorporated with a solar heat source and found it useful in preserving agricultural products which require a constant temperature for a certain periods.

### 1.3 Types of geometries for TES

Thermal energy storage systems consist of three major components or parts;

- Storage medium
- Heat transfer fluid
- Container system

The storage medium describes the type of storage material used, whether it is a sensible or latent storage material. For this research, the storage medium used is PCM. The heat transfer fluids mostly used are water, air, steam and thermal oil. The container system describes the type of geometry used for the thermal energy storage unit.

Various geometries are used for thermal energy storage, they include: Shell and tube geometry, rectangular geometry, spherical geometry. The geometries have PCM or HTF flowing through the tubes as shown in Figure 1:3. Figure 1:3(a) shows the HTF flowing through the tubes and the space within the main shell filled by PCM. Figure 1:3(b) describes a case where the PCM is within the tube and the space within the shell is filled by the HTF. Also, it may flow through channels that have a rectangular cross-section (e.g. plates). Wang et al. (2015b) carried out research which involved the HTF flowing through zigzag channels and Kurnia et al. (2013) carried out computational fluid dynamics analysis on research using serpentine tubes. Other geometries used include; straight tubes, pipes, rectangular channels etc. Much research has been done with various geometries as shown in Figure 1:4, different arrangements of the PCM and HTF.

Qianjun (2016) mentioned that the tube in shell is the most commonly used storage tank in CSP plants. Several researchers utilise the shell and tube geometry, it is also the most applied in industry. To enhance heat transfer, some applications use finned tube in shell. There is also rectangular shaped system, though often popular for use with sensible heat storage.

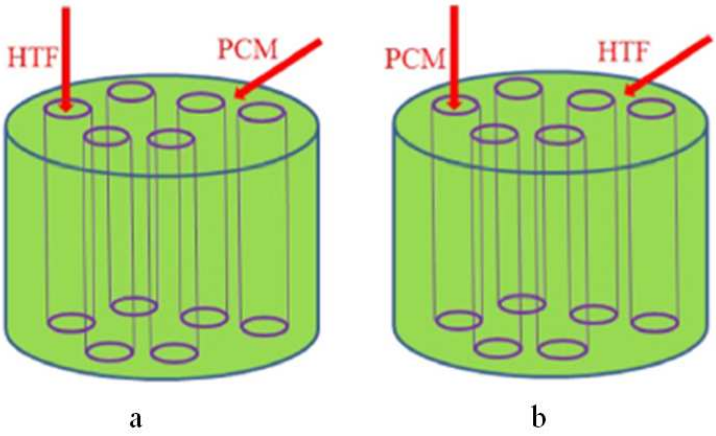


Figure 1:3: Tube in shell arrangement. Qianjun (2016)

Liu (2012) mentioned that the material used for the compartment containing the PCM should also be taken into consideration since it should be compatible (chemically and mechanically) with the PCM being used; for instance the container should be resistant to the corrosive nature of the PCM. Dincer and Rosen (2011) cited an example of the tendencies of paraffin based PCM to soften some plastics, but are compatible with most metals. However, metal containers may easily corrode when exposed to salt hydrates. Containers also have to be capable of withstanding the expansion of the PCM when it melts and the commensurate reduction in volume when it solidifies.

Trp (2005) carried out experimental and numerical investigation of transient behaviour of PCMs in a shell and tube LHS. The model developed was based on enthalpy formulation for non-isothermal behaviour of PCM. The results were validated with paraffin used as the PCM. Ismail and Henriquez (2002) used a numerical model to simulate heat transfer in a LHS, using ethylene glycol as its heat transfer fluid and a packed bed of spherical capsules filled with water as the PCM. The effect of varying the HTF inlet temperature, mass flow rate, material used for the spherical capsule were investigated experimentally and numerically to understand their effect on the storage unit's overall heat transfer performance. Barba and Spiga (2003) used three different geometries for the PCM container to analyse the behaviour of encapsulated salt hydrates (PCM) in a domestic hot water tank. Their findings showed the spherical geometry showed better response time in charging and discharging when compared to the tray and cylindrical geometry. The spherical geometry also produced the largest energy density when compared to the others. Belleci and Conti (1993) used the enthalpy method to numerically study the behaviour of PCM solar shell and tube

energy storage system. Esen et al (1998) studied the behaviour of solar water heating systems incorporated with a latent heat system with a cylindrical geometry. Different PCMs were analysed using the same geometry.

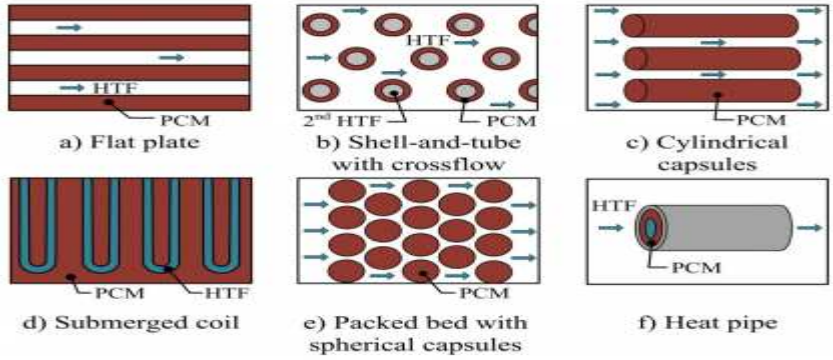


Figure 1:4: Different types of PCM storage geometries D'Avignon (2015).

The thermal behaviour of the phase change material and type of geometry used as a heat exchanger is vital to the performance of the thermal energy storage. The charging and discharging is highly affected by these factors. Thus it is important that the heat exchanger used should have a large surface area for effective heat transfer between the storage material, geometry used and the heat transfer fluid (Abhat (1980).

Campos-Celador et al. (2014) compared a conventional 500 litre hot water tank used for domestic application with a rectangular finned plate heat exchanger and discovered that the plate heat exchanger allows the required volume to be reduced to half of the conventional hot water tank. Also, the advantage of producing the plate heat exchanger using a simple manufacturing process, high modularity, high surface to volume ratio and the ability to easily integrate the rectangular shaped plate heat exchanger in spaces within domestic homes makes them suitable over conventional cylindrical shaped heat storage sources. Flat plate heat exchangers can easily be integrated in structures of the building and, with the concerns of space in residential homes, it provides a good advantage over other types of geometry used to produce heat exchangers. Due to the modular nature of the plates, it is possible to arrange the plates in parallel or in series based on the kind of arrangement desired. Liu et al. (2014) concluded that flat plate LHTES systems are adaptable and heat enhancement structures can easily be integrated. Polymers are suitable for use with PCMs because they do not react with the PCM and are resistant to pitting, bubbling and precipitation (Dinker et al. (2017). Based on such findings, the polypropylene plate heat exchanger was studied in this

research. The PP sheet with a thin walled plate spacing of 4mm and narrow channels which allows HTF to flow through is used to construct the PHE thermal store. This allows for effective heat transfer between the wall of the PP sheet, HTF and PCM. The modular nature of the PP sheet makes it possible to arrange them in series or parallel. Stacks of the PP sheet can be arranged to obtain the required capacity from the PHE store. Parameters such as PCM thickness, flow rate and thermal properties of the PCM are analysed in this thesis.

## 1.4 Heat transfer

Heat transfer can be defined as the movement of thermal energy between two or more systems as a result of difference in temperature. Heat transfer is the flow of energy from a region of higher temperature to a lower temperature. There is no heat transfer if both media exist at the same temperature. Heat can be transferred in three ways, namely: conduction, convection and radiation. A short description is made for each process. For this research, radiation is not applicable; hence it will not be discussed in detail in this thesis.

### 1.4.1 Conduction

Conduction can be described as the transfer of heat through or via vibration of molecules in a solid body or fluid. Due to the arrangement of the molecules, often close together, heat is transferred from contact source to other parts of the body. For example, heating one end of a metal bar results in transfer of heat across other parts of the bar after a specified time. Metals are very good conductors of heat, whereas air, wood and cloths are poor conductors of heat. Materials that are poor conductors of heat are referred to as insulators. The thickness and thermal conductivity of the material determines the rate of heat transfer per unit area. The rate of heat transfer is also dependent on the temperature difference across the medium and the type of geometry. The rate of heat conduction though a plane layer is proportional to the area and temperature difference across the plane, but inversely proportional to the thickness of the plane Cengel and Ghajar (2011).

The equation used for conduction is based on Fourier's law, mathematically it is expressed as shown in Equation 1.4:

$$\dot{Q}_{cond} = -kA\frac{\partial T}{\partial x} \quad (\mathrm{W}) \qquad 1.4$$

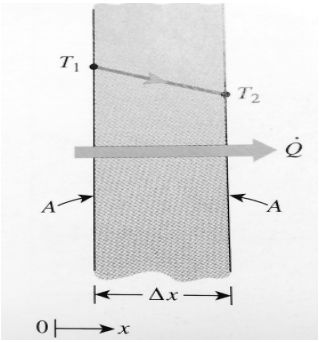


Figure 1:5 : Conduction in a wall. Cengel and Ghajar (2011)

The heat flux is rate of heat transfer per unit area normal to the direction to the direction of heat flow. Equation 1.5 expresses this relationship.

$$\dot{q} = \frac{\dot{Q}}{A} \quad (\mathrm{W/m^2}) \qquad 1.5$$

Heat conduction equation can be expressed for two dimensional cases for rectangular and cylindrical coordinates. It is assumed that the thermal conductivity is constant. Equation 1.6 and Equation 1.7 shows the heat conduction equation for rectangular and cylindrical co-ordinates respectively.

$$\frac{\delta T}{\delta t} = \frac{k}{\rho C_p}\left[\frac{\partial^2 T}{\partial x^2} + \frac{\partial^2 T}{\partial y^2}\right] \qquad 1.6$$

$$\frac{\delta T}{\delta t} = \frac{k}{\rho\, C_p}\left[\frac{1}{r}\frac{\delta}{\delta r}\left(r\frac{\delta T}{\delta r}\right)\right] \qquad 1.7$$

For both cases, thermal diffusivity is expressed as, $\alpha = \frac{k}{\rho C_p}$. The thermal conductivity expresses how quickly heat travels through any chosen material. For example, the thermal conductivity of copper (400 W/mK) is greater than that of aluminium (205 W/mK). Based on this, the rate of heat transfer in copper is higher

than aluminium. Thus, the higher the thermal conductivity value of any material, the higher the rate of heat transfer.

### 1.4.2 Convection

This mode of heat transfer is described as the mode of transfer of energy between a solid surface and the fluid adjacent that is in motion; it involves the combination of conduction and motion in the fluid Cengel and Ghajar (2011). When there is no fluid motion, heat transfer between a solid surface and adjacent fluid is solely by conduction. The rate of convection heat transfer is proportional to the temperature difference, expressed in Equation 1.8 as:

$$\dot{Q}_{conv} = hA_s(T_s - T_\infty) \qquad (\mathrm{W}) \qquad 1.8$$

## 1.5 Summary

This chapter describes the various types of thermal energy storage and the applications where TES is used are discussed in detail. The various modes of heat transfer are discussed except for radiation, as this is not applicable to this thesis. The governing equation that describe the conduction and convection heat transfer modes are highlighted.

An overview of the objective of this research and the thesis outline is discussed. Sensible and latent heat are explained with detailed examples of each given. The equation that describes this type of heat is highlighted as it concerns thermal energy storage. Various types of geometries and arrangement used for thermal energy storage are discussed.

# 2 Literature review

## 2.1 Latent Heat Thermal Energy storage

### 2.1.1 Phase change Material

Phase change materials are classified as organic or inorganic materials. PCMs are available for a range of different phase change temperatures. Organic PCMs are further divided into paraffins and non-paraffins. Figure 2:1 shows the classification of PCMs.

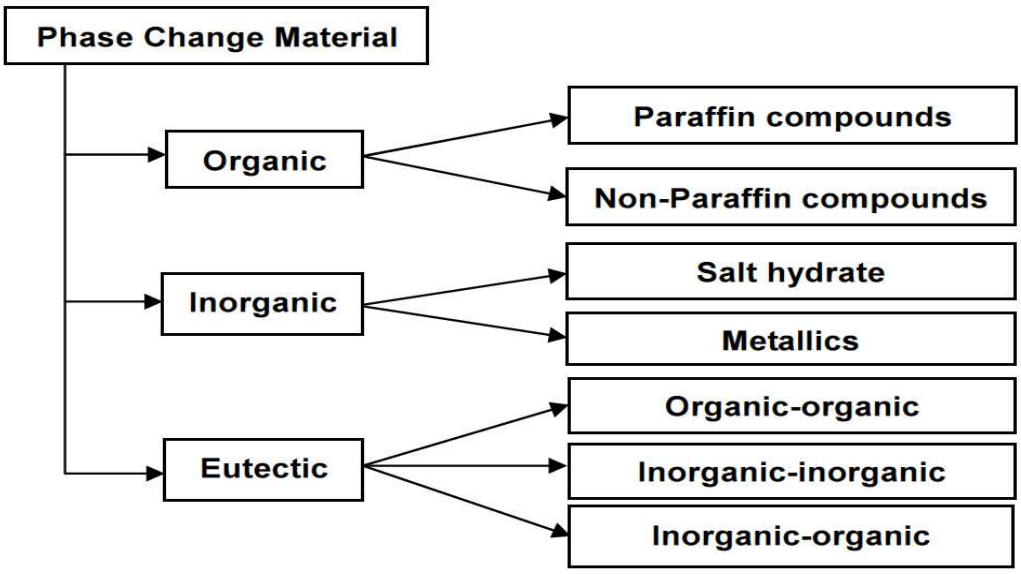


Figure 2:1: Classification of PCM. Sharma et al. (2009)

### 2.1.2 Classification of PCM.

Organic PCM such as fat and paraffin have been shown to be thermally stable after several cycles using the DSC(differential scanning calorimeter), showing little or no degradation of the latent heat and phase change temperature range Zalba B (2003). Sharma et al. (2009) mentioned that organic PCMs are regarded as PCMs with “poor thermal conductivity” and not ideal for effective thermal energy storage. However the advantage they provide with thier unique ability to undergo congruent melting, non-toxic nature, self-nucleating (ability to form structures or crystallize on its own) properties has made this class of PCM useful or relevant in latent heat thermal energy storage. Pure paraffin is known to belong to the family of saturated hydrocarbons, which means they contain only carbon and hydrogen of a general formula $C_{no}H_{2no+2}$ .The number of carbon atoms in the chain determines the melting point of the paraffin;

paraffin with values of n between 5 and 15 are regarded as liquid paraffin at room temperature. Also the longer the carbon chain, the higher the melting temperature and latent heat of fusion of the PCM Sharma et al. (2005). Lane (1989) mentioned that paraffin is known to be the most utilized viable heat storage PCM and in terms of cost, paraffins are regarded to be cheaper when compared to inorganic PCM.

Inorganic PCMs, include salt hydrates which possess good thermal conductivity when compared to organic PCM. The composition of elements that make up inorganic PCMs are different from organic PCMs. A Eutectic is a homogeneous mixture of substances that freezes at a temperature lower than that of the individual components. The configuration of the eutectic mix is a ratio or percentage of the constituent substances that has a lower melting point than any other composition of those substances Kotzé (2014). An example of an eutectic is calcium chloride hexahydrate and Magnesium chloride hexahydrate, having an individual melting point of 29.54°C and 117°C respectively, but at a percentage or ratio of 66.6% and 33.3%, they melt at a temperature of 25°C. The melting temperature is called the eutectic temperature. A eutectic system may comprise of a number of substances, most often binary or ternary. They have higher volumetric thermal storage density. However, Abhat (1983) observed that they are corrosive and possess poor nucleating properties which results in subcooling of the liquid PCM before solidifying. Subcooling is a phenomenon whereby a PCM only starts to crystallize at a temperature lower than the phase change temperature (melting point). Sub cooling delays the commencement of solidification in phase change material and this inhibits good thermal storage. It is significant in most inorganic phase change material Mehling and Cabeza (2008).In some application, Farid et al. (2004) stated that a small amount of subcooling might be insignificant, however a large amount of subcooling would hamper the performance of the thermal energy storage. Ataer (2006) mentioned that it is important to consider the following when designing a latent heat thermal energy system; a PCM with a desired phase change temperature, storage medium for the PCM and an effective heat transfer fluid which can transfer heat effectively. The selection of a PCM was based on the PCM melting temperature, chosen at a temperature interval below the operating temperature of the application (heat pump). Lane (1989) proposed an interval less than 5°C to prevent excessive degradation of heat within the system and reduction of efficiency. The latent heat, thermal conductivity and phase change temperature of the

PCM play a vital role in determining the size of the heat exchanger. The choice of paraffin for this research was based on cost, non-toxicity and its stability over a number of cycles of charging and discharging.

### 2.1.3 PCM Selection

Oró et al. (2013) stated that the selection of the suitable PCM required in any application is vital, as it plays an important role with regards to cost, thermal efficiency and utility of the thermal energy storage. PCM undergo several cycles of melting and freezing as they are charged and discharged respectively, hence it is important to take into cognisance, thermal cycling stability, based on the PCMs properties. It is also important for the PCM not to exhibit phase segregation, sub cooling and their thermal properties should be constant over a long period. Requirements of properties of desired PCM has been debated by several researchers; Mehling and Cabeza (2008) mentioned that two key requirements for a PCM to be used in any TES are a high latent heat of fusion and suitable phase change temperature, while Zhou et al. (2012) stated that three key properties are essential in determining the PCM to use for any system: suitable melting temperature, high heat of fusion and thermal conductivity Some researchers have grouped requirements for selecting PCM as; Physical, Technical and Economical. Table 2.1 describes the way the requirements are grouped .The properties of PCM required were explicitly discussed by various researchers.(Sharma et al. (2009), Zalba et al. (2003), Lane (1989)). Differential scanning calorimeters (DSC) has been used by various researchers to determine their thermo physical properties.

Commercial PCM is available from Rubitherm, Cristopia, Climator, TEAP and some can be prepared using reagents from chemical companies. From the list of commercially available PCM and those identified by other researchers, Agyenim and Hewitt (2012) stated that a selection of PCM in the temperature range of 50-60°C are regarded suitable for hot side of a vapour compression heat pump. The choice of the PCM is determined by the application or operating temperature.

Organic PCMs have low conductivity, which require heat enhancement to be used in thermal storage. The choice of selection of a PCM is based on the PCM melting temperature. It should be chosen at a temperature interval below the operating temperature of the application (heat pump). Klimes et al. (2012) stated that the thermal properties of PCM are vital for numerical modelling because they affect the numerical simulation. Esen et al. (1998) mentioned that the thermo physical properties and

geometry design of the store are to be considered together in designing a thermal energy storage system. This was evident in Esen et al. (1998) experiments using four different phase change materials (Calcium chloride hexahydrate (CCHH), Paraffin, Sodium sulphate decahydrate (SSDH) and Paraffin wax). CCHH stored heat energy faster than the other three PCM, because it has the highest conductivity. Also, the PCM melting time for smaller radii geometry was better than larger radii. This is because the thicker the PCM mass the lower the temperature gradient, the slower the heat transfer and the longer it takes to melt.

Table 2:1: Required properties of PCM. Dincer and Rosen (2011)

| Thermodynamic | Kinetic | Chemical | Economic |
|---|---|---|---|
| Melting temperature in desired range | High nucleation rate | Completely reversible | Low cost |
| High latent heat of fusion per unit mass | High rate of crystal growth | Chemical stability | Availability |
| High thermal conductivity | | Non corrosive | |
| High specific heat and high density | | High freeze/melt stability | |
| Small volume changes on phase transition | | Non-toxic, non-flammable and non-explosive material. | |
| Complete melting | | | |
| Small vapour pressure at operating temperatures | | | |

Based on the aforementioned, the research commenced with determining the thermal and physical properties of the PCM available.

## 2.2 Enhancing thermal conductivity of PCM.

PCMs with low thermal conductivity are not adequate for latent heat thermal energy storage (LHTES),this prolongs the charging and discharging time (Tian and Zhao

(2009), Chiu (2011)) .The higher the thermal conductivity, the higher the heat transfer in the medium which reduces the charging and discharging period. To enhance their thermal conductivity various methods have been utilized by researchers; Colella et al. (2012) added naturally expanded graphite matrix to paraffin (RT 100) to achieve the heat fluxes needed for a medium scale LHTES for district heating systems. Heat transfer enhancement is dependent on the type of application. Velraj et al. (1999) stated that in an application, such as water heat recovery which involves a process that is intermittent; for heat to be recovered in a short time, heat transfer enhancement required is for charging. If the application involves a case where the heat is available at a constant rate for a longer period of time and needed to be released quickly as in the case of a solar domestic hot water application, then heat transfer enhancement required is for solidification.

Weinstein et al. (2008) mentioned that the effect of the low thermal conductivity of PCMs reduces their effectiveness in a TES application with large volumes by creating larger thermal differences within the PCM. Weinstein et al. (2008) used graphite nanofibers (GNF) to enhance the thermal conductivity of the PCM with a phase change temperature of 56°C. The thermal performance was found to be dependent on the GNF loading. As the GNF weight loading increased, the thermal response increases initially, but at high GNF loading the effect on the thermal response is negligible. However, it was discovered that certain portion of the PCM did not undergo phase change, which means the latent heat of fusion was not fully utilized in the LHTES. Arasu and Mujumdar (2012) reported that by adding a certain amount of alumina particles to paraffin wax, the thermal conductivity could be increased. (Halalwa (2005), Farid (1990)) proposed ensuring minimal distance between PCM and fins of heat exchangers or pipes, which requires using thin plate arrangement to enhance heat transfer. Shatikian et al. (2005) carried out a numerical study using fin spacing of 0.5 to 4 mm. The fins were made from aluminium with a thickness of 0.15 mm to 1.2 mm. Fins are mostly made from copper, steel, aluminium or magnesium. They are used to enhance the thermal conductivity into and out of the PCM. High thermal conductivity of the fins and large surface area help to enhance the performance of a latent heat thermal energy storage. Frazzica et al. (2017) compared two different heat exchangers based on the latent heat storage concept. The heat exchangers were an asymmetric plate heat exchanger and a fin and tube heat exchanger. The plate spacing for the plate heat exchanger was 3 mm and fin spacing was 5 mm. Frazzica et al. (2017) mentioned

that the spacing dimensions were chosen in order to have an effective heat transfer between the heat exchangers and PCM. The fin and tube heat exchanger with welded fins performed better than the plate heat exchanger in terms of heat transfer. This is attributed to the presence of fins, which enhance heat transfer between the heat exchanger and the PCM. ACT (2018) stated that an optimal fin spacing of 1.27mm to 2.54 mm was used for a PCM heat sink for advanced cooling technique (ACT). It is observed that it takes a shorter time for the PCM to melt when there are more fins, and it takes a longer time for the PCM with the same volume to melt, when there are fewer fins.

For this research, the choice of using a plate heat exchanger made from polypropylene with a plate spacing of 4mm on the water side is based on the fact that an effective heat transfer would exist between the heat exchanger and water. The PP sheet as shown in Figure 6.4 provides a thin walled structure (0.3mm) which is suitable for effective heat transfer between the HTF, wall and PCM on top of the PP sheet during charging and discharging process. PP sheet is chemically resistant to attack from PCMs and due to the thin walls, it will be useful as an effective PHE.

There have been reports by some researchers that heat transfer could be increased by addition of nanoparticle copper to the PCM (nano fluid). Elgafy and Lafdi (2005) used carbon nano fibres (CNF) to enhance the thermal conductivity of a paraffin wax with a melting temperature of 67°C. Reddy (2007) used different number of fins attached to the PCM-water system to enhance heat transfer of a solar-integrated collector storage water heating system with PCM. However Chiu (2011) stated in his thesis that having larger number of fins to enhance thermal conductivity of PCM, could lead to reducing the IPF(Ice packing factor) of the PCM, which in turn reduces the energy storage capacity. The increase in cost of fabricating fins and difficulty of filling the PCM in the system prompted Chiu to state that the storage design is vital in improving the thermal performance of the PCM used. Dutil et al. (2011) stated that more fins also decreases the volume of PCM. This research looks at using low cost plate heat exchanger concept using polypropylene sheet with channels and a serpentine heat exchanger to enhance heat transfer in the thermal store.

Hassan (2014) studied three different models with pipes that have no fins, four fins and eight fins. He discovered the heat transfer was enhanced for the pipes with fins

compared to the pipe without fins as shown in Figure 2:2. Also, using multiple loop arrangement of pipes with different pipe diameters (40mm, 42.4mm and 46.64mm) in a 3D model, it was discovered that the largest pipe melted faster compared to the other two. Hassan's simulations are not backed up with experiments. He claims the only way to improve the heat transfer of a PCM with low thermal conductivity was by increasing the heat transfer area. Increasing the HTF inlet temperature, varying the mass flow rate, geometry etc. was not considered in his analysis.

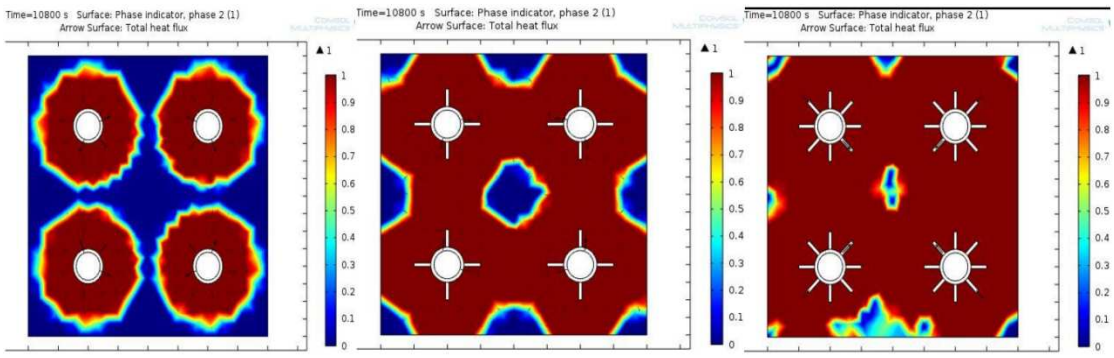


Figure 2:2: Melting phase comparison for the different models.Hassan (2014)

The type of geometry has been known to affect the overall heat transfer performance of a thermal storage unit. Various types of geometries exist such as plate heat exchanger, shell and tube heat exchanger, U-tube, U-tube with inline fins, U tube with staggered fins and festoon design etc. Figure 2:3 shows an image of various geometries used for thermal storage.

The melting time of each of these designs for thermal energy storage varies. Kurnia et al. (2013) concluded that the serpentine design shown in Figure 2:2 (d) offers the best heat transfer when compared to other geometrical design; U-tube, U-tube with inline fins, U tube with staggered fins. Paraffin wax was used for the study and the mathematical model was based on conjugate heat transfer between the heat transfer fluid (water) and PCM. The U tube with fins shown in Figure 2:2(c) improved heat transfer compared to the U tube without fins shown in Figure 2:2(a), which fortifies the advantages the use of fins brings to a TES. The addition of fins enhances the heat transfer surface, thus improving heat transfer. However, the conclusion by Kurnia cannot be validated because it was based on computational analysis and without any experimental analysis.

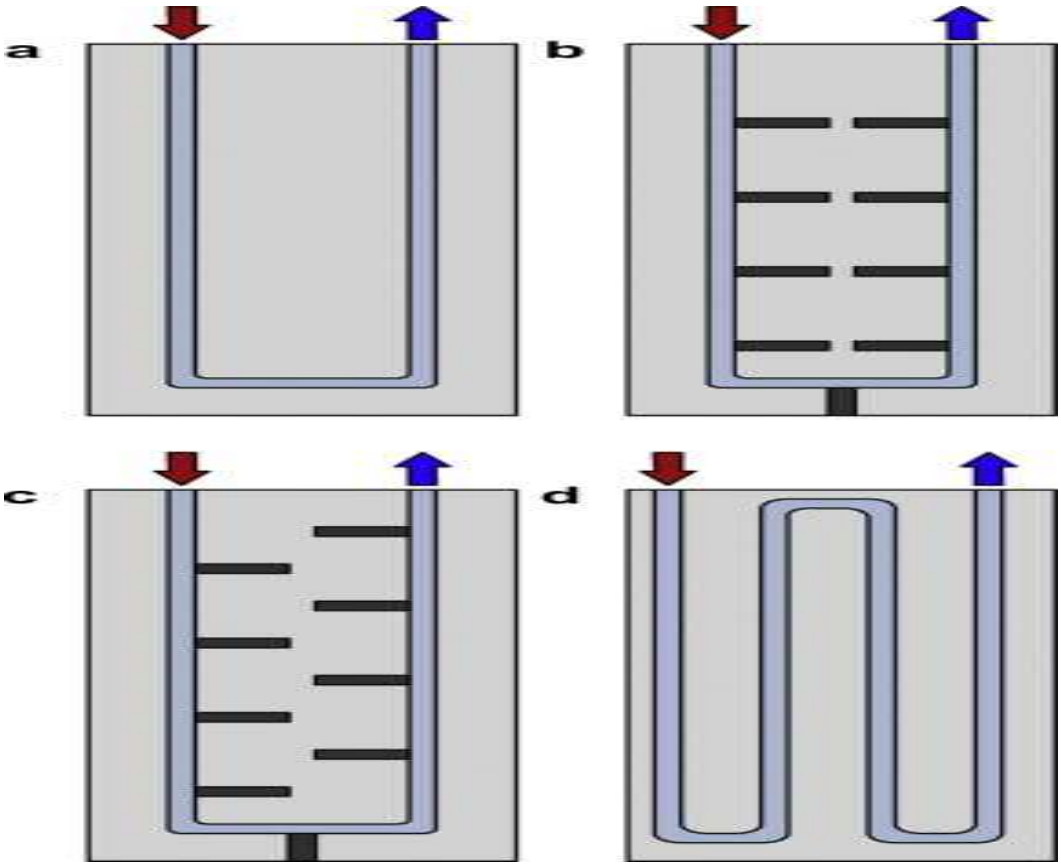


Figure 2:3: Schematic drawing of a) U-tube, b) U-tube with fins, c) U-tube with staggered fins and d) festoon design. Kurnia et al. (2013)

## 2.3 Modelling Of PCM

It is difficult to analyse the behaviour of phase change systems due to its non-linearity at moving boundary problem. The analytical method is complex but applicable to one dimensional case and physical situations with simple geometries. A numerical method of solving phase change material behaviour is better than the analytical method (Al-abidi et al. (2013). Dutil et al. (2011) and Verma et al. (2008)) described explicitly the various mathematical and numerical methods used by researchers in their reviews. The effect of different geometry and application, mathematical fundamentals of PCM were determined. Dutil et al. (2011) stated that predicting the behaviour of PCM is complex because of its non-linear nature at moving interfaces by which the displacement rate is controlled by latent heat loss. Sharma et al. (2009) describes that numerical method using finite element and finite difference method could be used for various applications, thus mostly used for practical application involving phase change. The most suitable and mostly used method for solving phase change problems is the

enthalpy method (Dutil et al. (2011), Alexiades (1993)). The enthalpy method is based on the energy equation which has temperature as the only dependent variable (Sharma et al. (2009). This solution is based on weak solution of partial differential equation (Lamberg et al. (2004), Hu and Argyropoulos (1996)).
The variation of the enthalpy with temperature can be illustrated in Figure 2:4

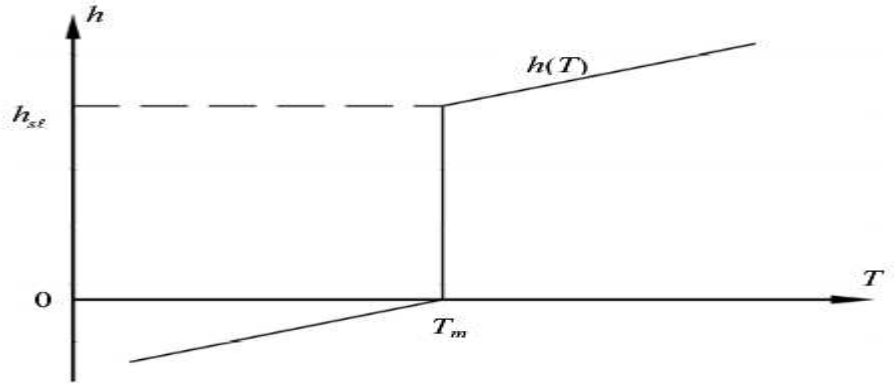


Figure 2:4: Enthalpy as a function of temperature. Mehling and Cabeza (2008)

Scrinivas (2006) discovered better convergence using the enthalpy method in his design of a transient heat conduction of a passive cooling device to model phase change of a heat sink made with aluminium and paraffin, utilizing MATLAB and COMSOL Multiphysics. Chiu (2011) mentioned that his heat transfer model was also created using MATLAB and COMSOL. The model was based on 2-D fixed grid finite difference enthalpy based simulation. A gelled salt hydrate was used in his experimental rig using a finned shell and the result was validated. A numerical model of an industrial tank filled with encapsulated PCM was studied by Bedecarrats (2009).

Several analytical and numerical methods have been developed to describe the behaviour of PCM in a geometry. Some researchers have been able to validate their findings, while others simply carried out experiments or simulations, without any validation of their study.

Recent approach by researchers involves using computational fluid dynamics software to simulate melting and solidification. Such software include: Fluent software by ANSYS, COMSOL multiphysics and Star-CMM+. Self-developed programs using Matlab, Fortran, C++ Al-abidi et al. (2013). Fluent program is mentioned to be the most frequent used. The fluent software uses a model that can simulate engineering

problems such as casting, melting and solidification, crystal growth. For the self-developed programs, various discretization methods are used; Finite difference method (FDM); Finite element method (FEM) and Finite volume method (FVM).

In most heat transfer simulation involving phase change, sub cooling is often ignored. Mehling and Cabeza (2008) stated that subcooling is evident during recovering of heat; when the latent heat is not released having attained the phase change temperature. The effect of sub cooling makes it important to reduce the temperature below the melting temperature so as to commence crystal growth or crystallization and to release the latent heat stored. The effect of subcooling in a thermal store could hamper the overall efficiency of the thermal store, because if there is no latent heat, then the store will be storing only sensible energy. Bony and Citherlet's (2007) research on simulation of heat transfer in phase change considered the effect of both hysteresis and subcooling on the model. They concluded that the hysteresis effect takes place during cooling of the PCM and that it delays the phase change process.

## 2.4 Research on Thermal Storage Using PCM

Kürklü et al. (1996) developed a model which was validated with an experiment to predict the thermal performance of a square-section PCM store based on conservation of energy. He used Sodium sulphate, sodium chloride with other additives as the PCM and air as the heat transfer fluid. He discovered that as the air mass flow rate increased, there is a corresponding decrease in the phase change time of the PCM (complete freezing). Nallusamy (2016) carried out experiment based research and observed that as the flow rate increases, the time required for complete charging reduces. Using flow rates of 2, 4 and 6 kg/min; he discovered charging time was smaller at 6kg/min. This is because when the flow rate increases, it results in an increase in surface heat transfer coefficient between the HTF and the PCM. This means the flow rate has an effect when charging and discharging.

Esen et al. (1998) investigated the performance of a solar assisted cylindrical energy storage tank which is part of a domestic heating system. For his model, he used the enthalpy method, solving by Gaus-sieldel iteration process. He discovered the cylindrical wall material and radius of tank were not appropriate due to the size of the cylinder. He recommended smaller radii and higher thermal conductivity material which would increase PCM melting time. The effect of the mass flow rate at a given

time affects the amount of stored energy. This is because more heat is removed from HTF, consequently more heat stored in the PCM.
(Agyenim and Hewitt (2012), Agyenim and Hewitt (2010)) carried out an experiment similar to this research using RT58 as the PCM. They used a finned longitudinal shell and tube heat exchanger because of the low thermal conductivity of RT 58 and the advantage of preventing sub-cooling of PCM through nucleation. From his experiment, as the temperature of the inlet HTF temperature increases, so does the heat transfer and the amount of heat energy charged. They increased the inlet HTF from 62.9°C to 76.7°C and concluded that full melting of the PCM occurred at 71°C and 76.7°C and that any temperature below that means complete melting did not take place. Agyenim's experiment had a bypass valve connected to the hot water bath which is PID controlled, so as to have a set value of inlet temperature before charging starts. This was utilised in this research's experimental work.

Agyenim and Hewitt (2012) discovered that when RT58 PCM is charged it cannot be melted (has not even reached its phase change zone) within four (4) hours at any value of inlet HTF temperature. He recommends twenty-four (24) hours of charging, ie. a whole day to complete heating of the system. This means the maximum time of charging under economy 7 cannot be achieved; hence it's important to design an advanced heat exchanger system whereby the PCM can be charged within the period of electricity tariff reduction.

In thermal storage using phase change material, using multiple PCMs (m-PCM) has enhanced the performance of the storage unit compared with using only a single PCM. The arrangement of multiple PCMs in decreasing order of their melting temperature during charging results in higher heat transfer rate. Various researchers have experimentally tested the performance. Tian et al. (2012) arrangement of the multiple PCM was in increasing order of melting during charging as shown in Figure 2:5, which is a different approach to other researchers as shown in Figure 2:6. This arrangement would decrease the heat transfer rate when HTF flows from a PCM with a low melting point to one with a higher melting point. Tian's arrangement will be useful for the discharging process but not the charging process. Tian's arrangement is not ideal, because the PCM melting temperature was not considered for the cascading storage. It is not possible to have an effective heat transfer with that storage. The right order

should be PCM3, PCM 2 and PCM1 in order to maintain similar temperature differences between the PCMs and HTF.

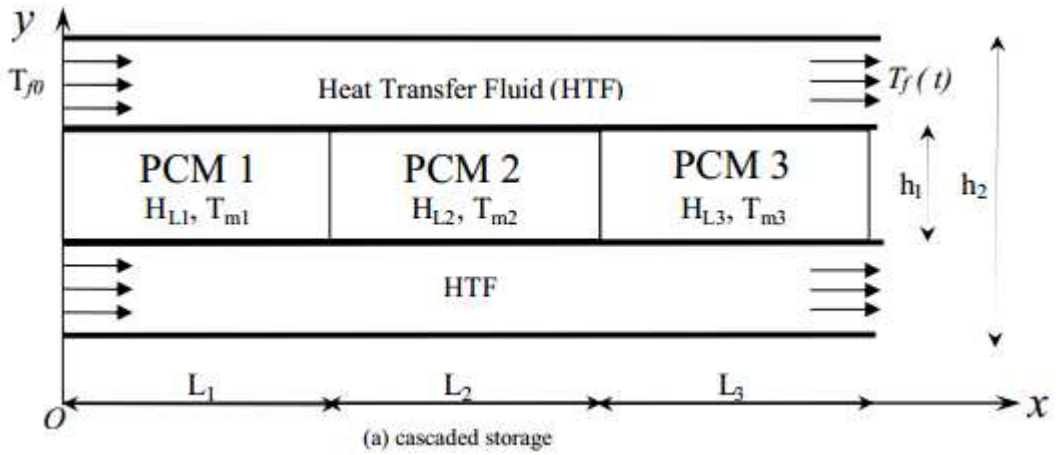

(a) cascaded storage

| PCMs | Melting temperature (℃) | Density ($kg/m^3$) | Latent heat (kJ/kg) | Specific heat (kJ/kg ℃) | Thermal conductivity (W/m K) |
|---|---|---|---|---|---|
| PCM 1 | 31 | 880.0 | 169.0 | 2.1 | 0.2 |
| PCM 2 | 50 | 880.0 | 168.0 | 2.1 | 0.2 |
| PCM 3 | 82 | 880.0 | 176.0 | 2.1 | 0.2 |

Figure 2:5: Cascaded thermal storage unit with thermal properties. Tian et al. (2012)

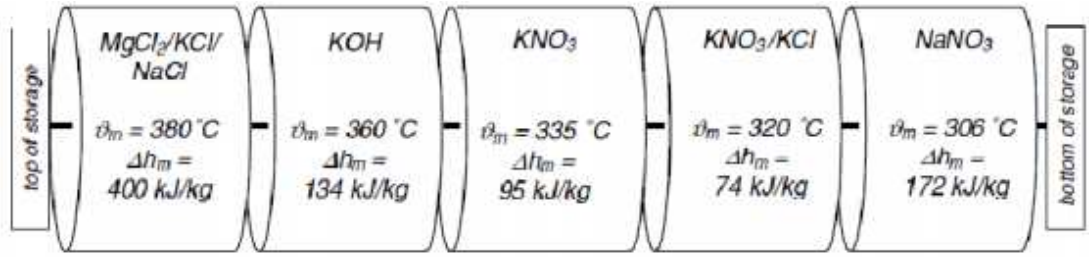


Figure 2:6: Cascaded thermal storage unit. Horst Michels and Pitz-Paal (2006)

Wang et al. (2015a) carried out a numerical simulation using three (3) PCMs contained between zig-zag configuration plates as shown in Figure 2:7. The arrangement of the PCM are in the order of PCM1, PCM 2and PCM 3 in the flow direction of the heat transfer fluid with decreasing order of their phase change temperature(PCM-1>PCM-2>PCM-3). A similar arrangement was investigated by Jegadheeswaran and Pohekar (2009) as shown in Figure 2:8, who used five different PCMs in a shell and tube heat exchanger.

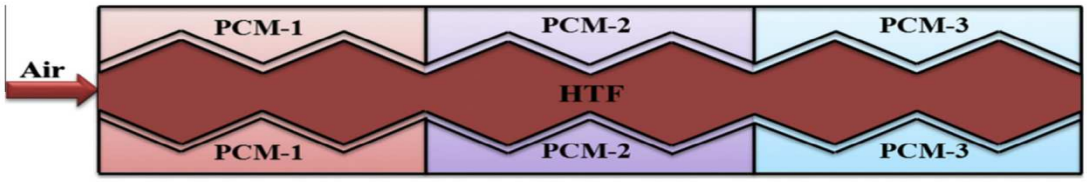


Figure 2:7: : Schematic representation of the zigzag configuration.Wang et al. (2015a).

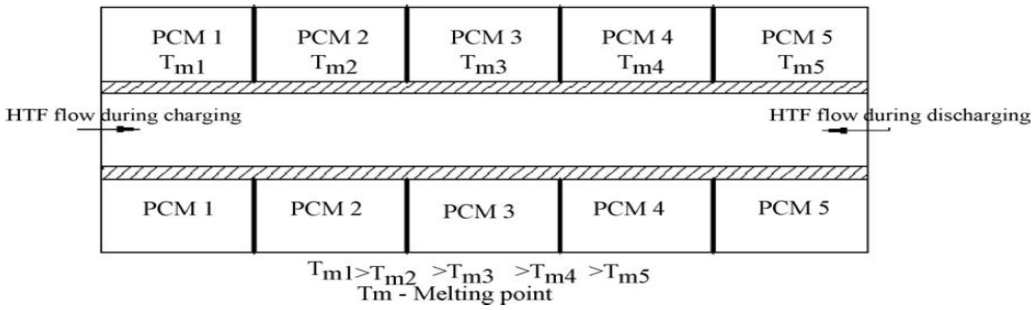


Figure 2:8:Multiple PCM arrangement in a shell and tube exchanger.Jegadheeswaran and Pohekar (2009).

## 2.5 Summary

The classification of PCMs and the advantages they possess over each other is discussed in detail. The mode of selection of PCM is discussed and their properties required for various TES application. The types of PCM and geometry used by other researchers are discussed. The various ways PCM can be enhanced by cascading, modifying the geometry (use of fins) and encapsulation is discussed in this chapter. The cascading method is used to give a more uniform temperature difference between HTF and store such that a more constant heat (charge rate) is maintained and as much energy extracted from the HTF as possible as it applies to enhancing the properties of the PCM as the various types of PCM are arranged according to their thermal properties (with the PCM with the highest melting point arranged in descending order).

The various modelling methods used by other researchers are discussed and the advantages they possess over each other are explained. The type of software used to solve the modelling problem is mentioned. Various ways in which the performance of TES can be enhanced are discussed, with mention of cascading and how to improve the thermal conductivity in PCMs with low thermal conductivity (Paraffins).

# 3 Phase change materials

## 3.1 Classification of PCM.

Phase change materials can be classified as organic or inorganic material. They possess the ability to absorb or release energy during change of process. Figure 3:1 shows the phase change cycle undergone by the PCM as it is heated or cooled.

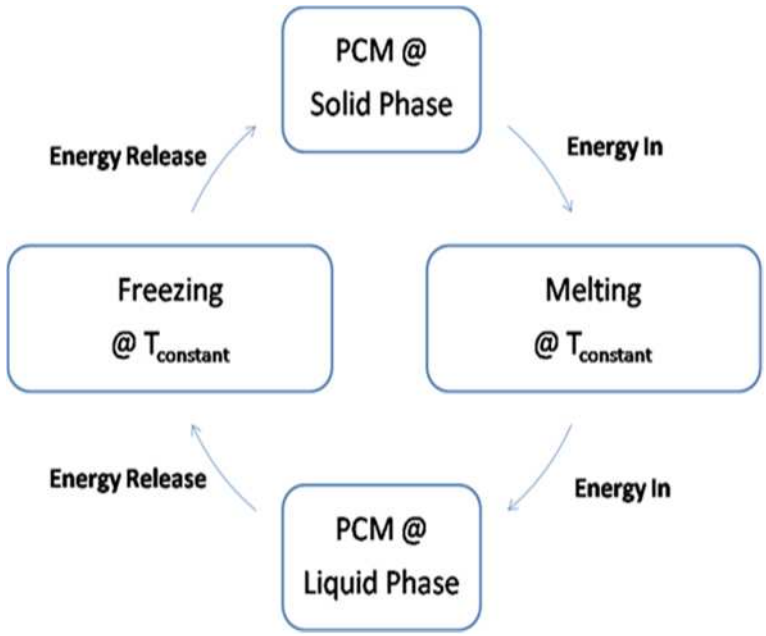


Figure 3:1: Phase change process. Al-Hallaj and Kizilel (2012).

## 3.2 Phase change material selection

Choosing the right PCM for the desired application or operating range is vital to the efficiency of the TES. The following criteria are considered when choosing a phase change material. For effective use in application, some properties are desirable. They have certain physical, thermal and chemical properties Sharma et al. (2009);

**Physical Properties**

- Small volume change
- Low vapour pressure
- High density
- Good phase change equilibrium

**Thermal properties**

- High thermal conductivity
- High latent heat of fusion
- Suitable phase change temperature

**Chemical properties**

- Non toxic
- compatible with heat exchanger geometry
- stable after undergoing several cycles
- Inflammable

## 3.3 Subcooling

Subcooling is a phenomenon where the PCM starts to crystallize only at a temperature lower than the phase change temperature (melting point) as shown in Figure 3:2. Latent heat is only released during energy recovery or discharge process. The temperature must be below the phase change temperature for crystallization to commence. During the recovery of energy (discharge process), the effect of subcooling of the PCM affects the overall performance of the latent heat thermal energy storage. It is important to reduce or eliminate subcooling, for it affects the overall performance of the latent heat thermal energy store Mehling and Cabeza (2008).

Subcooling delays the commencement of solidification in phase change material and this inhibits good thermal storage. It is significant in most inorganic phase change material Mehling and Cabeza (2008). Farid et al. (2004) stated that in some application, a small amount of subcooling might be insignificant; however large amount of subcooling would hamper the performance of the thermal energy storage. Lane (1989) mentioned that the selection of a PCM was based on the PCM melting temperature, chosen at a temperature interval below the operating temperature of the application (heat pump). An interval less than 5°C has been proposed to prevent excessive degradation of heat within the system and reduction of efficiency. The latent heat, thermal conductivity and phase change temperature of the PCM play a vital role in determining the size of the heat exchanger. The choice of paraffin for this research

was based on cost, non-toxicity and its stability over a number of cycles of charging and discharging.

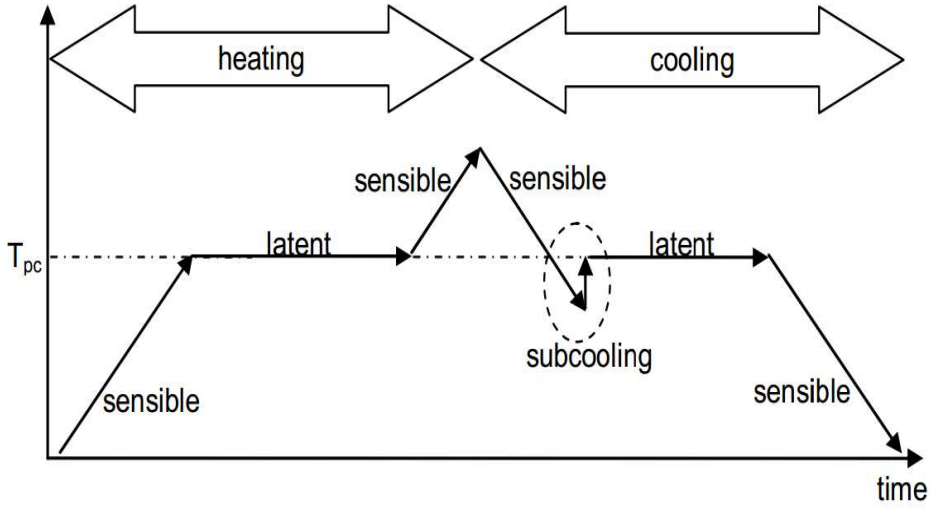


Figure 3:2: Investigation of subcooling. Mehling and Cabeza (2008).

In most heat transfer simulation involving phase change, subcooling is often ignored. Mehling and Cabeza (2008) stated that subcooling is evident during recovering of heat; when the latent heat is not released having attained the phase change temperature. The effect of sub cooling makes it important to reduce the temperature below the melting temperature so as to commence crystallization or crystal growth and to release the latent heat stored. Subcooling can be prevented by the use of nucleating agents, which have a crystal structure similar to that of the parent substance. Other means of eliminating or reducing subcooling involve the use of metallic heat exchanging surfaces in contact with PCM to promote heterogeneous nucleation, mechanical stirring, cold finger technique and PCM encapsulation. Mehling and Cabeza (2008).

The effect of subcooling in a thermal store could hamper the overall efficiency of the thermal store, because if the latent heat cannot be recovered, then the store will be storing only sensible energy. There is often some confusion between subcooling effect and thermal hysteresis. Thermal hysteresis is defined as the deviation in temperature between the heating and cooling temperature corresponding to the heating and cooling curve from the enthalpy-temperature graph. Figure 3:3a and Figure 3:3b; show the effect of both subcooling and thermal hysteresis respectively on a PCM (SP21EK), a Rubitherm product which has melting temperature of 21°C. The PCM has a subcooling temperature of 0.8°C and hysteresis of about 1.2°C. The pink colour line

on Figure 3.3 a, shows the plot of temperature against time, from which the enthalpy measurement was obtained, (Figure 3.3b). Figure 3.3a shows the temperature difference between melting and solidification area of the PCM; SP21EK, (22-20.8)°C =1.2°C, which is termed as hysteresis. The subcooling effect is observed on the solidification area, between 20.8°C and 20°C, where the PCM temperature drops to 20°C, before the solidification process commences.

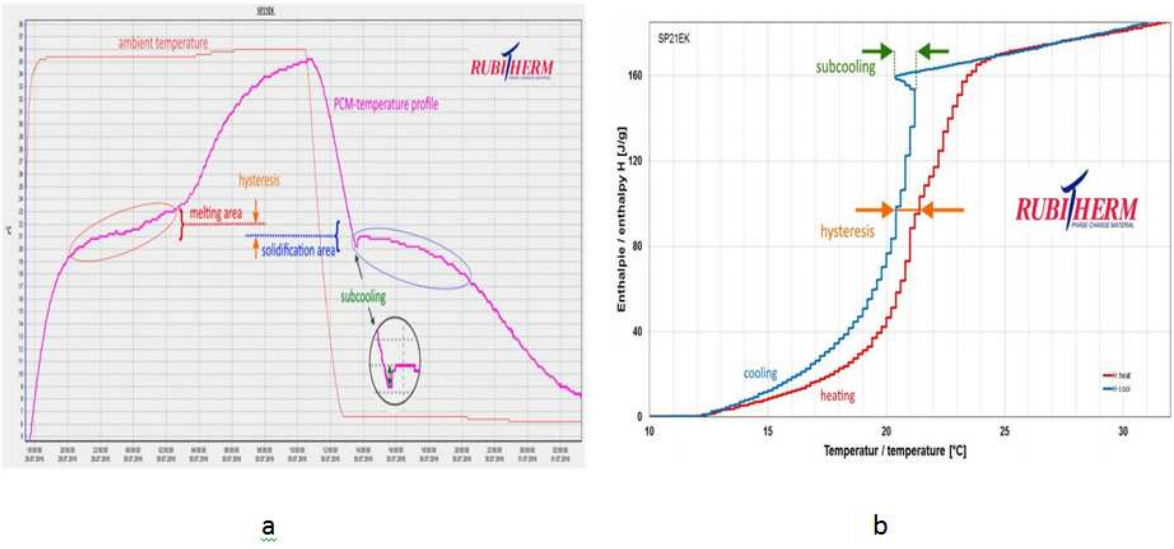


Figure 3:3: Temperature profile showing subcooling and hysteresis. Rubitherm (2017).

The result obtained from measured heating and cooling enthalpy curves could indicate both curves are far apart. This could be attributed to the presence of subcooling or thermal hysteresis. This effect could be checked by running the DSC measurement at different heating and cooling rate or step method. Günther et al. (2005) proposed three different methods could be used to confirm or produce a result with high accuracy for the thermal properties of PCM; using the DSC, T-history method and air flow apparatus.

## 3.4 Mathematical and Numerical analysis of latent heat thermal energy storage.

This chapter gives an overview of modelling of PCM in a latent heat thermal energy storage (LHTES). Numerical methods are used to solve phase change; they are discussed in detail in this chapter.

Modelling of PCM is based on a transient, non-linear phenomenon with a moving solid-liquid interface, which is called moving boundary problem. Over the years, several solutions to phase change have been proffered. Analytical method is not used due to moving boundary problem and can only be used to solve one dimensional case and simple geometries, thus numerical method has been regarded as the best solution to phase change problem. Several researchers have used this method for different geometry and storage applications.

### 3.4.1 Stefan Problem

Stefan problem is a type of boundary value problem for a partial differential equation with regards to solidification and melting in a phase change medium. Phase change material behaviour when it solidifies or melts is an example of a boundary value problem. Jozef Stefan, a physicist, was accredited with providing a general class for such problems in 1889. The Stefan problem is the most utilised solution for one dimensional moving boundary problem and simple geometries. However due to complex geometries and boundary conditions, varying thermo physical properties various transport mechanism (conduction, convection) within a domain, numerical methods are used for solving moving boundary problem that relates to phase change Hu and Argyropoulos (1996).

The problem when the PCM starts to melt is that it consists of a mixture of liquid and solid phase, which is regarded as the mushy region, of which they are separated by a moving interface. The non-linearity of the equation makes it difficult to solve analytically, hence a numerical method is developed to solve it. (Verma et al. (2008), Voller (1997), Dincer and Rosen (2002)) have undertaken reviews of the general numerical methods for solving phase change problems.

There have been several numerical methods used to solve the problem of phase change; effective capacity method, enthalpy method etc. The enthalpy method is the most commonly used numerical method. Figure 3:4 shows the relationships between these solutions.

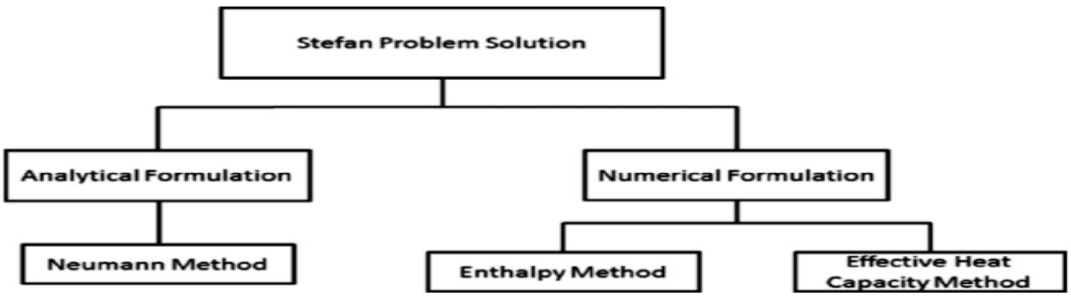


Figure 3:4: Relationship with Stefan problem. Iten and Liu (2014).

### 3.4.2 Effective heat capacity method

Effective heat capacity method involves the energy equation in terms of heat capacity. The method utilises the behaviour of the PCM into the heat capacity calculation. The heat capacity represents the quantity of heat required to raise the temperature of the PCM. The result from the differential scanning calorimeter is useful in solving the phase change problem. The latent heat of melting is key to this solution. This method is expressed with Equation 3.1. Based on this, there is only one unknown parameter, temperature.

$$\rho C_p \frac{\delta T}{\delta t} = \nabla \left( k \nabla^2 T \right) \qquad 3.1$$

There is a similarity between the effective heat capacity and enthalpy method, however for the enthalpy method; there are two unknown variables; enthalpy and temperature. Figure 3:5 shows the relationship between both methods.

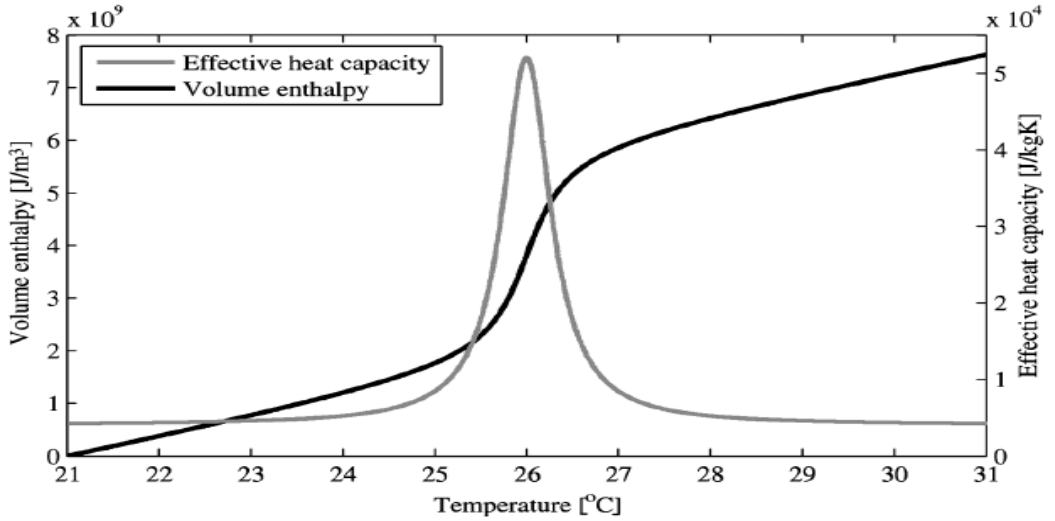


Figure 3:5: Relationship between the enthalpy and effective heat capacity method. Klimes et al. (2012).

### 3.4.3 Enthalpy method

The enthalpy method is used in solving non-linear heat equations in phase change problems which involve a moving boundary. The relationship between temperature and enthalpy is used to solve the phase change problem. The enthalpy method was developed by Voller (1997) and it is one of the most utilised methods for the treatment of phase change boundary. The method involves an enthalpy–temperature relationship of the phase change material expressed in Equation 3.2.

$$\rho \frac{\delta H}{\delta t} = \nabla \left( k \nabla^2 T \right) \qquad 3.2$$

The solution to Equation 3.2 is based on the enthalpy-temperature relationship. Both variables are combined together through their relationship which is obtained from the DSC. The enthalpy method assumes the enthalpy into the energy equation of sensible and latent heat. Enthalpy is the summation of the sensible heat and latent heat of the phase change as shown in Equation 3.3 to Equation 3.5.

$$H(T) = \text{sensible heat} + \text{latent heat}$$

$$H(T) = h(T) + \rho L f_i(T) \qquad 3.3$$

$$\mathrm{h(T)} = \int_{T_l}^{T} \rho C_p dT \qquad 3.4$$

$$H(T) = \int_{Tl}^{T} \rho C_p dT + \rho L f_i(T) \qquad 3.5$$

The liquid fraction is expressed as shown in Equation 3.6 for solid, mushy and liquid phase respectively

$$f_i(T) = \begin{cases} 0 & \mathrm{T} < T_s \\ \dfrac{T - T_s}{T_l - T_s} & T_s \le T \le T_l \\ 1 & T > T_l \end{cases} \qquad 3.6$$

The enthalpy method can be applied directly to the three phases (solid, liquid and mushy phase). The liquid fraction represents the state of the PCM at the nodes based on the temperature of the PCM; solid ( $f_i(T) = 0$); Mushy region ( $0 \le f_i(T) \le 1$ ) and liquid ( $f_i(T) = 1$).

Klimes et al. (2012) stated that different numerical methods such as finite difference, finite volume method, and finite element method can be used to solve this method. Most researcher model latent heat thermal energy storage with several tubes as one tube in order to save computation time. The energy stored by the system is the product of the number of tubes in the storage and energy stored in one of the unit that has been modelled. This is applicable in both shell and tube geometry as well as flat plate geometry.

### 3.5 Summary

The chapter deals with PCMs based on their classification, selection process of use in thermal storages. The selection of a PCM was based on the PCM melting temperature, chosen at a temperature interval below the operating temperature of the application (heat pump). The key properties that are desirable for PCMs to be used are discussed in detail. The effect of subcooling on the performance of thermal energy storage and its difference to hysteresis are mentioned using a case study of a PCM tested in the laboratory by Rubitherm. Knowing the difference between subcooling and hysteresis from results obtained from the differential scanning calorimeter is key to understanding the nature of the PCM and accuracy of the result obtained from the DSC. The different methods (Enthalpy, effective heat capacity) used for solving phase change problems are discussed. The Stefan problem is discussed and the various mathematical and numerical methods explained. The problem that phase change

problem are restricted in analytical solutions is explained. Most solutions are simple geometry and one dimensional. Hence the need to use numerical methods to solve phase change problem. Finite difference, finite element and finite volume method were some of the methods used to solve phase change problems.

# 4 Experimental Thermal Material Analysis

## 4.1 Introduction

For this research, thermal analysis test of the phase change material (PCMs) was carried out using the hot disk and differential scanning calorimeter (DSC). This is to study the thermophysical properties of the PCMs, which is essential in the design of the thermal store to optimise performance. This chapter covers this thermal measurement and how the PCMs were prepared for testing, while chapter 5 and chapter 6 contain details of the results from the thermal measurement and experimental setup using the chosen PCM based on the thermal analysis of the modular design of a polypropylene sheet based plate heat exchanger concept in the laboratory respectively.

## 4.2 Thermophysical properties of PCM

The importance of the thermophysical properties of the phase change material cannot be overlooked, hence this research commenced with determining the thermal properties of the four different phase change materials. They are, Paraffin RT 52, Paraffin RT 58, Climsel C58 and a eutectic mix of magnesium nitrate hexahydrate and ammonium nitrate ($Mg(NO_3)_2.6H_20 + NH_4NO_3$). Paraffin RT 52 and 58 are classified as organic PCM, while the Climsel C58 and eutectic mix are classified as inorganic PCM. They were chosen because their melting point is in the range of the design temperature of the thermal store for domestic home application. The thermal conductivity of each PCM was determined using the hot disk instrument, whilst the differential scanning calorimeter (DSC) was used to determine its thermal behaviour (melting point, enthalpy, specific heat capacity etc.). The determination of the thermo-properties of the aforementioned PCMs helps in the experimental investigation of the use of the PCM with a polypropylene sheet based on a plate heat exchanger design concept and on the serpentine heat exchanger, based on a shell and tube heat exchanger concept. Water is used as the heat transfer fluid because of its high heat capacity and low viscosity, which makes it easy to pump.

## 4.3 DSC/Hot Disk measurement

The paucity of fully reliable data on thermophysical properties from manufacturers prompted the process of conducting tests on four different phase change materials. The phase change materials include Paraffin RT 52, Paraffin RT 58, Climsel C58 and a Eutectic mix ($Mg(NO_3)_2.6H_20$ & $NH_4NO_3$). Both paraffins (RT 52 & RT58) were

procured from Rubitherm Company. The eutectic mix was prepared in the laboratory using 61.5% of magnesium nitrate hexahydrate $Mg(NO_3)_2.6H_20$ and 38.5% of ammonium nitrate ($NH_4NO_3$). Both chemical components were procured from Fischer chemicals. Climsel C58 is a salt hydrate based PCM procured from Climator Ltd. It comprises of sodium acetate, water and additives. Climsel C58 is stored in aluminium pouches and based on the instructions from the material safety data sheet (MSDS), they are difficult to handle. The thermophysical properties of the PCMs was analysed by using the DSC. Each PCM was heated and cooled at a cooling rate of 2°C/min. At the end of this thermal testing, the thermophysical properties of the PCMs were considered for use in the thermal store and results obtained from the instruments were compared to values from literature and results validated.

### 4.3.1 Differential scanning calorimeter

The differential scanning calorimeter (DSC) is a device that is used to determine the phase change temperature or melting temperature, heat of fusion, crystallization temperature of the material placed in its crucible. The measurements are carried out under a controlled heating or cooling rate. The process measures the temperature and heat flow (mW or W/g) corresponding to the thermal performance of the sample, as a function of temperature and time. DSC provides quantitative and qualitative information on melting and solidification processes of the material that is sampled. Figure 4:1 shows an image of the SENSYS Differential scanning calorimeter device available at the University of Warwick and used to carry out these measurements.

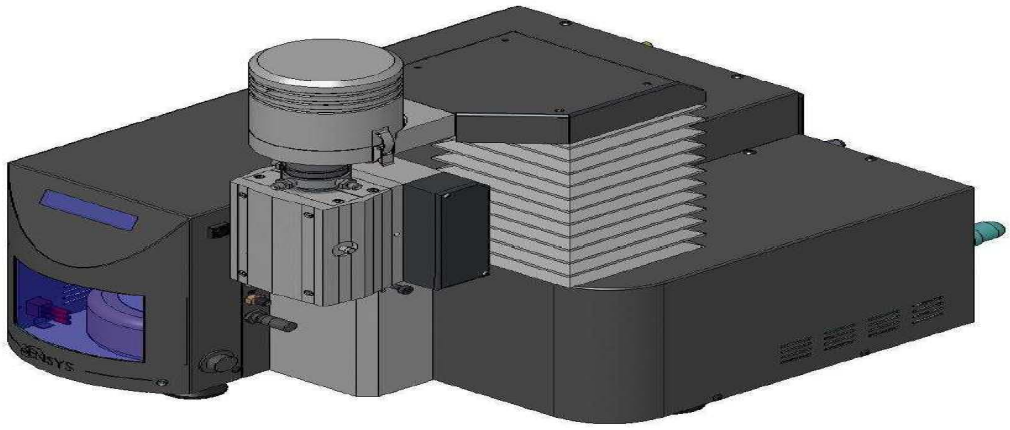

Figure 4:1: SENSYS Differential scanning calorimeter. Setaram (2005).

The DSC consist of the following parts; furnace, reference sample, material sample pan, thermoelectric sensor. The way the measurement is taken using the DSC involves the use of two pans; one holds the sample material, while the other pan is used as the reference. The heat flux between the reference and sample pan is measured. This is done by mounting the pans on separate thermoelectric sensor platform surrounded by a furnace. As the temperature of the furnace increases, heat is transferred to both pans through the thermoelectric platform they are mounted on. It should be noted that the DSC does not measure the temperature of the material. There is a sharp peak on the thermogram (heat flow against temperature plot) and deviation from the steady state profile. The latent heat of fusion is obtained from the area under the curve. A heating/cooling rate is chosen for the analysis. It is important to choose an appropriate rate, as it affects the result of the analysis. The mass of the sample is recorded before the test is carried out for quantitative analysis.

The heating or cooling rate affects the accuracy or deviation in DSC measurement. It was observed that at a higher heating or cooling rate, the DSC result was over predicted. To prevent this, DSC measurements are carried out at low heating and cooling rate (Günther et al. (2005). Günther et al. (2009) recommended using a heating or cooling rate in the range of 2 to 10°C/minute. The heating rate affects the point at which the phase change temperature peaks. Phase change shifts to a higher temperature, when heating rate increases. The higher the heating rate, the larger the melting peak.Drissi et al. (2015). Accuracy of the DSC measurement is dominated by the heating rate and sample size. Günther et al. (2005)

Araújo et al. (2010) carried out measurement on the DSC to determine the effect of heating or cooling rate. The result obtained from the DSC was evaulated using a sample mass of 2milligrammes. Zidovudine (AZT) was used as the sample material tested in the DSC. Figure 4:2 shows a DSC measurement carried out at different rates (1, 2,5,10 and 15°C/min. It was observed that the melting point was over predicted as the heating or cooling rate increases. From Figure 4:2, it was observed that at 5 to 15°C/min, the melting point of the sample was over predicted. At lower rates (1 to 2°C/min), the melting point are more accurate when compared to results obtained at higher heating or cooling rate. Based on DSC analysis carried out by various researchers, It was recommended that tests carried out using the DSC should be carried out at a lower heating or cooling rate.

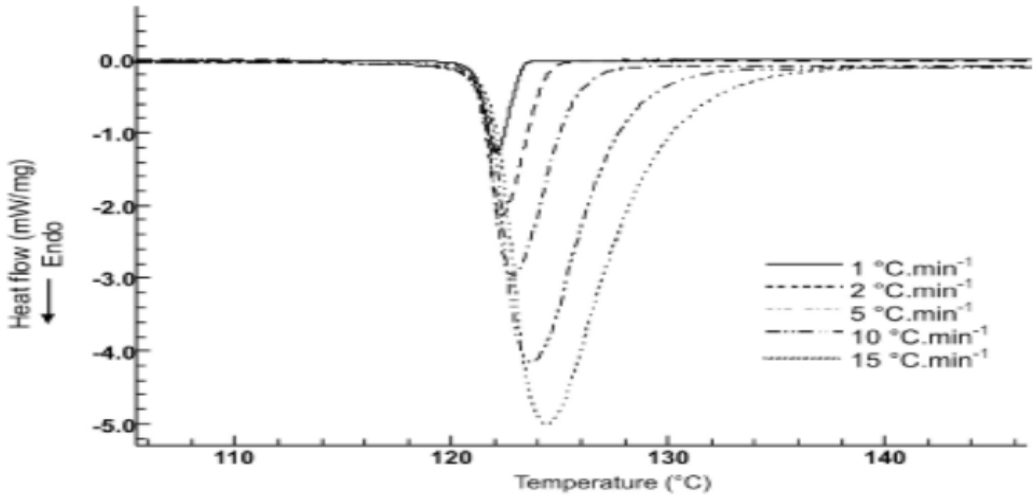


Figure 4:2: DSC curves of AZT at different heating rate;1,2,5,10,15°C(Araújo et al., 2010)

Figure 4:3 shows the calorimetric result using the dynamic mode on the DSC. The test was carried out at different heating rates (0.5 K/min, 1K/min and 2K/min) and using two different sample sizes (Sample A= 13mg and Sample B= 22mg). From the result, it is noticeable that the sample size and heating rate affects the peak temperature (melting temperature). As the sample size and heating rate increases, the peak was moved towards a higher temperatures. For example, the melting temperature of Sample B at heating rate of 2K/min was more than that of Sample A, at the same heating rate. This effect was as a result of an increase in thermal gradient in the sample.

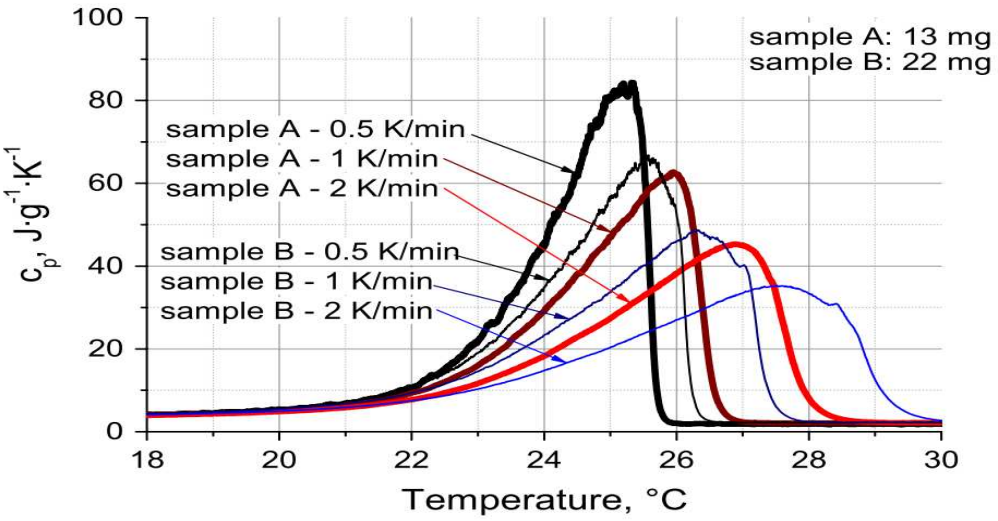


Figure 4:3: Dynamic mode DSC measurement at different heating rates and sample size. (Günther et al., 2009)

Another challenge faced using the DSC is that the temperature of the sensor was measured, not the sample. Due to the nature of PCM, sample temperature can be overestimated. PCMs are known to possess higher thermal storage capacity and in view of this, the amount of heat absorbed per volume is high Günther et al. (2009).

Calorimetry test using the DSC is carried out using either the dynamic mode or isothermal step mode. Günther et al. (2009) mentioned that the dynamic mode is not ideal to determine the enthalpy of PCMs, and proposed that the isothermal step mode be used since it offers better precision. All measurement carried out on the DSC for the aforementioned PCMs were carried out using the isothermal step mode.

Small sample geometry, low heating and cooling rates are recommended to minimise the thermal gradient during calorimetric measurement. Carrying out DSC measurement at low heating and cooling rates increases the duration in which the measurement is done. Using the step method reduces the duration of test on the DSC. Günther et al. (2005) stated that using the step method to test the PCMs offers the same precision for all sample materials without long duration of testing. Based on comparison of result obtained from the DSC for the four different PCM with literature, it can be deduced that the type of method, type of calorimetry device (DSC, T-history and air flow apparatus) affect the outcome of the result. When compared to other methods, the DSC can only measure a few milligrams of PCM for calorimetric testing. For example, Rathgeber et al. (2014b) carried out calorimetric test on a PCM; Pinacone hexahydrate using two different calorimetric test; DSC and T-history. The

result concluded that subcooling is highly reduced when measuring larger samples. Using the DSC resulted in huge subcooling due to the limitation of the sample size(small) permitted for testing, while larger sample size are possible using the T-history device.

The thermal behaviour of the PCM in application where tons of PCMs are required differs in reality to the result obtained by measuring only a small amount of PCM using the DSC. Effect such as crystal growth, phase separation need to be studied in sample of similar size to the application it is to be used. The T-history method was recommended based on the ability to measure large sample size and better precision. Günther et al. (2009).

### 4.3.2 Hot disk thermal conductivity instrument.

The Hot disk instrument measures the thermal conductivity of solid materials at ambient condition using a transient method. Thermal conductivity test was carried out on four different phase change materials (PCMs) using the hot disk TPS 2500S. TPS means transient plane source. This thermal constant analyser from hot Disk instrument is used to measure thermos-physical properties of solid, liquids, paste and powders. This instrument is also capable of testing the thermal diffusivity and specific heat capacity of various samples. The TPS 2500 meets ISO standard: ISO/DIS 22007-2.2. Figure 4:4 and Table 4:1 shows the image and specification of the hot disk device respectively.

Figure 4:4: Hot disk Transient Plane Source TPS 2500S.

Table 4:1: Table showing the specification of the TPS 2500.

| **Thermal Conductivity** | **0.005 to 500 (W/m K)** |
|---|---|
| **Thermal Diffusivity** | 0.1 to 100($mm^2/s$) |
| **Specific heat Capacity** | up to 5$MJ/m^3K$ |
| **Measurement time** | 1 to 1280 seconds |
| **Reproducibility** | Typically, better than 1% |
| **Accuracy** | Better than 5% Standard; ambient (room temperature only) |
| **Smallest sample dimensions** | 0.5mm high,2mm diameter |
| **Sensors types available** | Kapton and Mica |
| **Sensor design** | 5465 (3.189mm radius) |

The TPS sensor acts as a resistance thermometer for recording the time dependent temperature increase and also as a heat generating source; to increase the temperature of the sample. It operates by having a constant current pass through the probe of the TPS sensor, which generates a resistance hence, increases the temperature of the spiral probe. The probe also serves as a temperature sensor Manzello S (2008). The TPS probe consists of a sensor as shown on Figure 4:5. TPS sensor is made of nickel metal

double spiral with designed dimensions of the width, radii and number of windings. The nickel metal double spiral is encapsulated by either kapton or mica, which helps to increase the sensor mechanical strength, protect its shape and ensure it's electrically insulated. Kapton has a temperature range of -160°C to 300°C, while mica has an upper limit of 1000°C. For this measurement, kapton insulated TPS sensor was used with a radius of 3.189 mm. Figure 4:6 shows the setup of the hot disk sample holder with TPS sensor and cover.

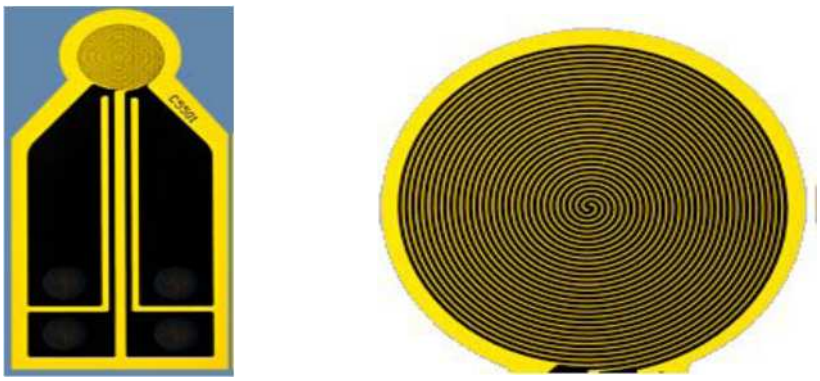

Figure 4:5: Typical image of the TPS sensor. KTH (2010).

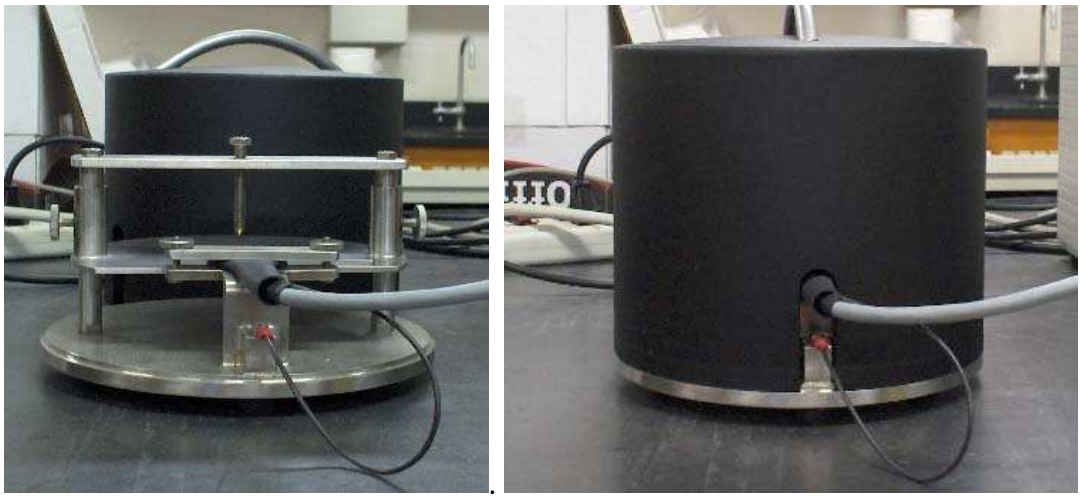

Figure 4:6: Hot disk sample holder with TPS sensor and cover.

### 4.4 Preparation of phase change material for measurement

The thermal properties of RT 52, RT 58, Climsel C58 and magnesium nitrate hexahydrate and ammonium nitrate are characterised at room temperature. Thermal conductivity was determined at room temperature using the hot disk. Preparation of the sample for the thermal conductivity test was done by melting the paraffin wax; RT 52, RT 58 and Eutectic PCM; 61.5% magnesium nitrate hexahydrate

($Mg(NO_3)_2.6H_2O$) and 38.5% ammonium nitrate ($NH_4NO_3$) in aluminium moulds and silicon mould respectively. The aluminium mould has a truncated cone shape, while the silicon mould is a round-shaped moulds. The moulds provide a contact surface that is flat for the measurement to be successful. Each PCM was heated in the oven to 59°C; the temperature at which the solid PCM does change to its liquid phase. The phase change temperature of each PCM was considered to set the temperature within the oven. The mould was allowed to cool before proceeding with test on the hot disk, TPS 2500S. The PCMs were allowed to cool for over 24 hours. This is to ensure the PCM are at room temperature and to prevent inaccuracy in data obtained from the hot disk measurement. For the Climsel C58, lumps with flat surface were used to measure its thermal conductivity. This is due to the nature of Climsel C58, which is a difficult sample to work with. The eutectic mix of 61.5% magnesium nitrate hexahydrate ($Mg(NO_3)_2.6H_2O$) and 38.5% ammonium nitrate ($NH_4NO_3$) was prepared by mixing the aforementioned chemical compounds at stated weigh percentage. Each chemical compound has a melting point of 89°C and 169.6°C respectively. Mixing each chemical compound in the stated proportion produces a congruent melt within a temperature range of 50-60°C. The result is a PCM produced in the laboratory.

To mount the sample PCM for measurement, the TPS sensor is sandwiched or placed between two layers of the samples as shown in Figure 4:7. The arrangement of the PCM (RT58) sample on the hot disk sample holder before the test is shown in Figure 4:8. The same arrangement applies to the other three phase change materials. It is essential that the cover for the hot disk sample holder unit is placed on the sample and sensor before commencing the test. Sufficient time interval between each experiment is important to allow the sample to be isothermal before the next measurement.

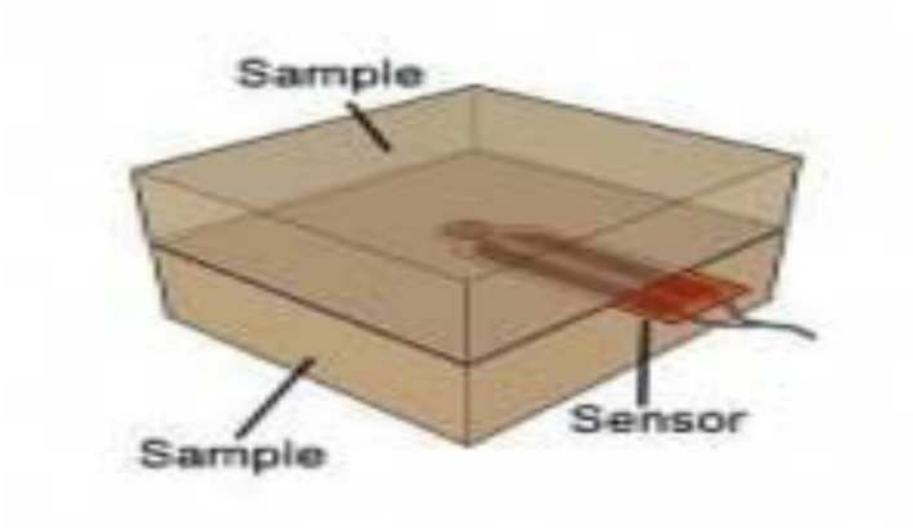


Figure 4:7: Schematic arrangement of sample on hot disk TPS 2500. KTH (2010).


Figure 4:8: Arrangement of PCM before measurement.

## 4.5 Summary

This chapter looked at the devices used to determine the thermal properties of the various PCMs used for this research, the hot disk and Differential scanning calorimeter (DSC) are the devices used to test each PCM. The method used to carry out the test is discussed in details. The precautions taken to obtain good data are discussed as well in this chapter.

Four different PCMs (two organic and two inorganic PCM) were tested, they have a phase change temperature range between 50 to 60°C. In the laboratory, a eutectic mix of magnesium nitrate hexahydrate ($Mg(NO_3)_2.6H_2O$) and ammonium nitrate ($NH_4NO_3$) was prepared successfully and its thermal behaviour tested alongside the other PCMs procured from manufacturers. Chapter 5 gives a detailed result of the test carried out on each PCM.

# 5 Thermal material analysis result and discussions

## 5.1 Experimental investigation of thermophysical results.

This chapter presents results from the thermal measurement done using the DSC and hot disk to measure the thermal properties of four different PCMs. Two organic PCMs (RT 52 and RT 58), which are paraffins made up of carbon and hydrogen atoms only ($C_{no}H_{2no+2}$) and two inorganic PCMs (Eutectic mix; 61.5% ($Mg(NO_3)_2.6H_2O$) & 38.5% ($NH_4NO_3$) produced in the laboratory and Climsel C58). The results were compared to data obtainable from manufacturer and other researchers.

### 5.1.1 Thermal conductivity result

From the result of the test on the hot disk, RT 58 and RT52 had the lowest thermal conductivity in the range of 0.22- 0.24W/m K and 0.22-0.23 W/mK respectively, while the eutectic mix has the highest values of thermal conductivity 0.56 - 0.73 W/m K. Climsel C58 value of thermal conductivity ranges from 0.51 to 0.55W/m K. The average of the values of thermal conductivity was estimated has shown in Table 5:1, for measurements taken for each phase change material.

The software of the hot disk thermal constant analyser also provides checks to indicate if data obtained from the measurement can be accepted or not. Total characteristic time ($T_{ct}$) should be in the region of 0.3 to 1.0. Appendix A shows the procedure in which the PCM's thermal conductivity was carried out using the hot disk . Equation 5.1 describes the relationship between the thermal diffusivity, time and radius of the sensor. Also the total temperature increase should be less than 2°C. Total characteristic time is dimensionless.

$$T_{ct} = \frac{\alpha t}{r_{TPS}^2} \qquad 5.1$$

Figure 5:1 shows a bar chart comparing the thermal conductivity of the PCMs. It shows the inorganic PCM have higher thermal conductivity than the organic PCM. The eutectic mix possesses the highest thermal conductivity of the PCMs tested. The thermal conductivity of the inorganic PCMs is almost three times the organic PCM

(RT 52 and RT 58). As discussed in Chapter three of this thesis, inorganic PCM possesses high thermal conductivity when compared to inorganic PCM, however its disadvantages in terms of toxicity, subcooling issues etc. hampers its use in latent heat thermal storage applications. Comparing the values of thermal conductivity from the hot disk TPS 2500S measurement, it is within the range specified in literatures and manufacturers data as shown on Table 5:2.

Table 5:1: Results from the Hot disk TPS 2500S.

| | **Thermal Conductivity(W/mK)** | **Temperature increase(K)** | **Total to characteristic time** |
|---|---|---|---|
| **PCM: Eutectic mix** | | | |
| **1** | 0.56 | 1.98 | 1.47 |
| **2** | 0.66 | 1.13 | 0.35 |
| **3** | 0.73 | 1.93 | 0.90 |
| **Average** | 0.65 | | |
| | | | |
| **PCM: Climsel C58** | Thermal Conductivity (W/m K) | Temperature increase(K) | Total to characteristic time |
| **1** | 0.55 | 1.34 | 0.64 |
| **2** | 0.54 | 2.34 | 0.48 |
| **3** | 0.51 | 2.31 | 0.35 |
| **Average** | 0.54 | | |
| | | | |
| **PCM: RT58** | Thermal Conductivity (W/m K) | Temperature increase(K) | Total to characteristic time |
| **1** | 0.22 | 2.00 | 1.31 |
| **2** | 0.23 | 1.95 | 0.78 |
| **3** | 0.24 | 1.83 | 0.80 |
| **Average** | 0.23 | | |

| PCM: RT52 | Thermal Conductivity (W/m K) | Temperature increase(K) | Total to characteristic time |
|---|---|---|---|
| **1** | 0.23 | 1.88 | 1.22 |
| **2** | 0.22 | 1.72 | 0.99 |
| **3** | 0.22 | 1.92 | 1.80 |
| **Average** | 0.22 | | |

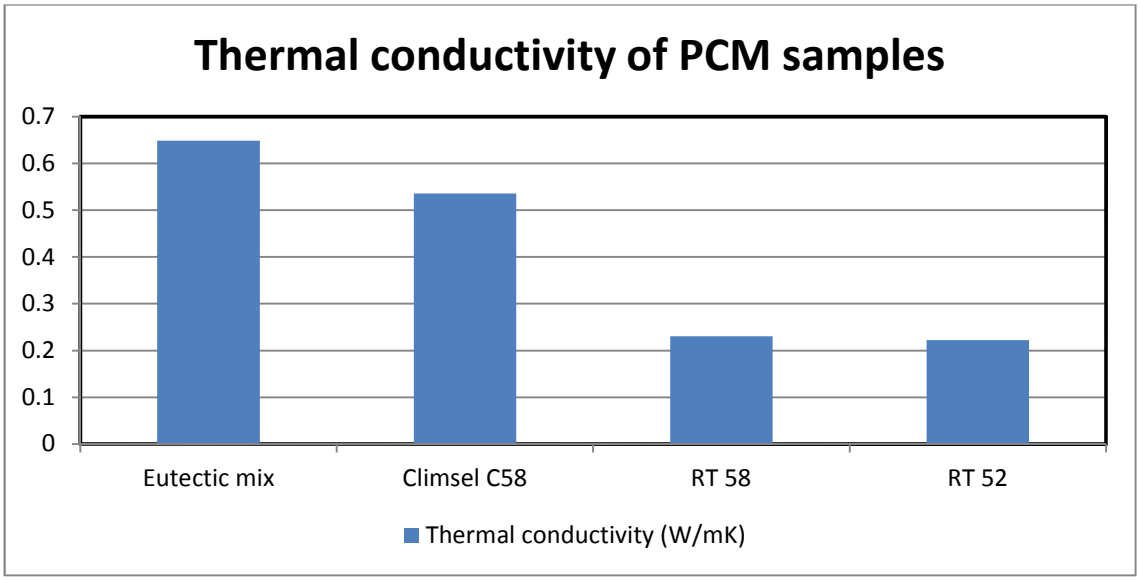


Figure 5:1: Thermal conductivity of the PCMs.

Table 5:2: Comparing hot disk measurement to values from other literatures.

| | **Thermal conductivity (W/mK)** | |
|---|---|---|
| **PCM** | Hot Disk Measurement | Literature values |
| **Eutectic mix** | 0.65 | 0.55. G.A.Lane (1980) |
| **Climsel C58** | 0.54 | 0.50 - 0.70 (Pär Johansson (2015), Climator (2016)) |
| **RT 52 and RT 58** | 0.22 and 0.23 | 0.20 Rubitherm (2013) |

Based on the result from the hot disk measurement, it shows good agreement with that from literature and manufacture's data, except for the eutectic mix which shows a difference of about 0.0962W/mK (approximately 15%).

### 5.1.2 Enthalpy.

The thermo-physical properties of the PCMs were analysed using a heat flux type DSC which uses Nitrogen as the purge gas. Each PCM was heated and cooled at a cooling rate of 2°C/min. Figure 5:2 (a-c) describes the specific heat input into the PCMs during heating and cooling phases for Climsel C58, eutectic mix and paraffin RT 58 respectively. Heat flow into the sample is indicated by positive values of the heat flux during the heating phase, phase change occurs, thus energy is stored by the PCM. Heat flow out of the sample is indicated by negative values of the heat flux during cooling process, thus energy is released by the PCM and the phase change is reversed.

Figure 5:2 a) and b) indicates that the inorganic PCMs (both Climsel C58 and eutectic mix) have a phase change occurring within a small temperature range. There is a difference the temperature at which heat is absorbed and released in the inorganic PCMs. The heat is released at temperatures less than they were absorbed. The eutectic mix has a difference of 6°C between the temperature at which heat was released and temperature at which heat is absorbed, while the Climsel C58 has a difference of 10°C. Based on this difference, there was need to check if the difference in the temperature at which heat was absorbed and released could be as a result of hysteresis or a problem of subcooling. For the RT 58, the heat is recovered at a similar temperature at which it was put in as shown in Figure 5:2c). RT 58 releases and absorbs heat put in over a wider range of temperatures when compared with the aforementioned inorganic PCMs.

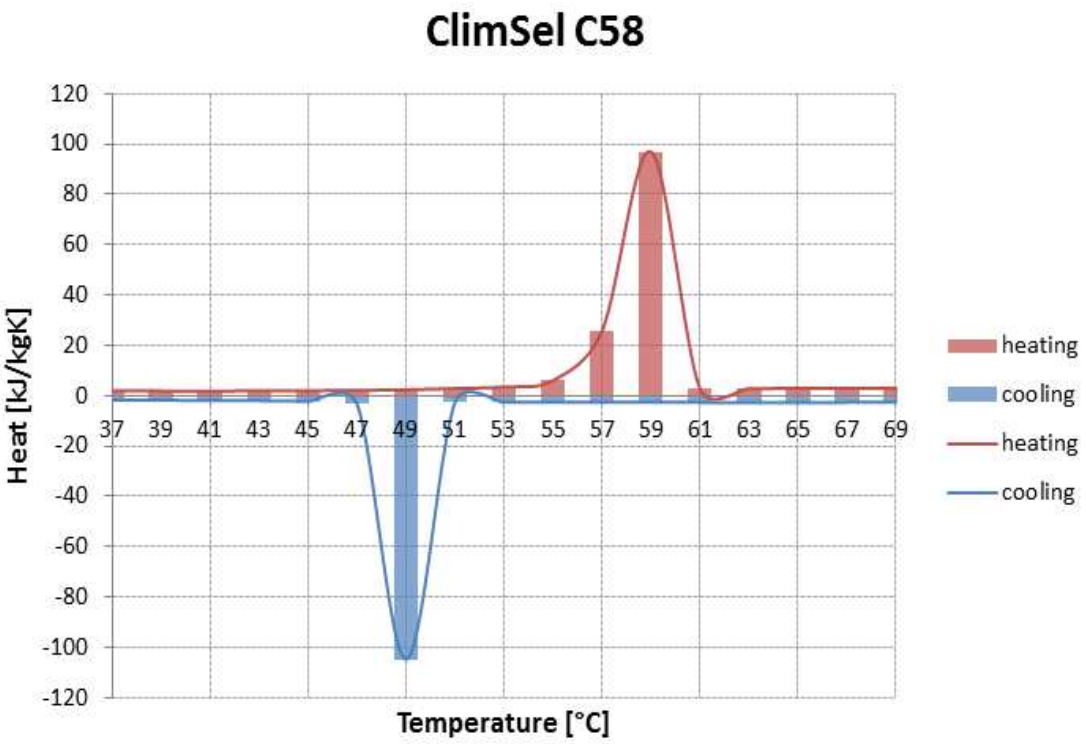


**(a) Climsel C-58**

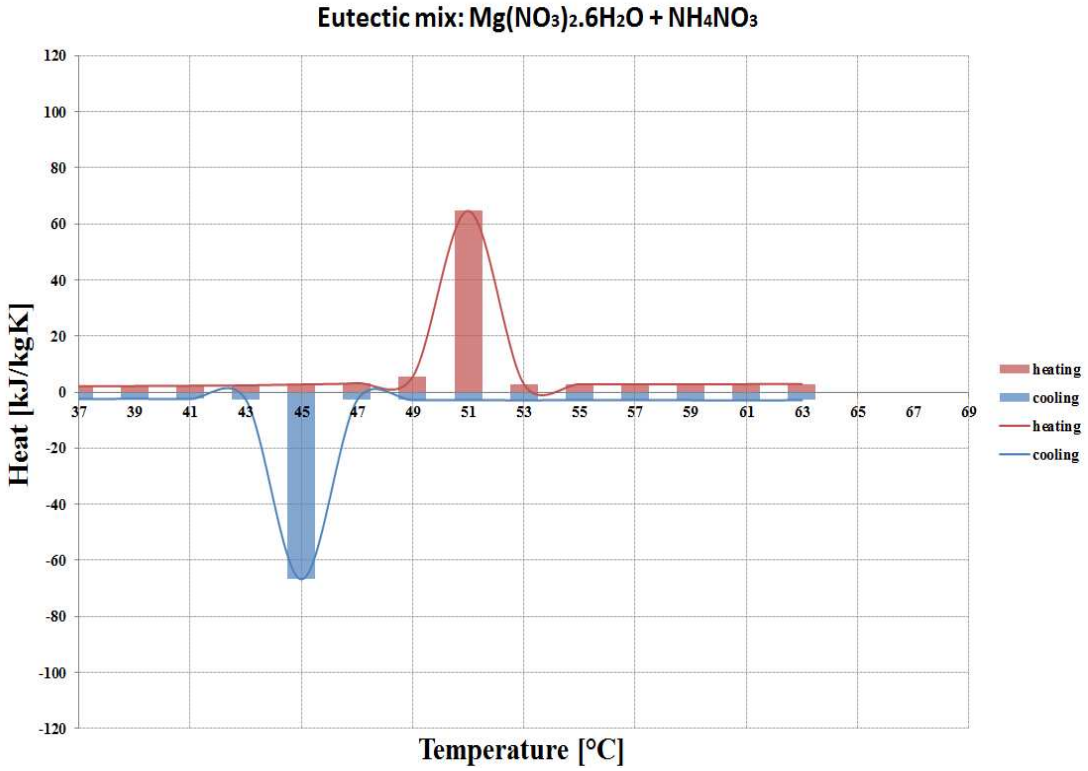


**(b) Eutectic Mix**

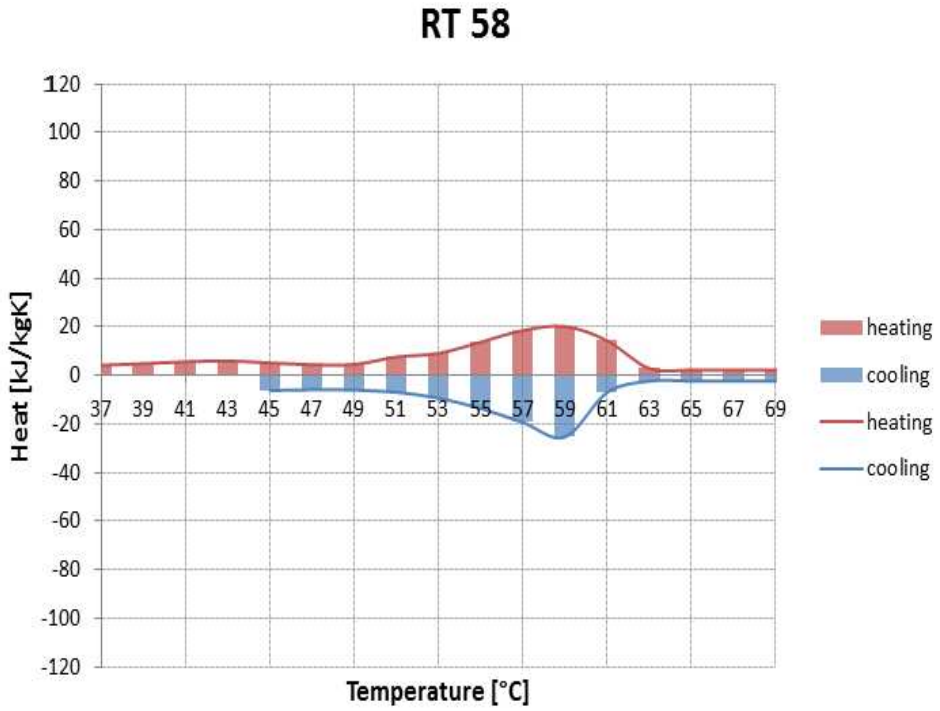


**(c) RT 58**

Figure 5:2: Specific heat input to sample PCMs.

Figure 5:3(a-d) shows the change in enthalpy in the PCMs during heating and cooling. It shows a cumulative curve of the heat fluxes in Climsel C58, eutectic mix, RT 58 and RT 52 respectively. Figure 5:3a) shows the change in enthalpy for Climsel C58 and it is observed that not all the heat put into melting the PCM was recovered. Though Climsel C58 shows promising thermal properties, it was difficult getting good results from the DSC. The tests of Climsel C58 using the DSC and hot disk provided some challenges due to the nature of the sample. For example, when the sample of C58 was prepared to be moulded, the sample did not melt in the oven, despite setting the oven to 60°C, which was above the PCM's melting point (52°C). Though the sample came in a sealed container, the additives of the PCM might have been affected over time as it was stored in a sealed container (loss of water from the sample). Another reason for the behaviour of this PCM could be as a result of some undisclosed additive present in the sample as delivered from Climator. Climsel C58 shows promising properties when compared to the other three PCMs, however, measures need to be taken to reduce the large subcooling required to initiate the phase change. From the specific heat capacity-temperature plot for Climsel C58 , it shows that there is a significant difference between the temperature at which heat is released and absorbed. The heat is released by these samples at temperatures below that at which the heat is absorbed.

For Climsel C58, the heat is released 10°C below the temperature at which it was absorbed. The DSC results show that not all the heat put into melting the Climsel C58 sample was recovered. During the calorimetric test, the sample temperature was taken above the optimum temperature specified by the manufacture. This affected the chemical composition of the material and affected its ability to return to the original state. During preparation of samples for the thermal conductivity test, there was difficulty in melting the sample to form the mould required for the test on the hot disk. The PCM shows promising properties but more work needs to be carried out in developing an effective way of reducing or minimise subcooling.

The behaviour of the eutectic mix made in the laboratory was different. It exhibits a sharp phase change, despite the presence of hysteresis in the heating and cooling curves. The material was selected based on its phase change temperature of 52°C, however from the test it shows heat was recovered at 44°C. This would make it unsuitable for the application intended. Figure 5:3c) shows the enthalpy change in the RT 58, it can be seen there is little hysteresis and there is no noticeable subcooling required to initiate phase change. From the low value of specific heat flux as observed from Figure 5:3c), the energy stored (140 kJ/kg) over the region of phase change (54-62°C) is similar to the eutectic mix. Difference between the charging and discharging temperatures exhibited by both salt hydrates could cause a significant problem running a thermal store, RT 58 does not exhibit such a problem; however, it does not have a sharp phase transition compared to the salt hydrates and has a low thermal conductivity (0.23 W/m K). For the RT 52, described in Figure 5:3 (d), it shows the energy stored (153 kJ/kg) over the region of phase change (51-55°C). The result shows that not all the heat was recovered as the PCM solidified. This can be attributed to hysteresis. However, the result obtained is comparable to manufacturer's data.

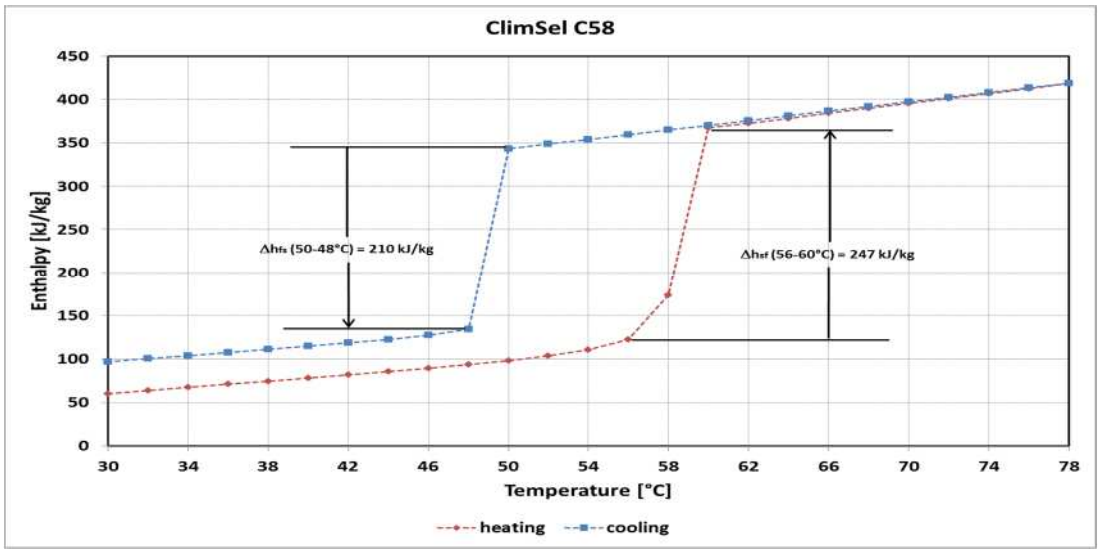
ClimSel C58
Enthalpy [kJ/kg]
Temperature [°C]
Δhfs (50-48°C) = 210 kJ/kg
Δhsf (56-60°C) = 247 kJ/kg
heating
cooling

**a)**

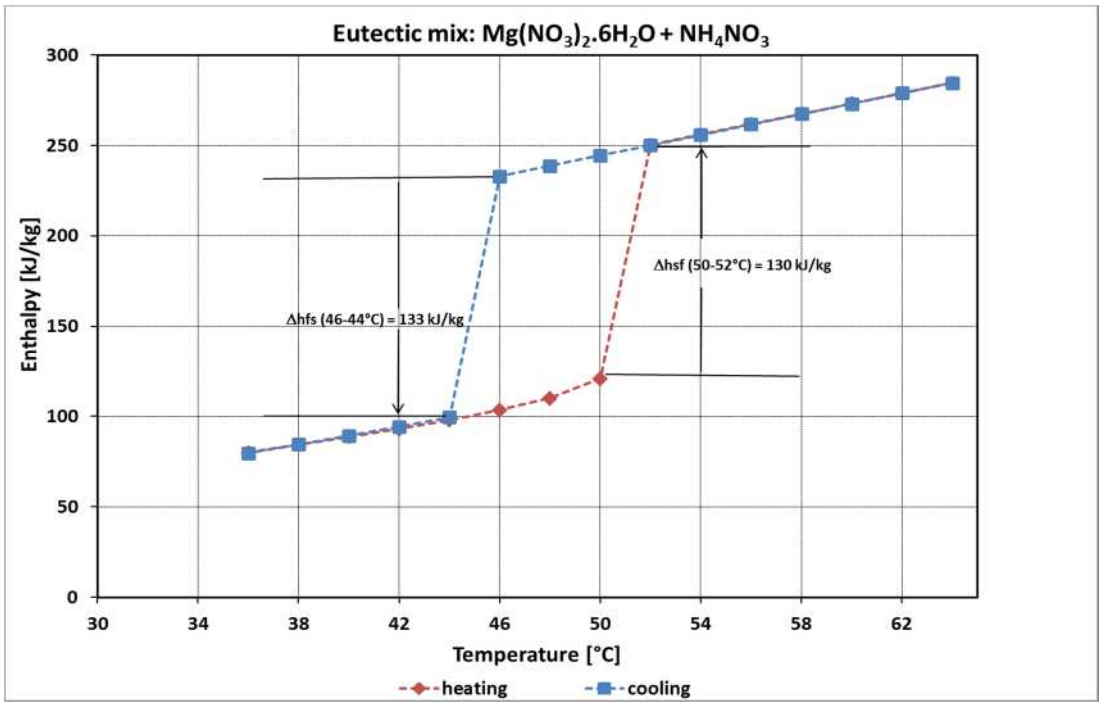
Eutectic mix: Mg(NO3)2.6H2O + NH4NO3
Enthalpy [kJ/kg]
Temperature [°C]
Δhfs (46-44°C) = 133 kJ/kg
Δhsf (50-52°C) = 130 kJ/kg
heating
cooling

**b)**

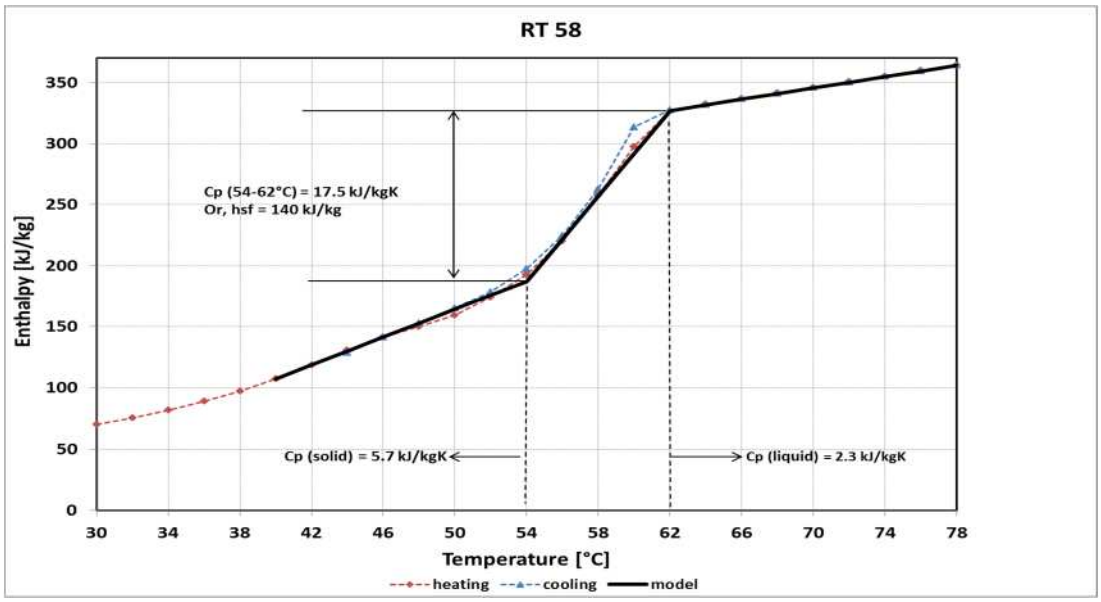


**c)**

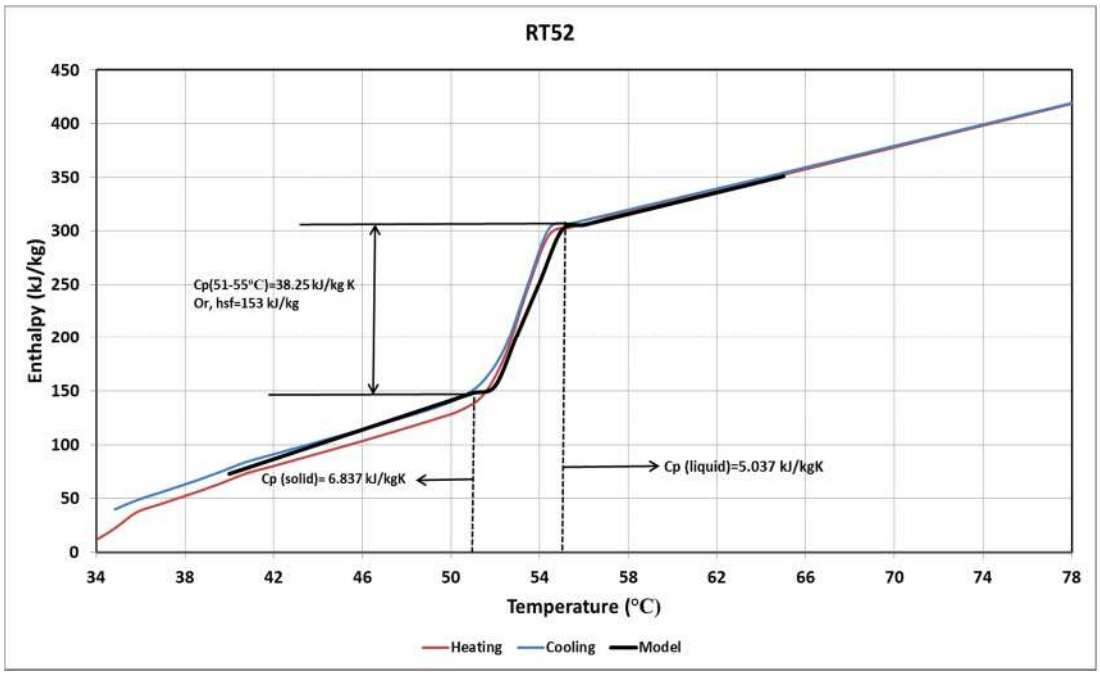


**d)**

Figure 5:3: Enthalphy change in the PCMs.

Based on the result from the hot disk and DSC measurements, Table 5:3 shows an overview of the results. It shows the eutectic mix has the highest thermal conductivty,while RT 52 and RT 58 have the lowest. Also, Climsel C58 has the highest enthalphy change within its phase change temperature.

Table 5:3: Properties of sample PCM.

| Material Properties | Eutectic mix | Climsel C58 | RT 52 | RT 58 |
|---|---|---|---|---|
| **Phase change temperature (°C)** | 44 – 52 | 48-60 | 51-55 | 54-62 |
| **Enthalpy (kJ/kg)** | 150 | 240 | 153 | 140 |
| **Thermal conductivity (W/mK)** | 0.65 | 0.54 | 0.22 | 0.23 |

In this research, it was observed that the paraffin and the eutectic mix behaved differently during the thermophysical test of the PCM using the DSC as described in Figure 5:3, which shows the enthalpy-temperature curve for both PCM; often times, researchers claim it is hysteresis that occur as the PCM is subjected to the process of charging and discharging on the DSC, where the amount of heat absorbed during change of phase differs from the heat recovery process, while others claim it is subcooling effect that takes place in the PCM.

It is difficult to establish whether the behaviour of the eutectic mix is actually sub cooling or hysteresis (See Figure 3:3b). Subcooling would hamper the performance of the thermal store, because it delays the commencement of solidification in the PCM. Hence, the reason why the organic PCMs (RT 52 and RT 58) are used for the experiments and simulation of the thermal store in this research.

Table 5:4: Comparision of DSC result with literature (Latent heat).

| Latent heat (kJ/kg) | | | |
|---|---|---|---|
| **PCM** | **DSC Measurement** | **Literature values** | |
| **Eutectic mix** | 150 kJ/kg (44-52°C) | 126 kJ/kg<br>131 kJ/kg | Sharma et al. (2009)<br>Krane (2009) |
| **Climsel C58** | 240 kJ/kg (48-60°C) | 260 kJ/kg<br>260 kJ/kg(55-58°C) | Shin et al. (2017)<br>Climator (2017) |
| **RT 52** | 153 kJ/kg (51-55°C) | 167 kJ/kg<br>173kJ/kg | Rubitherm (2013)<br>Huang and Hewitt (2011) |
| **RT 58** | 140 kJ/kg (58-62°C) | 160 kJ/kg (50-65°C) | Rubitherm (2013) |

Table 5:4 compares the latent heat of the PCMs tested using the DSC in the laboratory with values from literature. Based on the DSC result, it shows good agreement with values from literature and manufacturers' data, except for the eutectic mix which gave a 14-19% difference. The difference in values of the latent heat can be attributed to the conditions in which the test were carried out by different researchers and manufacturers. The phase change temperature range and the type of device used to carry out the thermophysical properties of the PCM were different to those used in the literature. The majority of the calorimetric results presented in literature or by manufacturers do not have full details of the temperature range used to determine the enthalpy change , DSC method used or sample size etc. Rathgeber et al. (2014a) stated that it is difficult to compare calorimetric results of PCM from different laboratories due to deviations in purity of the samples and measuring accuracy. Results from T-history are mostly carried based on self-built instruments, thus difficult to compare result obtained from it with DSC results. Calorimetric test done on nine different samples by Rathgeber et al. (2014a) using both DSC and T-history method showed that measured melting temperatures agreed with literature and manufacturers.

## 5.2 Summary

From the DSC results, both inorganic PCMs, which are also salt hydrates, released their stored heat at temperatures below the temperature at which it was absorbed. This difference between the charging and discharging temperatures could cause a significant problem running a thermal store with these salt hydrates. RT 52 and RT 58 do not exhibit such a problem; however, paraffin does not have a sharp phase transition compared to the salt hydrates and has low thermal conductivity. Both organic PCMs are chosen based on the fact that they do not show any hysteresis and heat is stored and released at the same temperature. This makes them ideal PCM to use in the thermal store, since their behaviour is easier to control.

The results from the DSC and hot disk device were compared to manufacturer's data, and they show good agreement with the obtained results. Several researchers ((Antony Aroul Raj and Velraj (2011), Lin Qiu and Min Yan, 2012, Celador et al., 2013) considered the thermal conductivity of the solid and liquid phase of the PCM to be constant. To simplify the model for the PHE store, the thermal conductivity of the organic PCMs (RT 52 and RT 58) were assumed to be constant for both solid and liquid phase.

# 6 Experimental setup of Plate heat exchanger thermal store.

The experiments and simulation in this research involve two different types of heat exchangers, the plate heat exchanger and serpentine heat exchanger (based on a shell and tube concept). Chapter 6 highlights the experimental setup of the modular design using polypropylene sheet based on a plate heat exchanger as a thermal store; to study the behaviour of the chosen PCMs (RT 52 and RT 58) and the next chapter; chapter 7 deals with the experimental study of a modular design of a serpentine heat exchanger based on shell and tube concept. Based on the results from the hot disk and DSC measurement, the aforementioned PCMs are used for both experiments due to the advantages they possess over the inorganic PCM as discussed in the earlier chapter. The materials and apparatus used for this experiment are also discussed in detail in this chapter.

## 6.1 Material

### 6.1.1 Heat transfer fluid (HTF)

Water was used as the heat transfer fluid (HTF) due to its thermal properties. Water is cheap and readily available. It does exhibit excellent heat transfer properties.

The important properties are:

- Density
- Thermal conductivity
- Viscosity
- Specific heat capacity.
- Latent heat of fusion

The properties of water vary with temperature. It is essential to utilize the properties based on its temperature, thus all simulation and calculation involved in this research was based on the corresponding temperature with reference to the properties. In some research, water is used as a PCM. This means water could be used as a heat transfer fluid or phase change material. The reason why water is not often used as a PCM is due to its melting and freezing temperature despite the fact that it has a high latent heat of about 330kJ/kg. It is used in air conditioning systems but the temperature is slightly too low and causes condensation of water from the air.

### 6.1.2 Phase change material (PCM) properties

Based on the design of the thermal store, the operating range of the phase change material studied ranges from 44 to 58°C. The selection of a PCM was based on the PCM melting temperature, chosen at a temperature interval below the operating temperature of the application (heat pump). An interval less than 5°C has been proposed to prevent excessive degradation of heat within the system and reduction of efficiency Lane (1989). Organic PCMs, RT 58 and RT 52 and inorganic PCMs; Climsel C58 and eutectic mix of magnesium hexahydrate and ammonium nitrate were tested on the DSC and hot disk. The aforementioned PCMs have their phase change temperature within a suitable range for domestic heat pump applications. For the experiment and simulation of the thermal store for this research, RT 58 and RT 52 were used. Various thermal parameters were taken into consideration, which include:

- Latent heat
- Density
- Melting temperature range
- Specific heat capacity
- Thermal conductivity
- Enthalpy-Temperature relationship.

## 6.2 Apparatus

### 6.2.1 Water bath

The water bath (Polystat R6L) designed by Cole Parmer was used to pump the water at the required temperature to the thermal store. The bath is proportional-intergral - derivative (PID) controlled, it uses a programmable controller. It allows for a set point temperature to be set as it heats or cools. An image of the water bath is shown in Figure 6:1.


Figure 6:1: Hot water bath (Cole Palmer Polystat R6L).

The device possesses an ability to heat or cool the fluid,however the system does not provide cooling over the full range of temperatures. The cooling system commences for set points less than 35°C ColePalmer (2016). Thus a drain valve had to be provided to release hot fluid as cold water is poured into the bath to aid cooling. This is because experiments in this research were all above the set point temperature that allows for cooling. Table 6.1 shows the specification of the Polystat R6L hot water bath or circulating bath. More information on the bath is available in Appendix D.

Table 6:1: Specification of circulating Bath(Polystat R6L). ColePalmer (2016)

| **Technical Data** | |
|---|---|
| Bath volume | 6litres |
| Temperature range | -20 to 200 °C |
| Heating power | 1 kW |
| Cooling power @20 °C | 0.29 kW |
| Pump delivery | 15 l/min |
| Electrical requirement | 230VAC, 50Hz, 10 Amps. |
| Overall dimension | 0.25 x 0.55 x 0.4m |
| Refrigerant | R134A |

### 6.2.2 Data acquisition (DAQ)

Temperature data were logged using TC-08 Thermocouple data logger. This device has a USB interface. It is an eight (8) channel temperature logger; as shown in Figure 6.2.

Key attributes of the TC08

- Measure from 1 to 8 thermocouples
- Measures from -270 to +1820 °C
- Automatic cold junction compensation
- High resolution- 20 bits
- Temperature accuracy- Sum of ±0.2% of reading and ±0.5 °C
- Fast sampling rate — up to 10 measurements per second
- USB interface

Figure 6:2: Pico temperature logger TC-08. Picotech (2014).

Appendix B has a description of the specification of the USB TC-08 used for the plate heat exchanger experiment to record and save temeprature records.

### 6.2.3 Thermocouples

Thermocouples were used for measuring the temperatures. K-type thermocouples were used for the experiment to take temperature at different locations. They are connected to the temperature logger; TC-08. Two types of type K thermocouples were used, and they are shown in Figure 6:3.

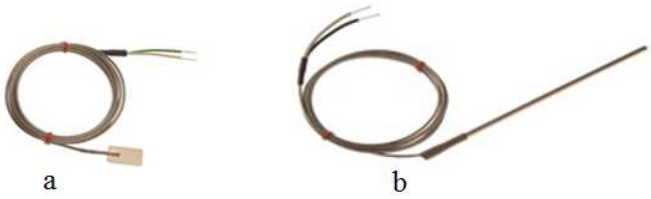


(a)Type K Stainless Steel Shim Labfacility leaf thermocouple

(b)Type K Probe Thermocouple; 1mm diameter.

Figure 6:3: Different types of K type thermocouples used.

Appendix C shows the locations where the Type K Stainless Steel Shim Labfacility leaf and Type K Probe thermocouple were placed on the PP (polypropylene) sheet to monitor the temperature of the PCM , HTF(heat transfer fluid) and room temperature during the experiment.

### 6.2.4 Polypropylene/Acrylic

The polypropylene (PP) sheet used was procured from Twinplast Company. The sheet has a layout of channels that could be used as a heat exchanger for this chosen application; thermal energy storage. Figure 6:4 shows the channels on the PP sheet. Efforts were made to weld the PP sheet, but it was not possible to find anyone capable of welding it. There were concerns about the thickness of the sheet being too thin to weld; however, it can be bonded using adhesives. Several adhesives were tested, to confirm which was well suited to bond the sheet to the PVC pipe required for inlet and outlet flow of water on the rig. The following adhesives were used in the final design.

1. DP 8005, procured from 3M Products
2. Ultimate instant grab: this is used on the inner part of the wood in contact with the hot surface.
3. All in one sealant, adhesive and filler MS polymer. Used on the exterior part of the wood.
4. Araldite.

Further experiment involved the replacement of the wooden frame with PVC strips of 30cm width. DP 8005 was used to bond the PVC strips on to the polypropylene surface. It was discovered that this bonding was better than using wood strips.

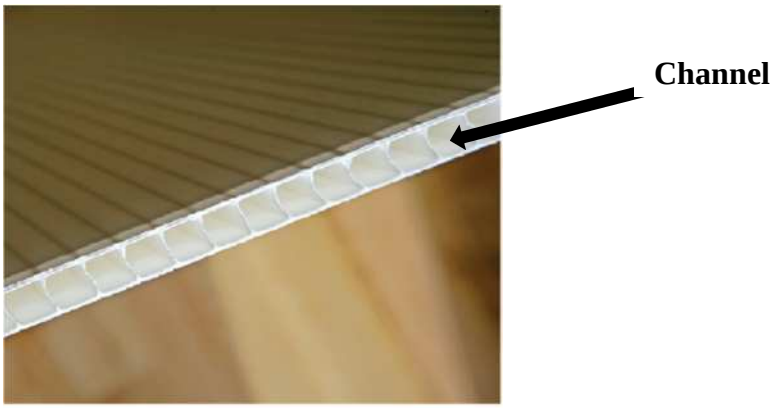


Figure 6:4: Polypropylene sheet with channels.

### 6.2.5 Electric wax heater:

The wax heater was used to melt the solid PCM on to the thermal store. It has a temperature range up to 200°C. It has a control switch which is used to set the desired temperature to heat the material or sample. This device is only used for heating; it is not designed for cooling the material. Figure 6:5 shows the electric wax heater unit and an image of paraffin wax melting in it.

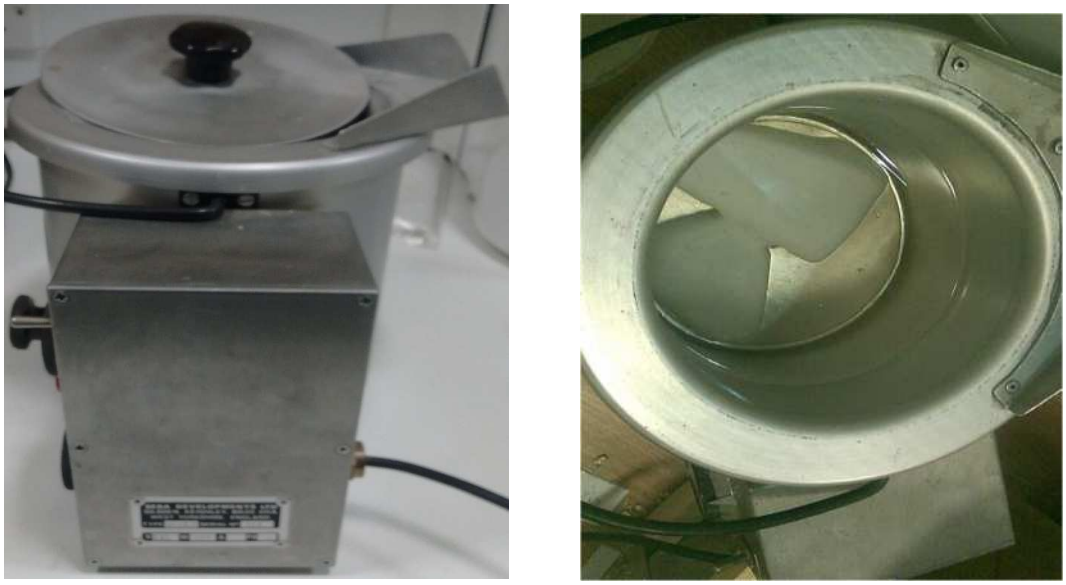

Figure 6:5: Electric wax heater.

### 6.2.6 Coriolis mass flow meter

The mass flow rate of the fluid flow for the experiment was monitored by a Coriolis flow meter manufactured by Emerson (Micro Motion Inc.). The flow meter can measure fluid flow up to a temperature of 200°C. The Coriolis mass flow meter has a flow range of 2g/s to 100g/s. It comprises of a flow transmitter and mass flow sensor; shown in Figure 6.6.

(a)Flow transmitter (b) Mass flow sensor

Figure 6:6: Coriolis mass flow meter. Emerson (2017)

The flow meter operates based on the “Coriolis principle” where the change in frequency or amplitude as a result of the fluid flowing through the vibrating tubes is produces a linear flow signal. When there is no fluid flow, the tubes within the unit oscillate at the same frequency. However as flow passes through the unit, there is a phase difference in the frequency. The signal from the sensors mounted on the tube at the inlet, middle and outlet of the unit with the aid of the transmitter gives the mass flow of the fluid travelling through it Emerson (2017). This device can also determine the density of the fluid passing through it. Coriolis meter accuracies for mass flow is ± 0.10% of the flow rate. Emerson (2018)

## 6.3 Statistical analysis

The mean, standard deviation and standard deviation mean of the measurement from the thermocouples, Platinum RTD and coriolis mass flow meter were estimated. Equation 6.1 to Equation 6.3 shows the relationship between the mean, standard deviation and standard deviation mean. Table 6:2 show the results of the calculation for each measurement.

Mean,

$$\overline{X} = \frac{\sum_{i=1}^{n} x_i}{n} \qquad 6.1$$

Standard deviation,

$$\sigma = \sqrt{\left( \frac{1}{n-1} \sum_{i=1}^{n} \left( x_i - \overline{X} \right)^2 \right)} \qquad 6.2$$

Standard deviation mean,

$$\sigma_m = \frac{\sigma}{\sqrt{n}} \qquad 6.3$$

Table 6:2: Statistiscal parameters of measured instrument.

| **Parameter** | **Thermocouples (°C)** | **RTD (°C)** | **Flow meter (g/s)** |
|---|---|---|---|
| **Standard deviation** | **0.795** | **0.02** | **0.5** |
| **Variance** | **0.632** | **0.0004** | **0.25** |
| **Standard deviation mean** | **0.459** | **0.0133** | **0.177** |

From Table 6:2, the uncertainty for the thermocouples, RTD and flow meter are determined. The deviation amongst the K-type thermocouples used for the plate heat exchanger experiment was less than 1°C. K-type thermocouples were used with a Pico logger data logger. The uncertainty in the thermocouples used for the plate heat exchanger (PHE) are determined as ±0.795°C. The uncertainty of the resistance temperature detector (RTD) is 0.02°C. The uncertainty in the flowmeter was determined by taking the standard deviation of the flow. The uncertainty of the coriolis flow meter is ±0.5 g/s.

## 6.4 Experimental setup plate heat exchanger (Polypropylene sheet)

### 6.4.1 Charging

The assembly of the rig using the polypropylene (PP) sheet based on plate heat exchanger concept consists of an acrylonitrile butadiene styrene (ABS) pipe at each end of the PP sheet and a rectangular frame to act as containment for the PCM. The rectangular frame was changed from wood to polyvinyl chloride (PVC), when the adhesion between the wooden frame and PP sheet failed. The PVC frame was bonded to the PP sheet with 3M Scotch-weld DP 8005(Acrylic structural adhesive). The internal part of the frame was sealed with silicone sealant to improve the seal and eliminate little holes that could be present in the DP8005. High temperature adhesive (Polycarbonate) was applied, due to close contact with the PCM during charging and to prevent any reaction that could occur. The exterior part of the frame was sealed with a sealant (instant Grab). Before bonding the frame to the PP sheet and pouring in the PCM, proper levelling of frame and PP sheet was done. Figure 6:8 shows the layout of where the adhesives are applied to the PP sheet for bonding.

For the flow of HTF in and out of the rig, an ABS pipe was used and bonded to the PP sheet using solvent weld. Prior to bonding the ABS pipe to the PP sheet, strips of ABS were bonded to the PP sheet using super glue, this is to provide a rigid layer for the ABS pipe to be bonded onto the PP sheet . Two pipes of same diameter were fixed at each end of the PP sheet. Each pipe had a slot to accommodate the channels of the PP sheet before bonding the sheet, a picture of this assembly is shown in Figure 6:7.

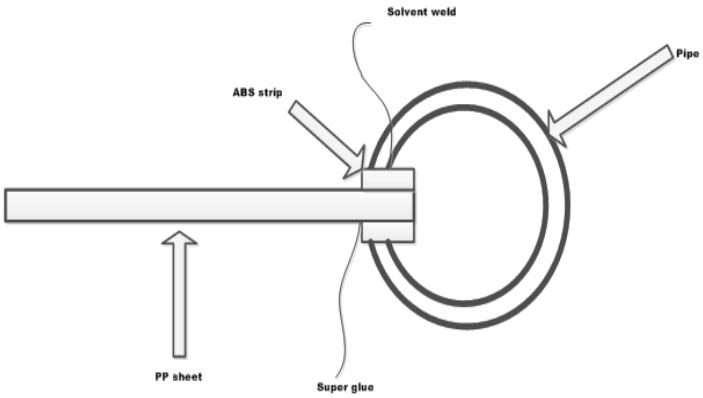


Figure 6:7: Imaging showing how the pipe is bonded to PP sheet.

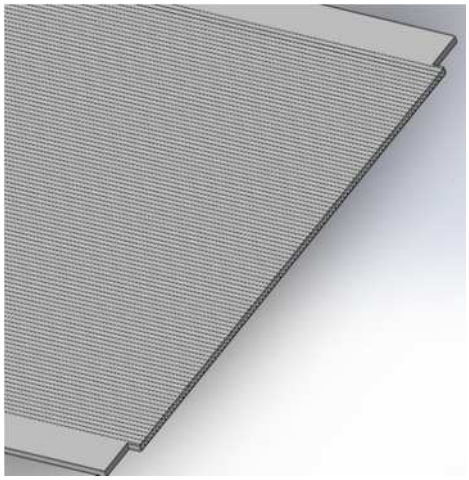

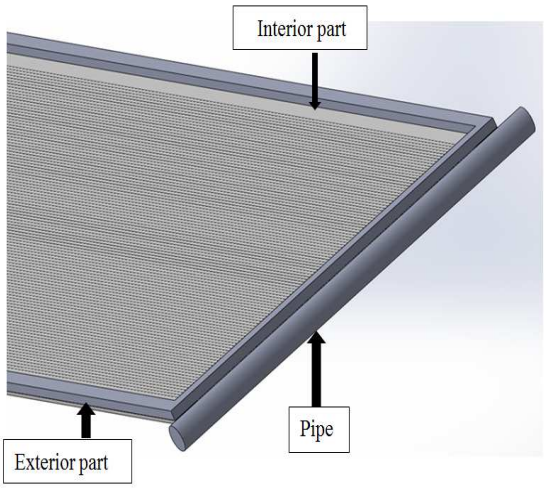

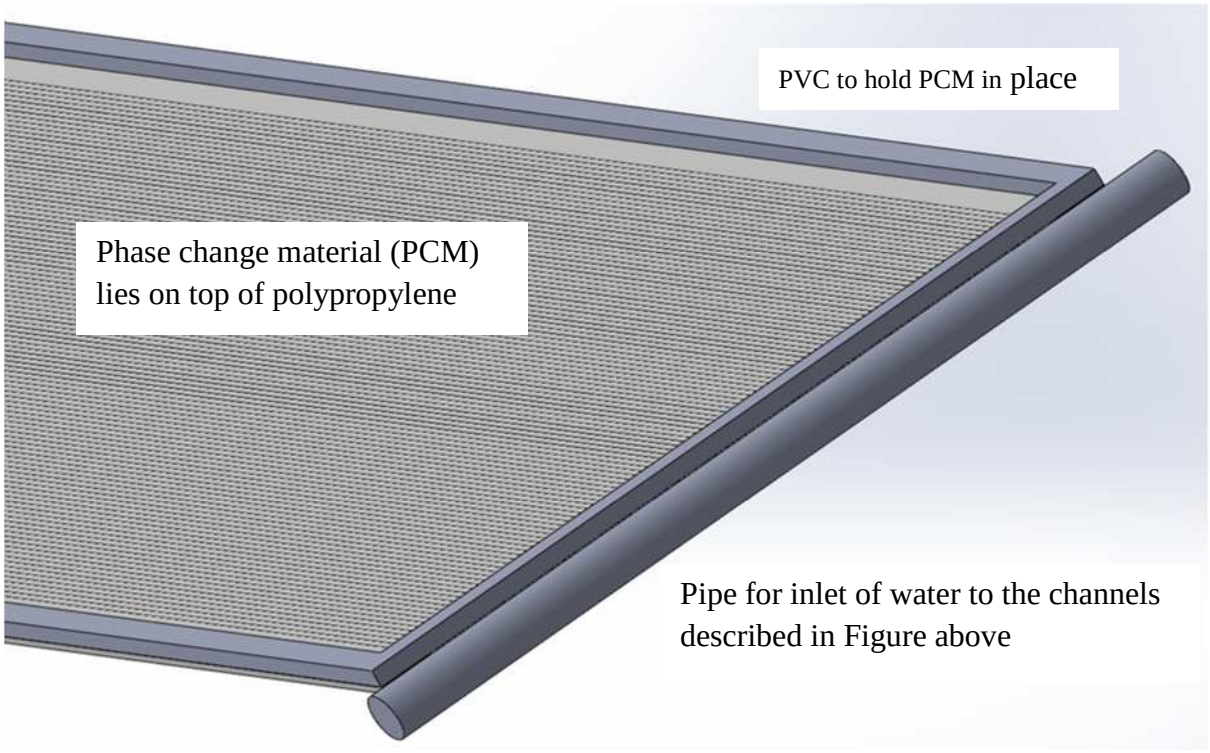


Figure 6:8: Drawing of the assembly of the polypropylene sheet.

The set up for the charging process involves the arrangement of the pipe lines from the water bath to the polypropylene sheet. The initial arrangement of the rig involved a connection to the inlet and outlet of the polypropylene sheet from the hot water bath. At the commencement of the charging process, it was observed that the desired HTF temperature at the inlet was not reached, but water flowed through the PP sheet channel causing the PCM to be heated before the desired inlet temperature is attained. Thus, modification was made to the flow from the circulating water bath to the rig by fixing a three-way valve on the inlet bath side. This facilitates recirculation of water from the bath inlet to its outlet until the desired HTF temperature is achieved. Upon achieving this temperature, the position of the handle on the three-way valve is changed, thus directing water to the inlet pipe of the polypropylene sheet and then through the channels to the entire length of the sheet. The water flows to the outlet pipe mounted on the outlet end of the rig and back to the bath. Figure 6:9 shows the layout, where the 3-way valve is mounted. The water flow through the sheet is in a Z-arrangement, in order to give a uniform flow across the sheet.

The setup of the experimental rig as shown in Figure 6:9 and Figure 6:10 consists of a horizontally positioned flat sheet made up of 4 mm thick polypropylene with a channel width and height of 3.6 mm and 3.3 mm respectively. From literature,

researchers designed plate heat exchanger using metals, with a plate spacing of 3mm (Frazzica et al.(2017)), 0.5 to 4mm (Shatikian et al(2005)) to promote effective heat transfer. This research made use of polymer material, polypropylene to design and build a PCM thermal store using a plate spacing of 4mm. Appendix K shows the design calculations done prior to construction of the PHE store. The dimension of the material is 1900 × 400 mm. Table 6:3 shows an overview of the dimension of the PHE, including the mass of PCM used and insulation. Water was used as the HTF from a water bath that was PID controlled. A layer of the PCM (RT 52 or RT 58) with a mean depth of 10mm was contained on top of the sheet and Celotex insulation board (brand name is Celotex) used to cover the test rig to prevent heat loss. The insulation board is made from Polyisocyanurate (PIR), procured from Wickes. For this experiment, two different PCMs were used. Using RT 58, the experiment was carried out at high flow only. This was due to the fact that the initial experimental set up was designed for only a single flow, this was modified to accommodate different flows when using RT 52, which possesses a higher latent heat than RT 58. For the experiments done using RT 52, modification was made by installing a gate valve on the inlet side of the water bath, allowing experiments to be done at three different flows (low, medium and high flow). Figure 6:9 shows a schematic representation of the rig. The PCM is located on top of the PP sheet (between the PP sheet and celotex insulation). The PCM temperatures are monitored using T3, T4 (inlet region), T5 and T6 (outlet region) thermocouples.

Table 6:3: Dimensions of the polypropylene sheet and other parameters.

| | |
|---|---|
| Polypropylene sheet width [mm] | 400 |
| Polypropylene sheet length [mm] | 1900 |
| PVC thickness [mm] | 30 |
| Mass of PCM [kg] | 6.7 |
| Channel width [mm] | 3.3 |
| Channel length [mm] | 3.6 |
| Celotex insulation [W/m.K] | 0.44 |
| Insulation thickness [mm] | 50 |

Using RT 58, the HTF temperature was set to 65°C and pumped through the channels (111) within the sheet to melt the RT 58. The temperature of the inlet and outlet water from the sheet was recorded as well as the temperature of the phase change material at four points.

Using RT 52, the HTF temperature was set to 60°C and experiment carried out at 35g/s, 47g/s and 65g/s, termed low, medium and high flow respectively. This was done for charging and discharging processes.

The measured experimental inlet water temperature was used in the numerical simulation in order to compare the water outlet temperature with measured experimental values. This was done to validate the heat transfer model for the system written in MATLAB.

.

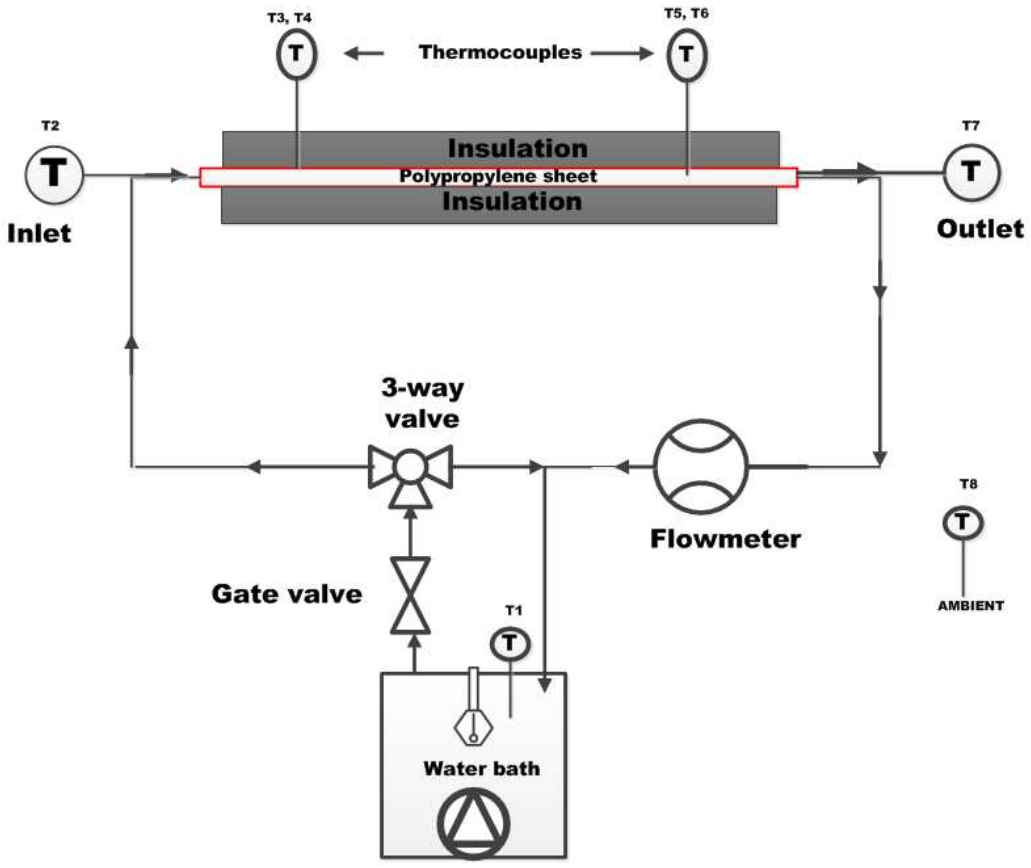


Figure 6:9: Schematic representation of the rig.

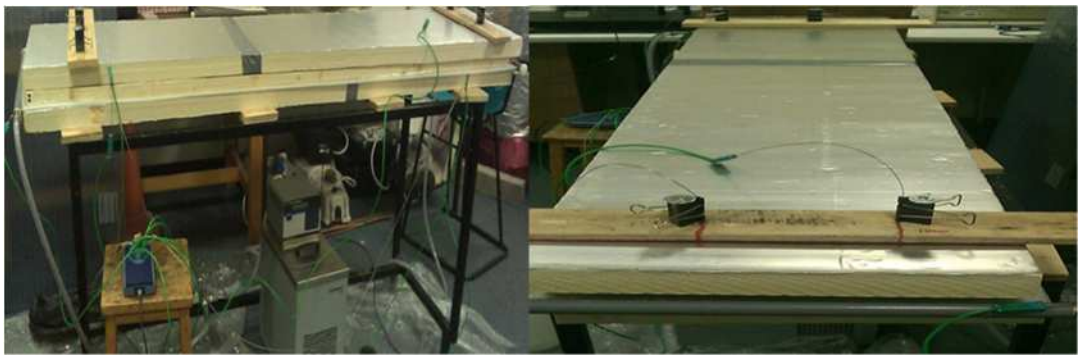

Figure 6:10: Schematic respresentation and picture of the experimental bench top test rig .

Figure 6:11 (a-c) shows the image of the plastic heat exchanger with the phase change material melting as the heat transfer fluid flows through the channels. Figure 6:11 (a) shows the paraffin in granules before melting starts, while Figure 6:11 (b) shows the deformation of the solid granules with a mushy look as meltinng commences across the rig. The paraffin is fully melted as shown in Figure 6:11 (c), where there is a clear liquid across the rig.

(a) Before melting (b) Melting starts (c) Complete melting

Figure 6:11: PCM Images on the plate heat exchanger.

Figure 6:12, shows the thermal image of the rig during melting without insulation. The image was taken by an infra-red camera. There is a noticeable bright patch as the PCM was heated. This is due to thinner layer of PCM in those areas, as a result of the wave-like deformation of the PP sheet. The figure also shows dark streaks on the plate, which

indicates blocked channels. Dark streaks on the sheet indicate low flow in channels which were partially blocked during fabrication by adhesive used in bonding. Software was used to interpret the temperature from the infrared camera image taken during the experiment. It also shows there is little variation of temperature across the plate.

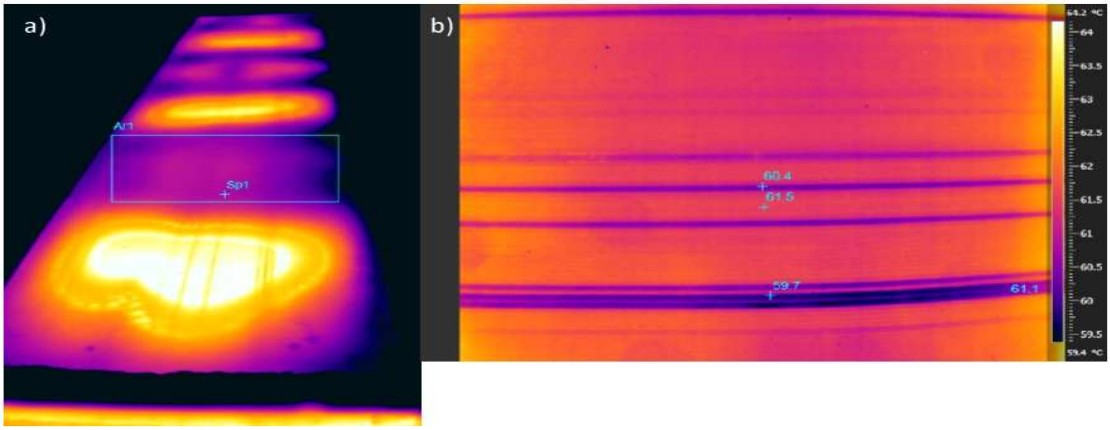


a) Hotter pools of wax indicate thinner area where the PP sheet has deformed in a wave pattern b) view of water channel from beneath.

Figure 6:12: Thermal image of the rig during melting.

Parameters used for calculation and simulation of the experimental results obtained include;

**Hydraulic diameter,** $D_h$ for the rectangular cross-section of the channel (fully filled). Equation 6.4 to Equation 6.7 shows how the hydraulic diameter is calculated.

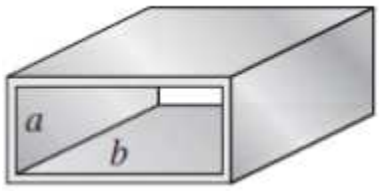


$$D_h = \frac{4A_c}{P} \qquad 6.4$$

$$A_c = a.b \qquad 6.5$$

$$P = 2(a+b) \qquad 6.6$$

$$D_h = \frac{2a.b}{(a+b)} \qquad 6.7$$

The Reynolds number which is the ratio of the inertia to the viscous force is expressed in Equation 6.8 as;

**Reynolds Number, Re**

$$\mathrm{Re} = \frac{\rho v D_h}{\mu} \qquad 6.8$$

Equation 6.9 relates the velocity of flow and mass flow rate,

$$\dot{m} = \rho v A \qquad 6.9$$

Thus;

$$v = \frac{\dot{m}}{\rho A} \qquad 6.10$$

Substituting Equation 6.7 and Equation 6.10 into Equation 6.8, Reynolds number can be expressed as described in Equation 6.11; as a function of the mass flow rate, dynamic viscosity, width and height of the rectangular duct (non-circular pipe).

$$\mathrm{Re} = \frac{2\dot{m}}{(a+b)\mu} \qquad 6.11$$

The Reynolds number of the flow in a rectangular duct is calculated based on using Equation 6.11.

However for the PP sheet, the mass flow rate measured by the Coriolis flow meter is for the flow through the width and length of the PP sheet, thus the Reynolds number was calculated based on flow per channel. The width of the sheet is 400mm, within this span; there are a number of channels, (N =111). Equation 6.12 to Equation 6.16 is used to calculate the velocity and Reynolds number of the flow through a channel.

The volumetric flow rate, $\dot{V}$ is related to the mass flow rate by Equation 6.12

$$\dot{m} = \rho \dot{V} \qquad 6.12$$

Equation 6.13 expresses the volumetric flow rate per channel as;

$$\frac{\dot{m}}{\rho N} \qquad 6.13$$

Thus from Equation 6.13, the velocity of flow through the channel is expressed by Equation 6.14 as:

$$v = \frac{\dot{m}}{A_C \rho N} \qquad 6.14$$

The Reynolds number for the flow through the channel is calculated using Equation 6.15 or Equation 6.16.

$$\mathrm{Re} = \frac{\rho \left( \frac{\dot{m}}{A_C \rho N} \right) D_h}{\mu} \qquad 6.15$$

$$\mathrm{Re} = \frac{\dot{m} D_h}{\mu A_C N} \qquad 6.16$$

The result obtained from calculating the Reynolds number using Equation 6.16 is presented on Table 6:4

Table 6:4: Reynolds number results.

| | **Reynolds Number** | | |
|---|---|---|---|
| **Inlet HTF Temperature (°C)** | **Low flow** | **Medium flow** | **High flow** |
| **60** | **193** | **259** | **359** |
| **65** | **n.a** | **n.a** | **386** |

The type of flow is determined based on the range of the Reynolds number using Table 6:5. This describes the type of flow; whether it is laminar ,transitional or turbulent flow. Based on the Reynolds number calculations, the flow in the channels is Laminar.

Table 6:5: Flow regimes

| | |
|---|---|
| **Laminar flow** | **Re<2300** |
| **Transitional flow** | **2300<Re<4000** |
| **Turbulent flow** | **Re>4000** |

**The charge and discharge rate rate** are calculated from the result obtained from the experiment using Equation 6.17 and Equation 6.18 respecively.

$$\dot{Q} = \dot{m} Cp(T_{in} - T_{out}) \qquad 6.17$$

$$\dot{Q} = \dot{m} Cp(T_{out} - T_{in}) \qquad 6.18$$

### 6.4.2 Discharging

When the PCM is fully melted, the discharging process is started by dropping the temperature in the bath gradually to 20°C. This is achieved by adjusting the temperature controller mounted on the bath to the aforementioned temperature. However, the cooling mode does not start until the temperature of the water in the bath is less than 35°C. To achieve this, the drain line on the outlet is opened and hot HTF released to a bucket as cold water is poured into the bath. When the set temperature of 35°C is reached the bath starts the cooling process. As the HTF of lower temperature flows through the polypropylene channels, heat transfer between the HTF and PCM causes the PCM to start to release its energy, hence solidification process begins. The circulation of HTF continues until all the PCM is solidified. Temperature readings are recorded with the aid of the temperature data logger. The store is discharged at different temperatures but kept at the same flow rate it was charged.

## 6.5 Summary

The materials and apparatus used for the experiment are discussed, stating the specification of each apparatus and properties of the materials used for the experiment using the polypropylene sheet (Plate heat exchanger). The advantages of using water over other types of heat transfer fluid (HTF) are also highlighted. The reason why the K-type thermocouple was chosen as the suitable thermocouple for this experiment is based on its temperature range and availability in abundance, in the workshop.

The experiment methodology using RT 52 and RT 58 as the suitable PCM on the PP sheet for the charging and discharging process is discussed in detail. The properties of the polypropylene sheet, hot water bath etc. used for the experiment are presented in detail in this chapter. The advantage of identifying the thermophysical properties of the PCM was vital in order to determine the PCM used. The thermal behaviour of RT 52 and RT 58 in the experimental rig demonstrates the potential for a plastic heat exchanger to be used for thermal energy storage. The plate heat exchanger concept used, allows a higher ratio of PCM to water within the store. The PCM thickness can be optimized for the anticipated charge/discharge rate and required storage density. The size of the channels also has an effect on heat transfer. The use of small channels allows good heat transfer at low flow rates and with a low pressure drop (small pumping power).

The work has demonstrated that an effective thermal store can be constructed from polypropylene. The plate heat exchanger design and heat transfer characteristics of the mini channels allow the store to be charged with only a small (<5°C) temperature difference.

# 7 Serpentine heat exchanger store design

## 7.1 Introduction

Serpentine heat exchanger (SHE) based on a shell and tube concept was designed and used as a thermal store. The purpose of this was to compare heat transfer characteristics of the plate heat exchanger and the serpentine heat exchanger in their use as a latent heat thermal energy storage device.

For this experiment, the apparatus used for the flat plate heat exchanger were also used for the serpentine rig. The difference in the set-up between the two heat exchangers is the type of heat exchanger used. Basically, from Figure 6:9, the PP sheet is replaced by the modular SHE. Another type of temperature logger; M&C USB 1616HS logger was used for the experiment on the shell and tube design based concept. This is because the Pico temperature logger had only eight(8) channels to measure temeperature ,while fourteeen (14) channels were required for the aforementioned shell and tube rig. The temperature logger; USB 1616HS, produced by M&C computing. MCCDAQ (2016) is used alongside the Picotech temperature logger for obtaining temperature data from the experiment. The Picotech temperature logger is used for only taking room temperature, while the USB 1616HS is used to measure the HTF at the inlet and outlet of the rig and the PCM temperatures at different locations. Details of the USB 1616HS logger are described below.

### 7.1.1 M&C computing USB-1616HS

The USB 1616HS logger is a multifunctional measuring and control board device built for the USB bus. It is supported by Microsoft Windows operating system. The USB 1616HS provides eight differential or sixteen single ended analog inputs with 16bit resolution. Eight of the analog inputs can be configured as differential thermocouple (TC) inputs. It has a built in cold junction sensors for each of the screw-terminal connections, which makes it possible for any TC to be easily attached to the eight thermocouple channels. Figure 7:1 shows the M&C computing USB-1616HS logger, it has a provision for two loggers to be connected as shown, thus providing more measuring channels. An analog input expansion module (AI-EXP48) which connects directly to the logger can increase the inputs to twenty-four (24) differential or forty-eight (48) single-end inputs to the logger.

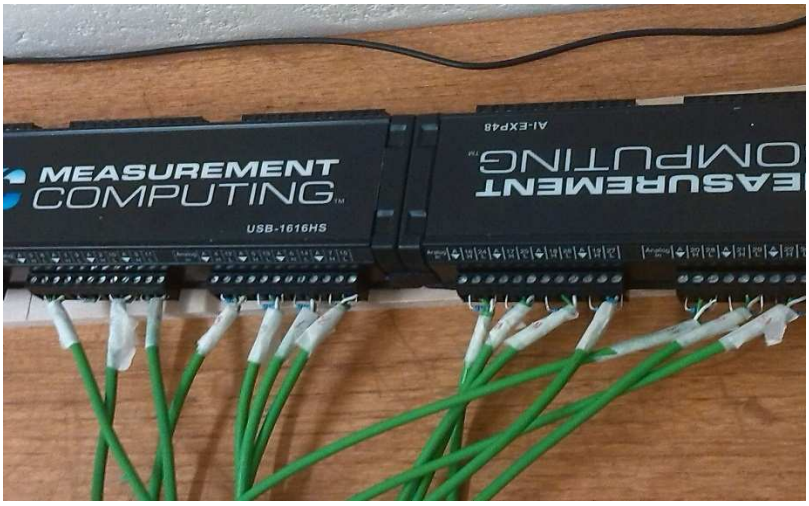


Figure 7:1: Image of the Measurement computing USB-1616HS.

Signal lines are connected to the logger's removable screw terminal blocks. The connections could be either voltage or thermocouple signals. Figure 7:2 shows a detailed description of these connections. Voltage connections (V1 and V2) are single ended or differential connections. Thermocouple signals are differential connection used in this research for obtaining temperature measurement. The negative (red line) connects to the channels LO connection, and the positive (blue line) connects to the HI connector. It is important to select the option to use differential input mode for thermocouple connections when using the software.

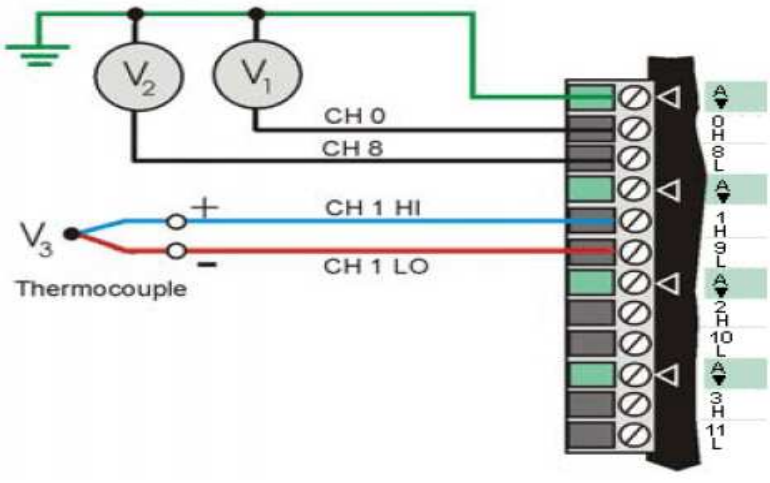


Figure 7:2: Voltage connections and differential thermocouple connections. MCCDAQ (2016).

The logger is calibrated at the factory using a digital NIST traceable calibration method. The NIST traceable calibration method works by using a correction factor for each range on the unit at time of calibration. Software called INSTACAL can also be used to calibrate the device without the need of an external instrument or device. INSTACAL was installed and used to calibrate this logger before commencement of experiment. It works in conjunction with a LabVIEW and MATLAB software to store and retrieve temperature data.

For thermocouple measurements, the logger can operate in an averaging mode, taking several readings on each channel, applying digital filtering and cold-junction compensation, and converts to readings in temperature. For the experiment with serpentine rig, the Picotech temperature logger was only used to take and monitor room temperature, while the M&C computing data logger was used to monitor temperature of the heat transfer fluid and phase change material on the rig. Table 7.1 gives a detailed description of the logger's specification.

To ensure accurate reading using this logger, the following precautions were taken:

- The USB 1616HS and thermocouples wire were allowed to warm up before commencing the experiment to ensure thermal stability.
- Shielded thermocouples are used, to reduce noise.
- Room temperature should be thermally stable, within the range of 20°C to 30°C.
- The USB 1616HS logger is mounted on an even surface.

Table 7:1: USB 1616 HS logger specification.

| **USB-device type** | **USB 2.0 high speed mode (480Mbps)** |
|---|---|
| **Operating temperature range** | -30°C to +70°C |
| **Storage temperature range** | -40°C to +80°C |
| **Dimensions** | 0.269m x 0.092m x 0.045m |
| **Connector type** | Screw terminal |
| **Compatible expansion product** | AI-EXP 48 expansion module with screw terminals |
| **Power range** | 6 to 16 VDC |
| **Weight** | 0.431 kg |

## 7.2 Experimental Procedure (Serpentine heat exchanger)

Two different compact latent heat storage modules were developed in the laboratory based on plate heat exchanger and a serpentine heat exchanger (shell and tube concept). This chapter discusses the latter. The store arrangement comprises of a rectangular tray made from 3mm aluminium sheet. This is the tray in which the PCM is contained as illustrated in Figure 7:4. Copper pipes run across the width of the rectangular aluminium tray. The dimension of the tray is 1970 x 620 x 50mm. The inner diameter of the copper pipe is 6.27mm and the outer diameter is 8.22mm. The dimensions of the serpentine rig were chosen, so that the layout would be identical to that of the plate heat exchanger (PHE). This would allow the experiments results to be comparable. The pitch was chosen (500mm) because the copper pipe could not be bent further to prevent kink, which could hinder flow of fluid during experiment. The jig fabricated in the workshop to aid the bending of the copper pipe was designed to accommodate the pitch desired. A minimum bending radius is required to ensure that the copper pipe was not damaged when it was bent. In the case of the copper pipes used for the serpentine heat exchanger, the minimum bending radius was 50mm. (Kragbaek and Reinholdt (2011)) proposed that a certain minimum bending radius is needed during construction of heat exchanger pipes with fins for a concentrated solar power plant. This is to prevent damage to the pipe during bending. A bending radius of 20mm was used for a pipe with outside diameter of 20mm. Kragbaek and Reinholdt proposed that the bending radius be equal to the pipes outside diameter. However this is difficult to obtain in constructing in the workshop, since preventing kinks in the pipe can be quite challenging, thus a jig was used.

Appendix I shows the solidworks drawing of the SHE arrangement. The copper pipe runs like a coil (serpentine pattern) across the entire width of the tray, similar to a shell and tube arrangement. During fabrication of the serpentine heat exchanger, kinks were avoided by using a bending jig, produced in the workshop. The presence of kinks causes flow rate restriction in this type of heat exchanger. The jig also ensures that a uniform spacing of 100mm between pipes is maintained throughout the entire length of the heat exchanger. The overall length of the pipe is 10200mm. Water is used as the heat transfer fluid, while the PCM (RT 52) occupies the spaces around the pipe within the rectangular tray. The store dimensions are shown on Table 7.2.

Table 7:2: Store dimensions from experimental work.

| **PCM tray width [mm]** | **620** |
|---|---|
| **PCM tray length [mm]** | 1970 |
| **PCM tray height [mm]** | 50 |
| **Volume [L]** | 60 |
| **Copper Coil length [mm]** | 10200 |
| **Copper Tube OD (ID) [mm]** | 8.22 (6.27) |
| **PCM fraction [%]** | > 90 |
| **Polystyrene insulation [W/m.K]** | 0.038 |
| **Insulation thickness [mm]** | 100 |

The rig was connected to the hot water bath with the outlet and inlet of the rig connected to the inlet and outlet of the bath. A 3-way valve is mounted on the inlet side of the water bath as described for the PHE. The flow rate was varied using a valve. Thermocouples were positioned at the inlet and outlet of HTF to the SHE; this was to monitor and record temperature of the HTF during the experiment. Figure 7:3 shows the schematic drawing of the rig.

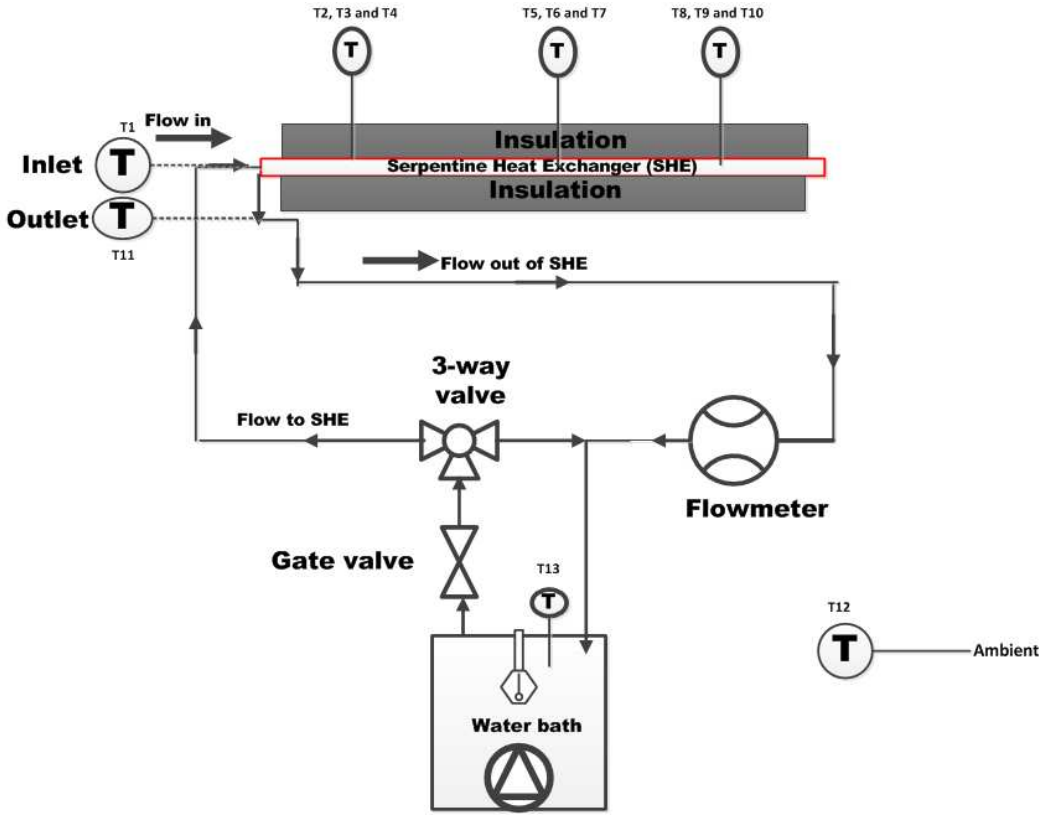


Figure 7:3: Schematic drawing of the serpentine rig.

The thermocouples were made in the laboratory using a 2-core screened PVC thermocouple cable (0.2mm) of a length of 25m. To make each thermocouple, the cable was cut to the desired length and welded. The other end was connected to the USB1616HS logger. The k-type probe (1mm) was used for monitoring the HTF temperature. These thermocouples are positioned at the inlet and outlet of the copper pipe. The eight thermocouples made in the laboratory were used to monition the PCM temperature. As shown in Figure 7:4, the thermocouples are positioned between two copper pipes. They are located on the same axis at six different locations; A1-A3; B1-B3 and C1-C3. Two thermocouples are placed at D1 and D2; to measure the PCM temperature at the regions where there are no copper pipes. The ambient temperature is also monitored by connecting the thermocouple to the TC-08 logger.

The PCM temperature is monitored using thermocouples mounted or positioned at A3BC3, A2B2C2 and A1B1C1. Figure 7:4 shows how the thermocouples are positioned radially and axially across the rig. A1B1C1, A2B2C2 and A3B3C3 are regarded as the axial positioning of the thermocouples, while A1A2A3, B1B2B3 and C1C2C3 are regarded as radial positioning of the thermocouples. The thermocouples are kept at a distance of 750mm apart from one another as shown in Figure 7:4. The

PCM thermocouples are inserted from above the insulation. Each thermocouple is placed in the middle of two copper pipes, which have a pitch distance of 100mm. The thermocouples positioned close to the inlet are A3B3C3, while those close to the outlet of the rig are A1B1C1. Thermocouple positions, A2B2C2 are thermocouples in the middle of the serpentine heat exchanger. Thermocouples at D1 and D2 monitor PCM temperature at the front and rear of the aluminum tray, where the copper pipes are not present. The positioning of the thermocouples was based on the orientation from the copper pipe. The flow of the HTF through the pipe and the heat transfer to the PCM relates to the axial and radial term used for positioning of the thermocouples.

The experiment looked at comparing the PCM temperatures at the radial and axial position of the thermocouples along the copper pipe. It also looked at comparing the temperature drop, charge rate and energy stored with the PHE result. In Chapter nine, the results and discussion will be based on different inlet HTF temperatures (60, 65 and 70°C), different flow rates (7, 15 and 30g/s) regarded as low flow, medium flow and high flow respectively, and, different position across the rig (axially and radially).

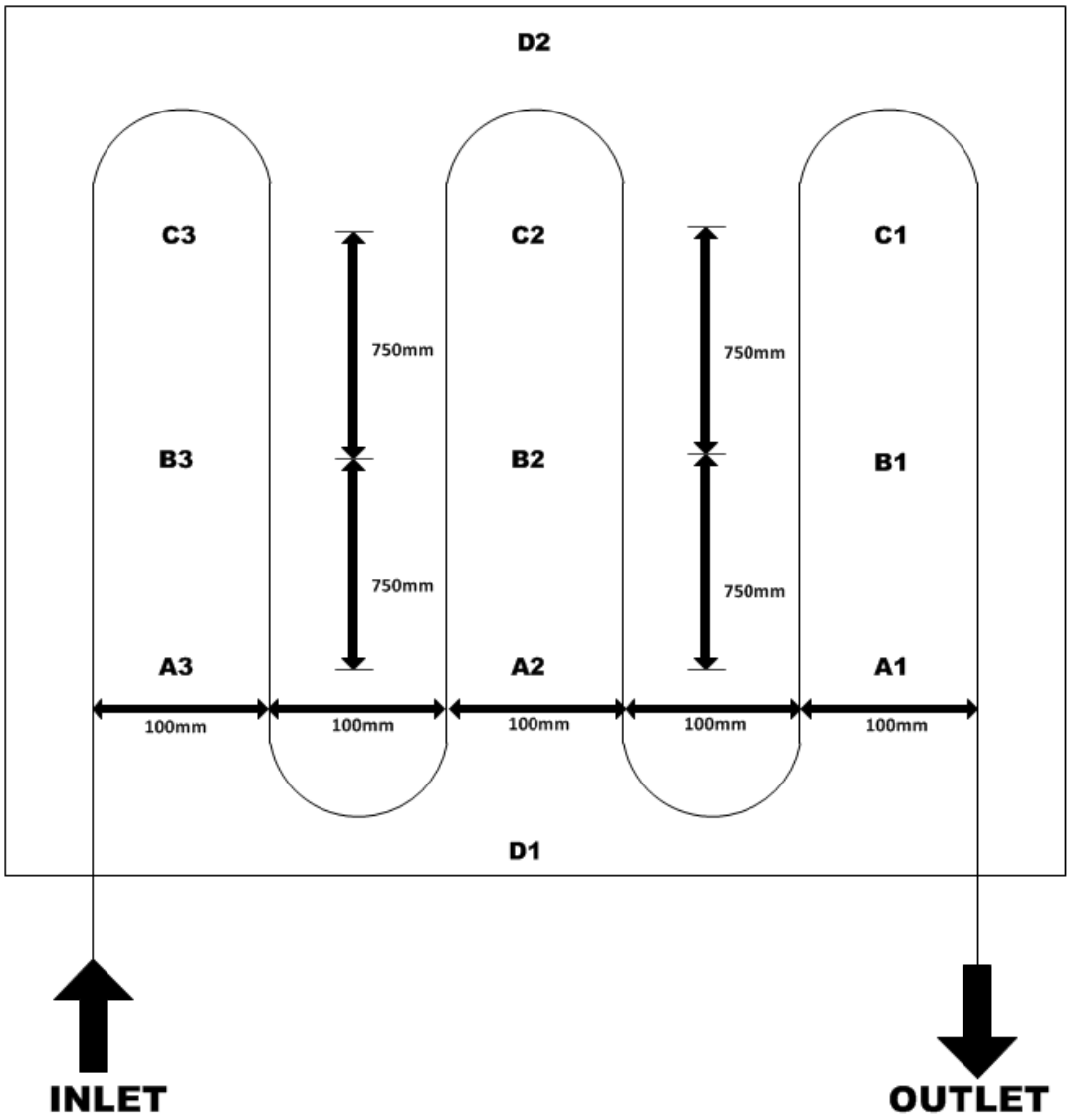


Figure 7:4: Position of thermocouples on the serpentine rig.

The copper tube coil arrangement is positioned at mid-depth of the PCM tray to ensure the same amount or even distribution of PCM above and beneath it. The rig is well insulated using polystyrene board, which has a thermal conductivity of 0.038W/mK. The polystyrene board has a thickness of 100mm to prevent heat loss to the surrounding. The Polystyrene board is placed above and beneath the Aluminium tray. The entire SHE thermal store module was placed horizontally and supported by a frame. Figure shows layout of the rig after being insulated. It shows the insulation above and beneath the thermal store module to prevent heat loss during the experiment.

During the experiment using the serpentine rig, there was a need to repeat all the experiment because it was observed that the sample reading stopped after 25,000 samples, meaning no temperature was logged after the maximum sample value set as 25000. This caused an abrupt end to the data logging as soon as the maximum sample is reached. The effect of this is that the experiment was still running, while data logging has stopped. New experiment was done and the sample maximum increased to 250,000 at a sample rate of 2 Hz.

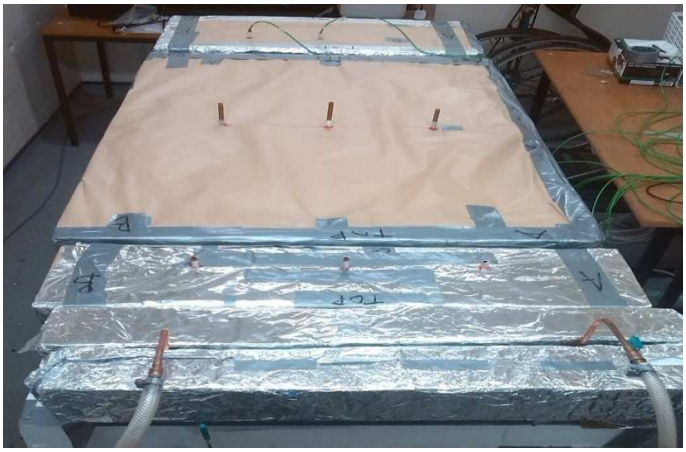

Figure 7:5: Experimental rig after being insulated.

Before the commencement of the experiment, the HTF was pumped through the entire length of the copper pipes with the aid of the hot water bath, to check for leakages along the soldered joints on the pipes. Also, the tray was filled with water to check for leakages from the welding points of the Aluminium tray fabricated in the workshop. Figure 7:6 shows the rig being tested for leaks.

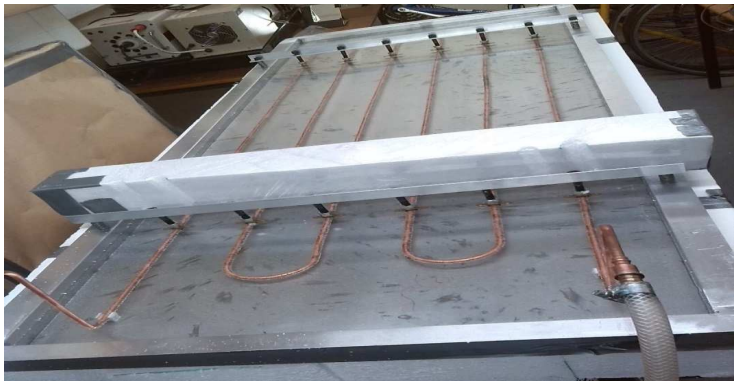

Figure 7:6: Water leakage test on Serpentine rig.

For the PCM, thermocouples are fixed at different length of the tank to monitor the temperature of the PCM during charging and discharging. The mass flow rate is

monitored by the Coriolis flow meter. The paraffin wax (RT 52) used was procured from Rubitherm. The mass of PCM used was 28.5kg. Figure 7:7 shows the rig filled up with the PCM before commencement of the charging process.

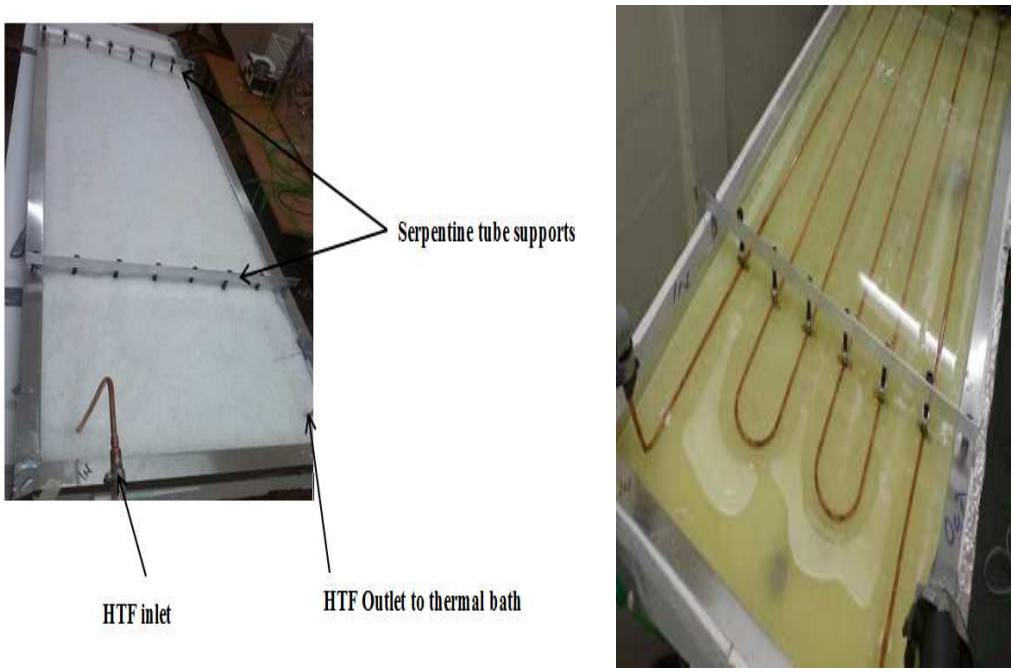


Figure 7:7: PCM filled rig.

Figure 7:8 (a) shows the image of the rig with the paraffin almost fully melted. The image shows the inlet and outlet of the rig, with the PCM on the inlet side almost melted, while in comparison the outlet has more PCM to melt. Figure 7:8 (a) also shows that the PCM around the serpentine melts faster, compared to regions without the copper pipes. This foremost section of the rig relies on the heat transfer from the already melted PCM to commence or be fully melted. This shows the importance of positioning the heat transfer pipes (copper pipes) for effective heat transfer. It takes a longer time for PCM further from the pipes to melt. Figure 7:8(b) shows image of the rig after complete melting.

(a) (b)

Figure 7:8: Image of the rig during charging.

The experiment is carried out in two modes; charging and discharging. For the charging mode; the initial state of the PCM was solid before the commencement of the experiment, basically at room temperature. The experiment was done at different inlet HTF temperatures and flow rates. The heat transfer fluid (HTF) was pumped with the aid of the hot water bath through the copper pipes at a set temperature within the range of 60-70°C.The experiment for the charging process was carried out at three different inlet HTF temperatures; 60, 65 and 70°C. This was done at different flows; low flow, medium flow and high flow. However for an inlet HTF of 60°C, only the charging and discharging result for high flow is presented due to the length of time required to charge the store at low and medium flow. As the water flows through the copper pipes, heat transfer via conduction takes place in the PCM. The charging was regarded as completed when all the PCM in the tray was fully melted. Temperature readings are taken every minute with the aid of the temperature logger.

For the discharging mode; the temperature of the HTF is dropped to a temperature below the melting point of RT 52. The HTF flows through the pipe to recover the heat stored in the PCM. Discharging process is carried out at 30°C for all flows. Temperature reading is also taken, until the entire PCM on the rig is solidified.

Table 7:3 shows the description of the flow term, position of the valve and flow rate at the aforementioned flows for the inlet, into the serpentine heat exchanger.

Table 7:3: Description of flow in the serpentine heat exchanger

| | Position of valve | Flow rate value (g/s) |
|---|---|---|
| High flow | Fully opened | 30 |
| Medium Flow | Half opening of the valve | 15 |
| Low flow | Lowest possible opening | 7 |

Reynolds number for a circular pipe is expressed using Equation 7.1;

$$\mathrm{Re} = \frac{\rho v D_h}{\mu} \qquad 7.1$$

Equation 7.2 to Equation 7.4 describes the relationship between the mass flow rate and the hydraulic diameter for a circular pipe, with inner diameter, D.

$$\dot{m} = \rho v A \qquad 7.2$$

$$A = \frac{\pi D^2}{4} \qquad 7.3$$

Thus substituting Equation 7.3 into Equation 7.2, velocity can be expressed as shown in Equation 7.4.

$$v = \frac{4\dot{m}}{\rho \pi D_h{}^2} \quad (\mathrm{D} = D_h) \qquad 7.4$$

Hence, substituting Equation 7.4 into Equation 7.1, Reynolds number can expressed as shown in Equation 7.5 for a pipe.

$$\mathrm{Re} = \frac{4\dot{m}}{\mu \pi D_h} \qquad 7.5$$

The Reynolds number is calculated for each flow at different HTF temperatures. Thus the viscosity of water at these temperatures is used in the Reynolds number calculations. The specific heat capacity and viscosity at 60°C, 65 °C and 70°C are obtained from tables. The calculation result for the Reynolds number is presented in Table 7:5. The viscosity and specific heat capacity of heat transfer fluid is shown in Table 7:4.

Table 7:4: Heat transfer fluid thermal properties

| **HTF Temperature** | **60°C** | **65°C** | **70°C** |
|---|---|---|---|
| **viscosity ( $Ns/m^2$)** | 0.000467 | 0.000436 | 0.000404 |
| **Specific heat capacity(kJ/kgK)** | 4.185 | 4.187 | 4.19 |

Hydraulic diameter, $D_h$ for a circular pipe is calculated using Equation 7.6 to Equation 7.8;

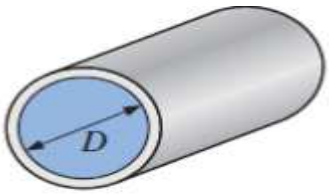


$$D_h = \frac{4A_c}{P} \qquad 7.6$$

$$A_c = \pi r^2 = \frac{\pi D^2}{4} \quad \text{(D=2r)} \qquad 7.7$$

$$P = 2\pi r = \pi D \qquad 7.8$$

Thus, Equation 7.9 gives the hydraulic diameter as;

$$D_h = \frac{4 x \frac{\pi D^2}{4}}{\pi D} = D \qquad 7.9$$

The hydraulic diameter is substituted into Equation 7.5 to obtain the Reynolds number.

Table 7:5: Reynolds number at different flow rate

| | Reynolds Number | | |
|---|---|---|---|
| **Inlet HTF temperature** | Low flow | Medium flow | High flow |
| **60°C** | 3043 | 6522 | 13043 |
| **65°C** | 3260 | 6985 | 13971 |
| **70°C** | 3518 | 7539 | 15077 |

The Reynolds number of the flow calculated based on Equation 7.5 through the pipe determines what type of flow regime goes through the tubes. Table 7:6 shows the regions that determine whether a flow is turbulent, laminar or in the transitional region.

Table 7:6: Flow regime for circular pipes

| | |
|---|---|
| **Laminar flow** | **Re<2300** |
| **Transitional flow** | **2300<Re<4000** |
| **Turbulent flow** | **Re>4000** |

Based on the calculation of the Reynolds number, the flow through the serpentine tube is transitional for low flow and turbulent for medium and high flow. The flows have an increment of about twice the flow, from the low flow to the high flow.

### 7.3 Calibration of Thermocouples

The thermocouples used for this research are type-K chrome thermocouples. Thirteen thermocouples were used on the rig, positioned at different location on the rig. All thermocouples were calibrated with the aid of a platinum resistance temperature device (RTD). The hot water bath in conjunction with the RTD and thermocouples were used for the calibration. The water bath was heated gradually to a temperature range of 11-70°C. All thermocouples were placed in the hot water bath as the temperature was varied within the working range of the planned experiment. The micro computing data logger was used to record the temperature data. Table 7:7 presents the results from the calibration.

Table 7:7: Calibration of the thermocouples.

| | | | | | | | | |
|---|---|---|---|---|---|---|---|---|
| **Platinum RTD reading (°C)** | **10.73** | **14.66** | **19.58** | **29.39** | **39.93** | **49.80** | **59.66** | **69.63** |
| **Inlet water Thermocouple(°C)** | **10.64** | **14.71** | **19.63** | **29.36** | **39.86** | **50.00** | **59.52** | **69.64** |
| **Outlet water Thermocouple (°C** | **10.54** | **14.64** | **19.75** | **29.45** | **39.85** | **49.96** | **59.71** | **69.49** |
| **A1 Thermocouple (°C)** | **10.62** | **14.58** | **19.56** | **29.64** | **39.92** | **49.82** | **59.78** | **69.44** |
| **A2 Thermocouple (°C)** | **10.61** | **14.46** | **19.77** | **29.39** | **40.09** | **50.05** | **59.56** | **69.46** |
| **A3 Thermocouple (°C)** | **10.43** | **14.90** | **19.55** | **29.48** | **39.90** | **49.76** | **59.99** | **69.34** |
| **B1 Thermocouple (°C)** | **10.77** | **14.71** | **19.35** | **29.37** | **40.02** | **49.90** | **59.87** | **69.38** |
| **B2 Thermocouple (°C)** | **10.22** | **14.69** | **19.59** | **29.92** | **40.10** | **49.80** | **59.83** | **69.23** |
| **B3 Thermocouple (°C)** | **10.65** | **14.51** | **19.76** | **29.69** | **39.84** | **49.43** | **59.88** | **69.62** |
| **C1 Thermocouple (°C)** | **10.68** | **14.59** | **19.58** | **29.57** | **39.84** | **49.83** | **59.56** | **69.69** |
| **C2 Thermocouple (°C)** | **10.63** | **14.57** | 19.51 | **29.50** | **40.18** | **50.15** | **59.22** | **69.61** |
| **C3 Thermocouple (°C)** | **10.82** | **14.69** | **19.73** | **29.18** | **39.90** | **49.68** | **59.37** | **70.00** |
| **Maximum deviation(°C)** | **0.50** | **0.25** | **0.23** | **0.53** | **0.25** | **0.36** | **0.44** | **0.40** |

Each of the thermocouple result was plotted against the measurement of the Platinum RTD and a calibration curve developed. A linear trend was applied to the plot of each thermocouple reading against the RTD temperatures. The reading was adjusted according to the result obtained from the curve and compared with the Platinum RTD readings. The maximum deviation (0.53°C) of the thermocouple reading when compared to the RTD was taken as the uncertainty of the thermocouple readings. A linear fit was applied to the result for the different temperature points and R-squared ($R^2$) between the range of 0.998 and 1 was obtained. R-squared is a statistical measure of how near the data points are to the fitted regression line. Figure 7:9 shows one of the plots used for calibration, in particular, the inlet HTF thermocouple. The same analysis was done for the remaining ten (10) thermocouples.

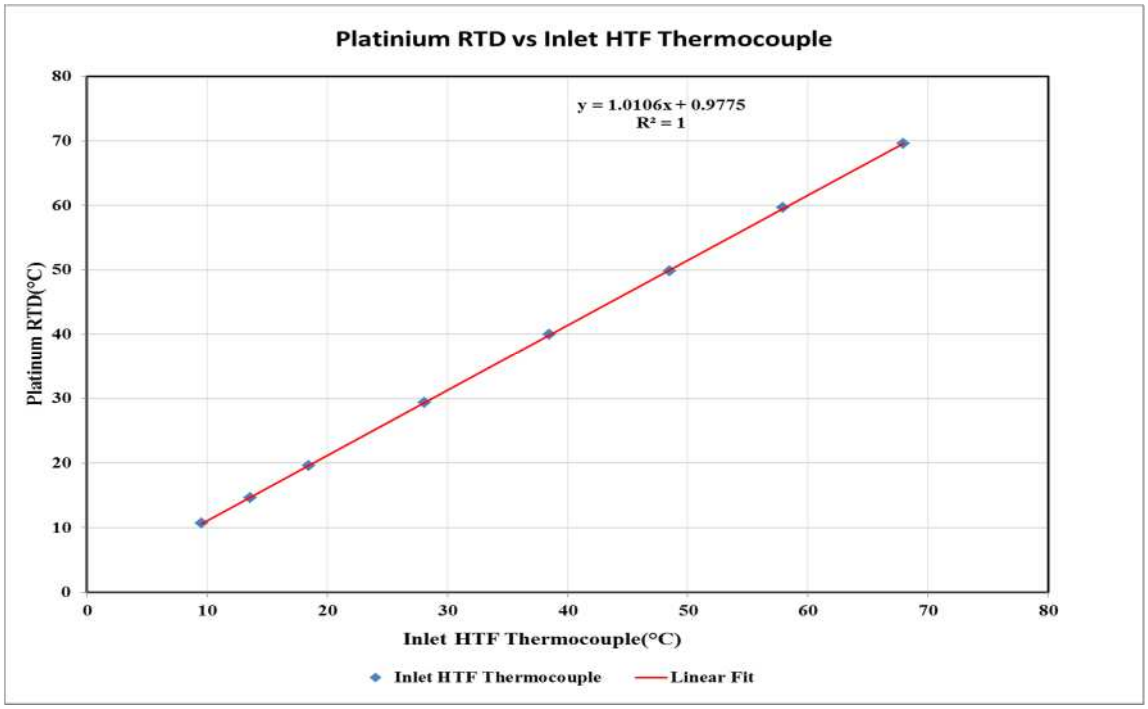


Figure 7:9: Calibration curve for inlet HTF thermocouple.

## 7.4 Summary

This chapter discussed the serpentine heat exchanger (SHE) and the additional devices used to carry out the experiment. A different logger (Picotech logger) from the previous experiment with the plate heat exchanger is used. The USB 1616 replaced the pico logger used in the previous experiment to record the temperature values. The charging and discharging experiment are discussed in details, where the charging process is carried out at three different inlet HTF temperatures (60, 65 and 70°C). The experiment was also carried out at three different flow rates (7, 15, and 30 g/s), which are expressed as low, medium and high flow. The discharging process was carried out at a constant HTF inlet temperature of 30°C. Experiment with the SHE was carried out using similar dimensions as the PHE .

# 8 Experimental result from the PHE thermal store.

## 8.1 Charging experiment (PHE)

Experimental results from the charging and discharging of the thermal store made from polypropylene using two different PCMs; RT 52 and RT 58 are presented in this section. The results for RT52 are discussed in detail and the results compared to the SHE thermal store comprising a serpentine heat exchanger with the same PCM. The inlet and outlet heat transfer fluid temperature, phase change material temperatures at the inlet and outlet of the rig are discussed in the experiment analysis. The result for RT58 are presented first as this was the first PCM used in the polypropylene PHE test rig before it was changed to RT 52, based on the phase change temperature and application in domestic homes. For the RT 58, there was no variation of flow rate, but the experiment was carried out at maximum opening of the valve and at an inlet temperature of 65°C. Experimental results for RT 58 are discussed using Figure 8:1, while experimental results for RT 52 are discussed using Figure 8:5 to Figure 8:7. Results are presented at different flow rate for the RT52 using plots of temperature against time.

Experiment results for RT 58 are discussed using Figure 8:1 which describes the temperature profile of the inlet and outlet HTF temperatures and PCM temperatures for the charging process. The temperature profile of the inlet and outlet HTF temperatures from the rig are studied and compared. Both profiles show similar pattern, with the inlet HTF temperature having a higher temperature profile, when compared to the HTF outlet temperature. The temperature drop of the heat exchanger is less than 3°C, this is because there is an effective heat transfer between the HTF and the PCM as it flows from inlet to the outlet of the heat exchanger. The PHE provides good surface area contact between the PCM and the HTF, thus facilitating good heat transfer. The conduction length is also shortened, because the PP sheet has a very thin wall thickness. Figure 8:1 shows the temperature -time graph of the HTF and PCM temperature at the inlet and outlet of the heat exchanger.

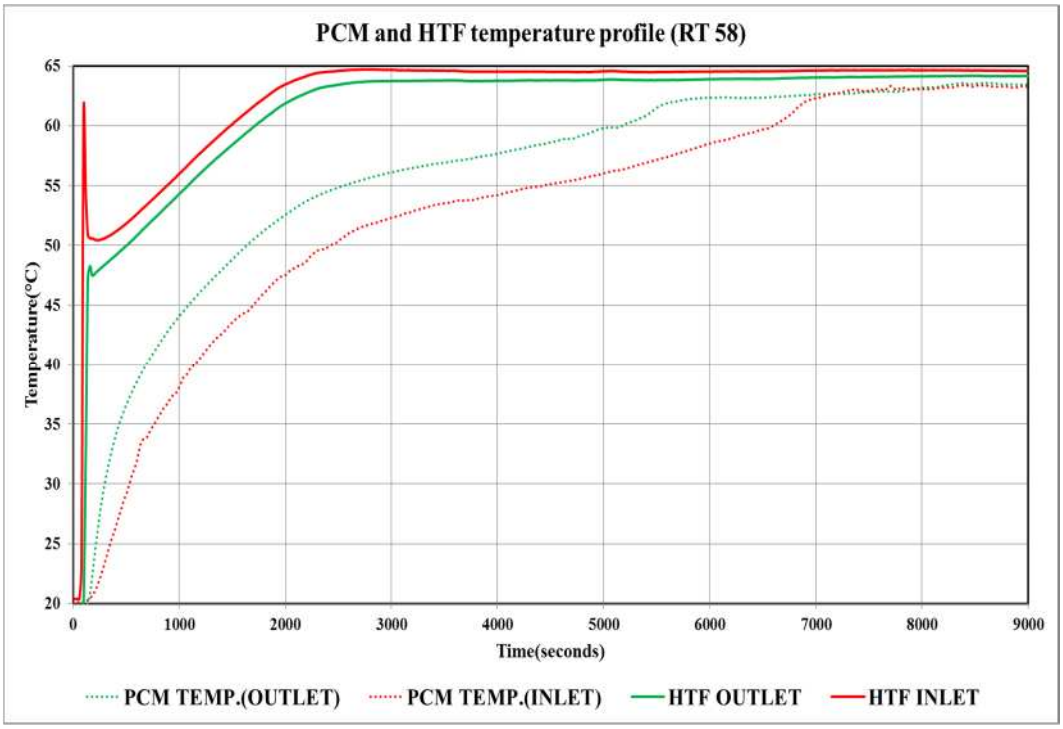


Figure 8:1: Plot of experimental result for inlet and outlet HTF and PCM temperatures.

Figure 8:1 shows that at the start of the experiment, the PCM temperature rises directly with time at the outlet zone and inlet zone. This region means the PCM is solid as sensible heating is experienced as heat transfer occurs between the PCM and HTF. On further heating, the PCM starts to melt, in the temperature region of 48-60°C; this region is regarded as the latent heat zone. PCM temperature rises further after 60°C, which means the entire PCM is fully melted. The more the PCM melts, the lesser the temperature drops across the store (between the inlet and outlet HTF temperature). The PCM behaviour on the rig during the charging process shows a transition of the temperature profile expected for the RT 58,however the PCM temperature at the inlet and outlet zone are different based on the positioning of the thermocouples on the rig. The experimental results for RT 58 were used for initial validation of the model.

The temperature drop using the PHE shows small variations between the inlet and outlet HTF temperature. Table 8:1 and Figure 8:2 shows the trend of the charge rate every half an hour from beginning to the end of the charging process. The results show the store is charged within 2.5 hours.

Table 8:1: Temperature drop and heating rate during the charging process.

| Time(seconds) | Temperature drop(°C) | Heating rate(W) |
|---|---|---|
| 900 | 1.69 | 459.72 |
| 1800 | 1.69 | 459.72 |
| 3600 | 0.81 | 220.34 |
| 7200 | 0.58 | 157.77 |
| 9140 | 0.40 | 108.81 |

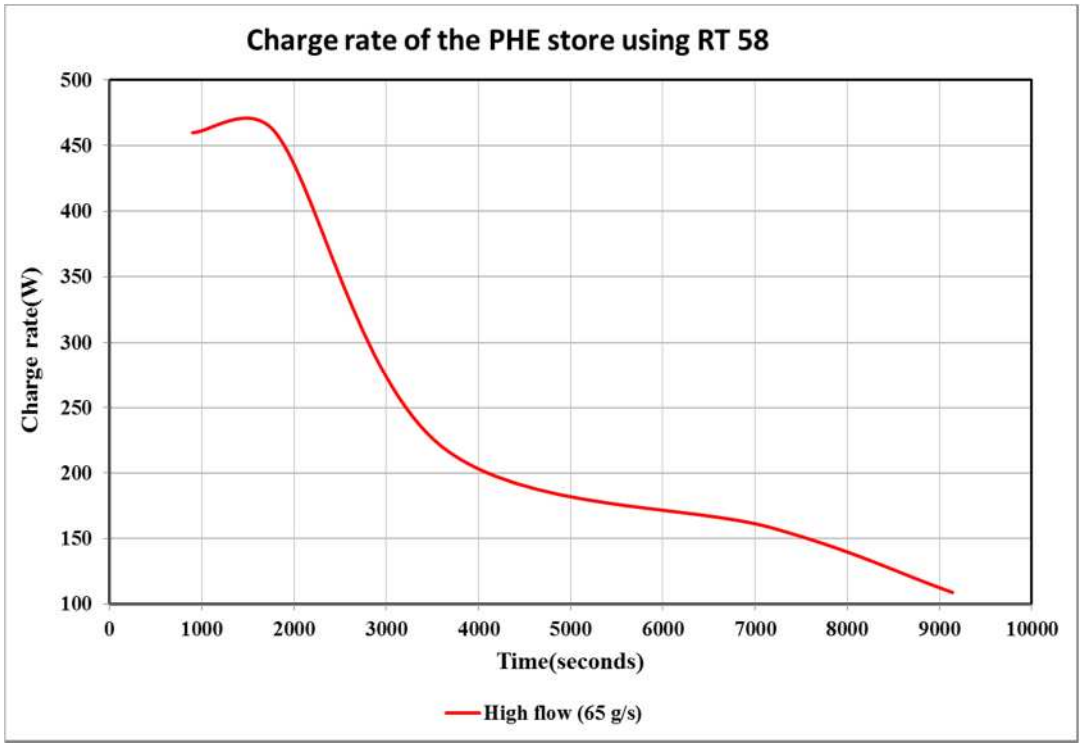


Figure 8:2. Charge rate from experimental result.

The power density of the plate heat exchanger thermal store using RT 58 was compared at different temperature difference. From Figure 8:3, it is observed that as the temperature drop increases, the power density increases. The power density is obtained by dividing the charge rate by the volume of the plate heat exchanger store.

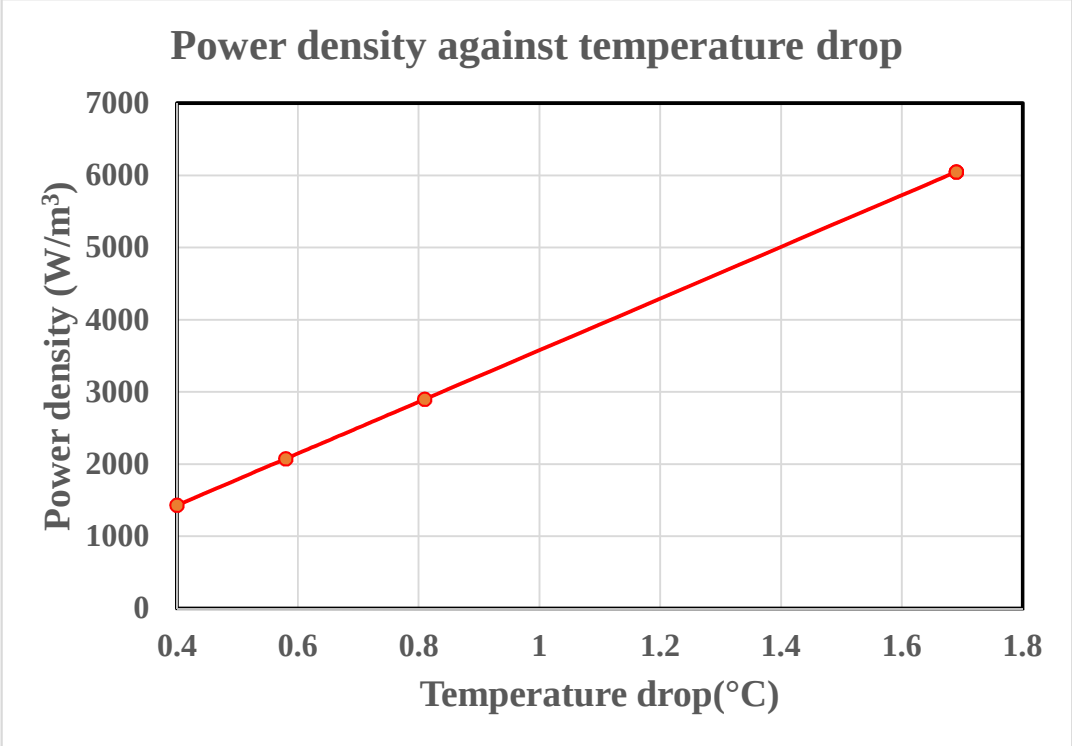


Figure 8:3: Power density of the PHE store using RT 58.

### 8.2 Experimental result using RT 52 on the plate heat exchanger.

The phase change material (RT 58) was replaced with another PCM (RT 52) and this PCM was used for the remaining part of the research for the plate heat exchanger and the serpentine heat exchanger. Using the same design of rig (plate heat exchanger), a new heat exchanger was made in the workshop for the RT52, with the same dimensions used for the previous one (RT58). The phase change material, RT 52 was filled onto the rig. It was easy to fill it on to the rig, because it came in spherical beads from the manufacturers, Rubitherm compared to the RT 58, which came in blocks of solidified PCM. RT 58 had to be cut into pieces and melted using the electric heater mentioned in Chapter 6. The experiment using RT52 commenced with varying the mass flow rate at a constant inlet HTF temperature of 60°C. The temperature profile for each mass flow rate is discussed for the charging process using Figure 8:6 to Figure 8:7, and for the discharging process, using Figure 8:10 to Figure 8:11.

#### 8.2.1 Effect of varying mass flow rate

The experiment was carried out by varying the flow rate into the rig. This was achieved by varying the position of the valve to obtain high flow (65g/s), medium flow (47g/s) and low flow (35g/s) into the polypropylene rig (PHE), at a constant inlet HTF

temperature of 60°C. All experiments commenced with the PCM at room temperature. The experiment result in which the flow rate of the heat transfer fluid was varied and compared to the experiment using the polypropylene rig. The inlet HTF temperature at different flow rates is described in Figure 8:5.

Table 8:2: Description of flow in the PHE.

| Flow type | Position of valve | Flow rate value (g/s) |
|---|---|---|
| High flow | Fully opened | 65 |
| Medium Flow | Half opening of the valve | 47 |
| Low flow | Lowest possible opening | 35 |

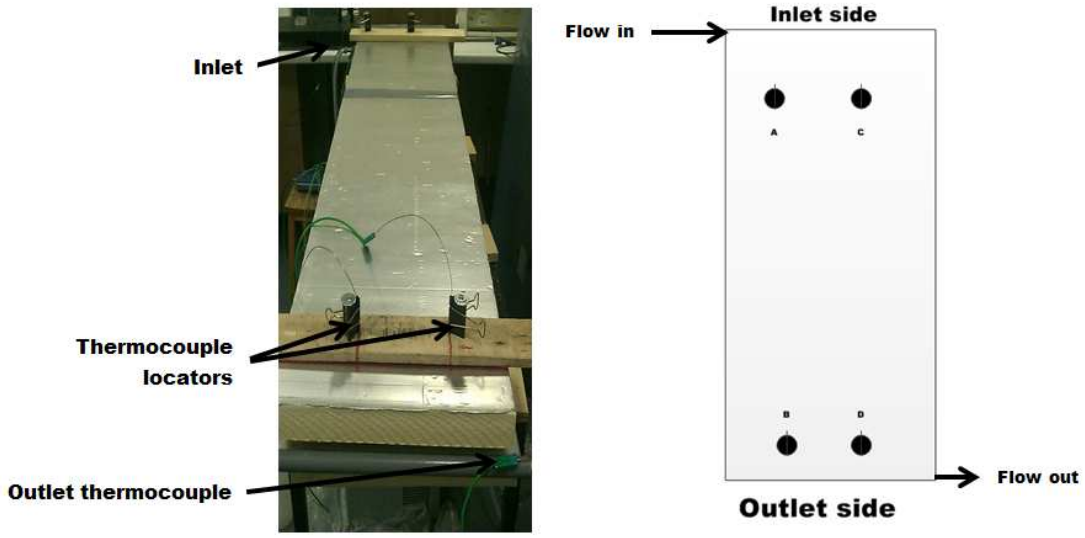


a) Thermocouple position b) Z flow arrangement of PHE

Figure 8:4: Position of thermocouples on polypropylene sheet.

Figure 8:4 shows the position of the thermocouples on the rig. Thermocouples A and B are the probe type thermocouples(1mm), while thermocouples C and D are steel shim as described in Figure 6:3. The thermocouples at the inlet are A and C, while thermocouples B and D are at the outlet of the rig. The thermocouple at point A (located at a distance of 418mm from the inlet end of the rig, while the thermocouple at B (located at a distance of 488mm from the outlet end of the rig). Both thermocouple

A and B are positioned along the channel flow path axis from the inlet to the outlet of the rig. The probe type thermocouples A and B are positioned at a depth of 5mm into the PCM.

Figure 8:5 (a-c) shows the temperature profile of the experiment during the charging process using RT 52 at different flow rates (low(35g/s), medium(47g/s) and high flow(65g/s)), it take a longer time for the PCM to melt at low flow compared with the other two types of flow. The temperature drop of the HTF at low flow is more than at medium and high flow before the PCM melts and even after the PCM is melted. The temperature profile of the HTF and PCM follow similar pattern for the different flows, though there is a difference in the temperature drop and the rate of melting of the PCM.

The PCM at the outlet zone of the thermal store melts faster in comparison to the PCM at the inlet zone for all the different flow rates used during the experiment. This result is not expected and could be attributed to the depth at which the thermocouples are located. Thermocouple at outlet (B and D) could be closer the PCM at the PP sheet surface during melting. Also, the PP sheet experienced deformation in a wave pattern as shown in Figure 6:12, this pattern is observed at the outlet side of the store. The wax is thin wax at this thermocouple locations, which explains the reason why the PCM temperature at the outlet end is higher than at the inlet end of the PHE.

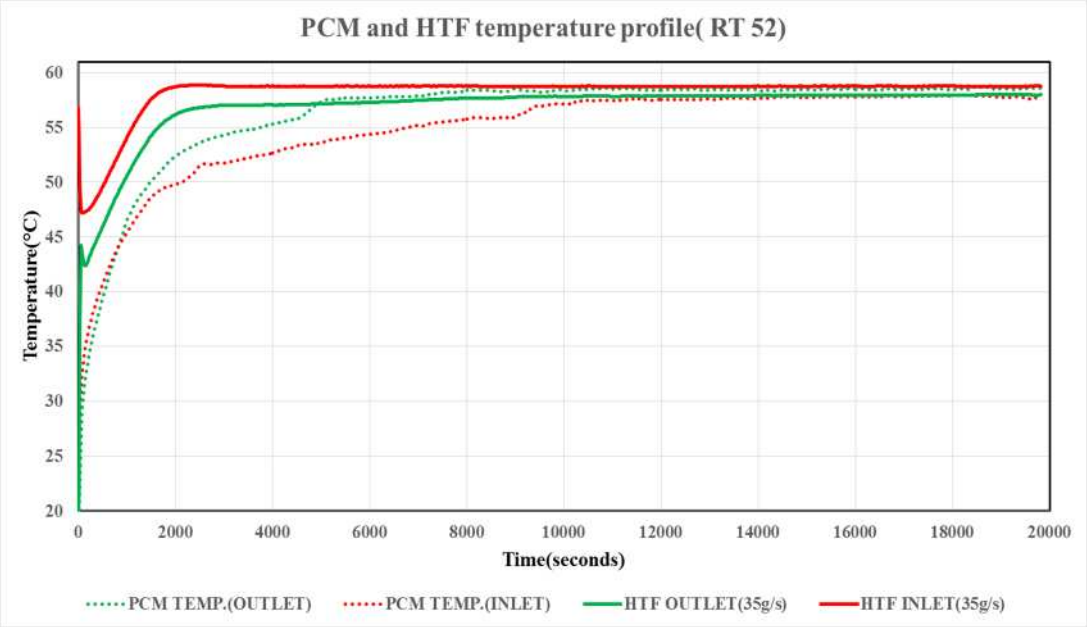


(a) Low flow (35g/s)

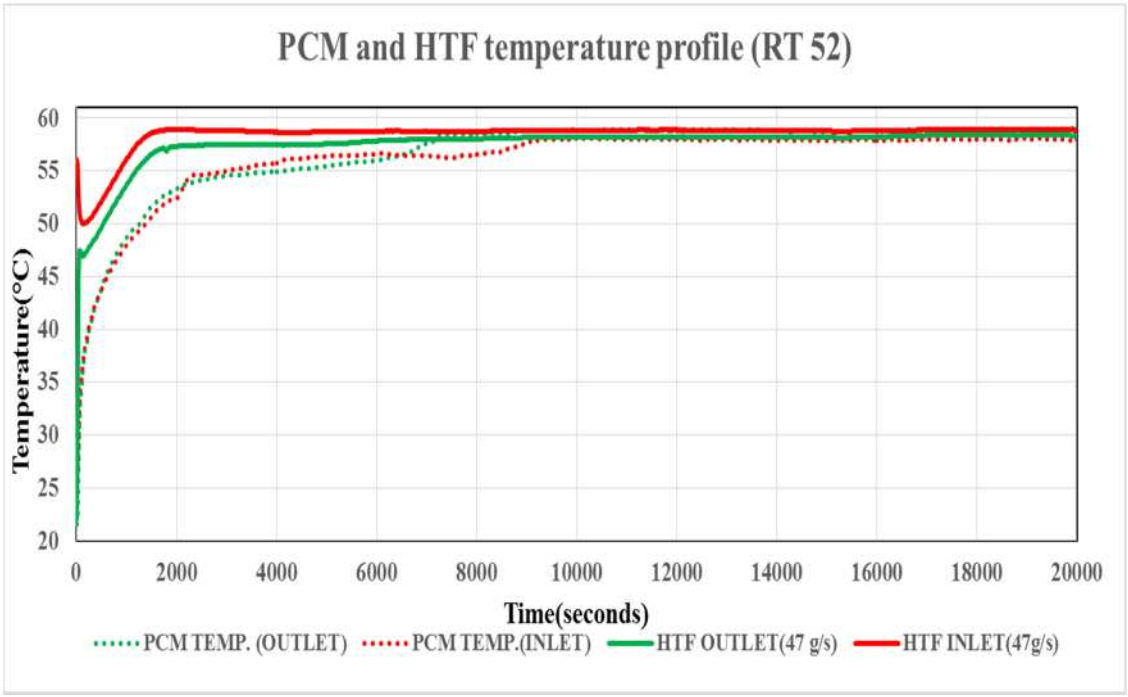


(b) Medium flow (47g/s)

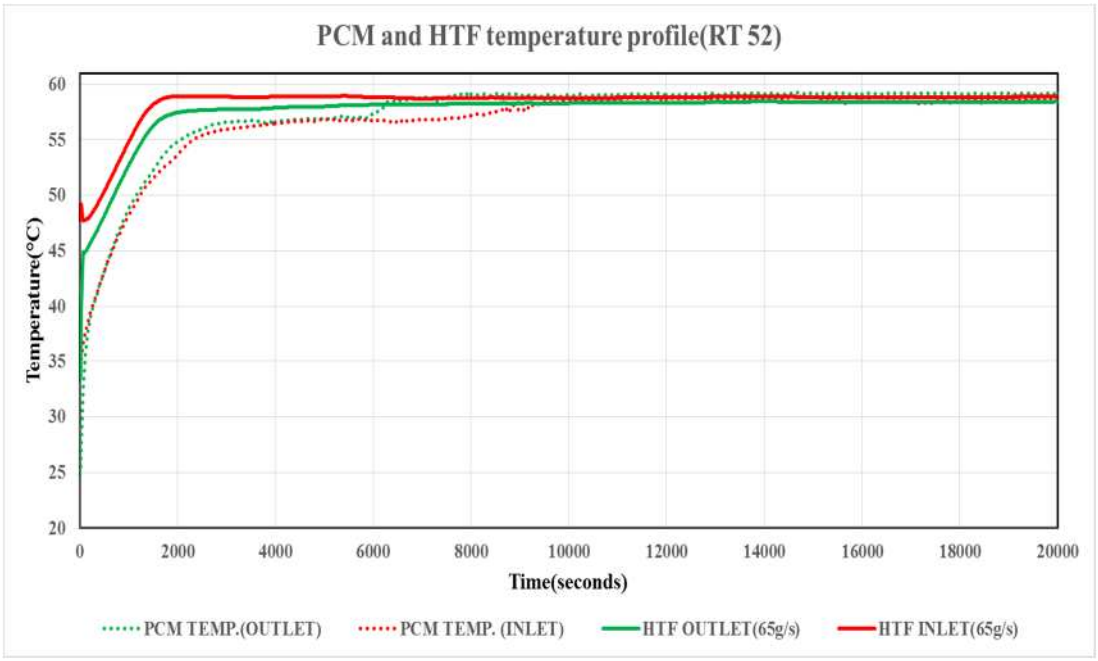


(c ) High flow (65g/s)

Figure 8:5: Charging process result for RT 52.

Comparing the temperature profile plots for each flow rates showing the HTF outlet temperature, PCM inlet and outlet temperature against time, there is a similar trend for all cases (65, 47 and 35 g/s).

With reference to results from Figure 8:5 (a-c), which shows there is a variation in the temperature difference between the HTF outlet and PCM temperatures, it can be observed that at higher flow rate of 65g/s, the temperatures are closer together, but at a lower flow rate of 35g/s, they are farther apart. This can be based on the rate of heat transfer that exists between the PCM and HTF's flow rate. The PCM inlet and PCM outlet thermocouples are on the same axis on the plate heat exchanger during the experiment, a pictorial view is available in Figure 8:4. Figure 8:6 and Figure 8:7 shows the temperature profile considering only the HTF inlet and outlet temperature respectively.

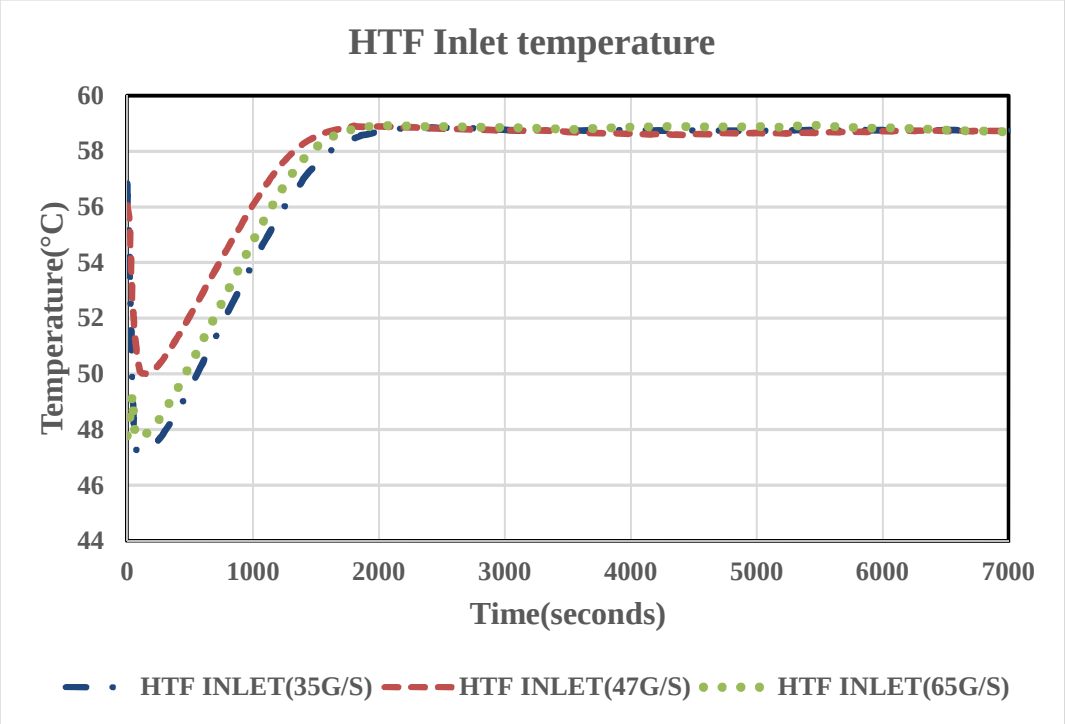


Figure 8:6: Charging RT 52, HTF inlet temperature at different flow rate.

Figure 8:6 shows the temperature profile during the charging process at each flow rate. The plot describes the inlet HTF temperature into the rig over a period of time. This is affected by the outlet HTF temperature from the rig based on the heat transfer between the PCM and HTF along the path of the heat exchanger, from the inlet to the outlet of the rig. The outlet HTF temperature is also changing based on heat transfer between the PCM, fluid and heat exchanger as shown in Figure 8:7. From Figure 8:6, there is a noticeable drop in temperature at the beginning of the experiment; this was because of the presence of a lower HTF temperature in the polypropylene channels before the start of experiment. The temperature drop was further enhanced as heat transfer occurs

between the PCM, which was at room temperature and the plate heat exchanger. Figure 8:6 shows the temperature rises till the 2000$^{th}$second, and then a constant temperature throughout the remaining part of the experiment as the thermal store becomes thermally stable. The rise in temperature is as a result of heat gained as the PCM starts to melt. Comparing the HTF inlet and outlet temperatures, it can be observed that they both exhibit similar temperatures after 2000 seconds. The temperature-time plot at different flow rates for the HTF inlet are close but for the HTF outlet; there is a noticeable difference in the temperature profile for the different flow rates.

Figure 8:7 shows the result obtained for the heat transfer fluid outlet temperature during the charging process of the PCM at different flow rate. The plot shows that the temperature-time for the three different flow rates follow a similar trend, with the flow rate of 35g/s (low flow) having the lowest temperature amongst the three flow rates temperature profile. The experiment was carried out at an inlet HTF temperature of 60°C. The effect of the heat transfer between the phase change material, polypropylene heat exchanger and heat transfer fluid can be seen on the temperature profile at the outlet of the rig. It is observed that the flow rate has little effect on the outlet HTF temperature from the rig. The result shows that at a lower flow rate of 35 g/s, there is bigger temperature drop due to longer residence time. Smaller temperature drops occur at medium and full flow when compared to low flow as shown in Table 8:3 to Table 8:5. Heat transfer is dominated by conduction through the PCM, so flow rate has little effect on heat transfer.

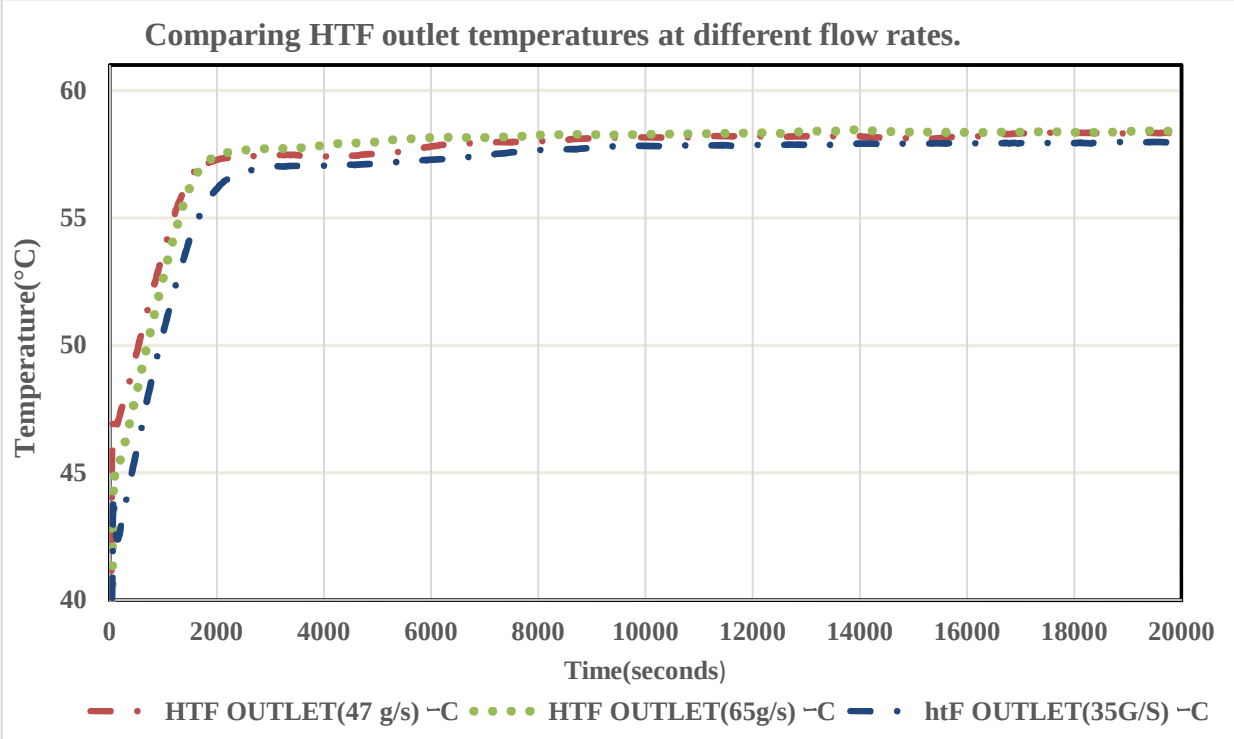


Figure 8:7: Charging RT 52, HTF outlet temperature at different flow rate.

With reference to the charge rate at different flow rate (low, medium and high flow) the power density of the PHE thermal store using the RT 52 was compared at different temperature difference. As shown in Figure 8:8, it is observed that as the temperature difference increases, the power density increases. Also the power density at high flow is larger when compared to the low and medium flow. It was observed that the power density at high flow for the experiment using RT 52 and RT 58, shows that the store's power density using RT 52 is higher than the store's power density using RT 58. This can be attributed to the latent heat of RT 52 being higher than RT 58 and a higher temperature difference(dT) using RT 52.

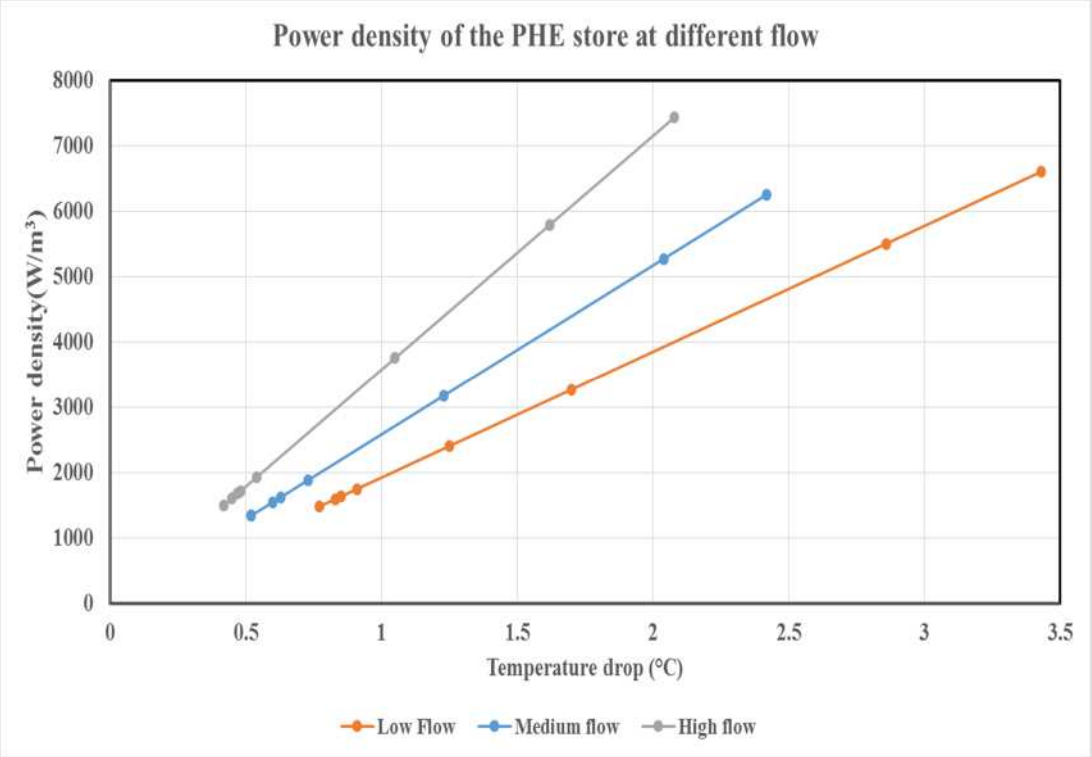


Figure 8:8: Power density at different flow rates using RT 52.

### 8.3 Discharging Experiment (PHE)

The discharging result for the RT58 is discussed first. The experiment using RT 58 was carried out without provision for varying the flow rate. For subsequent experiments using RT 52, the rig was modified by installing a valve, which allows the flow rate to be varied, varying the flow rate at three different flows; low, medium and high flows. The result for the discharge process from the experiment using RT 58 is presented in Figure 8:9. The temperature profile for the discharge process shows a spike at 2000 seconds for the HTF outlet temperature; this could be attributed to error in the thermocouple reading at that time. Comparing the PCM temperature (inlet and outlet) and HTF temperature (inlet and outlet) during the discharge process, it can be seen that the spike in temperature occurs at the same point or time the PCM reaches its phase change temperature (58°C). This can be attributed to latent heat release during solidification. During the discharging process, heat is gained by the HTF. There is a similar occurrence with RT 52 during discharging where the spike in HTF temperature occurs at the point RT 52 reaches its phase change temperature (52°C) during discharging. The melting or solidification temperature of each PCM (RT 52 and RT 58) is the point at which the latent heat is released as the PCM melts or

solidifies. However, after release of its latent heat, it shows a similar pattern with the HTF inlet temperature afterwards. Also, the PCM temperatures at the inlet and outlet zone of the PHE were also monitored as shown in Figure 8:9. During discharging, it shows that the PCM at the inlet zone has a higher temperature when compared to the PCM at the outlet zone. There was a drop in temperature, and then it plateaued and drops further with time as the rig is discharged at 20°C. The experiment using RT 58 was the first experiment done on the rig before modifications were made to study its behaviour at different flows as well as change the PCM to RT 52.

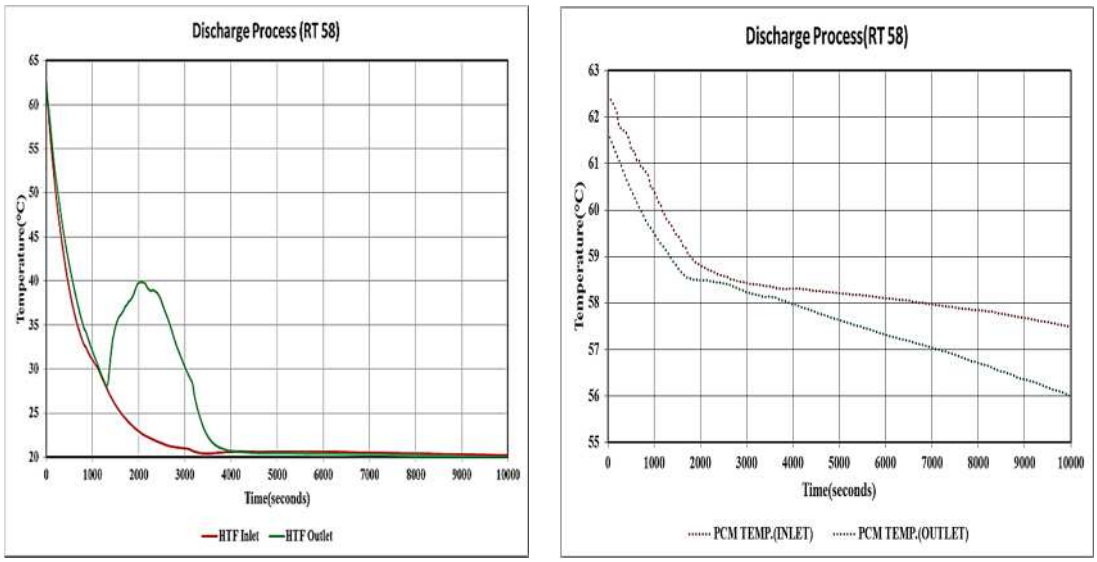


Figure 8:9: Discharge process result using RT 58.

### 8.3.1 Effect of varying mass flow rate.

Discharge process using RT 52 was done at the same flow rate as the charging process for each flow rate. The discharge process was done at different heat transfer fluid temperatures. Discharge process commences immediately the entire PCM on the heat exchanger is totally melted. The discharge of the thermal store ends when the entire PCM is solidified. The discharging process for the three flow rates were done at different temperature. The store was discharged at different HTF temperatures. For the flow rate of 47g/s, the thermal store was discharged at a temperature of 47°C, while for the flow rate of 35g/s it was discharged at a temperature of 40°C. The high flow (65g/s) was discharged without the use of the hot water bath. This effect was noticeable by the temperature of the PCM during discharging.

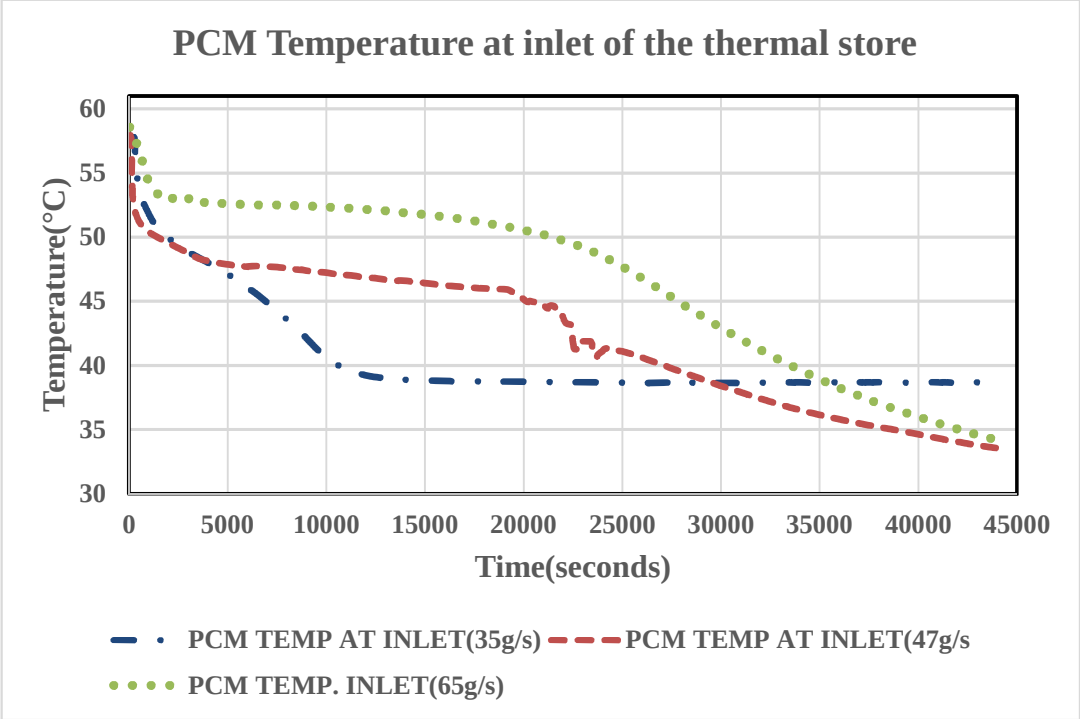


Figure 8:10: Discharging RT 52, PCM temperature at inlet of the rig at different flow rate.

Figure 8:10 shows the temperature profile for the phase change material situated at the inlet end of the rig, where a thermocouple positioned in that location takes temperature measurement. The temperature profile shows that the PCM temperature drops rapidly at flow rates of 65g/s and 47 g/s, however at lower flow rate of 35g/s, the store maintains a temperature of about 38°C. The rapid drop in the PCM temperature for medium and high flow could be as a result of the discharge temperature being different for each flow rate.

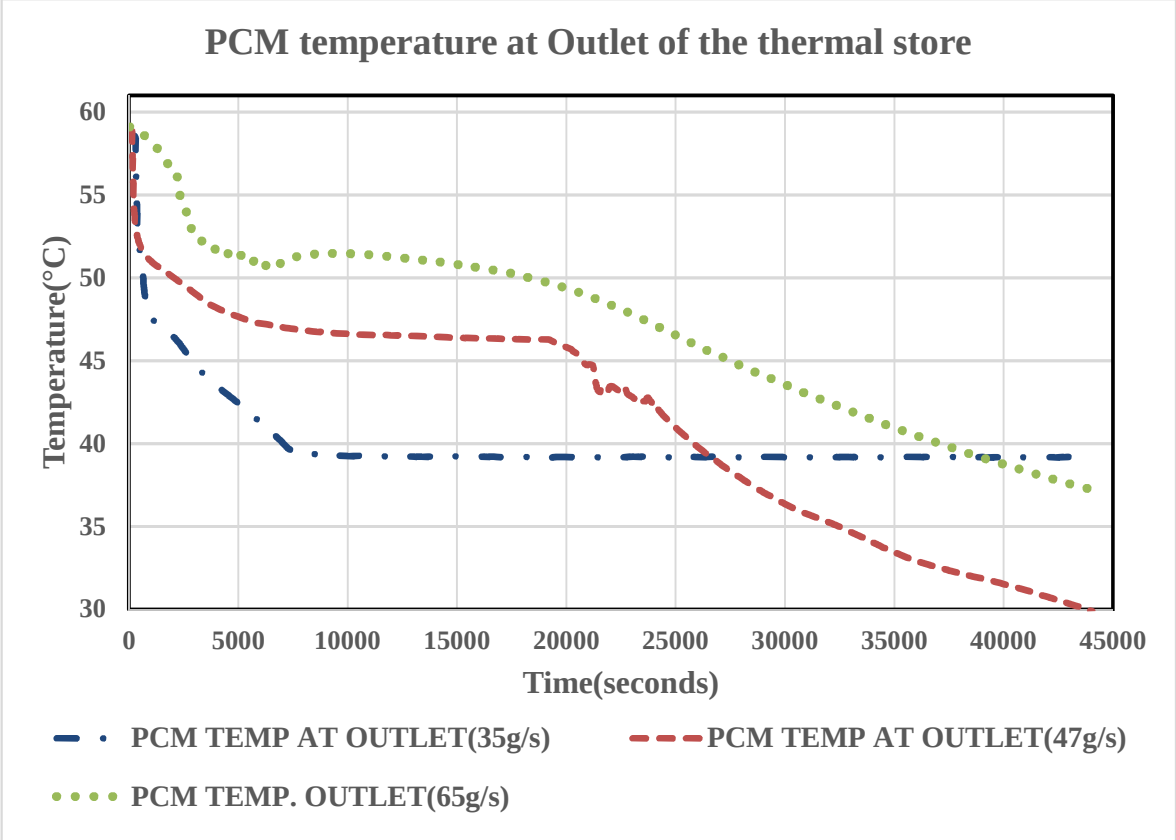


Figure 8:11: Discharging RT 52, PCM temperature at outlet of the rig at different flow rate.

Figure 8:11 shows the temperature profile for the phase change material situated at the outlet end of the rig. Figure 8:10 and Figure 8:11 shows that at the end of the experiment, the temperature of the PCM at a flow rate of 35g/s is higher than at 65g/s and 47g/s at the end of the experiment. However, the temperature at the PCM was consistently higher throughout the duration of the discharging process at a higher flow rate of 65g/s, when compared to the flow rate of 47g/s and 35g/s. The temperature of the PCM starts to drop at the end of the experiment due to the discharging inlet temperature into the rig.

The results from the experiment were used in a model. The model was written in MATLAB to optimize the thermal store in such a way that the flow rate, thickness of PCM, PCM thermal properties and size of the channels can be varied. The aim is to study the response of the store to the changes, which in turn determines the right parameters for the thermal store that would give the best thermal performance. The experiment is also used to validate the model result where the inlet temperature from

the experiment is used to predict the heat transfer fluid temperature at the outlet of the rig.

The heating or charge rate was calculated from the experimental results at different flow rates. Table 8:3 to Table 8:5 shows the values of the heating rate from different flow rates. The results show that the heating rate is higher at high flow rate compared to the other two flow rates.

Table 8:3: Temperature drop and heating rates (low flow).

| Time(seconds) | Temperature drop (°C) | Heating rate(W) |
|---|---|---|
| 900 | 3.43 | 502.41 |
| 1800 | 2.86 | 418.92 |
| 3600 | 1.70 | 249.01 |
| 7200 | 1.25 | 183.09 |
| 9800 | 0.91 | 133.29 |
| 14400 | 0.85 | 124.50 |
| 18000 | 0.83 | 121.57 |
| 21600 | 0.77 | 112.79 |

Table 8:4: Temperature drop and heating rates (medium flow).

| Time(seconds) | Temperature drop (°C) | Heating rate(W) |
|---|---|---|
| 900 | 2.42 | 476.00 |
| 1800 | 2.04 | 401.26 |
| 3600 | 1.23 | 241.93 |
| 7200 | 0.73 | 143.59 |
| 9800 | 0.63 | 123.92 |
| 14400 | 0.60 | 118.02 |
| 18000 | 0.52 | 102.28 |
| 21600 | 0.52 | 102.28 |

Table 8:5: Temperature drop and heating rates (high flow).

| Time(seconds) | Temperature drop (°C) | Heating rate(W) |
|---|---|---|
| 900 | 2.08 | 565.81 |
| 1800 | 1.62 | 440.68 |
| 3600 | 1.05 | 285.63 |
| 7200 | 0.54 | 146.89 |
| 9800 | 0.48 | 130.57 |
| 14400 | 0.47 | 127.85 |
| 18000 | 0.45 | 122.41 |
| 21600 | 0.42 | 114.25 |

Figure 8:12 shows the relationship between the charge rate and mass flow rate of the store. It shows that at the start of the charge process, the higher the mass flow rate, the higher the charge rate. Generally for all flow rates, as the temperature gradient reduces, the effect of mass flow rate becomes negligible as the PCM melts. The result shows that the charge rate of the low flow is higher than the medium flow, which is not expected. The closeness of the low and medium flow could account for this behaviour. The difference between the flow rates is close (47-35=12g/s). Figure 8:12 shows that the charge rate stays at 100W, this can be attributed to heat loss to the ambient via the celotex insulation placed at the bottom and top of the PHE store.

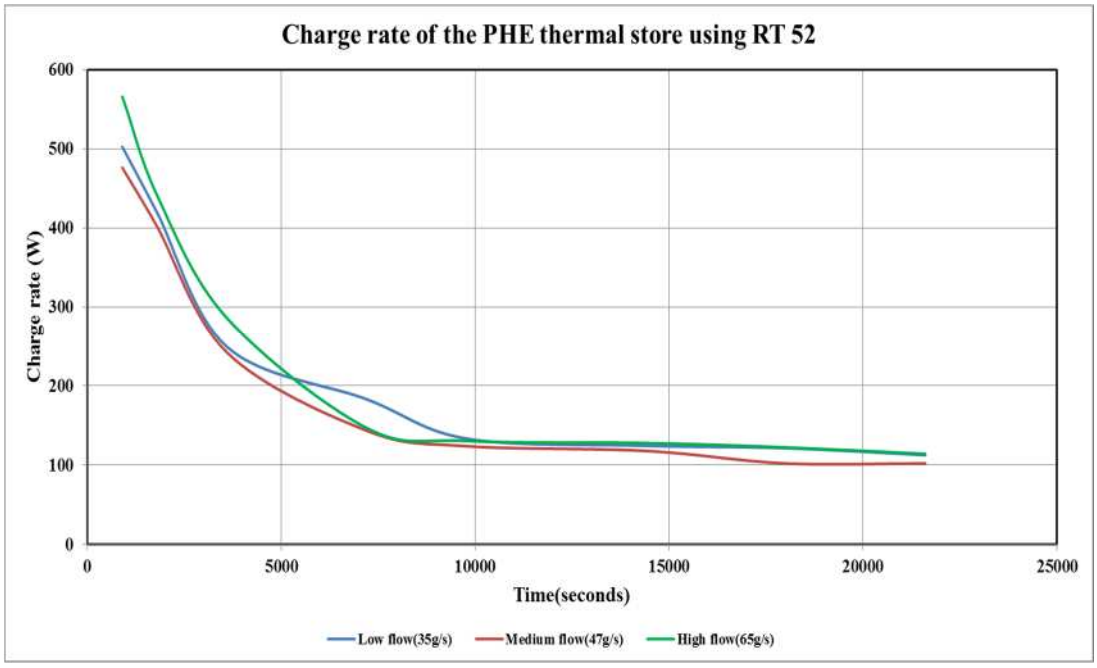


Figure 8:12: Charging rate of the store using RT 52

Figure 8:13 (a-c) shows the temperature profile for both the HTF and PCM during the discharging process at different flow rates. The store was discharged at different temperature; for the low flow (38°C), medium flow (47°C) and for Figure 8:13(c ), the store was allowed to discharge without use of the hot water bath. At low flow, there is a fluctuation in both the inlet and outlet HTF; this can be attributed to the interchange from the charging to the discharging process. A similar pattern is evident in medium flow, where the process is being stabilised after changing temperature from 60°C to the discharging temperature of 47°C.

Figure 8:13(c), shows that it is evident that it will take a long time for the PCM to solidify as there is no flow through the channels to facilitate heat transfer quicker on the rig. The temperature difference between the PCM and HTF is huge.

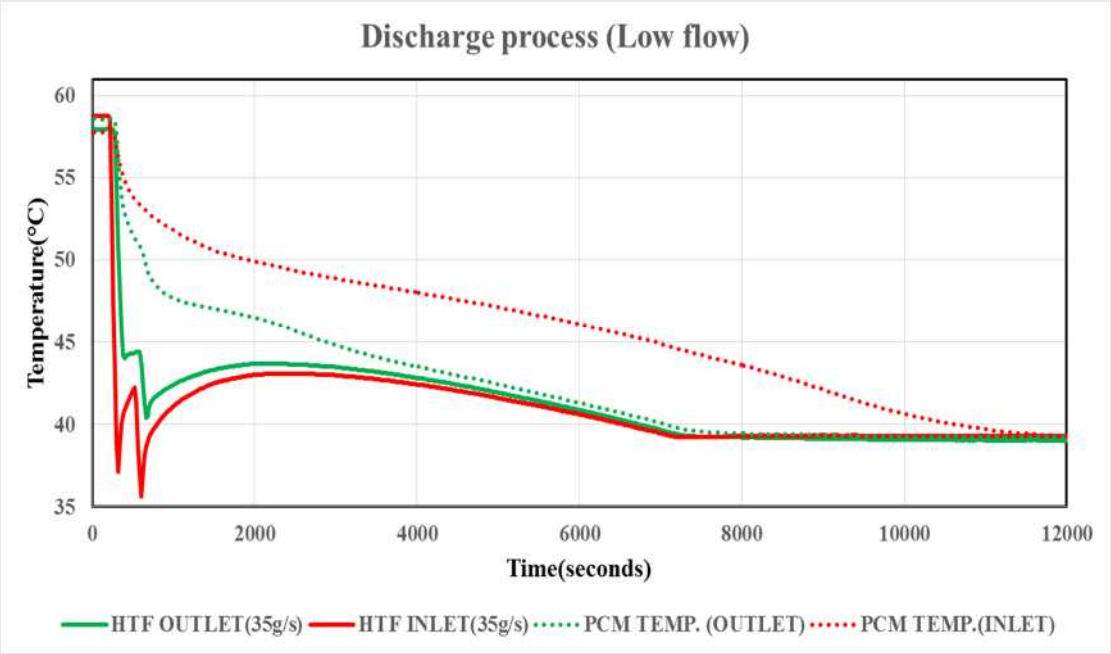


(a)

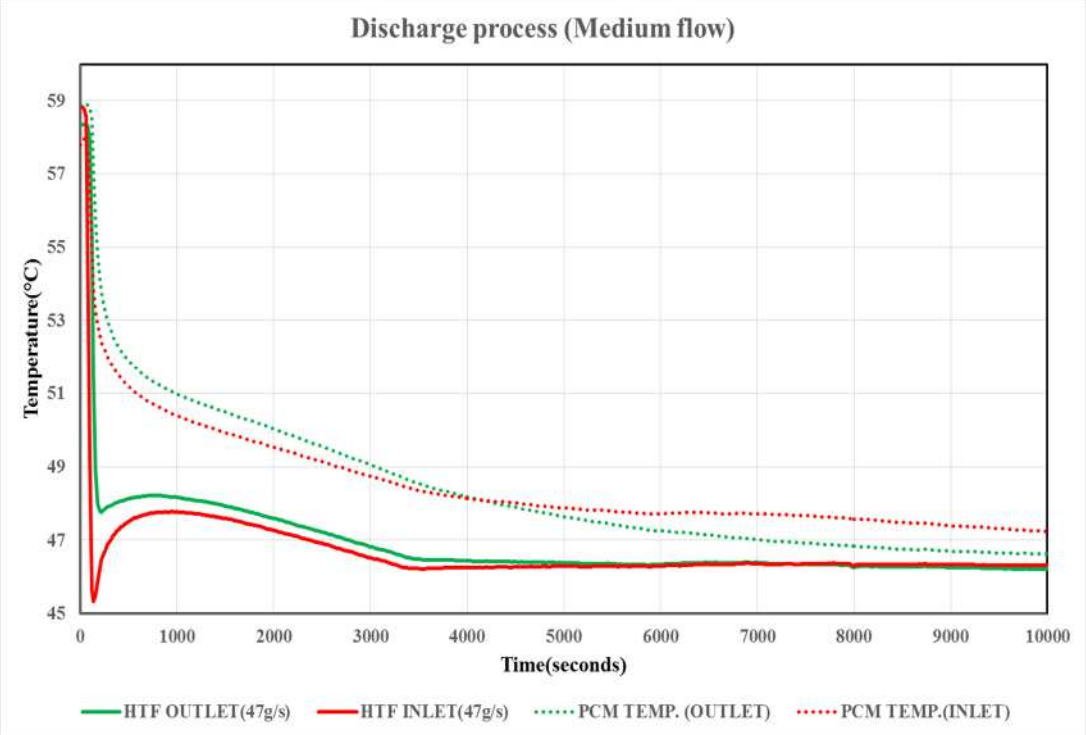


(b)

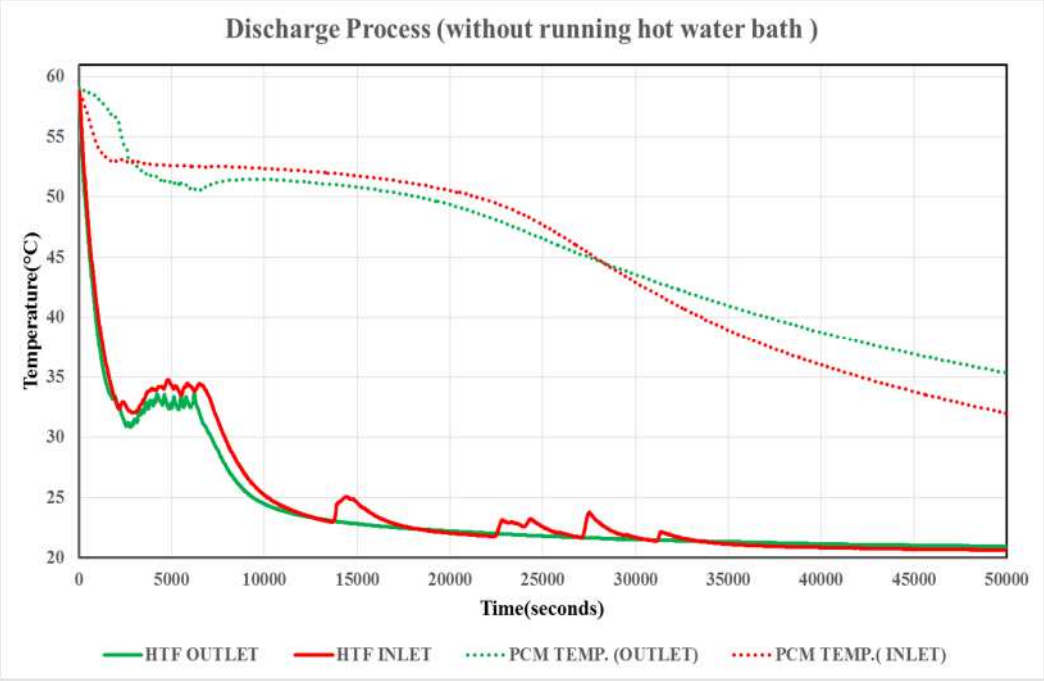


(c )

Figure 8:13: Temperature profile for the discharge process at different flows.

Table 8:6 and Table 8:7 shows a summary of the temperature drop and cooling rate (Watts) at specified periods. The temperature drops for the low flow result are higher than that for the medium flow at the same time, though the thermal store is discharged at different inlet HTF; 40°C and 46°C respectively. The results show that as the flow rate increases, the temperature drop decreases.

Table 8:6: Temperature drop and cooling rate(Low flow)

| Time(seconds) | Temperature drop | Cooling rate(W) |
|---|---|---|
| 900 | 1.05°C | 153.58 |
| 1800 | 0.65°C | 95.07 |
| 3600 | 0.40°C | 58.51 |
| 7200 | 0.02°C | 2.93 |

Table 8:7: Temperature drop and cooling rate(Medium flow)

| Time(seconds) | Temperature drop | Cooling rate(W) |
|---|---|---|
| 900 | 0.39°C | 76.60 |
| 1800 | 0.33°C | 64.82 |
| 3600 | 0.22°C | 43.21 |
| 7200 | 0.00°C | 0.00 |

## 8.4 Summary

Plate heat exchanger was used in the experiment using two different PCMs, RT 58 and RT 52. This was to facilitate and compare experimental and modelling results. Results obtained from the experiments shows that the use of this type of modular design of a plate heat exchanger could be beneficial and suitable for domestic application in conjunction with the heat pump. Three different flow rates (low, medium and high) were studied from the experiment and the effect on the heat transfer of the store. The experimental results for the charging and discharging processes show that the flow rate has little effect on the heat transfer during charging and discharging. Increasing the Inlet temperature of the HTF improves heat transfer. Also the power density of the plate heat exchanger thermal store increases with increase in temperature difference. The effect of varying the flow rate of the PHE store using RT 52 shows that the power density increases with increase in flow. The next chapter(Chapter 9) will look at the experimental result obtained by varying the inlet HTF temperature and flow rate to study the effect it has on a different kind of heat exchanger; serpentine heat exchanger. Chapter 10 focuses on the numerical model of the PHE store, where the experimental result for charging and discharging are validated.

# 9 Results from serpentine heat exchanger experiment.

## 9.1 Design of flow in serpentine heat exchanger

The result obtained from the experiment using the serpentine heat exchanger is discussed for both charging and discharging process. Similar flow terms as the plate heat exchanger are used; there are three flow terms, high flow, medium flow and low flow. The flow is termed “high flow” when the valve is fully opened; “medium flow” is a flow in the intermediate while “low flow” is the lowest possible flow allowable for the rig to operate.

The Reynolds number was calculated for each flow at different HTF temperatures. The viscosity of water at these temperatures was used in the Reynolds number calculations. The result of the calculation of the Reynolds number is presented in Table 9.1.

Table 9:1: Reynolds number at different flow rate and inlet HTF temperature.

| | **Reynolds Number** | | |
|---|---|---|---|
| **Inlet HTF temperature** | Low flow | Medium | High |
| **60°C** | 3043 | 6522 | 13043 |
| **65°C** | 3260 | 6985 | 13971 |
| **70°C** | 3518 | 7539 | 15077 |

Based on the Reynolds number calculations, the medium and high flows are regarded as turbulent flow, while the low flow is a transition flow. The Nusselt number and heat transfer coefficient can be determined based on Nusselt correlation. The heat transfer coefficient is calculated using Equation 9.1 and Equation 9.2.

$$Nu = \frac{hD_h}{k} \qquad 9.1$$

$$\Pr = \frac{C_p \mu}{k} \qquad 9.2$$

The Dittus-Boelter Nusselt Correlation (Equation 9.3) was used for the turbulent flow while Gnielinski correlation (Equation 9.4 and Equation 9.5) used for the low flow, because it falls within the transition flow regime. Cengel and Ghajar (2011) stated that the Gnielinski correlation could be used as rough estimates of the friction factor and heat transfer coefficient in the transition region. Kakaç et al. (1987) mentioned that, based on the range of the Reynolds numbers and Prandtl number, that the Nusselt correlation by Gnielinski could be used in the fully developed transition region. It is assumed the copper pipe used for the SHE are smooth pipes; thus friction factor (f) based on Gnielinski correlation was applied.

$$Nu = 0.023\,\mathrm{Re}^{0.8}\,\mathrm{Pr}^{n^*} \quad \begin{matrix}(n^*=0.4 \text{ for heating}) \\ (n^* = 0.3 \text{ for cooling})\end{matrix} \qquad 9.3$$

For the Dittus-Boleter correlation to be used The following conditions needs to be met; Reynolds number should be greater than or equal to 10000($\mathrm{Re} \geq 10000$) and the Prandtl number should be in the range of; $0.7 \leq \mathrm{Pr} \leq 160$.

Gnielinski correlation is expressed as shown in Equation 9.4. Equation 9.5 is used to calculate the friction factor (f) based on the assumption that the serpentine pipe is smooth. The Reynolds number and Prandtl number should be in the range of $3\text{x}10^3 < \mathrm{Re} < 5\text{x}10^6$ and $0.5 \leq \mathrm{Pr} \leq 2000$ respectively for the Gnielinski correlation to be used.

$$Nu = \frac{\left(\frac{f}{8}\right)(\mathrm{Re}-1000)\,\mathrm{Pr}}{1+12.7\left(\frac{f}{8}\right)^{\frac{1}{2}}\left(\mathrm{Pr}^{\frac{2}{3}}-1\right)} \qquad 9.4$$

$$f = \left(0.790\ln \mathrm{Re} - 1.64\right)^{-2} \qquad 9.5$$

The results of the calculation are presented using Table 9:2 to Table 9:4. Both correlations were used to calculate the Nusselt number and heat transfer coefficient for the transition flow.

Table 9:2: Gnielinski correlation result (Low flow)

| | | | | Gnielinski correlation | Gnielinski correlation |
|---|---|---|---|---|---|
| Flow type | Temperature(°C) | Prandtl Number | Frictional coefficient(f) | Nusselt Number | h(W/m$^2$K) |
| Low | 65 | 2.77 | 0.04 | 18.01 | 1892.76 |
| Low | 70 | 2.55 | 0.04 | 19.12 | 2022.18 |

Table 9:3: Dittus-Boelter correlation result (Low flow)

| | | | Dittus-Boetler correlation | Dittus-Boetler correlation |
|---|---|---|---|---|
| Flow type | Temperature(°C) | Prandtl Number | Nusselt Number | h(W/m$^2$K) |
| Low | 65 | 2.77 | 22.35 | 2349.21 |
| Low | 70 | 2.55 | 22.99 | 2431.33 |

Table 9:4: Dittus-Boelter correlation result (Medium and high flow).

| Flow type | Temperature(°C) | Prandtl Number | Nusselt Number(Nu) | h(W/m$^2$K) |
|---|---|---|---|---|
| High | 60 | 2.99 | 69.86 | 7286.41 |
| High | 65 | 2.77 | 71.60 | 7525.40 |
| High | 70 | 2.55 | 73.66 | 7788.58 |
| Medium | 65 | 2.77 | 41.12 | 4321.96 |
| Medium | 70 | 2.55 | 42.31 | 4473.60 |

Figure 9:1 shows the relationship between the Reynolds number and Nusselt number from the SHE experiment using both correlations. It shows that as the Reynolds number increases, so does the Nusselt number. Based on Equation 9.1, the Nusselt number is directly proportional to the heat transfer coefficient, thus as the Nusselt number increases, so does the heat transfer coefficient. The higher the Nusselt number or heat transfer coefficient, the more the dominance of convection in the heat transfer. Based on calculations considering the Dittus-Boelter and Gnielinski correlation, Figure 9:1 shows that there is deviation in the Nusselt number considering each correlation. The results show that at lower flow (Re<9000), the Nusselt number is overestimated if Dittus-Boelter correlation is used. However at higher flow (Re>9000), the Nusselt number is underestimated. From the calculation of the Nusselt number and heat transfer coefficient using Gnielinski and Dittus-Boelter correlation for the transition flow as shown in Table 9:2 and Table 9:3, it was observed that there is a percentage difference of 21.52% and 18.37% at 65°C and 70°C fluid temperatures respectively. This difference is significant, thus it is important to use the appropriate correlation for each flow regime. Table 9:4 shows the result obtained for the medium and high flow using Dittus-Boleter correlation. It was observed that the heat transfer

coefficient at the same inlet HTF temperature, but different flow rate differs. Heat transfer coefficient is higher at high flow when compared to the medium flow.

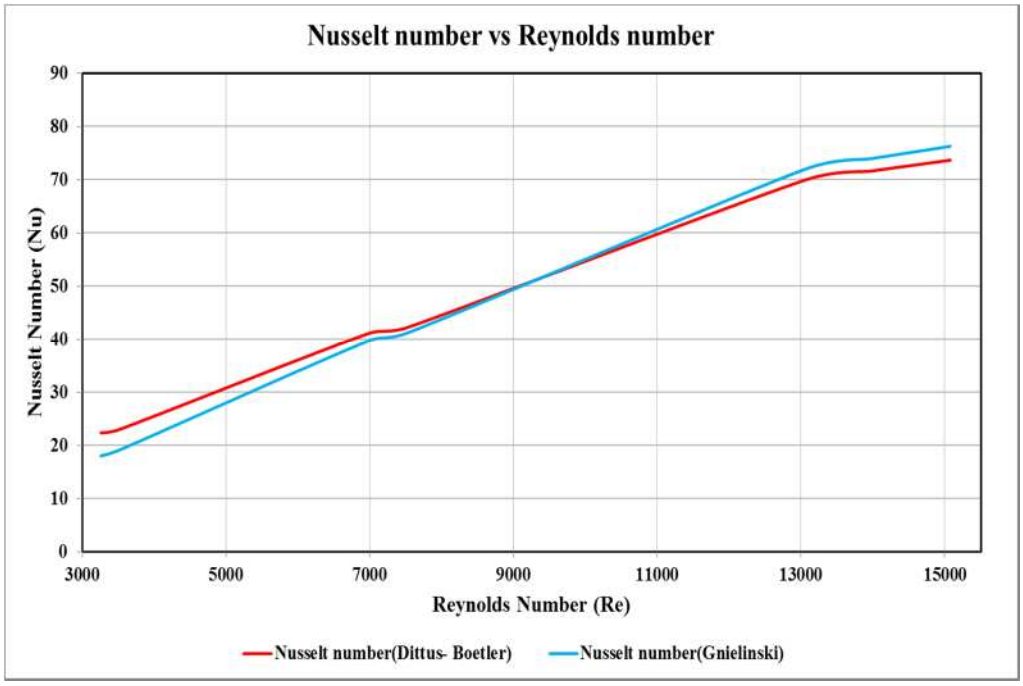


Figure 9:1: Plot of Nusselt number and Reynolds number.

## 9.2 Charging experiment (SHE).

The charging process is discussed based on the temperature drop, charge rate and amount of energy given by the HTF during charging. Figure E1 to Figure E7 shows the temperature drop that occurs over time, as a result of the heat transfer between the PCM and HTF flowing through the copper pipes. Appendix G shows the room temperature at which each experiment was carried out. The temperature drop is the difference between the inlet HTF temperature and the outlet HTF temperature. The discussion of the charging process is based on the effect of varying flow rates (low, medium and high flow), inlet HTF temperatures (60, 65 and 70°C) and comparing the temperature drop between the inlet HTF and outlet HTF temperature. The store is fully charged when the PCM temperatures exceeds its melting temperature of 52°C. This was observed from the temperature readings of the nine thermocouples located at A1 to C3, which measured the PCM temperature on the rig.

### 9.2.1 Effect of varying mass flow rate.

For this research, the mass flow rate was changed thrice by changing the valve's positions; to obtain high (30g/s), medium (15g/s), and low flow (7g/s). This is to study

the effect of the mass flow rate on the thermal behaviour of the PCM on the rig and its rate of melting as the HTF flows through the copper pipe. The temperature drop throughout the charging process is described using Figure E1 to Figure E7 and Table 9:6. Low and medium flows were charged at two different inlet HTF temperatures; 65 and 70°C. Results for high flow involve three different inlet HTF temperatures (60, 65 and 70°C). Table 9:5 shows an overview of the mass flow rate and inlet HTF temperatures used for the charging process.

Table 9:5: Overview of charging process

| Flow type | Flow rate value (g/s) | Inlet HTF temperatures |
|---|---|---|
| Low flow | 7 | 65 and 70°C |
| Medium Flow | 15 | 65 and 70°C |
| High flow | 30 | 60,65 and 70°C |

The concept of using an inlet heat transfer temperature of 60°C was discontinued at lower flow rates (15g/s and 7g/s), because the time of melting resulted into long hours of constant charging for the store to be fully charged. As the concept is to melt the PCM quickly and recover the energy at a lower cost of electricity, experiments at HTF inlet temperature of 60°C were discontinued for low and medium flows. The temperature difference between the phase change temperature and the inlet HTF at 60°C is about 8°C (60-52=8°C), which could have accounted for the long melting time. Heat loss could also be a contributing factor to the lengthy charging time. Experiment at inlet HTF temperature of 60°C was only done with the valve fully opened (high flow).

### 9.2.2 Temperature drop during charging process.

Figure E1 to Figure E2 shows the temperature drop that occurs at a flow rate of 7g/s (low flow) for two different inlet HTF temperatures (65°C and 70°C). The temperature drop at inlet HTF temperature of 70°C is more than at inlet HTF temperature of 65°C. Both figures show a similar pattern in the temperature–time graph; where there is an initial huge temperature difference and as the PCM melts, the temperature drop reduces towards the end of the experiment. Figure E2 shows that the melting time is shorter for an inlet HTF temperature of 70°C when compared to Figure E1 for an inlet

HTF temperature of 65°C at the same flow rate. This is due to the time it takes the PCM to attain its melting temperature as shown in Figure 9:15, Figure E18 and Figure E19 for inlet HTF temperature of 65°C and Figure 9:16, Figure E20 and Figure E21 for inlet HTF temperature of 70°C .

The temperature profiles (Figure E1 to Figure E7) shows that the temperature drop at the start of the experiment is larger than at the end of the experiment. This can be attributed to the fact that at the beginning of the experiment, the PCM starts to melt gradually as the hot fluid flows through the copper pipes. Once the PCM starts to change phase (from solid to liquid), the HTF loses more heat to the PCM, hence the difference in the temperature drop at the start and end of the experiment. It is also noticeable at inlet HTF temperature of 60°C and 65°C, the temperature drop at the end is much smaller when compared to inlet HTF temperature of 70°C.It is observed that as the temperature of the PCM increases, the temperature difference between the inlet HTF and outlet HTF decreases for all experiment at this flow.

Rate of melting was faster at higher inlet HTF temperature. The greater the temperature difference between the PCM melting temperature and inlet HTF temperature, the faster it takes the PCM to melt. Table 9:6 shows the change of temperature drop at different times during the charging process.

Table 9:6: Overview of the temperature drop for the charge process.

| **Low Flow** | | | | | |
|---|---|---|---|---|---|
| **Charging temperature** | 3600sec. (1hour) | 10000sec. (2.7hours) | 20000sec. (5.6hours) | 300000sec. (8.3hours) | 40000sec. (11.1hours) |
| 65°C | 10.66°C | 8.33°C | 6.08°C | 5.70°C | 5.26°C |
| 70°C | 12.58°C | 10.62°C | 10.11°C | 10.03°C | 8.91°C |
| **Medium Flow** | | | | | |
| **Charging temperature** | 3600sec. (1hour) | 10000sec. (2.7hours) | 20000sec. (5.6hours) | 250000sec. (6.9hours) | |

| | | | | | |
|---|---|---|---|---|---|
| 65°C | 4.32°C | 4.49°C | 3.77°C | 1.28°C | |
| 70°C | 6.29°C | 6.12°C | 4.32°C | 3.75°C | |
| **High Flow** | | | | | |
| **Charging temperature** | **3600sec. (1hour)** | **10000sec. (2.7hours)** | **20000sec. (5.6hours)** | **30000sec. (8.3hours)** | |
| 60°C | 1.85°C | 1.61°C | 1.55°C | 1.40°C | |
| 65°C | 2.52°C | 2.59°C | 2.20°C | 1.75°C | |
| 70°C | 3.68°C | 3.51°C | 2.84°C | Fully melted | |

From Table 9:6, the highest inlet HTF temperature, 70°C possess the highest temperature drop, when compared to that at 60°C and 65°C at different flow rates. The charging time is affected by the inlet HTF temperature. The higher the inlet HTF temperatures, the quicker the charging time. For example, at flow rate of 30g/s, the charging time is longer for inlet HTF temperature of 60°C when compared to the charging time at 65°C and 70°C. Figure E5 shows the charging time to be 79,200 seconds (22 hours); this was due to the time it took for the store to be fully charged as shown in the PCM temperatures in Figure 9:10, Figure E8 and Figure E9. Figure E6 shows the charging time for an inlet HTF temperature of 65°C to be 39,600 seconds (11 hours) based on the PCM temperature on Figure 9:11, Figure E10 and Figure E11. Figure E6 shows the charging time for the highest inlet HTF temperature, 70°C to be 21,600 seconds (6 hours), since the PCM temperature melts quicker as shown in Figure 9:12, Figure E12 and Figure E13. For low flow, the charging time for inlet HTF temperature of 65°C is 79,200 seconds (22 hours) based on the PCM temperature as shown in Figure 9:15, Figure E18 and Figure E19. The charging time at the same flow rate for inlet HTF temperature of 70°C is 50,400 seconds (14 hours). The PCM temperatures are presented in Figure 9:16, Figure E20 and Figure E21. The charging time for inlet HTF temperature of 65°C and 70°C at flow rate of 15g/s (medium flow) are twenty-two and seven (7) hours respectively. Figure 9:13, Figure E14, Figure E15 and Figure 9:14, Figure E16 and Figure E17 shows the PCM temperature for each inlet HTF temperature. Based on the charging time to melt the PCM, it shows that the rate

of melting is higher at higher inlet HTF temperature. Also, the temperature difference between the inlet and outlet HTF temperature at high flow is smaller when compared to low and medium flow.

Figure 9:2 and Figure 9:3 are used to compare outlet HTF temperature profile at same inlet HTF temperature, but different flow rate. The experimental result of the outlet HTF temperature from Figure E1 to Figure E7 are compared using Figure 9:2 and Figure 9:3 for two different inlet HTF temperatures (65°C and 70°C) at varying mass flow rate. It shows that the highest outlet HTF temperature is at high flow, whilst the least outlet HTF temperature is obtained at low flow for both cases.

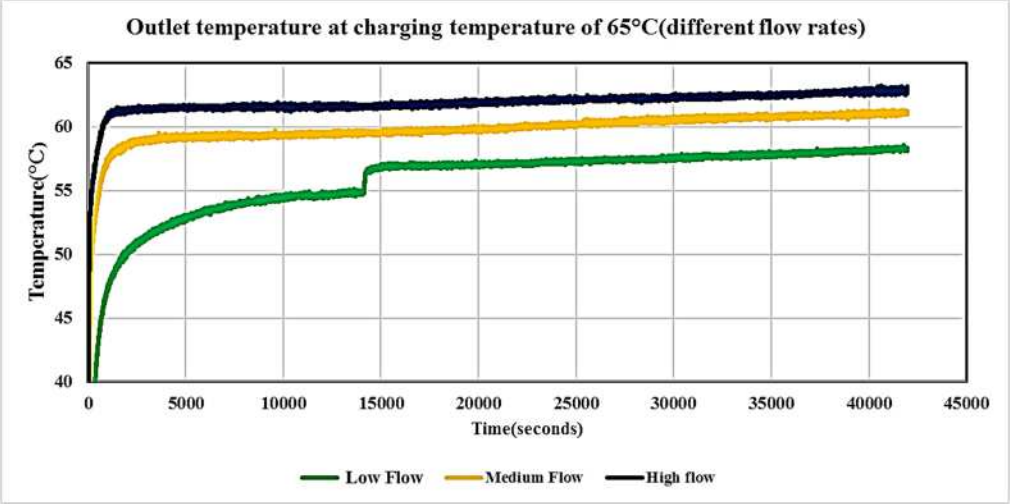


Figure 9:2: Outlet HTF temperature at different flow rate (inlet HTF 65°C).

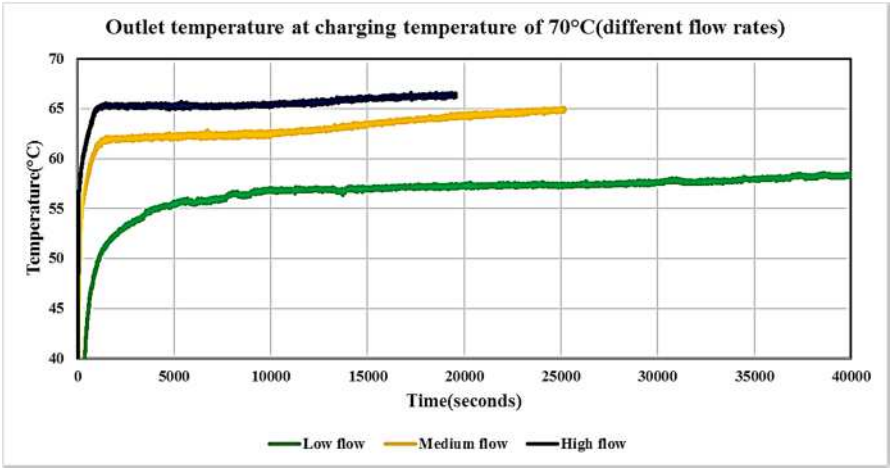


Figure 9:3: Outlet HTF temperature at different flow rate (inlet HTF 70°C).

### 9.2.3 Effect of the varying inlet HTF temperature and flow rate on the charge rate and energy.

Varying the HTF inlet temperature has a corresponding effect on the HTF outlet temperature, charge rate and amount of energy stored as the fluid flows through the serpentine rig. The heat transfer via conduction between the HTF within the copper pipes and the PCM caused the temperature change across the rig. Figure 9:4 and Figure 9:5 shows that the charge rate of the SHE at different flow rate for inlet HTF temperatures of 65°C and 70°C respectively. It shows that at the start of the charging process, the higher the mass flow rate, the higher the charge rate. However, as the charging process continued, the thermal gradient between the PCM and the HTF reduces and the effect of the mass flow rate becomes negligible. This effect is noticeable more at inlet HTF temperature of 65°C compared to inlet HTF temperature of 70°C. The charge rate at inlet HTF temperature of 70°C is higher than at an inlet HTF temperature of 65°C, as shown on Figure 9:4 and Figure 9:5.

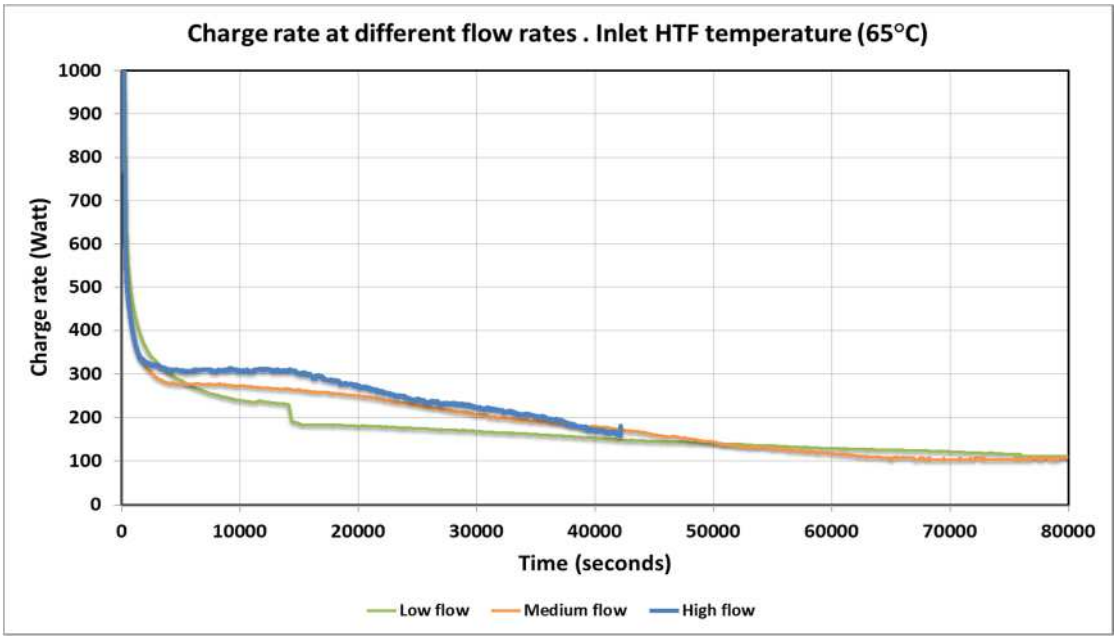


Figure 9:4: Charge rate at inlet HTF temperature of 65°C

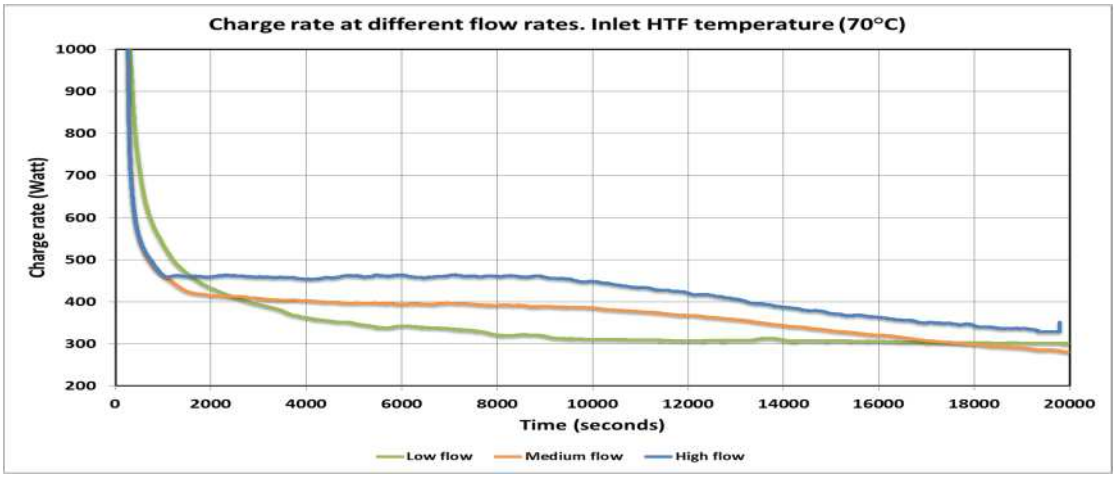


Figure 9:5: Charge rate at inlet HTF temperature of 70°C

Figure 9:6 to Figure 9:8 shows the effect of varying the HTF inlet temperature on the charge rate of the store. The length of time to charge the thermal store is different for each inlet HTF temperature. Figure 9:8 shows a shorter charging time during the charging process at inlet HTF temperature of 70°C when compared to results at inlet HTF temperature of 60°C and 65°C.

For the charge rate at low flow, medium flow and high flow, shown in Figure 9:6, Figure 9:7 and Figure 9:8 respectively, the charge rate increases as the inlet HTF temperature increases. The charge rate at inlet HTF temperature of 70°C is greater than at an inlet HTF temperature of 60°C and 65°C. The results show that the inlet HTF temperature variation has a significant effect on the charging process. Overall the higher the mass flow rate and inlet HTF temperature, the higher the charge rate as shown in the aforementioned figures.

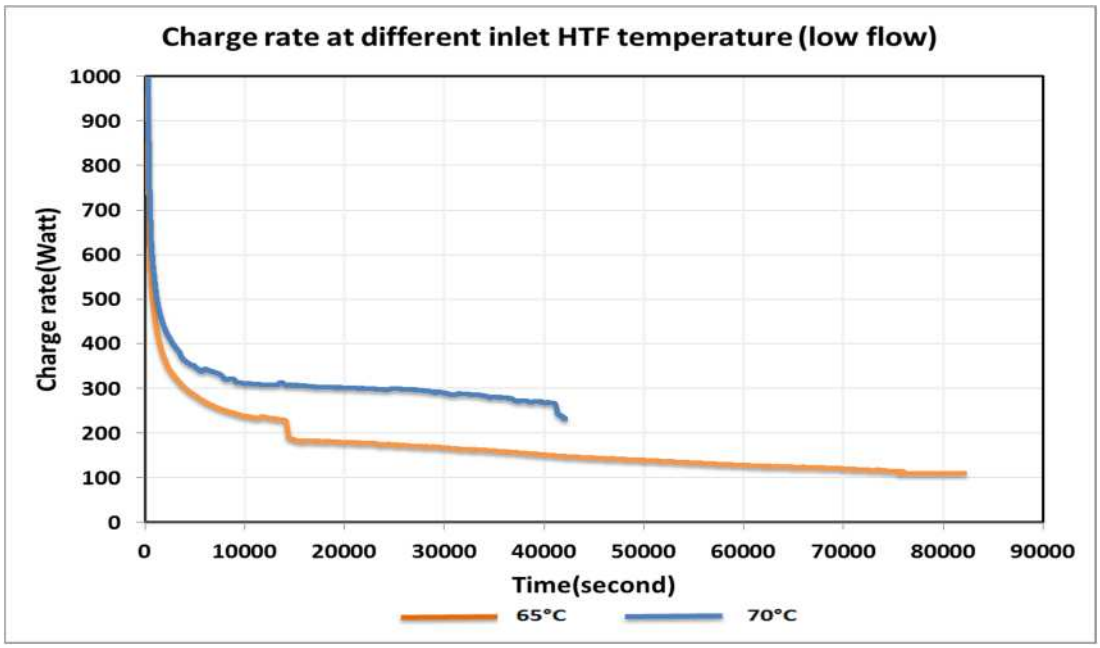


Figure 9:6: Charge rate at different HTF temperature (Low flow).

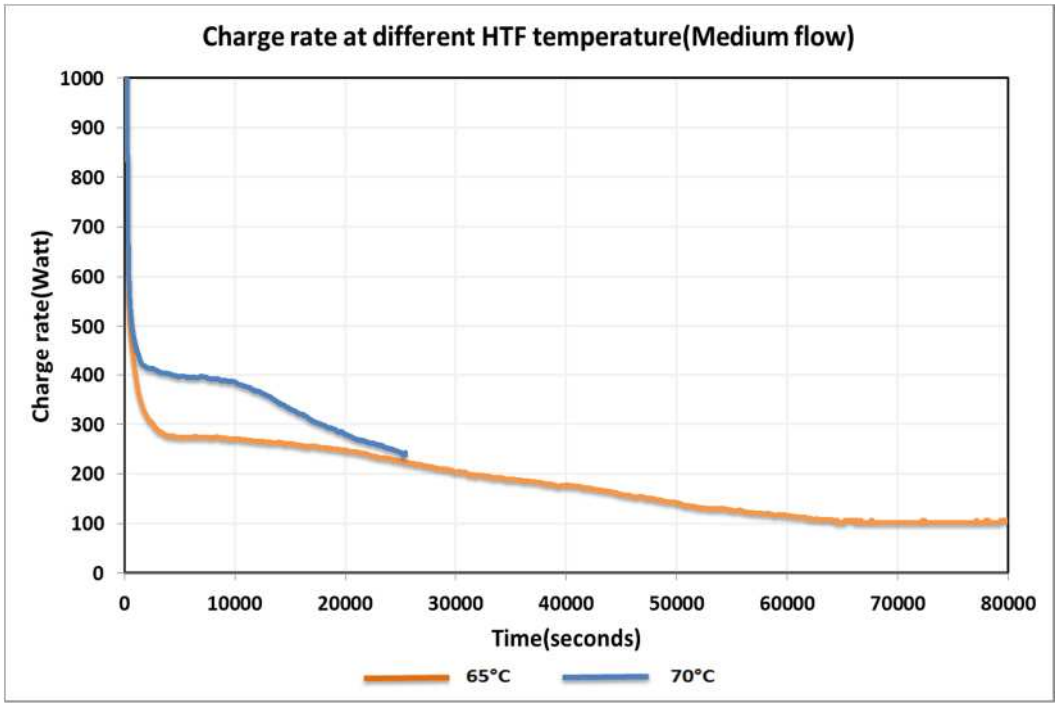


Figure 9:7: Charge rate at diffeent HTF temperature (Medium flow).

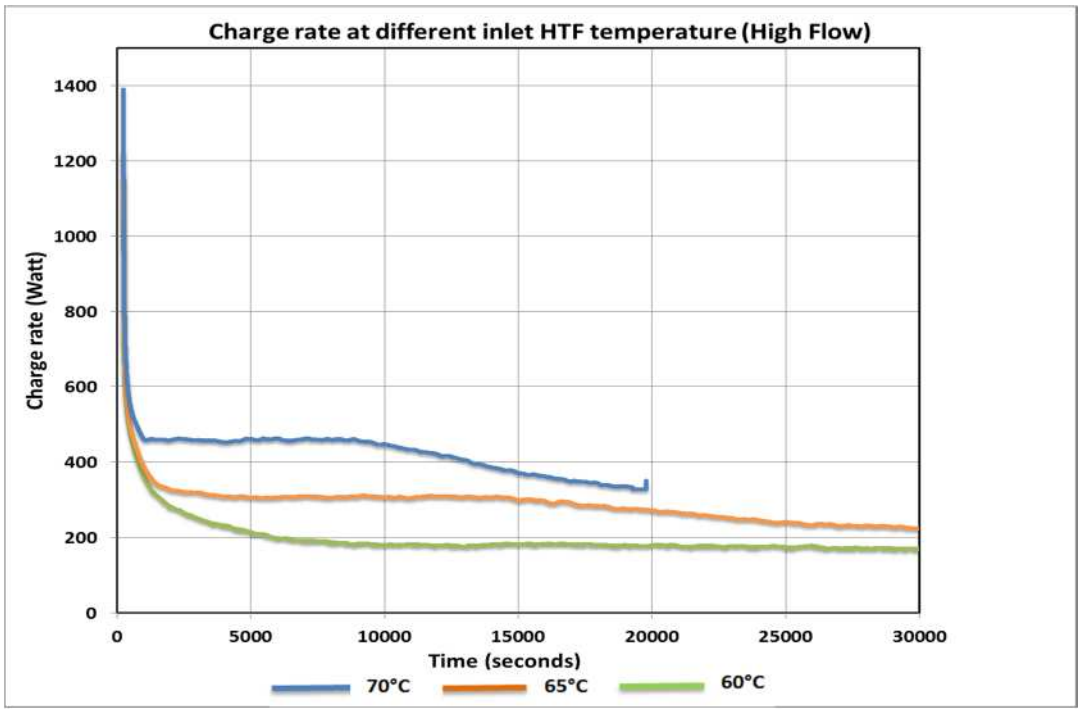


Figure 9:8: Charge rate at different inlet HTF temperature(High flow).

Figure 9:9 shows the amount of energy stored at high flow, when the store is charged at three different inlet HTF temperatures, 60°C, 65°C and 70°C. The amount of energy stored during the charging process at high flow shows that the higher the inlet HTF temperature, the higher the amount of energy stored. The results show that increasing the inlet HTF temperature, the time need to charge the store decreases. This is useful for determining the temperature at which the store can be charged within off peak electricity time.

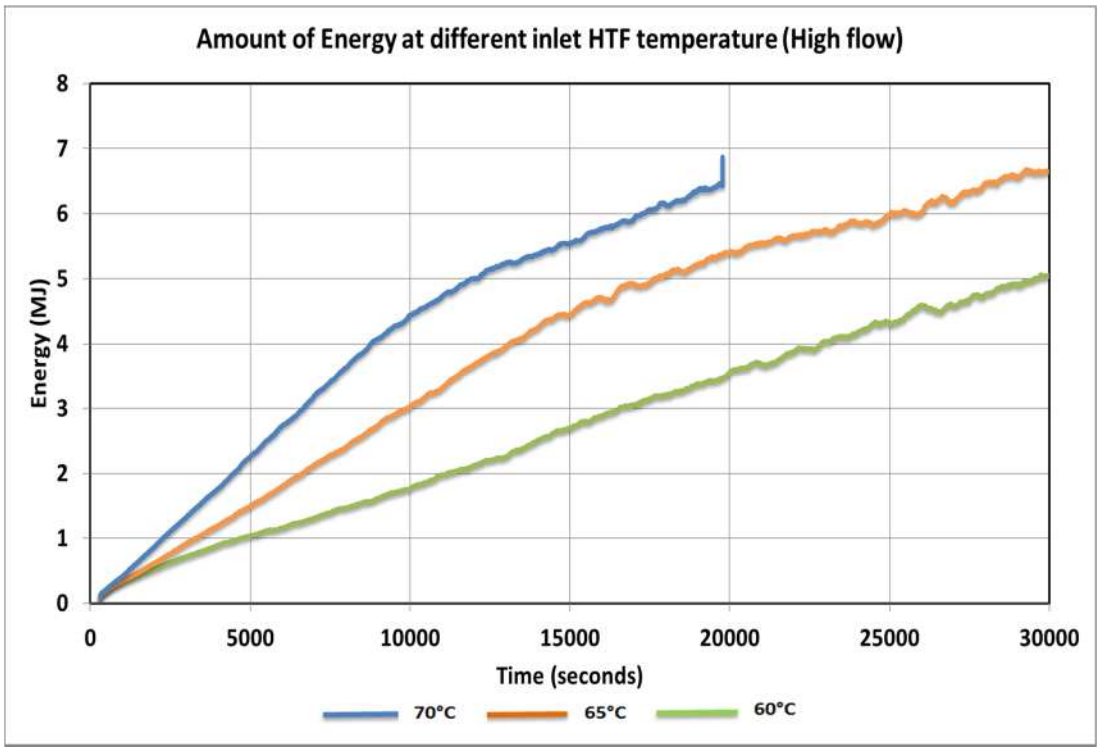


Figure 9:9: Amount of energy stored at different inlet HTF temeprature.

### 9.2.4 PCM temperature across the rig during the charge process.

Based on the result from the experiment using the serpentine heat exchanger, the phase change temperature across the rig was monitored using thermocouples positioned at different locations. The design of the rig and layout of how the thermocouples are positioned is presented in Figure 7:4. Figure 7:4 shows that the melting commences at the inlet side of the serpentine heat exchanger, as this has the highest temperature from the hot water bath. The thermal behavior of the PCM is discussed as it affects the HTF temperature during the experiment. The PCM temperature was monitored during charging and discharging process.Figure 9:10 to Figure 9:16 describes the thermal behavior of the PCM as the HTF flows through the copper pipes during the charging process. Also, the result from the experiment is discussed using Figures E1 to Figures E21 in Appendix E. The PCM temperatures at thermocouple positions; A2B2C2 and C1C2C3 are discussed in detail as well as references made to the figures in Appendix E.

Figure 9:10 to Figure 9:12 and Figure E8 to Figure E13 in Appendix E describes the PCM temperatures at high flow for different charging temperatures; 60°C, 65°C and 70°C. Figure 9:10 shows that the charging time at inlet HTF temperature of 60°C has the longest charging time, while Figure 9:12 shows that the charging time at inlet HTF

of 70°C is the shortest. Figure 9:11 shows the charging time at inlet HTF of 65°C is an intermediary between the aforementioned inlet HTFs. The PCM temperature at position C3 rises fastest when compared to A3 and B3 (see Figure E9, Figure E11 and Figure E13). This is unexpected, as A3 is expected to be the point with the highest temperature as result of its position, being the first point of heat transfer within the rig. However C3 has the highest temperature considering the pipe orientation (axially). This could be attributed to the position of the thermocouple into the PCM from the top of the thermal store. PCM at position A2B2C2 shown in Figure 9:11 exhibit a different trend as the thermocouples B2 and C2 have the highest temperature; although there is a small temperature change as the temperature of the PCM rises over time. PCM at A1B1C1 show a similar trend to the PCM at A3B3C3.The PCM temperature at C1 has the highest temperature when compared to B1 and A1 (See Figure E9).

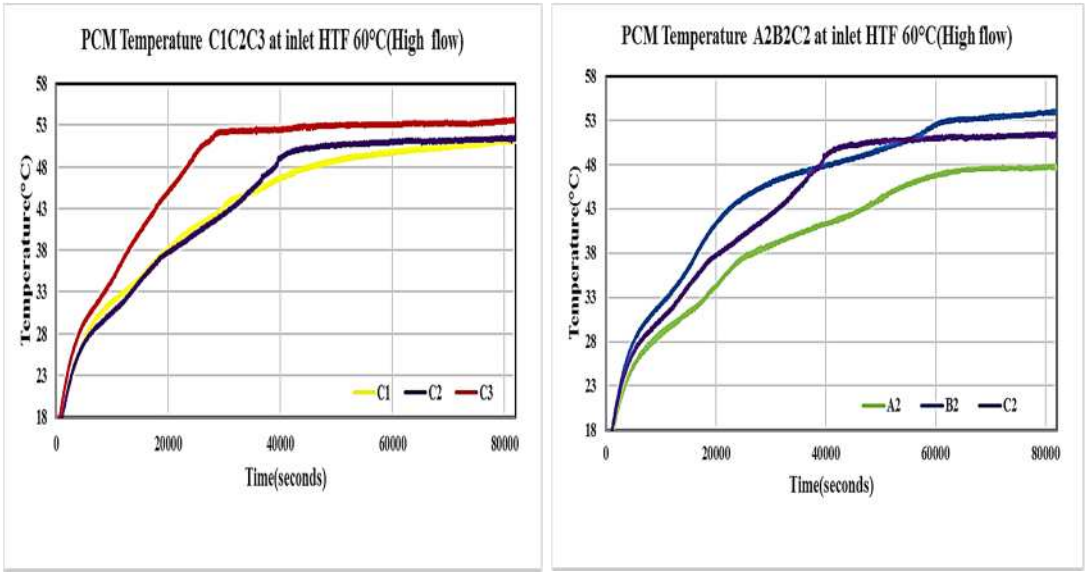


Figure 9:10: PCM temperature at radial (C1C2C3) and axial points (A2B2C2) at 60°C (high flow).

With reference to Figure 9:10, the radial effect of the heat transfer from the HTF to the pipe to the PCM outwardly, shows that the PCM at thermocouple position, C3 got completely melted before C1 and C2. This can be attributed to the position of the thermocouples at C1, C2, and C3 close to the inlet of the rig. The PCM close to the inlet has a higher temperature than other points as the PCM starts to melt within the rig. Radial positions, A1A2A3, B1B2B3 (see Figure E8) shows a different temperature trend, where the thermocouples located at the middle of the rig (B2, A2), PCM at this location behaves differently to the PCMs from the region of C1C2C3, result shows the

PCM temperature at A2 and B2 are greater than other radial points around it. This can be attributed to heat loss from edges of the tray due to the location of the PCM as shown in position of the thermocouple on the SHE(see Figure 7:4).

It is noticeable from Figure E8, that it takes a longer time for the PCM at A1-A3 and B1-B3 to reach its melting point of 52°C. The results show that having run the experiment for 80,000seconds (22hours), the entire PCM in the region A1-A3 and B1-B3 are not completely melted for the case of charging the store at 60°C (high flow).

Charging the thermal store at 65°C (high flow) as shown in Figure 9:11 shows that the PCM temperature profile is similar to the profile at C1-C3 (see Figure 9:10) for charging at 60°C. The result for charging the store at 65°C shows that PCM temperature at C3>C2>C1. The result also shows that the PCM temperature at A2 and B2 starts off being of a higher temperature than other radial points. The PCM melts faster while charging the store at 65°C than at 60°C. Figure 9:11 shows that all the PCM at the radial points; C1C2C3 and axial point; A2B2C2 respectively are fully melted with C3 and C2, the quickest to be melted. The PCM temperature along the path of the HTF flow (axially) shows that A1, A2, A3 have the lowest temperature profile (see Appendix E). From Figure 9:11, Figure E10 and Figure E11, it is noticeable that the PCM temperature at A1B1C1, A2B2C2, A3B3C3, rises in the following sequence; C3>B3>A3; C2>B2>A2 but for the PCM temperature at A1B1C1, it shows that the thermocouple at C1 rises rapidly but afterward plateaued. The PCM temperature at A3B3C3 has the highest temperature point as C3, followed by B3 and A3. Figure 9:11 shows that the PCM temperature at A2B2C2, B2 has the highest temperature, while the other points (A2 and C2) are closely packed with regards to temperature difference.

The results show that there are changes in the pattern at which the PCM temperature increases for all flows at different charging temperatures of 60°C, 65°C and 70°C. Considering the axial positions, where the thermocouples are positioned, to measure the PCM temperature; Figures E9, E11, E13, E15.E17, E19 and E21 from Appendix E shows that the PCM temperature at this thermocouple positions A3B3C3 for all three flows (low, medium and high), follow this sequence; C3>B3>A3.

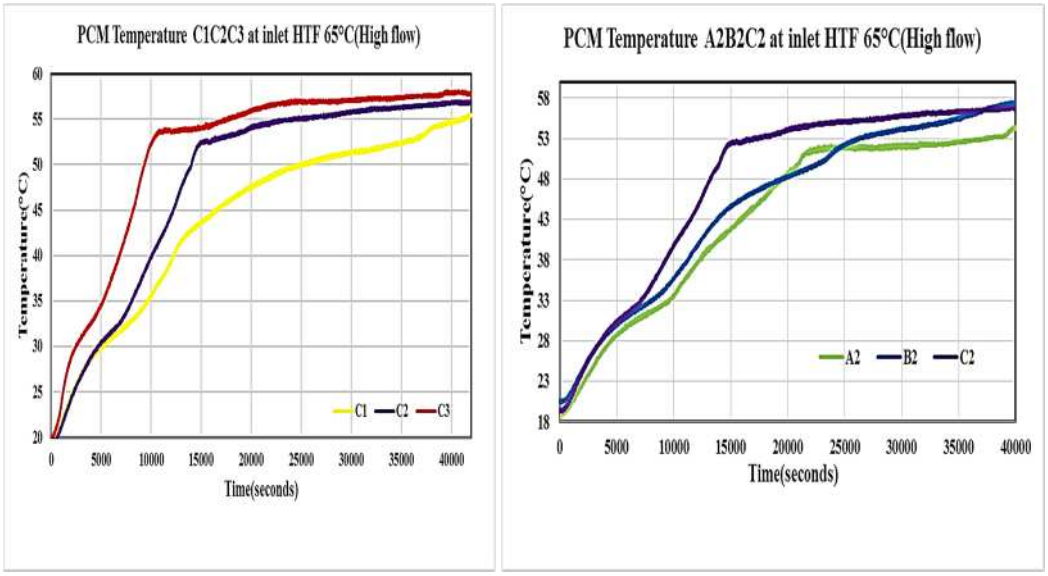


Figure 9:11: PCM temperature at radial (C1C2C3) and axial points (A2B2C2) at 65°C (high flow).

Figure 9:12 shows that the PCM has fully melted at 20,000seconds for charging the store at 70°C. The melting time for charging the store at 65°C as shown in Figure 9:11 was at 40,000seconds, while the longest charging time (80,000seconds) as shown in Figure 9:10 was at charging the store at 60°C. This shows that for high flow, the time of melting is increased, as the inlet HTF temperature decreases.

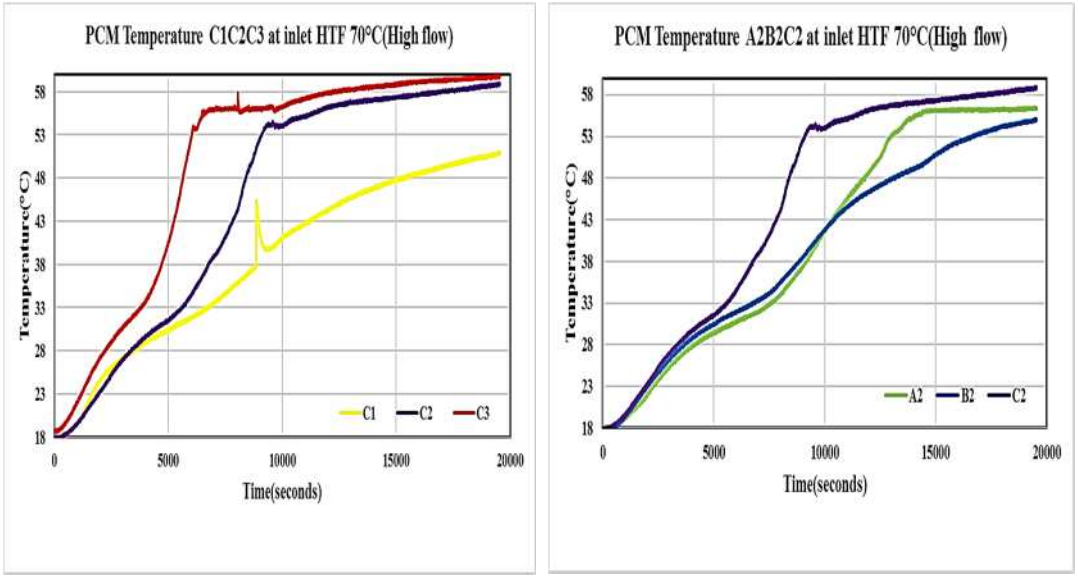


Figure 9:12: PCM temperature at radial (C1C2C3) and axial (A2B2C2) points at 70°C (high flow).

Figure 9:13 to Figure 9:14 and Figure E14 to Figure E17 in Appendix E, shows the experimental result from the medium flow when the store is charged at 65°C and 70°C, the charging time are 80000 and 25000seconds respectively. Based on this result, it means the experiment duration for charging PCM at medium flow was more than at charging the PCM at high flow for the same charging temperature.

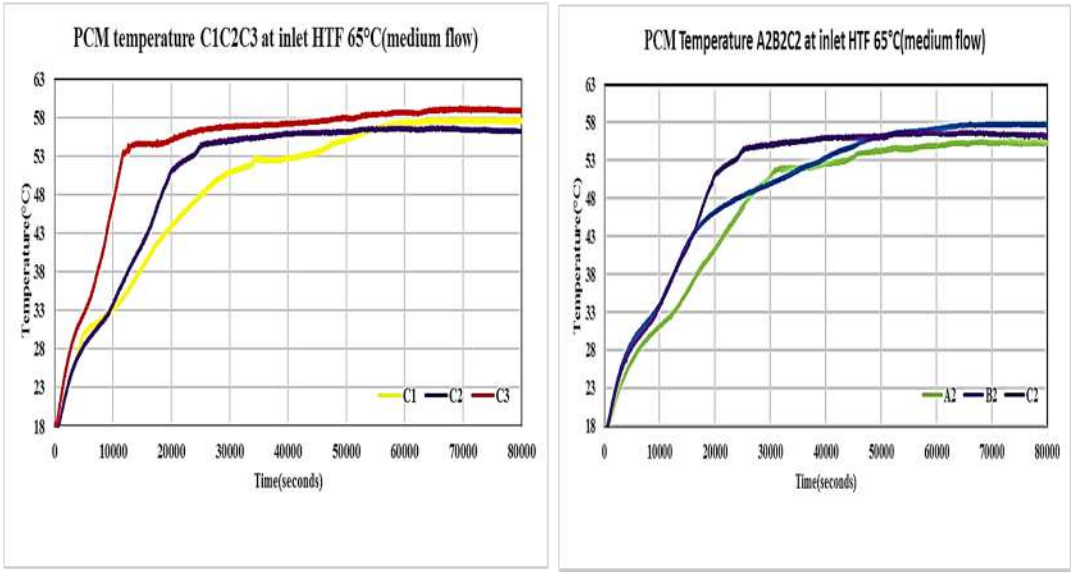


Figure 9:13: PCM Temperature for radial (C1C2C3) and axial (A2B2C2) points at 65°C (medium flow).

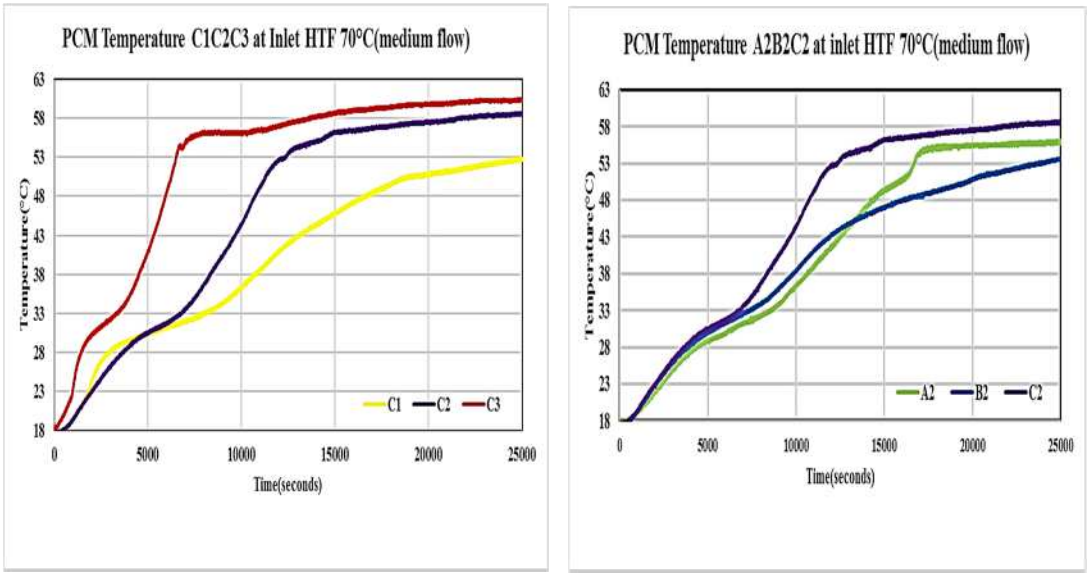


Figure 9:14: PCM Temperature for radial (C1C2C3) and axial (A2B2C2) points at 70°C (medium flow).

Figure 9:15 to Figure 9:16 and Figures E18 to Figure E21 in Appendix E, shows the PCM temperature from the experiment at low flow, when the store is charged at 65°C and 70°C.It is observed that the charging time when the store is charged at 65°C (80,000seconds) is more than when the store is charged at 70°C (45,000 seconds).

Figure 9:16 shows the PCM temperature when the store is charged at 70°C for the radial positioning of the PCM thermocouple vary, the highest PCM temperature are at C3, which is the closest to the inlet side of hot fluid entering the rig. The figure shows that C3>C2>C1, while Figures E16 shows the temperature profile at A3>A2>A1 and B3>B2>B1.

Considering the axial positioning of the thermocouple using Figure E21, it shows that the PCM temperature at thermocouple positions A1B1C1 increase in the order; C1>A1B1. PCM temperature at A1 and B1 are close together as they rise in temperature. Figure 9:16 shows the result that the PCM temperatures at A2B2C2 are close together as the temperature rises with C2 greater than A2 and B2 at the end of the charging process, though initially B2 was greater than A2C2 at the beginning of the charging process. Figure E21 shows that the heat transfer in this region is the first contact of the PCM with the hot fluid flowing from the bath. Thus, there is a faster response to melting of the PCM as C3 has a quicker rise in temperature when compared to B3 and A3. This region of the rig has the fastest response to the heat transfer between the HTF and the PCM.

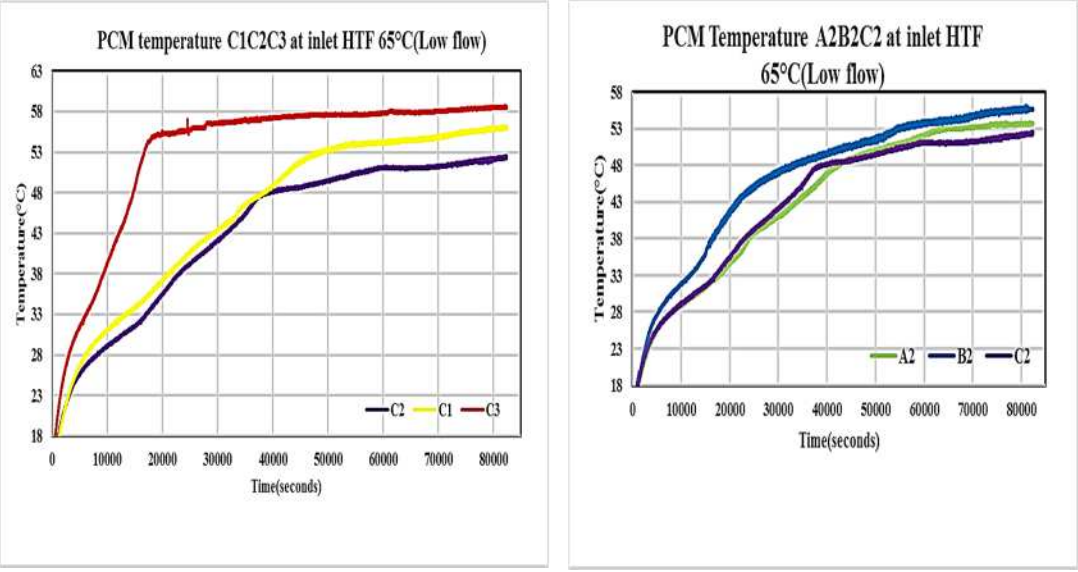


Figure 9:15: PCM Temperature for radial (C1C2C3) and axial (A2B2C2) points at 65°C (low flow).

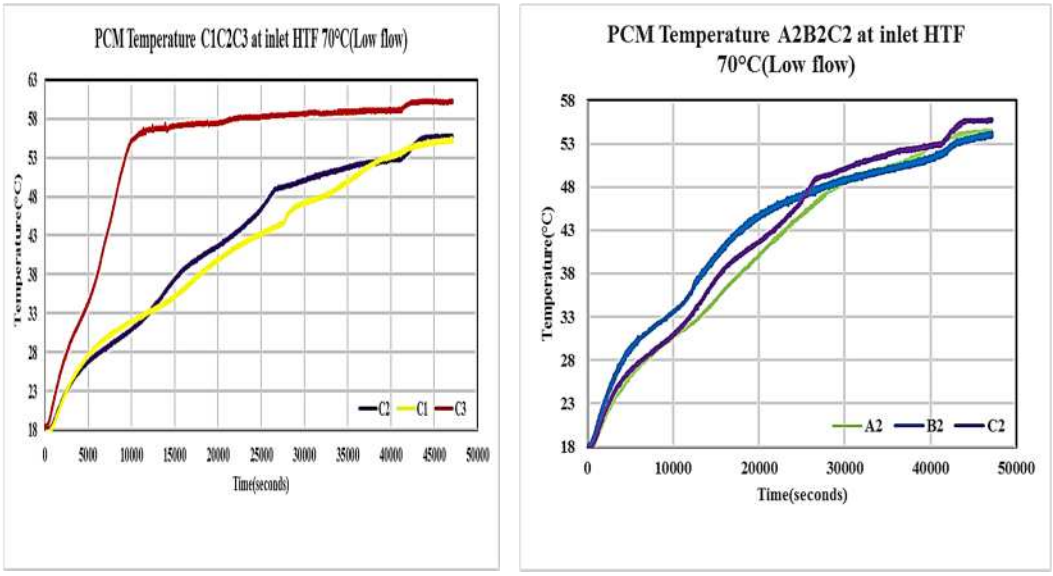


Figure 9:16: PCM Temperature for radial (C1C2C3) and axial (A2B2C2) points at 70°C (low flow) .

In general, the result for the PCM temperature at the thermocouple positioned axially at A1B1C1, A2B2C2 and A3B3C3 show that the PCM temperature at A1, A2 and A3 are the least. Considering the thermocouples positioned radially at A1A2A3, B1B2B3 and C1C2C3, it shows that A1, B1 and C1 has the least temperature profile trend. This means that the hottest zone on the rig (inlet) possesses the highest PCM temperature. The PCM temperature reduces radially away from the inlet to the outlet of the thermal store. The result shows that the entire PCM at different locations on the rig was fully melted; this can be verified by the PCM temperature at different thermocouple positions. The temperature must exceed the phase change melting temperature of the RT52, which is 52°C to be completely melted. However not all the points reach the PCM melting point when the store was charged at 60°C.

## 9.3 Discharging Experiment (SHE)

### 9.3.1 Effect of varying mass flow rate

The store was discharged at the same mass flow rate used in charging the store (same position of the valve on the valve). The discharge process was carried out at the same HTF inlet temperature or discharge temperature of 30°C in all cases. Figure F1 to Figure F7 shows the temperature drop at different flows (Low, medium and high).The figures show that discharge process at low flow has the highest temperature drop, while discharge process at high flow has the least. This means that during the discharge

or heat recovery process, the high flow results in a quick loss of heat within the store, when compared to other flows.

Results from the temperature drop within the thermal store at different flow rate, shows that the higher the flow rate, the higher the temperature drop (low temperature difference) that exist between the inlet and outlet HTF temperatures. The lowest temperature drops (high temperature difference) are obtained at the low flow, while the high flow has the highest temperature drop (low temperature difference). Table 9:7 shows the temperature drop at different times during the discharging process.

Table 9:7: Overview of the temperature drop for the discharge process.

| **Low Flow** | | | | | |
|---|---|---|---|---|---|
| **Discharging temperature** | **3600sec. (1hour)** | **10000sec. (2.7hours)** | **20000sec. (5.6hours)** | **300000sec. (8.3hours)** | **40000sec. (11.1hours)** |
| 65°C | 4.20°C | 3.21°C | 2.29°C | 1.29°C | 0.60°C |
| 70°C | 5.11°C | 3.90°C | 2.88°C | 1.42°C | 0.55°C |
| **Medium Flow** | | | | | |
| **Discharging temperature** | **3600sec. (1hour)** | **10000sec. (2.7hours)** | **20000sec. (5.6hours)** | **300000sec. (8.3hours)** | **40000sec. (11.1hours)** |
| 65°C | 2.59°C | 1.91°C | 1.43°C | 0.97°C | 0.22°C |
| 70°C | 2.52°C | 1.88°C | 1.57°C | 0.36°C | 0.13°C |
| **High Flow** | | | | | |
| **Discharging temperature** | **3600sec. (1hour)** | **10000sec. (2.7hours)** | **20000sec. (5.6hours)** | **30000sec. (8.3hours)** | |
| 60°C | 1.18°C | 1.11°C | 0.57°C | 0.29°C | |
| 65°C | 1.67°C | 1.17°C | 0.79°C | 0.28°C | |
| 70°C | 1.22°C | 0.99°C | 0.53°C | 0.30°C | |

Figure 9:17 and Figure 9:18 comprises of the outlet HTF temperatures result as the thermal store is discharged from 60°C,65°C and 70°C for different flows. Figure 9:17 shows the outlet HTF temperature at low flow from discharging the store from charging temperature of 65°C reduces to the set discharging inlet HTF temperature of 30°C at a longer time when compared to the other flows. The high flow is the quickest to drop in temperature.

Figure 9:18 shows a similar relationship with the result from Figure 9:17, where the results show that from discharging the store from 70°C. At high flow, the outlet HTF temperature drops quicker, when compared to the other flows. The store is discharged at inlet HTF temperature of 30°C. It also shows the store is discharged at a shorter time at high flow. Figure 9:18 shows the outlet temperature at low flow reduces to the set discharging inlet HTF temperature of 30°C at a longer time when compared to the medium and high flow. The thermal store discharges quicker at a higher flow compared to the low and medium flow results from the experiments. At low and medium flows, the thermal store gradually recovers heat from the PCM, as the HTF temperature slowly drops.

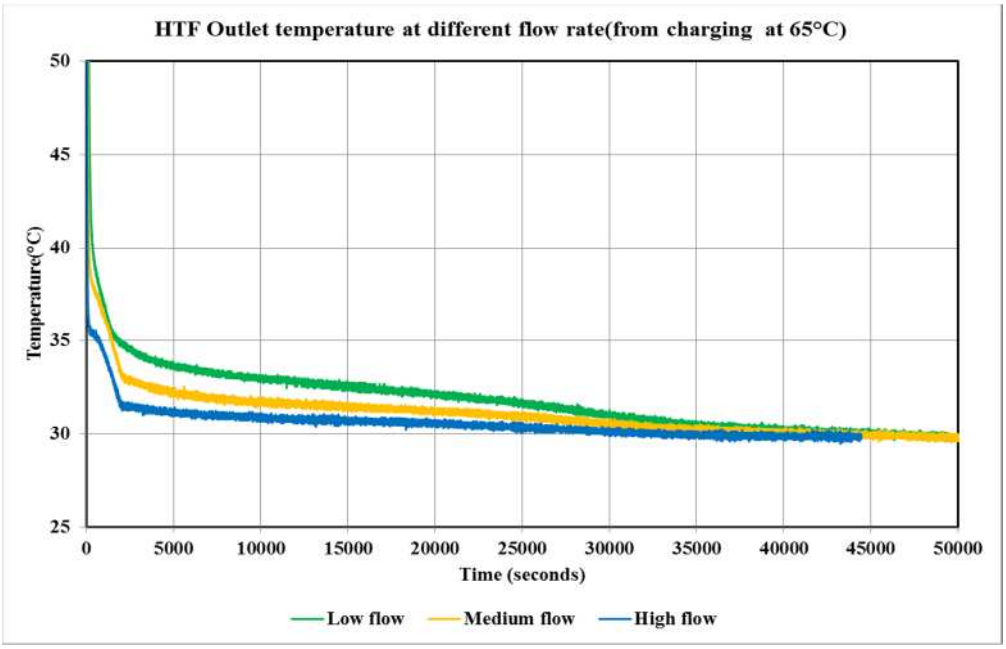


Figure 9:17: HTF outlet temperature during discharge at different flows from charging at inlet HTF temperature of 65°C.

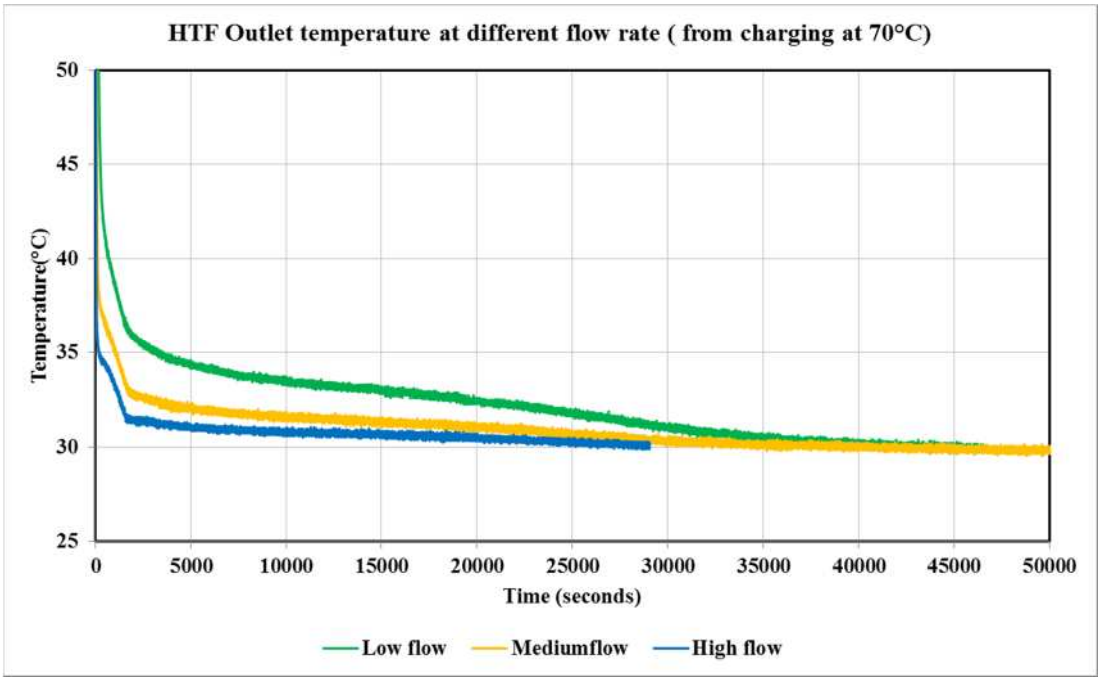


Figure 9:18: HTF outlet temperature during discharge at different flows from charging at inlet HTF temperature of 70°C.

Figure 9:19 and Figure 9:20 show the discharge rate at different mass flow rate. The results show that the discharge rate is faster at low flow when compared to the medium flow and high flow for both cases. The difference in discharge rate is not as significant as it showed for the charge rate with the same scenario (see Figure 9:4 and Figure 9:5). Experimental results showed that increasing the mass flow rate reduces the discharging time.

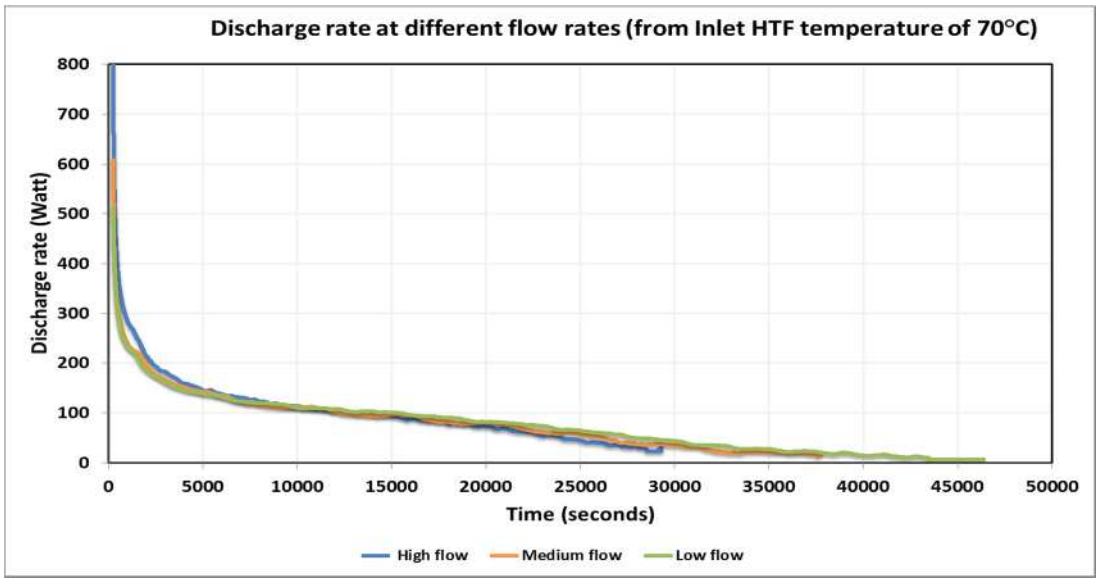


Figure 9:19: Discharge rate at different flow rate. (from charging at 70°C).

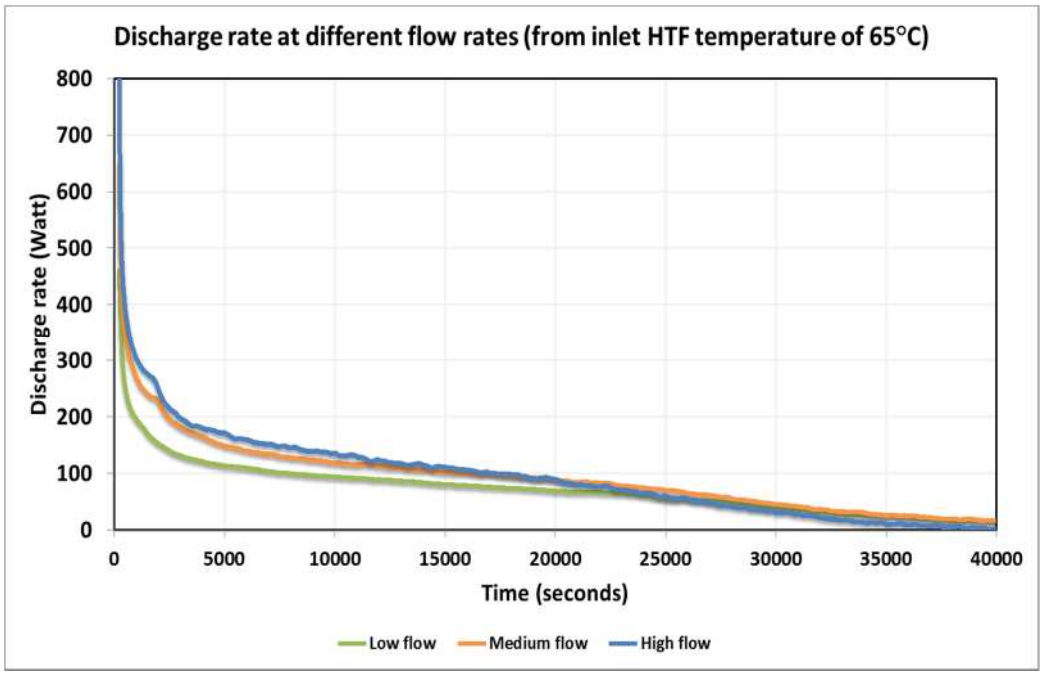


Figure 9:20:Discharge rate at different flow rate(from charging at 65°C).

Figure 9:21 shows the relationship between the discharge rate and time as the store was discharged at an inlet HTF temperature at 30°C. The store was discharged from the different charge processes; from charging inlet HTF temperatures of 60°C, 65°C and 70°C. The result shows that the least discharge rate was from discharging the store from inlet HTF of 70°C.

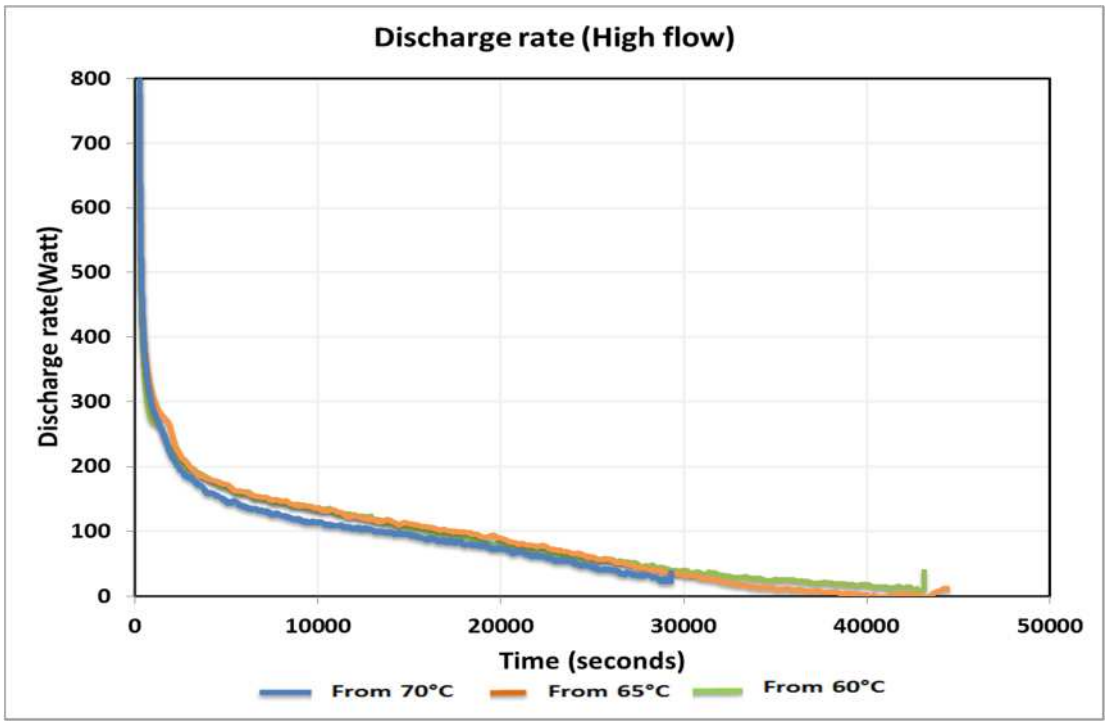


Figure 9:21: Discharge rate (High flow).

### 9.3.2 PCM temperature across the rig during discharge process.

This section discusses the PCM temperature across the rig. The thermocouples positioned axially and radially along the path of the copper pipe on the thermal store measures the PCM temperature as aforementioned for the charging process. For each figure, it shows that the PCM temperature is high at the start of the discharge process and the PCM is in its liquid state. The store is fully discharged when the difference between the inlet and outlet HTF temperature is zero and when the PCM is solid(less than 51°C based on result from the DSC.

Figure 9:24 to Figure 9:28 shows the outlet HTF temperature and PCM temperatures at A2B2C2 and C1C2C3 obtained from discharging the store at an inlet HTF temperature of 30°C for different flow rates. The figures compare the PCM temperatures at these points and the HTF outlet temperature during the discharging process. Appendix F shows further result for axial points A1B1C1, A3B3C3 and radial points A1A2A3 and B1B2B3 from the thermal store experiment result. Axial points A2B2C2 and radial point C1C2C3 are discussed using Figure 9:24 to Figure 9:28 to describe the discharging process. At the commencement of the discharging process, there is a noticeable trend for the PCM temperatures at the thermocouples positioned axially along the copper length. The PCM temperature shows that B2>C2>A2 from

discharging the store from charging temperatures of 65°C and 70°C(low flow) as described using Figure 9:24 and Figure 9:25 respectively. The PCM temperature at B2 is far apart from the PCM temperature at A2 and C2 from the commencement of the discharge till the outlet HTF temperatures match or reach the discharge temperature of 30°C. Figure 9:24 and Figure 9:25 shows the PCM temperatures of thermocouples positioned axially(A2B2C2) and radially(C1C2C3) along the path of the copper length to measure the PCM temperature from discharging the store from charging temperatures of 65°C and 70°C respectively at medium flow. The PCM temperature shows that C1>C3>C2 from discharging the store from charging temperatures of 65°C and 70°C. Based on the layout of the thermocouples on the thermal store, C1 is positioned farthest from the inlet of the heat transfer fluid into the store, thus it is expected to have PCM that are still molten or at a higher temperature when compared to C2 and C3. The PCM closest to the inlet, C3 and C2 are expected to solidify before C1 as shown in both Figure 9:24 and Figure 9:25.

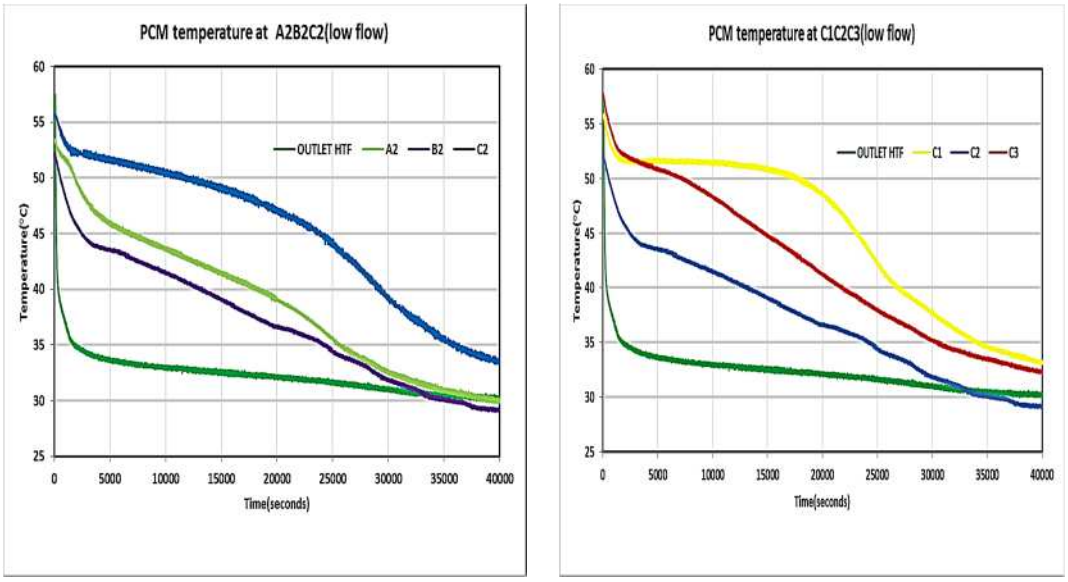


Figure 9:22: Discharging result from charging the store at 65°C; axial (A2B2C2) &radial (C1C2C3) points (low flow).

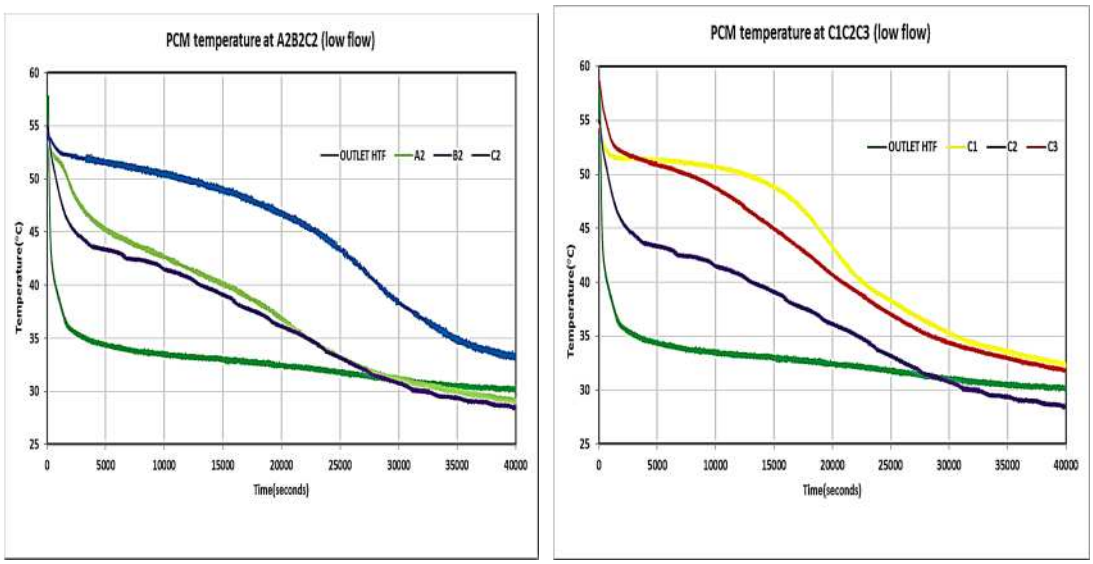


Figure 9:23: Discharging result from charging the store at 70°C; axial (A2B2C2) &radial (C1C2C3) points (low flow).

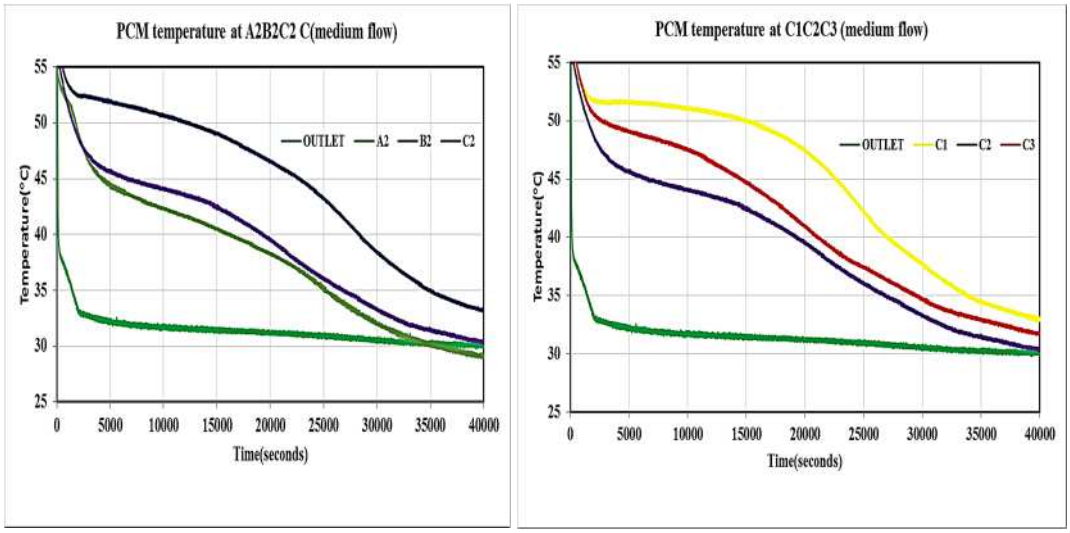


Figure 9:24: Discharging result from charging the store at 65°C; axial (A2B2C2) &radial (C1C2C3) points (medium flow).

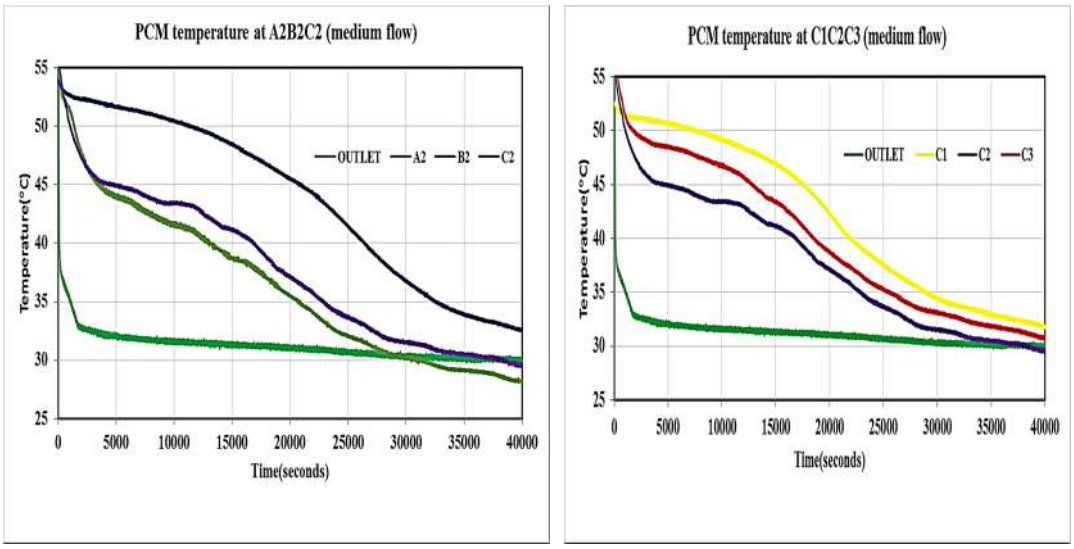


Figure 9:25: Discharging result from charging the store at 70°C; axial (A2B2C2) &radial (C1C2C3) points (medium flow).

The result obtained from the medium flow as the thermal store was discharged from 65°C and 70°C is similar at high flow as shown in Figure 9:26 to Figure 9:28. However, the discharging time is faster at high flow when compared to the medium flow. From Figure 9:27 and Figure 9:28, the results for the temperature of the PCM at thermocouples positions A2B2C2 (axial) shows similar trend, where B2>C2>A2 in both cases but at the end of the experiment in Figure 9:27 the temperature of the PCM is about 32°C and the other two points, A2 and C2 are less than 30°C. However from Figure 9:28; the PCM temperature at B2 was still at a temperature of 36°C while the other two points; A2 and C2 are close to the HTF outlet temperature of 30°C at the end of the experiment.

Considering the radial points, C1C2C3 in Figure 9:26 to Figure 9:28 for discharge result from discharging the store at 60°C, 65°C and 70°C respectively, the results shows that PCM temperature at C1 is greater than C2 and C3. The position of the thermocouples shows the temperature difference across these points. This means the PCM temperature at C1 solidifies after C2 and C3.

Appendix F comprises of the results for the other thermocouple positions that measure the PCM temperatures on the SHE. The results show that for axial and radial positions the PCM temperature followed this pattern; the PCM temperatures increase in this order for radial points (A1>A3>A2 and B2>B1>B3) as shown in Figure F8, Figure

F10, Figure F12, Figure F14, Figure F16, Figure F19 and Figure F20. The results show that the PCM temperature closest to the outlet of the rig has the highest PCM temperature as they solidify when compared to the other points. For radial points, B1B2B3, the result for all flows, show that B3, which is closer to the inlet of the rig solidifies quickly and has a temperature difference far apart from B1 and B2. For the PCM temperatures at the axial points, they follow this temperature pattern (C1>B1>A1 and C3>B3>A3) as shown in Figure F9, Figure F11, Figure F13, Figure F15, Figure F17, Figure F18 and Figure F21.

Based on the discharging result, it shows radially, A1 and C1; solidify slowly when compared to the other radial points. The case is different when considering the axial point; the PCM temperatures are closer to each other when compared to the radial points. Based on the result from this experiment, it shows that for the charging and discharging process, the inlet HTF temperature and mass flow rate affects the charging (melting) and discharging (solidification) time.

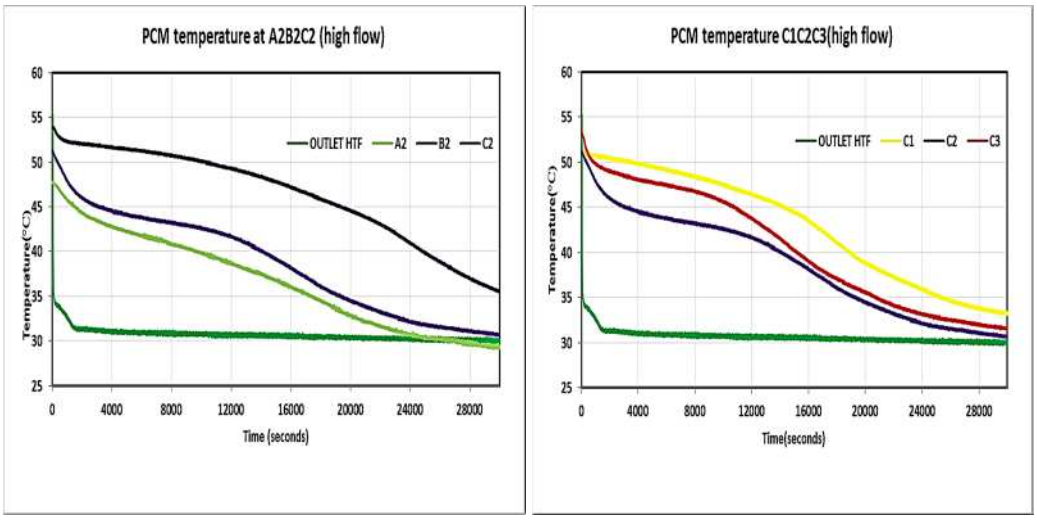


Figure 9:26: Discharging result from charging the store at 60°C; axial (A2B2C2) & radial (C1C2C3) points (high flow).

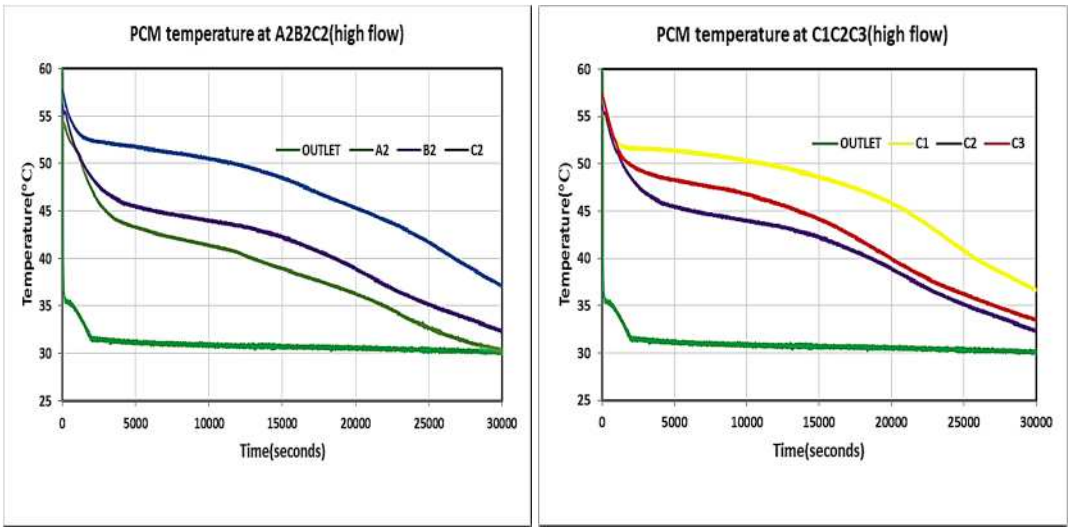


Figure 9:27: Discharging result from charging the store at 65°C; axial (A2B2C2) & radial (C1C2C3) points (high flow).

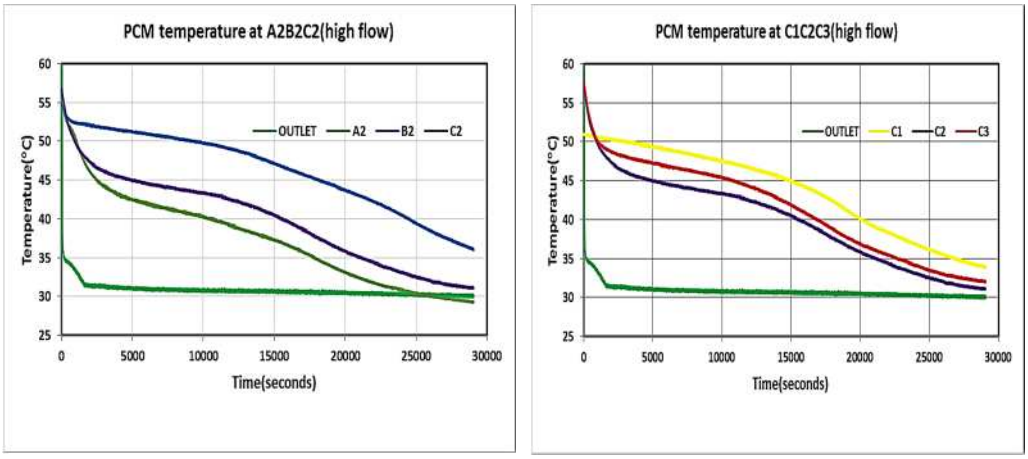


Figure 9:28: Discharging result from charging the store at 70°C; axial (A2B2C2) &radial points (C1C2C3) (high flow).

### 9.3.3 Comparison result of both geometries.

The experimental result using the PHE and SHE at low, medium and high flow showed that it takes a longer time to charge the thermal store using the SHE. Both heat exchangers used in this research are compared at high flow rate at the same inlet HTF temperature of 60°C using RT 52. The experiment using PHE was carried out at only one inlet HTF temperature (60°C), while the SHE arrangement was carried out at three different inlet HTF temperatures(60°C, 65°C and 70°C) . Similar dimensions were used for the design and construction of both bench test rig. The results obtained when the polypropylene sheet was used as the plate heat exchanger and the serpentine heat

exchanger, with the use of copper pipes are discussed. The result shows that the PCM melted faster at high flow rate using the plate heat exchanger when compared with the result from the serpentine heat exchanger at high flow. At inlet HTF temperature of 60°C, for the PHE, the entire PCM was melted between 4000-6000 seconds, while for the SHE, the PCM at thermocouple positions B1, B2 and C1-C3 were melted but the PCM at A1-A3 were not fully melted. This means there was an even distribution of heat between the PCM and HTF via the thin walls across the polypropylene sheet as the HTF flows through the channel running across the length of the sheet. This proves that the surface area and conduction path length in PCM are critical. For the SHE, only the PCM close to the pipe melt quickly and PCM farther way from the pipes takes a longer time for the PCM to melt, thus the charging time longer than the PHE. The quantity of PCM used for both heat exchangers differs. The PHE experiment was carried out using 6.7kg of RT 52, while 28.5 kg of the same PCM was used for SHE. The quantity of PCM affects the charging or discharging time, this depends on the surface area and conduction path length. The more the quantity of PCM, the longer the charging or discharging time. Varying the mass flow rate influences heat transfer to the store with the SHE arrangement. For the PHE rig, the type of flow is laminar for all cases, while for the SHE, the type of flow is transition and turbulent. The heat transfer coefficient for the PHE is 577 W/m$^2$K, while the heat transfer coefficient for the SHE arrangement is within the range of; $1890 \leq h \geq 7788$ W/m$^2$K.

The temperature drop of the SHE is greater than the PHE at high flow. After charging the store for an hour, the temperature drop for the PHE is 1.05°C, while for the SHE, the temperature drop is 1.84°C. At the end of the of six(6) hours of charging, the temperature drop for PHE is 0.42°C and 1.49°C for the SHE. It was observed that the charging process for the PHE at high flow was carried out for 20000 seconds (5.5 hours), though the entire PCM has melted at 6000 seconds(1.7 hours), while for the SHE was charged for 82,915 seconds (23 hours) at the same inlet HTF temperature and flow rate. The time it takes to charge the store and fully melt the PCM at an inlet HTF temperature of 60°C using the SHE is long, thus for faster charging time, it needed to be charged at a higher inlet HTF temperatures (65°C or 70°C). The inlet HTF temperature and flow rate can be varied to increase or decrease the time at which the thermal store is charged or discharged, though the mass flow rate has little effect on the heat transfer between the HTF and the PCM. The temperature drop at medium

and low flow for the SHE is greater than at the high flow as shown in Table 9:6. The same applies to the PHE at the two different flows as shown in Table 8:3 and Table 8:4.

For the discharge process, the PHE was discharged at different inlet HTF temperature. The SHE was discharged at 30°C for all the three different flows. The temperature drop for the PHE and SHE shows that the lower the flow rate; the higher the temperature drop as shown in Table 8:6, Table 8:7 and Table 9:7. This is similar to the trend observed during the charging process. For the SHE, the temperature drop for the low flow is higher than at medium and high flow. The high flow has the lowest temperature drop as shown in Table 9:7.

The results for the discharge process using the SHE arrangement showed that the PCM temperature goes below the inlet and outlet HTF temperature. This is not expected, since an inlet HTF temperature of 30°C is maintained throughout the experiment. Due to the difficulty in modeling such an action, numerical analysis was only done for the plate heat exchanger arrangement in Chapter 10. Also, the length of time to charge and discharge the SHE arrangement, when compared to the PHE arrangement prompted the decision to choose the PHE as the heat exchanger to be used for the purpose of this research.

### 9.3.4 Thermal Imaging of the serpentine rig

Thermal images were taken using the infrared camera (FLIR Camera) during the experiment. The thermal images are shown in Figure 9:29, which shows the changes that occur from the room temperature of the phase change material to when it was completely melted as the heat transfer fluid flows through the copper pipes. The image shows the temperature across the rig at different duration during the charging period. The first image is the temperature condition at the beginning of the experiment with the PCM at room temperature. The subsequent images show the image taken as the PCM melts gradually. The images show that the PCM in the inlet zone melt faster than at the outlet of the rig. It also shows PCM around the copper pipes melt faster when compared to other points on the rig. The melting involves heat transfer radially from the copper pipes to the surrounding PCM.

There are noticeable grey patches close to the copper pipes carrying the hot HTF, this indicates the PCM that is not fully melted yet which means the temperature at that

region is less, when compared with the PCM temperature around the copper pipes. The region on the rig without copper pipes melt slowly and depends on heat distribution from the PCM melted close to the heat exchanger.

.

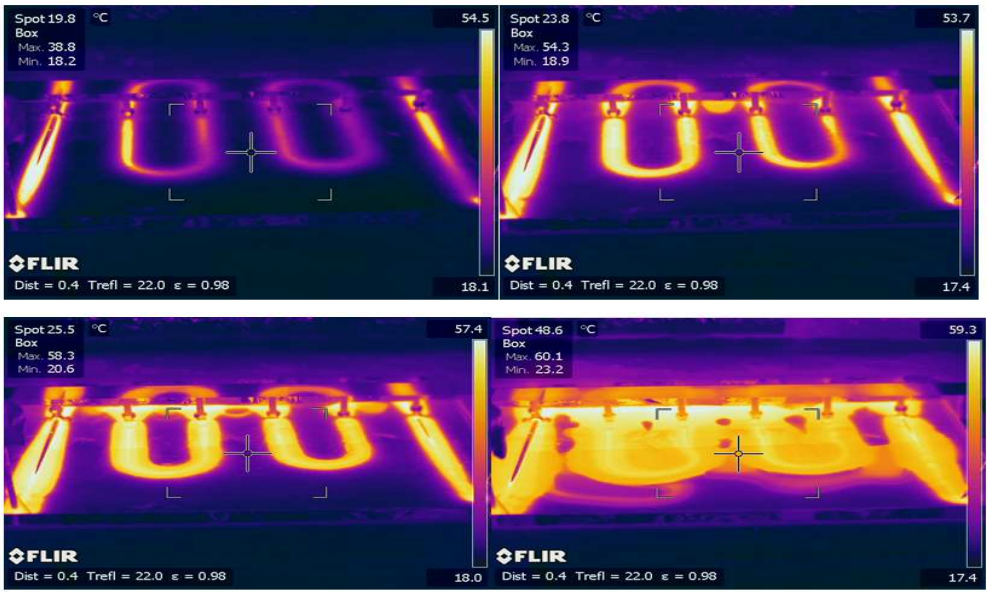


Figure 9:29: Thermal image of the rig at start and end of experiment.

Figure 9:30 shows these pockets of PCM in between the copper pipes that are not totally melted, however observing the thermal image; it is noticeable that PCM at the centre of two copper pipes shows PCM yet to melt fully. The highest temperature captured by the infrared camera using the 'spot' option which give a point temperature at a location, give a temperature higher than 50 °C and the phase change temperature of the PCM is 52°C.These thermal images give an overview of the temperature pattern across the rig and also confirm the PCM temperature obtained from the thermocouples measurement. Appendix H shows the pictorial view and thermal image of the entire rig during the charge process.

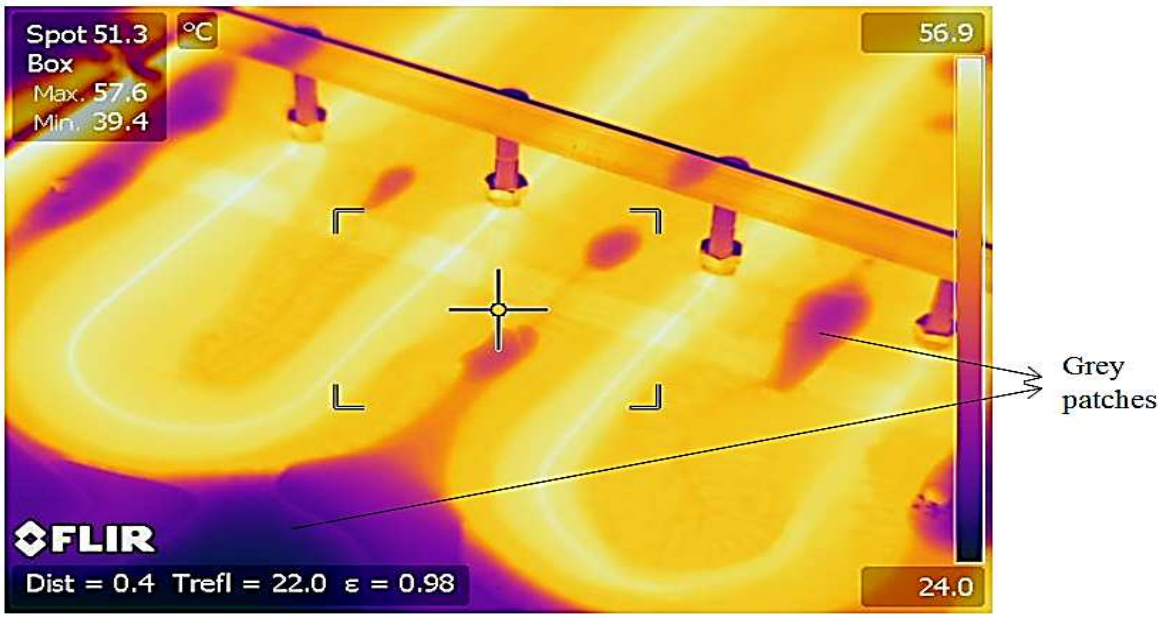


Figure 9:30: Thermal images showing the grey patches of PCM.

## 9.4 Summary

The experiment using serpentine heat exchanger as a thermal store and using RT 52 as the phase change material shows the thermal behaviour over time. The experiment looked at varying the mass flow rate and inlet heat transfer fluid temperature to study the effect on the behaviour of the thermal store during the charging and discharging processes. The thermal image of the serpentine heat exchanger was discussed at the beginning and end of the experiment. The HTF temperature profile of all figures shows that at the temperature drop at the start of the experiment is larger than at the end of the experiment. This can be attributed to the fact that at the beginning of the experiment, the PCM starts to melt as the hot fluid flows through the copper pipes but much heat is not lost by the HTF to the PCM, but once the PCM starts to change phase (from solid to liquid), the HTF loses more heat to the PCM, hence the difference in the temperature drop at the start and end of the experiment. The proposed use of the serpentine heat exchanger was discontinued due to the following reasons: Lengths of time required to charge and discharge the SHE thermal store and due to large conduction length using this arrangement. Plate heat exchanger (PHE) was modelled as discussed in Chapter 10; because it has a small conduction length and the store can be charged quickly as shown from the experiment result.

# 10 Modelling the PHE thermal store.

## 10.1 Description of Model

The model written in MATLAB is based on flow of the HTF, heat transfer to the polypropylene sheet, conduction through the wall of the polypropylene sheet and conduction through the PCM using enthalpy method. The simplifying assumptions the model relies on include; laminar flow and heat transfer in the HTF, zero span-wise heat transfer (2-D model), natural convection in the liquid phase of the PCM is negligible; and the PCM is homogenous and isotropic within each cell (at each node). The effect of natural convection in the PCM is neglected to simplify the model and also because the sheet has thin walls, making the conduction length the dominant heat path within the PCM.

The governing equations for the transient analysis of heat transfer in phase change material (solid-liquid PCMs) comprises of the Navier stokes equation, mass conservation equation and energy conservation equation. The energy equation is used for analysis of PCMs, because the Navier-stokes and mass conservation equation can be neglected as the convective term is negligible in the PCMs. Numerically, the transient partial differential equation representing heat transfer in PCMs is expressed thus,

$$\frac{\partial H}{\partial t} = \nabla(\mathrm{k}.\nabla T) \qquad 10.1$$

The type of phase change determines the nature of the relationship between the temperature and enthalpy using Equation 10.1. The boundary conditions used in the heat transfer equation over a range of temperature employing the enthalpy method are expressed using Equation 10.2.

$$\begin{aligned} H &= C_p T && \mathrm{T} < T_s \\ H &= C_p T + \frac{T - T_s}{T_l - T_s} \,.\, \mathrm{L} && T_s \le T \le T_l \\ H &= C_p T + L && T \ge T_l \end{aligned} \qquad 10.2$$

where, $C_p$ is the specific heat, L is the latent heat, $T_s$ and $T_l$ are the temperatures at which melting or freezing is initiated in the PCM when it is solid or liquid respectively.

The computational domain is discretized using nine (9) elements in the axial direction and twelve (12) elements in the y-direction. The enthalpy and temperature was determined in each node in the model built. The thermal resistance and temperature within the PCM was also considered in the simulation. Figure 10:1 describes the node distribution of the 2D model. The x-direction and y-direction are represented by m, n across the element to indicate position of the nodes. The time step of the simulation is represented by i (current time step) and the new time step by i+1.

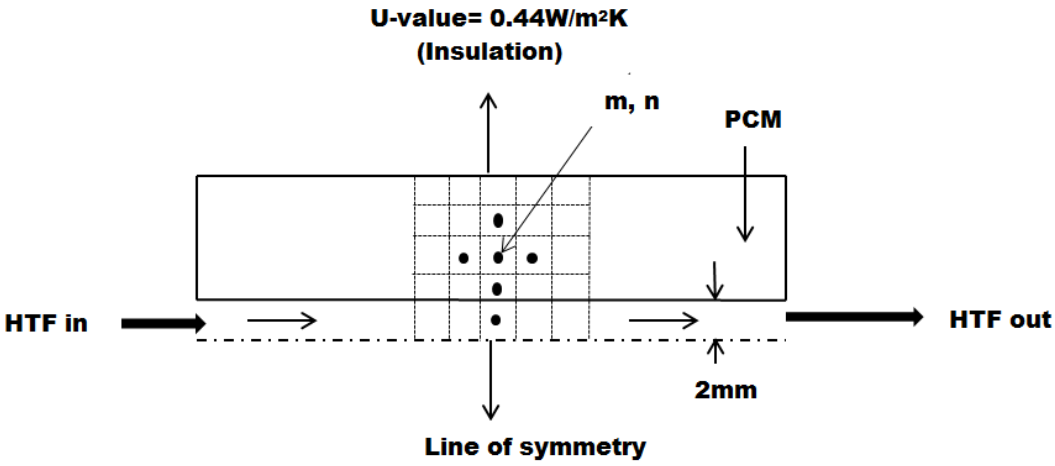


Figure 10:1: Schematic drawing of the rig showing the module

The following assumptions were made for this analysis:

- PCM initially at solid state for charging case.
- 2-D model
- Finite difference method
- Natural convection inside the PCM liquid phase is not considered.
- Enthalpy method is implemented.
- Isotropic case for solid and liquid PCM except the specific heat, which depends on the PCM temperature based on the DSC result.
- HTF thermal properties at specified temperatures are used.
- Flow is fully developed.

The thickness of the PCM used for the experiment is 10mm; same thickness is used for the validation of the MATLAB model. The store dimensions of the plate heat exchanger used for the experiment and modelling parameters is presented in Table 10:1.

Table 10:1: Store dimension used in the modelling

| | |
|---|---|
| **Polypropylene Sheet length [mm]** | **1900** |
| **Polypropylene Sheet width [mm]** | **400** |
| **PCM slab thickness [mm]** | **10** |
| **Area($m^2$)** | **0.76** |
| **Volume [L]** | **7.6** |
| **Channel width(mm)** | **3.6** |
| **Channel length (mm)** | **3.3** |
| **PIR Insulation board [W/m.K]** | **0.022** |
| **R-value($m^2K/W$)** | **2.25** |
| **Insulation thickness [mm]** | **50** |

The flowing HTF exchanges heat with the PCM via the wall of the polypropylene sheet. The wall thickness is small, however it is considered in the modelling of the store. The advantage of having a small wall thickness is that it allows heat to be transferred from the HTF to the PCM quickly. The axial direction (numx) is elements across the HTF in the channel and the numy is the elements through the PCM(y-direction) as heat transfer occurs from the HTF flowing the channels via the thin layer layered walls to the PCM. In order to reduce the computation time, the nodes were carefully selected. The domain is discretised along the x-axis of the polypropylene sheet in such a way that the PCM nodes along the x-axis and y-axis are equal. This is to ensure the PCM temperature across the sheet is well monitored to ascertain the heat transfer present between the PCM nodes due to the heat transfer (conduction) from the HTF and the wall of the sheet. The first two nodes along the y-axis are for the heat transfer fluid and the wall of the polypropylene sheet. Equation 10.3 expresses the number of element in the x-direction, while Equation 10.4 expresses the number of elements in the y-direction. For the simulation, the distance step in HTF flow direction; dx, is taken as 0.2. The distance steps in the PCM; dy is taken as 0.001.The length of the sheet; Lx spans across the x-direction; for the y direction; the n nodes are described thus; the first node is the HTF; n=1(HTF); the second node is the polypropylene wall; n=2(polypropylene wall) and the remaining nodes which describes the PCM domain

from n=3 to numy (n=3:12). For the m nodes; which covers the length of the channel (numx=1:9) for the HTF, wall and PCM.

$$numx = \frac{Lx}{dx} \qquad 10.3$$

$$numy = \frac{t_{\mathrm{PCM}}}{dy} + 2 \qquad 10.4$$

The Nusselt number is based on laminar flow in rectangular channels with a channel width ratio; 0 to 1. The channel width ratio of the geometry used for the PHE is determined using Equation 10.5.

$$\frac{channel\ width}{channel\ height} = \frac{b}{a} \qquad 10.5$$

$$\text{Channel width ratio} = \frac{3.6mm}{3.3mm} = 1.09$$

The Reynolds number for the flow in the channel is calculated as shown in Chapter 6 (Equation 6.16) and the flow was discovered to be laminar for all the different flow rates used during the experiment. Therefore based on the channel width ratio, the Nusselt number at constant surface temperature was used. The internal convection for fully developed laminar flow at constant surface temperature for a channel width ratio of 1 has a Nusselt number of 2.98 (Nu=2.98) Kays and Crawford (1993).

The hydraulic diameter ($D_h$) of the channel is used to calculate the heat transfer coefficient ($W/m^2K$) from water to the channel wall. Equation 6.7 is used to calculate the hydraulic diameter based on the wetted perimeter and the cross-sectional area of the closed channel. The Nusselt number is expressed as a function of the hydraulic diameter ($D_h$), thermal conductivity (k) and heat transfer coefficient (h); as shown in Equation 10.6 to Equation 10.7.

$$Nu = \frac{h.\mathrm{D_h}}{k} \qquad 10.6$$

The heat transfer coefficient ($W/m^2K$) is expressed using Equation 10.7.

$$h = \frac{Nu.k}{D_h} \qquad 10.7$$

Thus; for heat transfer fluid; $h_f = \frac{Nu.k_f}{D_h} = \frac{2.98x0.6587}{0.0034} = 577.52\ W/m^2K$

The PCM properties are included in the model based on result from the differential scanning calorimeter. The liquid fraction, which describes the state of the PCM, is expressed as shown in Equation 10.8:

$$X = \frac{T(m,\mathrm{n}) - T_s}{T_l - T_s} \qquad 10.8$$

$X > 1 \Rightarrow X = 1$ (liquid)
$X < 0 \Rightarrow X = 0$ ($solid$)
$0 < X < 1$ (Mushy)

The value of X, is defined as solid when X= 0; and 1, when it is liquid. The value of the liquid fraction between 0 and 1 is regarded as the mushy region. The specific heat capacity of the PCM is expressed based on the liquid fraction as shown in Equation 10.10; an additional specific heat capacity is added to consider the melting of the PCM as expressed in Equation 10.9.

$$C_{p_{p(\mathrm{melt})}} = C_{p_p(\mathrm{melt})} = \frac{L}{T_l - T_s} \qquad 10.9$$

$$C_{p_{p_{m,n}}} = X * (C_{p_p(liquid)} - C_{p_p(solid)}) + C_{p_p(solid)} \qquad 10.10$$

If the liquid fraction is in the mushy region; $if\ \ 0 < X < 1;$, the specific heat is expressed as shown in Equation 10.11

$$C_{p_{p_{m,n}}} = C_{p_{p_{m,n}}} + C_{p_p(\mathrm{melt})} \qquad 10.11$$

During the charging and discharging process, the thermal resistance to the heat transfer within the PCM is considered. North, south, west and east thermal resistance for the PCM is expressed using Figure 10:2.

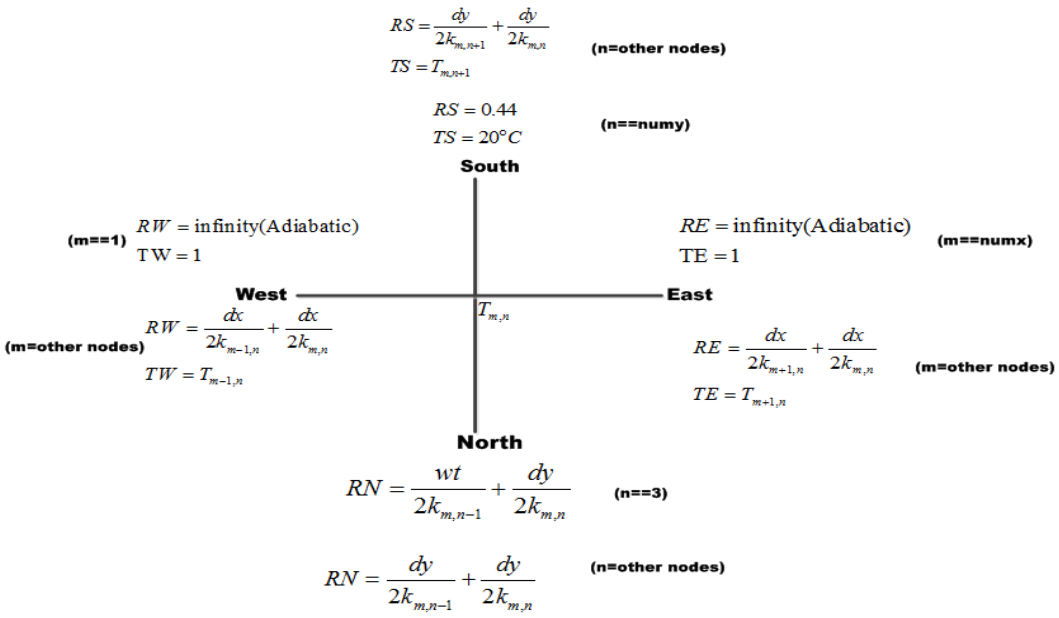


Figure 10:2: Schematic of the PCM nodes, showing the thermal resistance.

The thermal resistance for a rectangular or Cartesian coordinate is expressed as described in Equation 10.12.

$$R_{th} = \frac{thickness}{kA} \qquad 10.12$$

The thermal resistance, is used in the model; which is defined as a measure of the material resistance to conductive heat flow; the higher the thermal resistance, the more resistance it is to transfer heat.

$$\text{R-value} = \frac{thickness(m)}{thermal\ conductivty(W/mK)}\ (\text{m}^2\text{K/W})$$

The U-value is used in the simulation, considering the effect of the insulation on the heat transfer. The south resistance considers heat loss from the top of the rig as a result to the Celotex insulation and room temperature. The U-value of the Celotex insulation is used to determine the measure of heat loss. The R-value of the 50mm thickness

Celotex insulation board is 2.25m$^2$K/W, thus the U-value can be calculated as shown in Equation 10.13.

$$\frac{1}{R\text{-}value}\ (\mathrm{m^2W/K}) \qquad 10.13$$

$$U = \frac{1}{R} = \frac{1}{2.25}$$
$$U = 0.44 W / m^2 K$$

This U-value is used in the model, including a heat loss of 20°C. Two cases are considered with the Matlab model, case 1 is based on the experiment as shown in Figure 10:3a; case 2 is based on having multiple sheets as shown in Figure 10:3b.

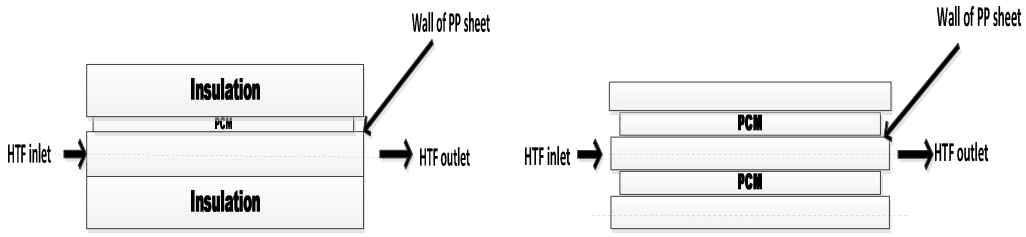


(a) Case 1 (b) Case 2

Figure 10:3: Arrangement of the store modelled.

The modelling of the PHE commenced with the consideration of case 1; where the PP sheet has insulation above and beneath it. This was verified with the experiment data. The Matlab model showed good agreement with the experiment result, where the experimental outlet HTF temperature was compared to the simulated outlet HTF temperature from the model. The model was used to study the behaviour of the store, when various parameters such as flow rate, latent heat capacity, thickness of the PCM and type of material used for the heat exchanger are varied. Figure 10:10 to Figure 10:13 describes the behaviour of the store when these parameters are varied.

## 10.2 Numerical analysis for the plate heat exchanger (PHE)

The explicit finite difference equations are derived for a transient case using energy balance. Equation 10.14 to Equation 10.16 shows the energy balance equation used for the analysis.

$$\sum_{All\ sides} \dot{Q}^i = \rho V_{element} C_p \frac{T_m^{i+1} - T_m^i}{\triangle t} \qquad 10.14$$

$$V_{element} = dxdy \qquad 10.15$$

$$\sum_{All\ sides} \dot{Q}^i = \rho dxdy C_p \frac{T_m^{i+1} - T_m^i}{\triangle t} \qquad 10.16$$

For each element or node, the mass of the water, mass of wall and mass of PCM in an element is described as shown in Equation 10.17 to Equation 10.19 respectively.

$$M_{htf} = M_f = dx.dy_{htf}.\rho_{htf} \qquad 10.17$$

$$M_{wall} = M_w = dx.wt.\rho_{wall} \qquad 10.18$$

$$M_{pcm} = M_p = dx.dy\ .\rho_{pcm} \qquad 10.19$$

The energy balance equation on the element for the HTF is related by Equation 10.20

$$E_{in} - E_{out} + E_{generated} = E_{accumulated} \qquad 10.20$$

Energy into the element is expressed as shown in Equation 10.21

$$E_{in} = \dot{m} C_{p_f} T\big|_x = \dot{m} C_{p_f} T \qquad 10.21$$

The energy out of the element, considering the convection between the HTF and wall is expressed in Equation 10.22 as;

$$E_{out} = \dot{m} C_{p_f} T\big|_{x+dx} + \mathrm{h_f}\ A\left(T_f - T_p\right) = \dot{m} C_{p_f}\left(T + \frac{\delta T}{\delta x}\Delta x\right) + \mathrm{h_f}\ A\left(T_f - T_p\right) \qquad 10.22$$

The accumulated energy on the content of the element is shown in Equation 10.23

$$E_{accumulated} = \rho V C_{p_f} \frac{\delta T}{\delta t} \qquad 10.23$$

For this case, there is no heat generation; $E_{generated} = 0$

Therefore, total energy on the element based on Equation 10.20 is expressed using Equation 10.24;

$$\rho A \Delta x C_{p_f} \frac{\delta T}{\delta t} = \mathrm{A h_f} \left( T_w - T_f \right) - \dot{m} C_{p_f} \frac{\delta T}{\delta x} \Delta x \qquad 10.24$$

Applying finite difference, explicit scheme; Equation 10.24 becomes Equation 10.25

$$T_{m,n}^{i+1} = T_{m,n}^{i} + \frac{\triangle t \, \mathrm{h_f} \, dx}{M_f C_{p_f}} \left( T^{i}{}_{w} - T^{i}{}_{f} \right) - \frac{\dot{m} \triangle t}{M_f} \left( T_{m+1,n}^{i} - T_{m-1,n}^{i} \right) \qquad 10.25$$

Rearranging Equation 10.25, the new temperature is expressed as Equation 10.26

$$T_{m,n}^{i+1} = T_{m,n}^{i} + \frac{\triangle t \, \mathrm{h_f} \, dx}{M_f C_{p_f}} \left( T^{i}{}_{w} - T^{i}{}_{f} \right) + \frac{\dot{m} \triangle t}{M_f} \left( T_{m-1,n}^{i} - T_{m+1,n}^{i} \right) \qquad 10.26$$

The first node of the HTF; $T_{1,1}$ is expressed using Equation 10.27;

$$T_{1,1}^{i+1} = T_{1,1}^{i} + \frac{\triangle t}{M_f} \left( \frac{\mathrm{h_f} \, dx}{C_{p_f}} \left( T^{i}{}_{1,2} - T^{i}{}_{1,1} \right) + \dot{m} (T_{in} - T_{1,1}^{i}) \right) \qquad 10.27$$

The remaining node (m=2: numx-1) across the HTF considers heat loss to ambient and expressed as described in Equation 10.28; (U=0.44W/m$^2$K)

$$T_{\mathrm{m},1}^{i+1} = T_{\mathrm{m},1}^{i} + \frac{\triangle t}{M_f} \left( \frac{\mathrm{h_f} \, dx}{C_{p_f}} \left( T^{i}{}_{\mathrm{m-1,1}} - T^{i}{}_{\mathrm{m,1}} \right) + \dot{m} (T_{m-1,1} - T_{m,1}^{i}) \right) + \frac{\triangle t}{C_{p_f} M_f} \left( \frac{0.44 dx}{C_{p_f}} \left( 20 - T^{i}{}_{1,1} \right) \right) \qquad 10.28$$

Equation 10.29 describes the last node on the HTF node, which is the outlet HTF temperature,

$$T_{\mathrm{numx},1}^{i+1} = T_{\mathrm{numx},1}^{i} + \frac{\triangle t}{C_{p_f} M_f} \left( \mathrm{h_f} \, dx \left( T^{i}{}_{\mathrm{numx},2} - T^{i}{}_{\mathrm{numx},1} \right) + \dot{m} (T_{\mathrm{numx-1,1}} - T_{numx,1}^{i}) \right) \qquad 10.29$$

For the wall node; the first node is $T_{1,2}$ (m=1, n=2) as shown in Equation 10.30. The equation considers the effect of convection between the wall and the HTF nodes; including the surrounding nodes of the PCM.

$$M_w C_{pw} \frac{T_{1,2}^{i+1} - T_{1,2}^{i}}{\Delta t} = \mathrm{h_f}\, dx\left(T^{i}_{1,1} - T^{i}_{1,2}\right) + \frac{wt.k_w}{dx}(T_{2,2} - T_{1,2}) + dx(T_{1,3} - T_{1,2}) \frac{2}{\frac{wt}{k_w} + \frac{dy}{k_{1,3}}} \quad 10.30$$

The temperature at this node is expressed in Equation 10.31 as;

$$T_{1,2}^{i+1} = T_{1,2}^{i} + \frac{\Delta t}{M_w C_{pw}} \left[ \mathrm{h_f}\, dx\left(T_{1,1} - T^{i}_{1,2}\right) + \frac{wt.k_w}{dx}(T_{2,2} - T_{1,2}) + dx(T_{1,3} - T_{1,2}) \frac{2}{\frac{wt}{k_w} + \frac{dy}{k_{1,3}}} \right] \quad 10.31$$

In the Matlab code, for the other remaining nodes across the length of the sheet, it is expressed ;( m=2: numx-1).

$$T_{\mathrm{m},2}^{i+1} = T_{\mathrm{m},2}^{i} + \frac{\Delta t}{M_w C_{pw}} \left[ \mathrm{h_f}\, dx\left(T^{i}_{\mathrm{m},1} - T^{i}_{\mathrm{m},2}\right) + \frac{wt.k_w}{dx}(T_{\mathrm{m}-1,2} + T_{\mathrm{m}+1,2} - 2T_{m,2}) + dx(T_{\mathrm{m},3} - T_{\mathrm{m},2}) \frac{2}{\frac{wt}{k_w} + \frac{dy}{k_{\mathrm{m},3}}} \right] \quad 10.32$$

Equation 10.33 describes the wall temperature at the last node; the equation considers the boundary with the PCM at n=3.It also considers the effect of convection between the wall and the HTF flow.

$$T_{\mathrm{numx},2}^{i+1} = T_{\mathrm{numx},2}^{i} + \frac{\Delta t}{M_w C_{pw}} \left[ \mathrm{h_f}\, dx\left(T_{\mathrm{numx},1} - T_{\mathrm{numx},2}\right) + \frac{wt.k_w}{dx}(T_{\mathrm{numx}-1,2} - T_{\mathrm{numx},2}) + dx(T_{\mathrm{numx},3} - T_{\mathrm{numx},2}) \frac{2}{\frac{wt}{k_w} + \frac{dy}{k_{\mathrm{numx},3}}} \right] \quad 10.33$$

The PCM nodes are m=1: numx and n=3: numy. For the phase change material; thermal resistance is considered across the nodes with PCM. The resistance are termed; North resistance (RN); South resistance, West resistance and East resistance. Figure 10:2 shows the conditions across each node.

The PCM nodes at the first and last nodes on the west and east (RW and RE) are regarded as adiabatic (no heat loss). Also for RS, the last node (n=numy=12) applies heat loss conditions at the top of the sheet; also includes the properties of the insulation used.

Applying the PCM conditions based on $C_p$, X and thermal resistance at the North, South ((n=3: numy), West and East zone (m=1: numx) of the PCM from nodes. Equation 10.34 expresses the PCM temperature. The thermal resistance; RS, RN, RE, RW and temperatures; TS, TN, RE, TW are expressed in Figure 10:2.

$$T_{\mathrm{m,n}}^{i+1} = T_{\mathrm{m,n}}^{i} + \frac{\Delta t}{C_{p_{p\,m,n}} M_p}\left(\frac{dx}{RN}TN + \frac{dx}{RS}TS + \frac{dy}{RE}TE + \frac{dy}{RW}TW - BT_{m,n}\right) \quad 10.34$$

Where B is the total thermal resistance around the nodes, as shown in Equation10.35

$$B = \frac{dx}{RN} + \frac{dx}{RS} + \frac{dy}{RE} + \frac{dy}{RW} \quad 10.35$$

The amounts of energy stored and charge rate of the store is obtained from the model and used for the analysis. The charge rate is expressed as;

$$\dot{m} C_{p_w} (T_{in} - T_{out}) \quad 10.36$$

### 10.3 Simulation result and analysis and Validation of model (PHE)

The Matlab model was used to validate the experiment result done using RT 58 and for RT 52; at different flow rates (low, medium and high flow). The Matlab code use for the validation of the experiment for both charging and discharging is presented in Appendix J. Figure 10:4 shows the result for the validation of the model using RT 58 experimental result. Figure 10:5 to Figure 10:7 shows the temperature profile of the inlet heat transfer fluid and outlet HTF during experiment and the outlet HTF temperature from the simulation using the MATLAB model for different flows using RT 52 data. The simulation result for the discharging process of RT 52 is presented

using Figure 10:8 and Figure 10:9. The inlet HTF temperature during the experiment was used in the simulation to compare the simulation HTF outlet temperature with measured experimental values. This was done to validate the heat transfer model for the system written in MATLAB utilising material properties from the DSC and hot disk instrument, along with properties of polypropylene (PP) sheet from literature. The results show that the outlet temperature predicted by the simulation is in accordance with the experimentally measured data, which means the model functions appropriately. The validated model is used to study the effects of varying the relevant parameters during charging and discharging.

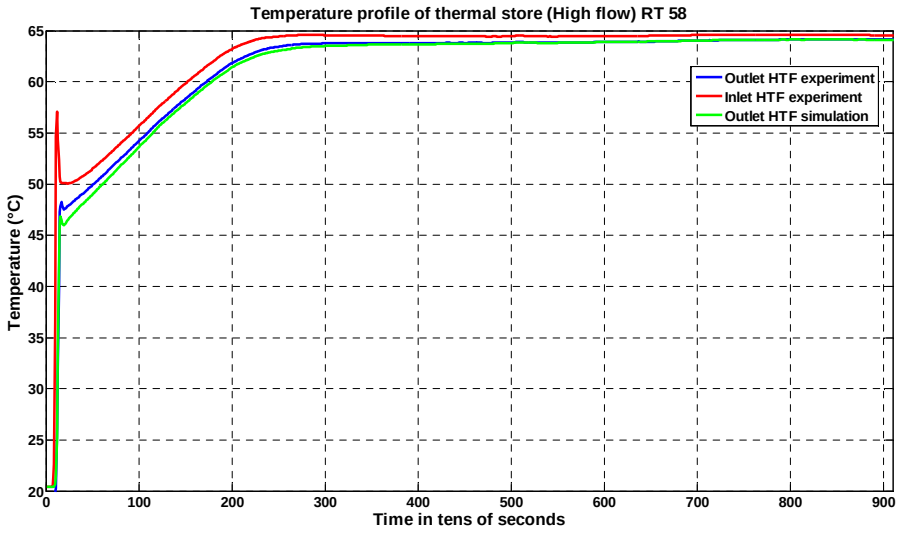


Figure 10:4: Temperature profile of validated model for RT 58 experiment.

The model was initially used to validate the charging result using RT 58 as shown in Figure 10:4, where the experiment was done at high flow only. With modification of the flow process to facilitate varying flow rates, a valve was installed before the commencement of the charging process using RT 52. The model was also used to validate experiment done using RT 52, which has different thermal properties (specific heat for when the PCM is solid and liquid, latent heat, melting point etc.), different flow rate (low, medium and high flow) and at an HTF inlet temperature of 60°C. Figure 10:5 to Figure 10:7 shows that the model was appropriate for the three different flow rates using RT 52 as the PCM for the thermal store. There is a noticeable difference between the outlet HTF temperature and the simulation outlet temperature at the beginning of the simulation for Figure 10:4 to Figure 10:7.

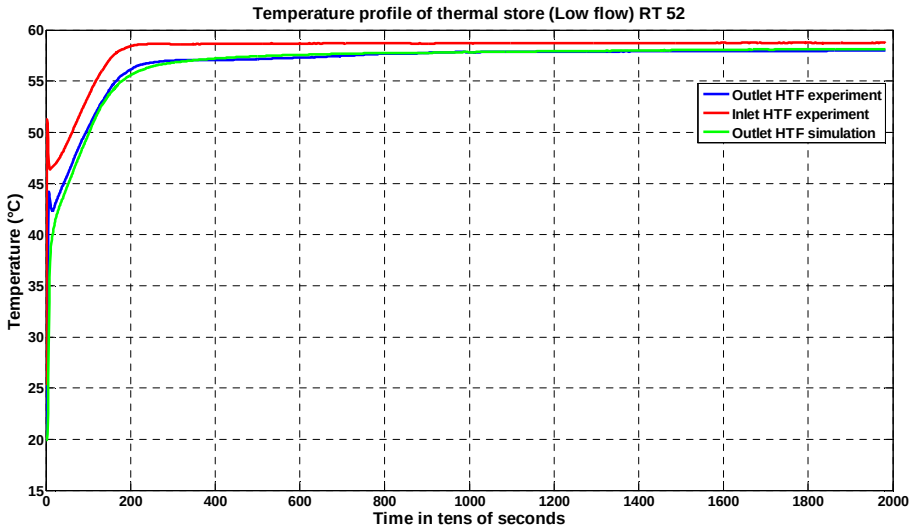


Figure 10:5: Temperature profile of the validated model for RT 52 at low flow rate.

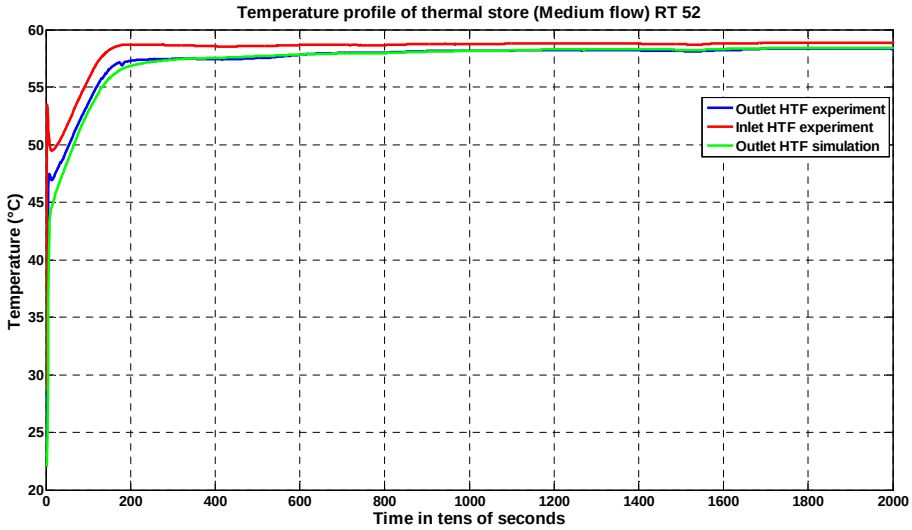


Figure 10:6: Temperature profile of the validated model for RT 52 at medium flow.

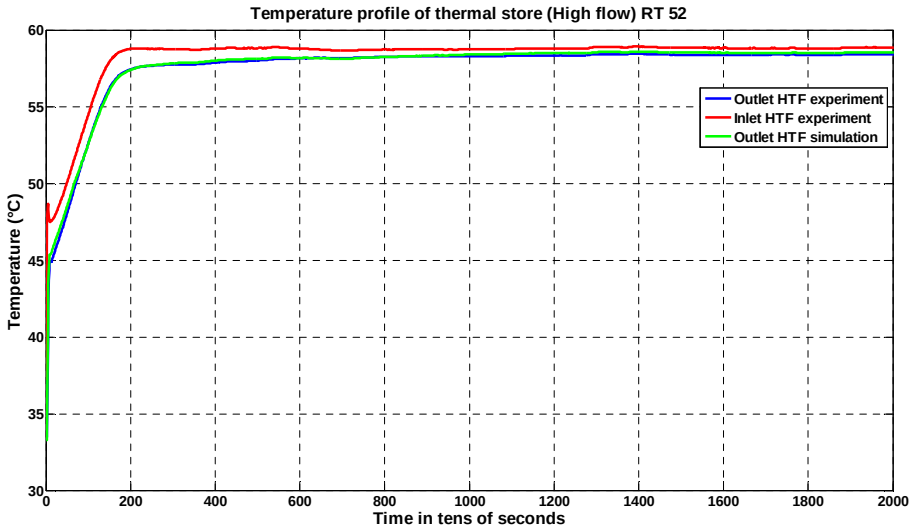


Figure 10:7: Temperature profile of the validated model for RT 52 at high flow.

For the validation of the discharge process based on experimental data using RT 52, the low and medium flows are presented for the discharge at different HTF temperatures; 38°C and 47°C respectively. The discharge process at high flow is not presented for the discharge was done, without the use of the hot water bath. Figure 10:8 and Figure 10:9 shows the result from the simulation, where the experimental inlet HTF temperature and outlet HTF temperature are plotted alongside the simulation outlet HTF temperature. The model does not exactly agree with the experiment results throughout the duration of the simulation. This can be attributed to the nature of the solidification process, where temperature variations could occur as a result of PCM forming layers on the heat transfer surface.

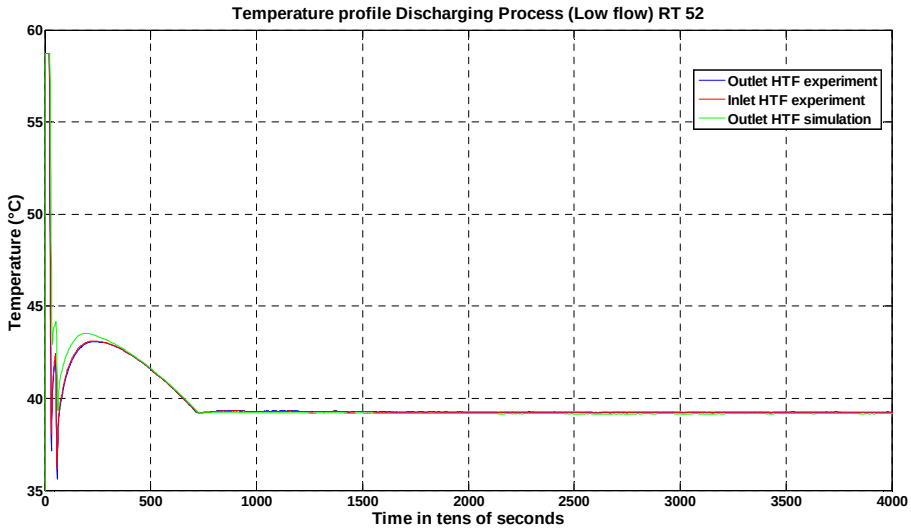


Figure 10:8: Temperature profile of the validated model for RT 52 at low flow (Discharge Process).

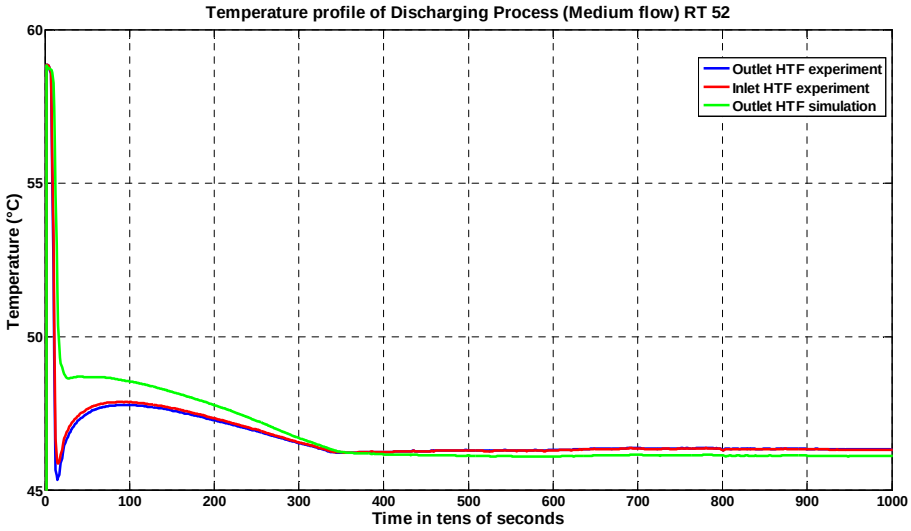


Figure 10:9: Temperature profile of the validated model for RT 52 at medium flow (Discharge process).

.

### 10.3.1 Varying the flow rate

Using the model, the properties of the sheet was varied for the RT 52 and RT 58. The simulation results obtained using RT 58 is presented in this section of the thesis, since the model works well for both cases. Various parameters such as thickness of PCM, latent heat, mass flow rate is discussed in this section. The mass flow rate is varied to study the effect it has on the amount of energy stored and thermal behaviour of the rig. From the result shown in Figure 10:10, it is observed that varying the mass flow rate has a significant effect on the temperature profile of the model. However, it has no effect on the amount of energy store profile; Figure 10:11 shows the energy profile. This agrees with findings from (Mohamed (2011))**,** which states that the heat transfer fluid mass flow rate has no significant effect on the accumulated stored energy. It is observed that when the mass flow rate is increased by a factor of 2 (130g/s), the simulation HTF outlet temperature trend (green line) moves upwards; away from the experimental result. However, reducing the mass flow by the same factor (32.5g/s), the simulation outlet temperature trend (green line) moves downwards as shown in Figure 10:10. The mass flow rate affects the melting time of the rig, because the rate of heat transfer increases with increase in the mass flow rate. However, increasing the mass flow rate does not increase the performance of the thermal store with regards the amount of energy stored. Based on the results from the experiment and the simulation using the MATLAB code, it is observed that it takes a longer time for the PCM to melt at low flow compared to the medium and high flow. This means the flow rate can be adjusted to suite the desired period of charging/discharging, depending on how much time the store is required to be charged during the off peak periods and how often charging and discharging is required throughout the day.

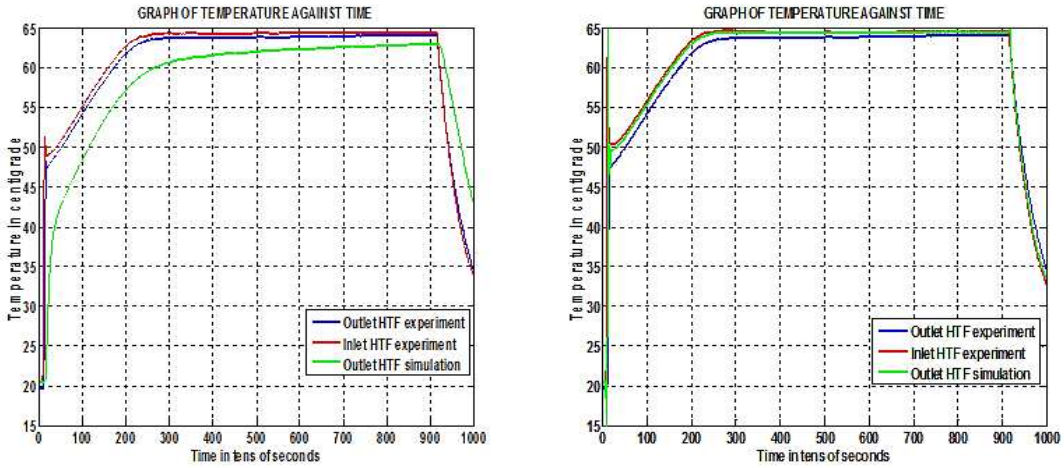


a) 32.5g/s b )130g/s

Figure 10:10: Model result increasing and reducing the flow rate.

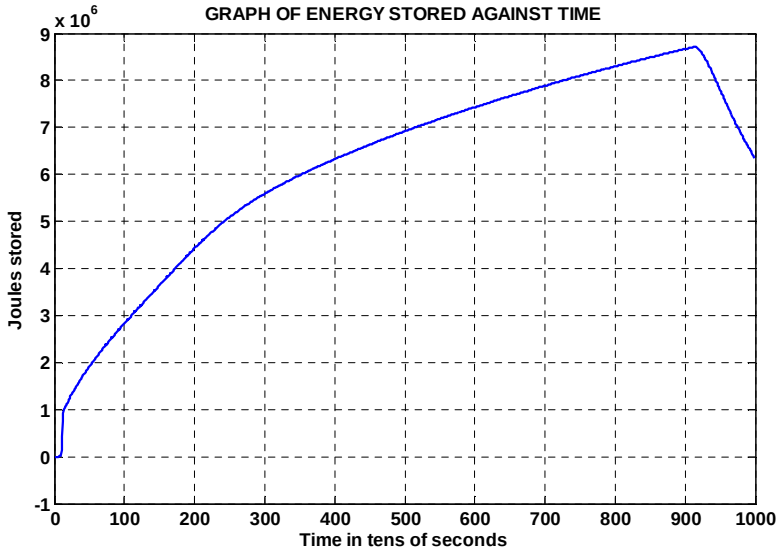


Figure 10:11: Energy stored against time for RT 58.

### 10.3.2 Varying the thickness of the PCM

The thickness of the PCM is varied using the Matlab code to study the effect on the thermal store performance. The thickness of PCM used for the experiment and to validate the model is 10mm. The original thickness of the PCM was halved (5mm) and quadrupled (40mm). Figure 10:12 shows the result of the simulation. There is an

increase in the amount of energy stored when the PCM thickness is increased by four times (quadrupled) the original value as shown in Figure 10:12 a). However, there is no change in the temperature profile. This was observed also, when the thickness of the PCM was halved. At half of the original thickness of the PCM, the amount of energy obtainable from the thermal store was less when compared to the original thickness of the PCM(see Figure 10:12 b)). The volume of PCM will result in an increase in the amount of energy obtainable from the thermal store. The result shows that when the thickness of PCM is increased by four times the original value, there is a corresponding increase in the energy obtainable from the thermal store, when compared to amount of energy stored when the thickness of PCM is halved. This means that the PHE thermal store output can be varied by changing the thickness. However, it was observed that the time it takes to run the simulation increases as the thickness of the PCM is increased; this is as a result of more simulation time required to melt the layers of PCM with respect to the thickness of the PCM in the thermal store.

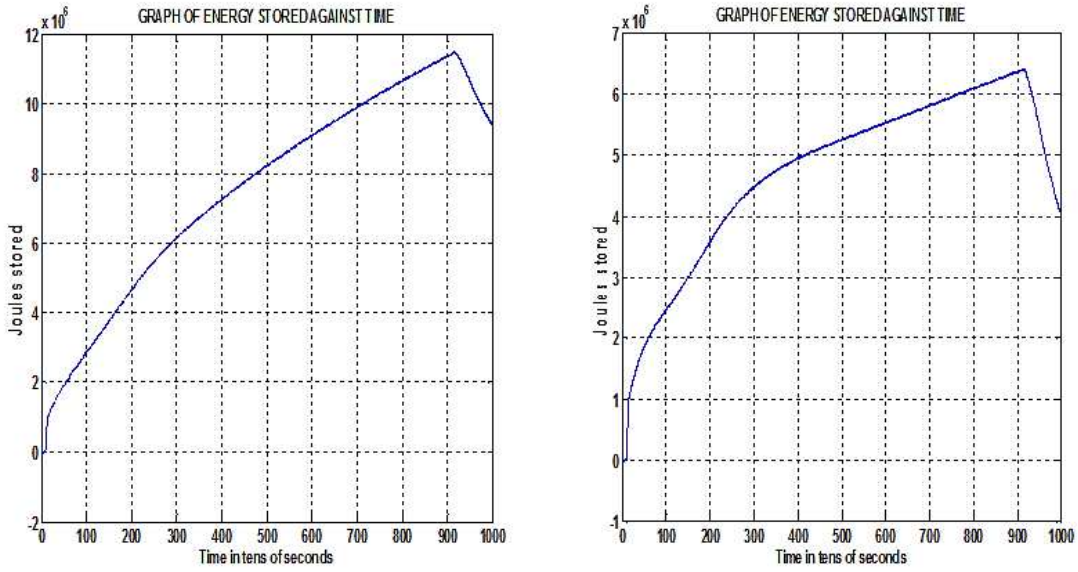


a)40mm thickness b)5mm thickness

Figure 10:12: Effect on varying the thickness of the PCM.

### 10.3.3 Varying latent heat of PCM used for experiment.

The latent heat of the PCM was doubled and halved to find out the effect on the performance of the store. From the DSC result for RT 58, the value of the latent heat is 140kJ/kg. This was doubled (280kJ/kg) and halved (70kJ/kg) to study the effect on

the thermal store using the model. Figure 10:13 b) shows the energy of the store rose up to 10MJ using a PCM with a latent heat of 280kJ/kg, while using a PCM with a latent heat of 70kJ/kg (see Figure 10:13 a)) resulted in about 8MJ of energy from the thermal store. The same result experienced with varying the thickness of the PCM was applicable to when the latent heat of the PCM was varied. Using a PCM with a higher latent heat, it would result in a higher amount of energy from the store, though other factors that determine selection of PCM needs to be considered. The temperature profile of the model was also not affected by varying the latent heat of the PCM in the simulation.

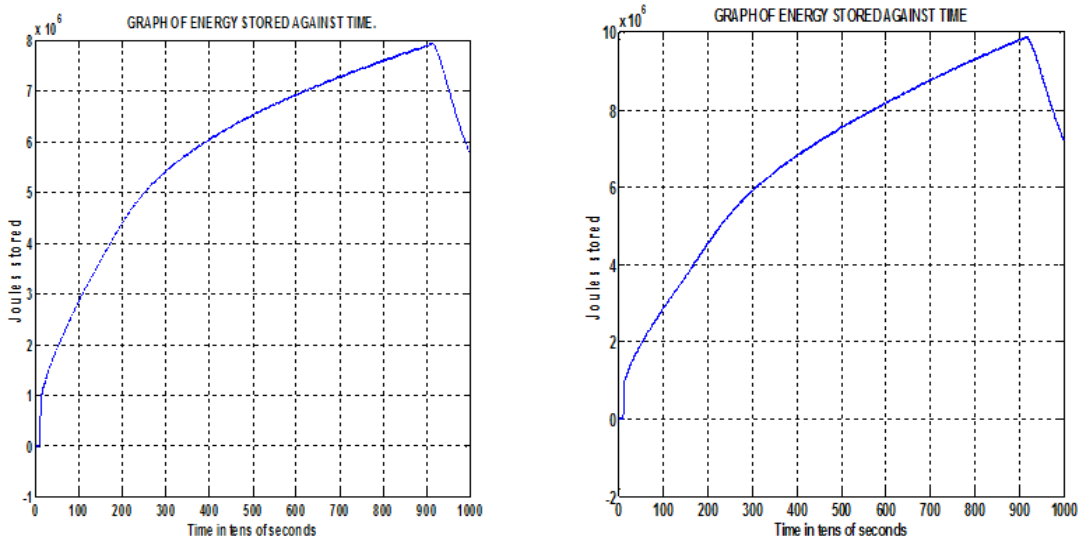


a)Latent heat (70kJ/kg) b)Latent heat(280kJ/kg)

Figure 10:13: Effect of varying the latent heat of the PCM.

## 10.4 Design Optimization

With the Matlab model verified, using the results from the experiments for both PCMs, further analysis was done using the model. The Matlab model was updated using Case 2 from Figure 10:3 to simulate another scenario, where the thermal store could accommodate stacks or layers of sheet to obtain the required power or capacity required for the PHE thermal store. The following changes were made to the model:

*Insulation top and bottom is neglected, heat loss to ambient is negligible.

*The thermal resistance is updated to meet the new conditions. South thermal resistance is updated to simulate an adiabatic case.

$$RS = \text{infinity(Adiabatic)}$$
$$\text{TS} = 1$$

*The experimental result is not used for this case, since the model has been validated. Real life scenarios where studied, where a constant inlet HTF temperature and initial temperature of the store can be varied.

* The specific heat capacity of water was halved to simulate that just half of the PP sheet is modelled to obtain the desired results for having the sheet with PCM at the top and bottom.

Based on the updated Matlab model, the charge rate and energy values obtained from the simulation are for a single sheet. This means if more than one sheet is considered in a stack, the corresponding charge rate or energy from the store should be multiplied by the desired number of sheets. The Matlab model was used to simulate different scenarios where the PCM thickness, flow rate, thermal properties are varied and the effect on the thermal store determined. PCM thickness was simulated based on 10mm, 20mm and 40mm thickness of wax for RT 58 and six different PCM thicknesses for RT 52 (10mm to 60mm). The application for this is that the capacity of the thermal store can be increased by the number of sheets. This is to help facilitate the design of an effective store for use in domestic application during off peak electricity periods. It would enable the thermal store to be charged during the off-peak periods with the use of a heat pump of 8kW capacity.

For the modelling, a single sheet was considered and half of the water channel (line of symmetry) used to simulate the behaviour of the store. There is a thickness of PCM above and below the sheet, so more heat or power is generated within the store. The melting point of RT 58 based on result from the DSC is 58°C, while it is 52°C for the PCM RT 52. The temperature difference between the inlet HTF temperature for RT 52 and RT58 are 8°C and 7°C respectively. Thus the charge rate of the store with a constant inlet HTF temperature (65°C) can be calculated using Equation 10.37

$$\dot{Q} = h_f A \Delta T \qquad 10.37$$

For the RT 58 PCM, the charge rate is calculated thus

$$\dot{Q} = 577.52 * 0.76 * (65 - 58)$$

$$\dot{Q} = 3.1kW$$

For the RT 52 PCM, the charge rate is calculated thus;

$$\dot{Q} = 577.52 * 0.76 * (60 - 52)$$

$$\dot{Q} = 3.5kW$$

Based on this, the thickness of the PCM on the sheet, flow rate and other parameters was varied to determine the optimal performance of the store. The time of melting the store was taken into consideration as the advantage of utilizing the store during off-peak periods as economy 7 tariffs, where cheaper electricity is targeted. The idea was to charge the store during off peak periods and recover the heat during peak periods for the domestic application.

The result from the DSC was used for the modelling of each PCM. Table 10:2 shows the thermal behaviour of the PCMs.

Table 10:2: Overview of the PCM thermal properties

| PCM | Thermal Conductivity | Phase change temperature range | Latent heat | Specific heat capacity(solid) | Specific heat capacity(liquid) |
|---|---|---|---|---|---|
| | W/mK | (°C) | kJ/kg | kJ/kgK | kJ/kgK |
| RT 52 | 0.22 | 51-55 | 153 | 6.8 | 5.0 |
| RT 58 | 0.23 | 54-62 | 140 | 5.7 | 2.3 |

### 10.4.1 Charge Process using RT 58

Using RT 58 for the charge process, the initial condition of the store was set at 50°C, while a constant inlet HTF temperature of 65°C was inputted in the model. The charge process and energy results are presented using Figure 10:14 and Figure 10:15 respectively. The PCM thickness was varied during the simulation for three different scenarios (10, 20 and 40mm). Figure 10:20 and Figure 10:21 shows the charge process result using RT 52, at a constant inlet HTF temperature of 60°C.

Figure 10:14 shows the charge rate of the thermal store at three different thicknesses. It shows that, the thicker wax has a higher charge rate and it takes the PCM a longer time to melt. However, at a thickness of 10mm, the PCM melts faster when compared to the charge rate at 20mm and 40mm. There is a maximum value of power as the heat

is transferred at the commencement of the charge process. This is due to the thermal gradient between the HTF and PCM was at maximum at the commencement of the charge process and the PCM thermal resistance is low. As the PCM starts to melt, the power reduces significantly due to the increase in PCM thermal resistance and reduction of the thermal gradient between the PCM and HTF.

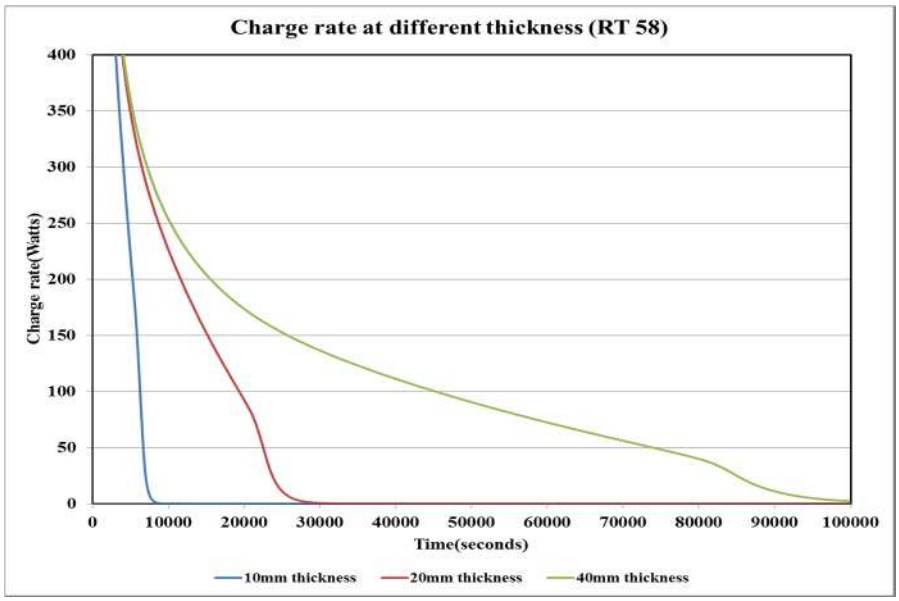


Figure 10:14: Charge rate at different thickness(RT 58).

The energy profile shown in Figure 10:15 shows that the thicker wax has the highest energy, while the thinner wax (10mm) has the least energy when compared to others. The stored energy is doubled as the wax thickness is doubled. Figure 10:15 shows the energy profile of the thermal store at three different thicknesses. As the thermal store is charged, the energy profile rises directly with time, as the PCM melts, the profile starts to change. The trend plateaus as soon as the PCM has completely melted and there is no further increase in energy into the store. This result shows that, the thicker wax takes a longer time to melt. However at a thickness of 10mm, it shows that the PCM melts faster, when compared to the charge rate at 20mm and 40mm. The result obtained from this profile would determine the thickness of wax to use to obtain the optimal charge rate and energy from the store within the off peak electricity tariff.

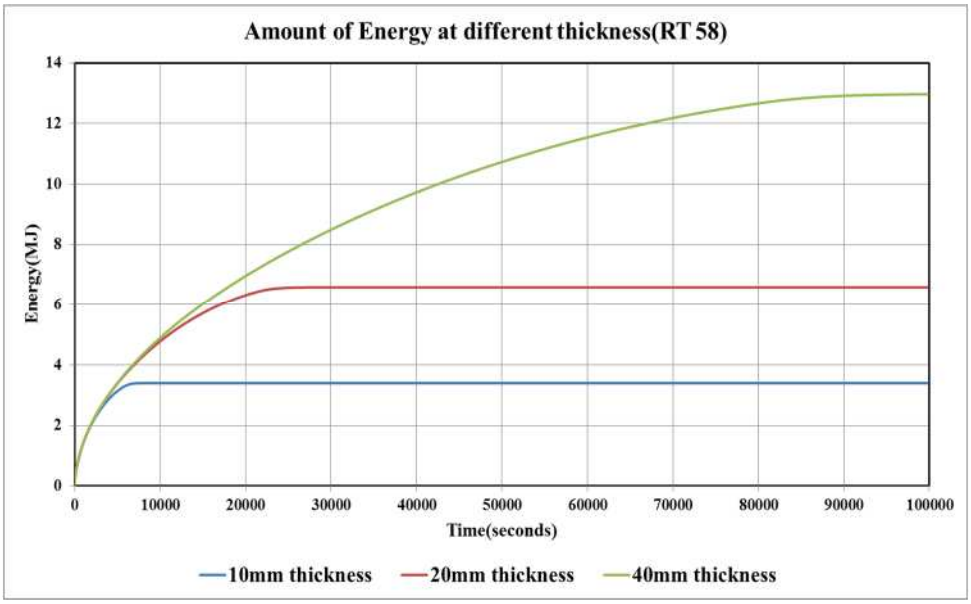


Figure 10:15: Energy profile at different thickness (RT 58).

Figure 10:16(a-c) shows the temperature change across the PCM as it melts from the initial store temperature of 50°C for a thickness of 10mm at different times(500,3500 and 4000 seconds). It is observed that the HTF and wall zones are at a higher temperature at the start of the charging process. The PCM temperature increases as it gains heat from the HTF via the wall of the PP sheet.

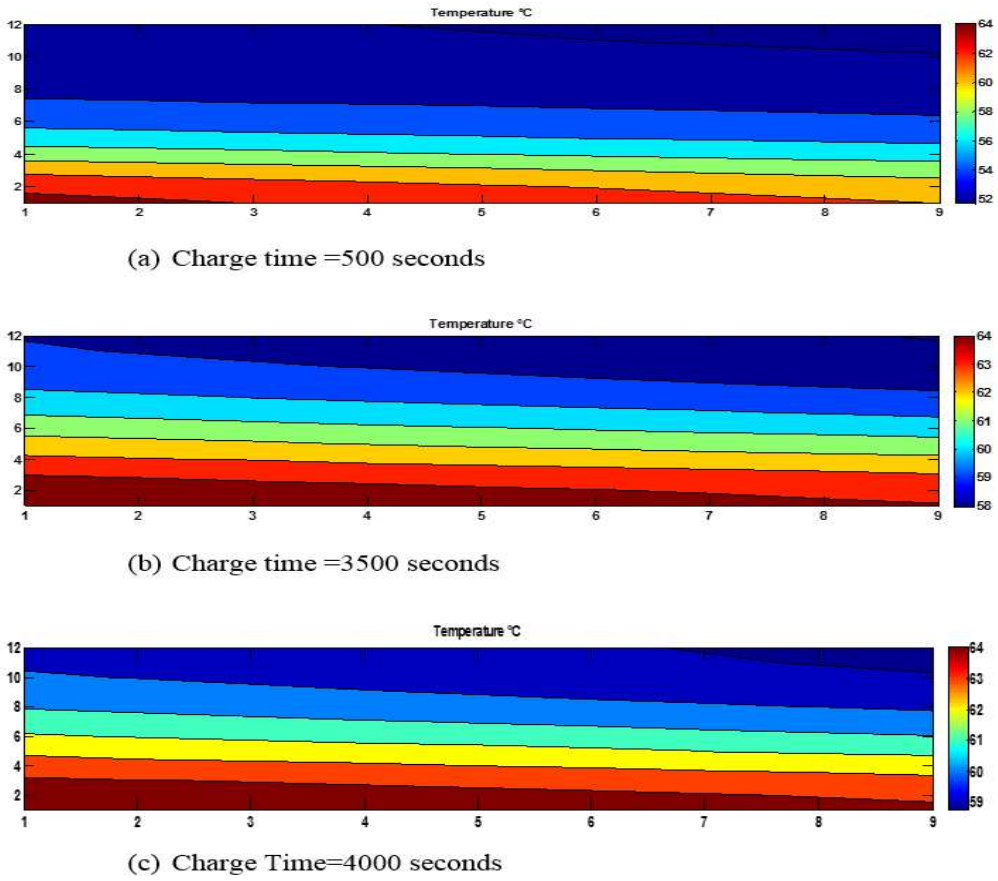


Figure 10:16: Colour map showing temperature distribution (charging process).

The profile shows the variation in temperature with time across the store as the PCM melts. The nodes closer to the HTF nodes melts quicker than the PCM nodes. Increasing the heat transfer fluid temperature causes the PCM to melt faster due to a higher temperature difference between the HTF and the PCM.

Figure 10:17 (a-c) and Figure 10:18(a-c) shows the temperature contour map of the PCM at different thickness, 20 and 40mm respectively, when it is charged at an inlet HTF temperature of 65°C. The temperature contour map snapshots were taken at the same time (500, 3500 and 4000 seconds) as the 10mm PCM thickness (Figure 10:16(a-c)). It takes a longer time to charge the PCM with thicknesses of 20mm and 40mm compared to the PCM with 10mm thickness. For example, at 4000 seconds, the PCM is entirely melted at 4000 seconds for 10mm thickness(See Figure 10:16c), while for 20mm and 40mm PCM thickness, melting is incomplete(See Figure 10:17c and Figure 10:18c respectively). From the temperature contour map, it can be observed that there was only a small temperature change across the store, and buoyancy forces are negligible, hence convection is not considered in the model for the thermal store.

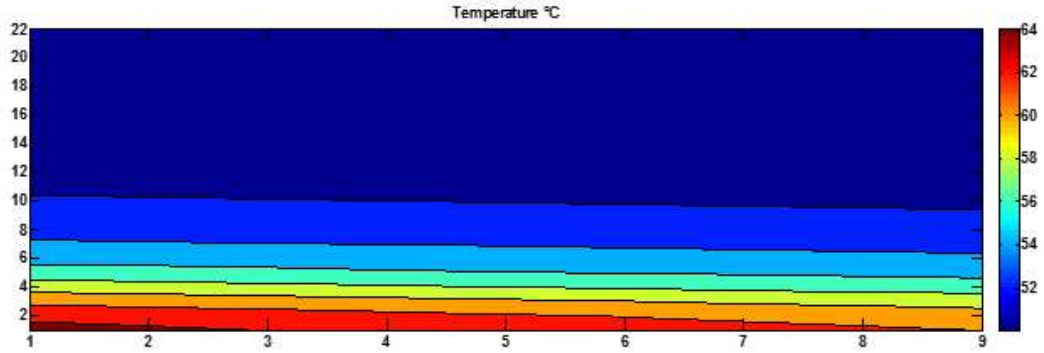


(a) Charge time =500 seconds (20mm PCM thickness)

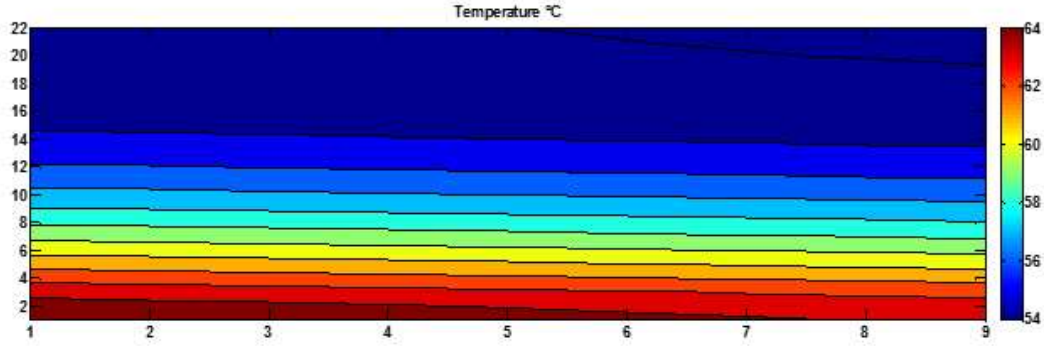


(b)Charge time =3500 seconds (20mm PCM thickness)

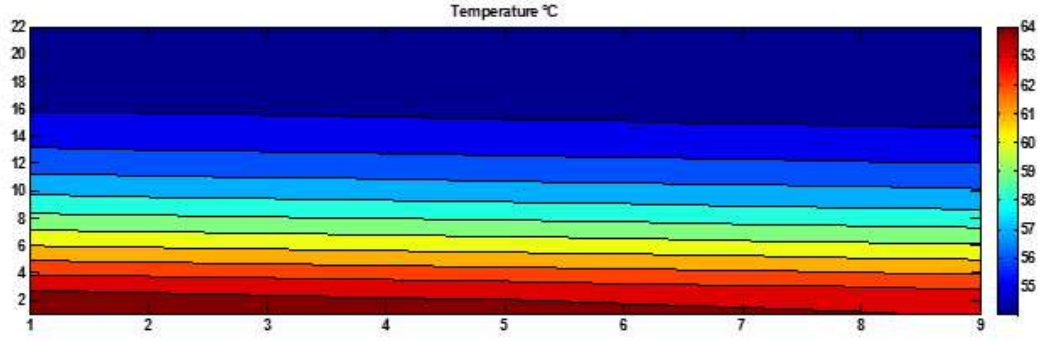


(c)Charge time =4000 seconds (20mm PCM thickness)

Figure 10:17: Colour map showing temperature distribution at 20mm PCM thickness (RT 58).

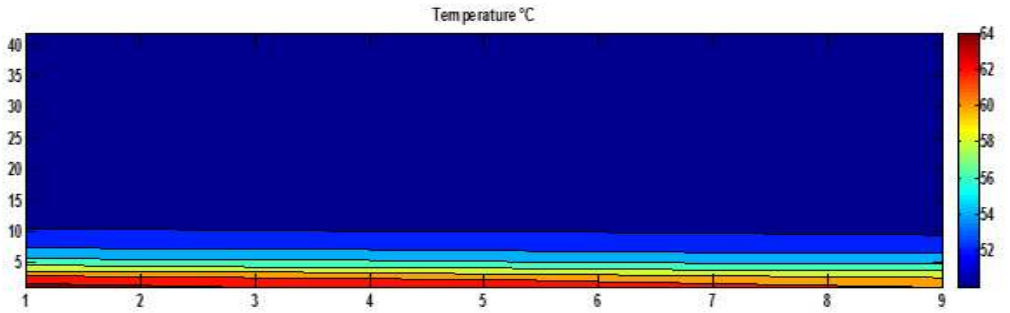


(a) Charge time =500 seconds (40mm PCM thickness)

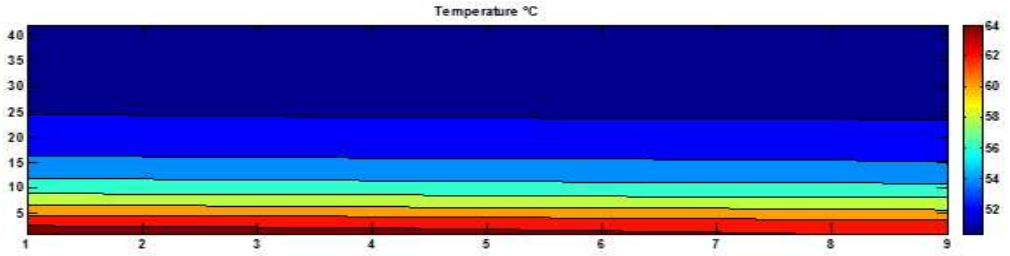


(b)Charge time =3500 seconds (40mm PCM thickness)

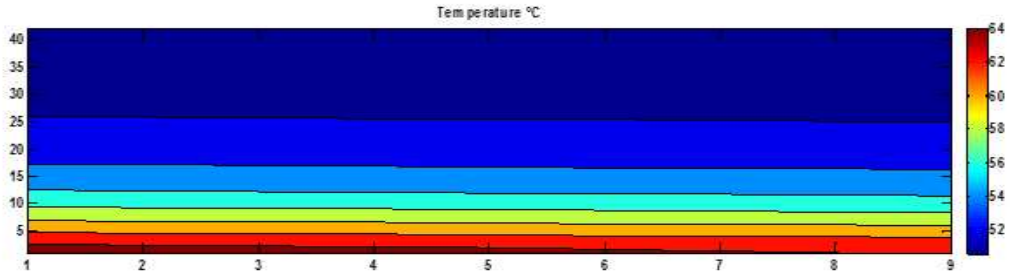


(c)Charge time =4000 seconds (40mm PCM thickness)

Figure 10:18: Colour map showing temperature distribution at 40mm PCM thickness (RT 58).

Using the energy profile of the thermal store, the behaviour of the store when it is fully charged and half charged can be deduced. Figure 10:15 shows when the store is half and fully charged, the energy of the fully charged store for 10mm, 20mm and 40mm PCM thickness are 3.4MJ, 6.5MJ and 13MJ respectively. Considering when the store is half charged, that will be half of the energy evolved when the store is fully charged for each PCM thickness. The time at which the PCM is half charged is located and the corresponding charge rate deduced from the charge rate result.

Table 10:3 shows the condition of the thermal store (using RT 58) when it is half charged for the charging process. Based on the MATLAB model, the charge rate obtained in Table 10:3 needs to be doubled to determine the actual charge rate, because

the model was done considering only half of the sheet. The results presented are obtained directly from the plot of the energy stored and charge rate.

Table 10:3: Full and half charge rate using RT 58

| Thickness (mm) | Full charge (MJ) | Half charge (MJ) | Charge rate (W) |
|---|---|---|---|
| 10 | 3.40 | 1.70 | 660 |
| 20 | 6.50 | 3.25 | 360 |
| 40 | 13.00 | 6.50 | 187 |

### 10.4.2 Charge Process using RT 52

The same analysis carried out using the Matlab model for PCM (RT 58) was done for RT 52, by updating the code with its thermal properties at high flow. The simulation was carried out at six (6) different PCM thicknesses. The PHE thermal store was charged at an inlet HTF temperature of 60°C from an initial store temperature of 50°C. The temperature profile of the PCM and HTF at a PCM thickness of 40mm is presented in Figure 10:19. It shows the HTF inlet and outlet temperature and PCM temperature. The result shows that at the start and end of the charging process, the temperature difference between the inlet and outlet HTF temperature reduces as the PCM melts. The PCM was completely melted at about 140000 seconds. The melting time is influenced by the PCM thickness.

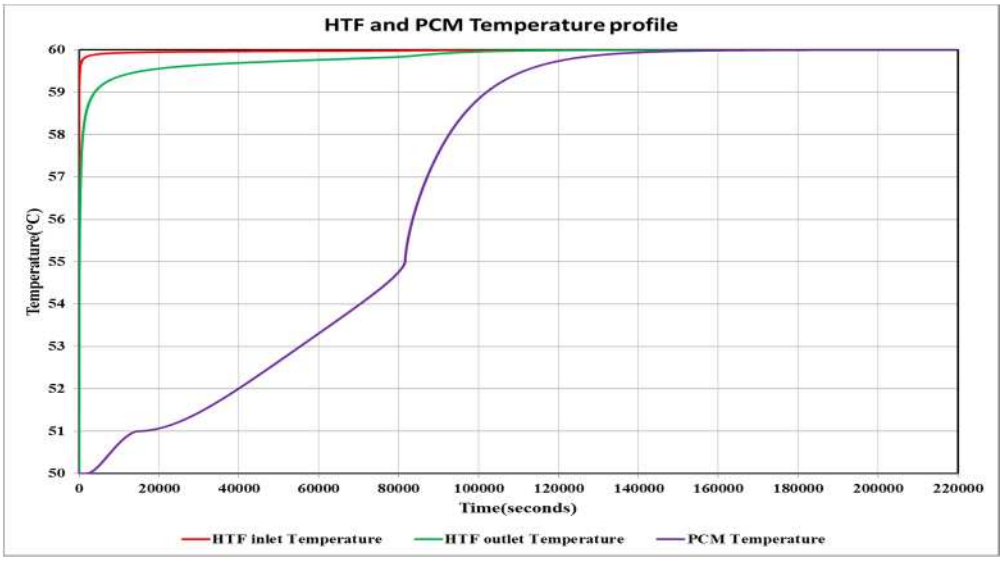


Figure 10:19: HTF and PCM temperature profile(40mm thickness).

The charge rate and energy stored at the six (6) different thicknesses are presented in Figure 10:20 and Figure 10:21 respectively. It is observed that the results follow a

similar trend to the results obtained from the simulation with RT 58. The simulation results at different thickness (10,20 and 40mm) shows that the energy profile at each thickness is more than that obtained using the properties of RT 58 at the same high flow. This could be attributed to the latent heat and specific heat capacities of RT52 being more than the properties of RT 58. Also, the temperature difference between the HTF and PCM is also higher; using RT 52 (60-52=8°C) compared to RT 58(65-58=7°C). Figure 10:20 shows that the rate of melting is faster at low thickness. The charge rate reduces with increase in PCM thickness.

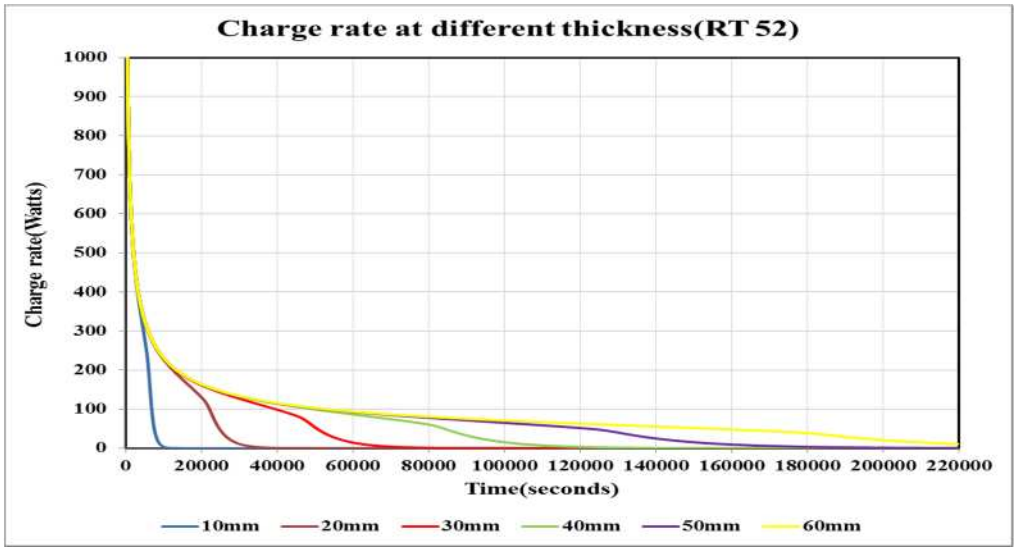


Figure 10:20: Charge rate at different thickness using RT 52 (Charging).

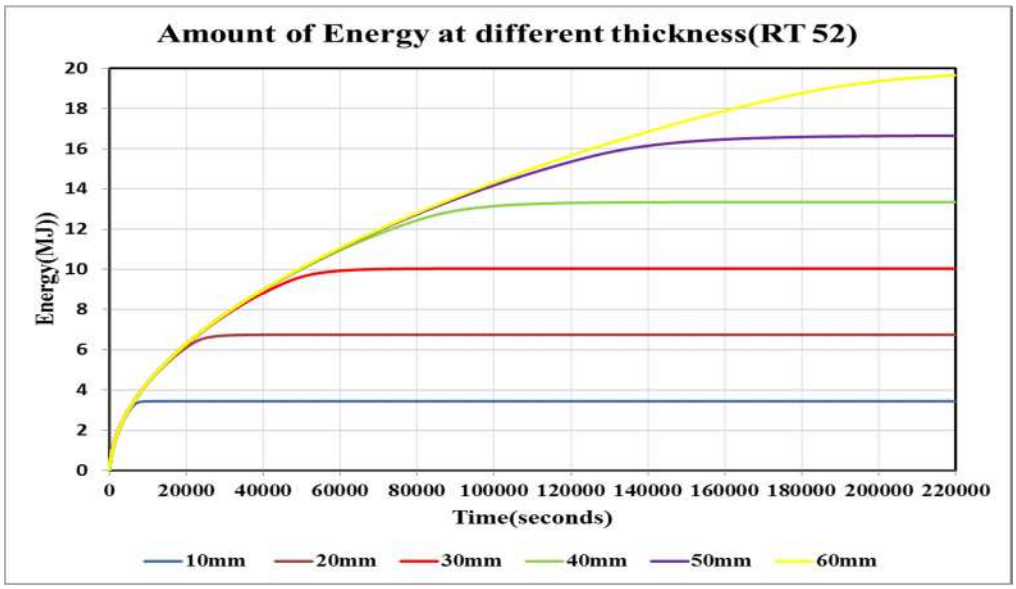


Figure 10:21: Energy stored at different thicknesses using RT 52(Charging).

At the same flow, the higher the thickness, the more the energy obtainable from the store. Table 10:4 shows the result of the thermal store (using RT 52) when it is half charged and fully charged for the charging process.

Table 10:4: Full and half charge rate using RT 52.

| Thickness (mm) | Full charge (MJ) | Half charge (MJ) | Charge rate (W) |
|---|---|---|---|
| 10 | 3.43 | 1.72 | 531 |
| 20 | 6.74 | 3.37 | 292 |
| 30 | 10.04 | 5.02 | 202 |
| 40 | 13.36 | 6.68 | 154 |
| 50 | 16.64 | 8.32 | 124 |
| 60 | 19.64 | 9.82 | 106 |

The results show that the store does not need to be fully charged for it to be used, for a higher charge or discharge rate is obtainable when the store is half charged. Based on the fact that it takes a longer time for the store to be fully charged, thus the store can be half charged within the off-peak periods where there is cheap electricity.

The thermal store capacity and charge rate can be increased by having more sheets combined together in parallel. The results from this modelling and experiment results can be used to determine the number of sheets that can be incorporated into a PHE thermal store for domestic heating application. For the required domestic application, an 8kW heat pump is proposed to operate based on Economy 7 tariff. Based on

Economy 7, there is about four (4) hours of off-peak electricity (8kWx 4hrs=32kWh). The thermal store is optimized for this purpose. The result from charging the store using RT 52 is used for this analysis. The sheet capacity $Q_{T_{AN}}$ (MJ) is calculated using Equation 10.38 and Equation 10.39. The calculation is done for the six (6) different thicknesses.

$$Q_{T_{AN}} = Q_p + Q_f + Q_w \qquad 10.38$$

$$Q_{T_{AN}} = \int_{T_{ini}}^{T_s} m_p C_{p_s} + \int_{T_l}^{T_F} m_p C_{p_l} + m_p h_{sf} + \int_{T_{ini}}^{T_F} m_f \frac{C_{p_f}}{2} + \int_{T_{ini}}^{T_F} m_w C_{p_w} \qquad 10.39$$

*where*;

$T_{ini} = 50^{o}C$

$T_s = 51^{o}C$

$T_l = 55^{o}C$

$T_F = 60^{o}C$

$T_s$ and $T_l$ is the phase change temperature range of RT 52 as shown in Table 10:2. The initial and final temperature of the store are $T_{ini}$ and $T_F$ respectively. The result for calculating the sheet capacity of the store based is presented in Table 10:5 , which also compares the result obtained from the model using Table 10:4.

Table 10:5: Comparing Model and anaylitcal result for total sheet capacity.

| | | **Analytical** | **Model** | |
|---|---|---|---|---|
| **Thickness(mm)** | **Thickness(m)** | **$Q_T$(MJ)** | **$Q_T$(MJ)** | **% Difference** |
| **10** | **0.01** | **3.23** | **3.43** | **5.74** |
| **20** | **0.02** | **6.33** | **6.74** | **6.13** |
| **30** | **0.03** | **9.42** | **10.04** | **6.17** |
| **40** | **0.04** | **12.51** | **13.36** | **6.33** |
| **50** | **0.05** | **15.61** | **16.64** | **6.21** |
| **60** | **0.06** | **18.70** | **19.64** | **4.78** |

The results obtained from the model and analytical calculations show a difference of 6% between both analysis. The analytical calculation took into consideration the

quantity of heat transferred through the water, wall and PCM. For the PCM, the sensible heat and latent heat were considered.

Based on Table 10:4, the charge rate and energy stored using results from the model for RT 52 can be used to deduce the total store capacity(MJ) obtainable when certain number of sheets are used. For example,

For the thickness of 30mm, at full charge, energy = 10.04MJ

Half charge = $\frac{10.04MJ}{2}$ = 5.02MJ

Using Figure 10:20 and Figure 10:21 , the charge rate at half charge is deduced as 202W. Based on the MATLAB model for the sheet which comprises of wax at top and bottom of the sheet, the charge rate is doubled; 2x202W=404W to get the actual charge rate.

Based on the desired output from the thermal store to be used for economy 7, where there is cheaper electricity for about 4 hours during the off-peak periods. Running the heat pump for four hours gives 32kWh. The total thickness required to deliver this output is determined using Equation 10.40 and Equation 10.41.

$$Q_{T_{Output}} = \rho_{\mathrm{PCM}} * A * t_{PCM_T} * \mathrm{h_{sf}} \qquad 10.40$$

$Q_{T_{Output}}$ =32kWh is converted to Joules (1kWh=3.6MJ) = 115.2 M J.

$$t_{PCM_T} = \frac{Q_{T_{Output}}}{\rho_{\mathrm{PCM}} * A * \mathrm{h_{sf}}} \qquad 10.41$$

The number of sheets can be calculated using Equation 10.42.

$$N = \frac{Q_{T_{Output}}(MJ)}{Q_{T_{MO}}} \qquad 10.42$$

The total charge rate of the PHE thermal store is calculated using Equation 10.43.

$$\dot{Q}_{s_T} = \dot{Q}_s * N \qquad 10.43$$

The total PCM thickness ($t_{PCM_T}$ =1.126m) required to deliver the required energy (32kWh) from an 8kW heat pump was obtained using Equation 10.41 . The total store charge rate; $\dot{Q}_{s_T}$ (W) is a product of the number of sheets (N) and the sheet charge rate $\dot{Q}_s$ (W) for a single sheet. Thus, Equation 10.43 is used to calculate the total store charge rate.

An overview of the result is shown on Table 10:6, showing the number of sheet, sheet charge rate and the total charge rate of the PHE store. The result shows that a PCM thickness of 30mm is suitable for integration with a 8kW heat pump. Using 22 sheets for a charge rate of 404W gave a total store charge rate of 8.89kW.

Table 10:6: Overview of the result

| Thickness (m) | Thickness($m^{-1}$) | Sheet charge rate(W) | Number of sheet(N) | Total store charge rate(kW) |
|---|---|---|---|---|
| 0.01 | 100 | 1062 | 66 | 70.09 |
| 0.02 | 50 | 584 | 34 | 19.86 |
| 0.03 | 33.33 | 404 | 22 | 8.89 |
| 0.04 | 25 | 308 | 16 | 4.93 |
| 0.05 | 20 | 248 | 12 | 2.98 |
| 0.06 | 16.67 | 212 | 10 | 2.12 |

The relationship between the charge rate and thickness of PCM was ascertained by plotting the results from the simulation based against the thickness of PCM. Results obtained from Figure 10:20 and Figure 10:21 were used to acquire this relationship as shown in Figure 10:22. The results show that as the thickness of the PCM increases, the charge rate reduces. This indicates that the charge rate is inversely proportional to the PCM thickness. A power fit was applied to the result for the six different points. Based on this relationship, a further plot of the charge rate and inverse of the thickness was used to get a linear relationship between both parameters. Figure 10:23 shows this linear relationship with a $R^2$ of 99.8%. The graph can be used to obtain the required thickness or charge rate for the thermal store. R-squared is a statistical measure of how near the data points are to the fitted regression line

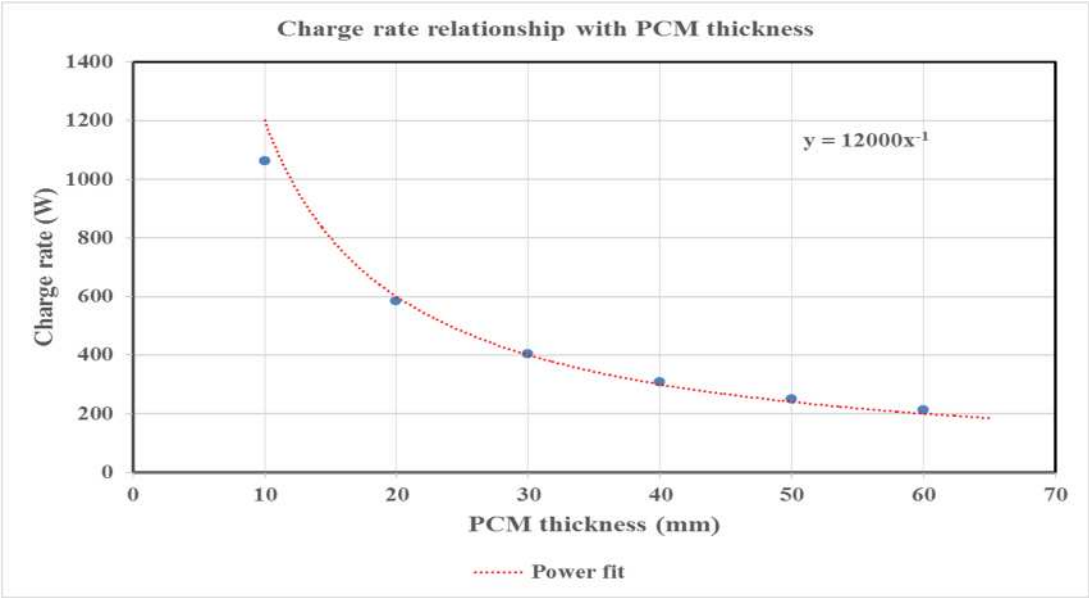


Figure 10:22: Relationship of charge rate and thickness of PCM (RT 52).

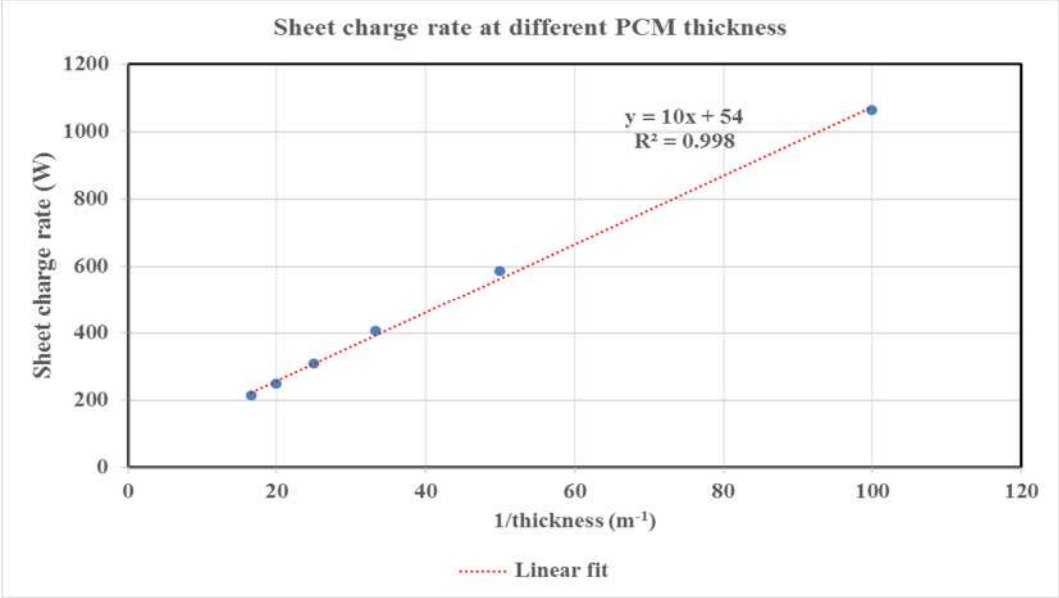


Figure 10:23: Single sheet charge rate at different thickness ($m^{-1}$).

The total store charge rate is a multiplication of the sheet charge rate and the number of sheets (N). Figure 10:24 shows the relationship between the total store charge rate and thickness ($m^{-1}$) of the PHE thermal store. From this graph, the thickness of |PCM required to achieve a charge rate of 8kW can be obtained and the number of sheets determined.

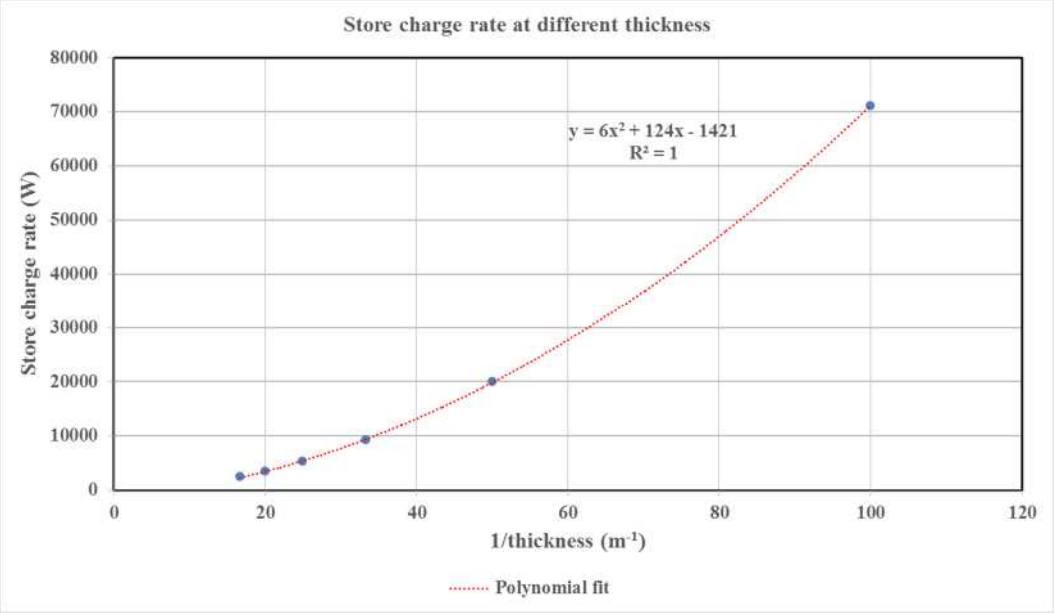


Figure 10:24: Store charge rate at different thickness ($m^{-1}$).

Based on this result, PCM thickness of 30mm will be suitable for the heat pump (8kW) to produce 32kWh of energy during off peak period with economy 7 tariff. The store charge rate at the aforementioned PCM thickness is 8.89kW. This can work in conjunction with a 8kW heat pump for domestic application. This makes it suitable for the thermal storage, where the energy from the heat pump can be utilized and the thermal store charged during the off peak period.

For a given store capacity, in this case;32kWh,the ratio of the store charge rate (kW) and storage capacity (kWh) gives the period (per hour) required to charge the store. Figure 10:25 shows how long is required to charge the store at a given charge rate for different thicknesses. The greater the thickness of the store, the lower the charge rate. From the graph, to charge the store for four hours, you require a period of 0.29 per hour, thus a thickness of 30mm is required to achieve a total store capacity of 32kWh. The time it takes to charge the store and thickness required can be obtained from Figure 10:25.

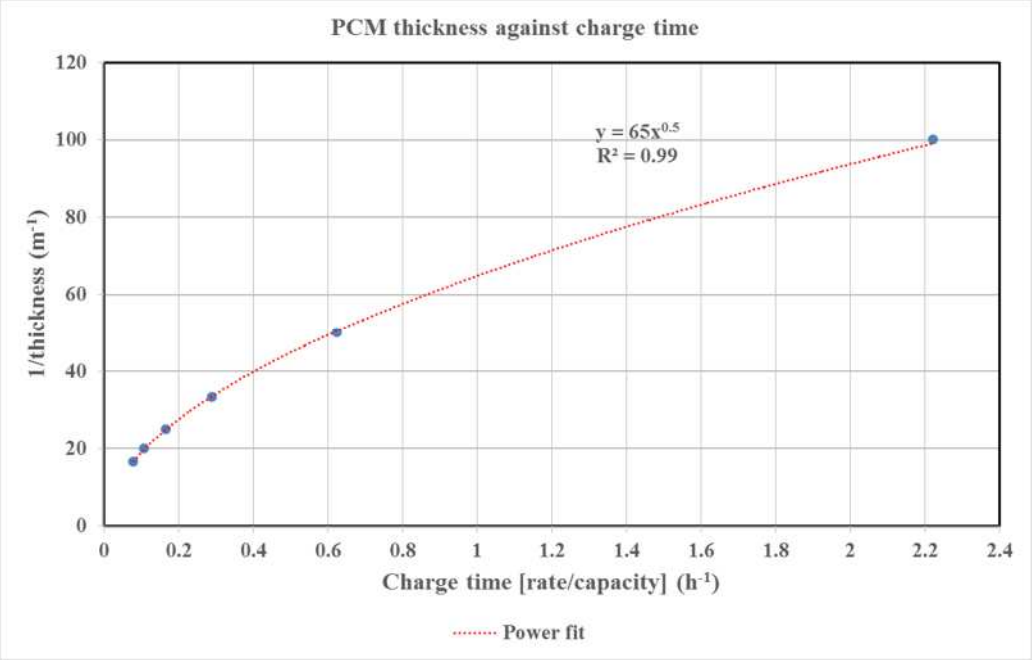


Figure 10:25: Plot of thickness against ratio of charge rate and store capacity.

### 10.4.3 Discharge Process using RT 58

The discharge process using the updated Matlab model was used to simulate the behaviour of the store when it is discharged from an initial temperature of 65°C to 40°C by setting the inlet HTF temperature to 40°C. Figure 10:26(a-c) shows the PCM temperature transition from the start of the discharge process till the store temperature achieves a temperature of 40°C. Figure 10:26(a-c) shows the temperature contour map across the element as it is discharged for a PCM thickness of 10mm over time(500, 2000 and 2800 seconds). It shows the region of the wall and HTF cools faster compared to the PCM zone. The PCM temperature drops gradually as it loses heat to the wall and HTF, till it solidifies. The store discharges quicker compared to the time it takes to charge it.

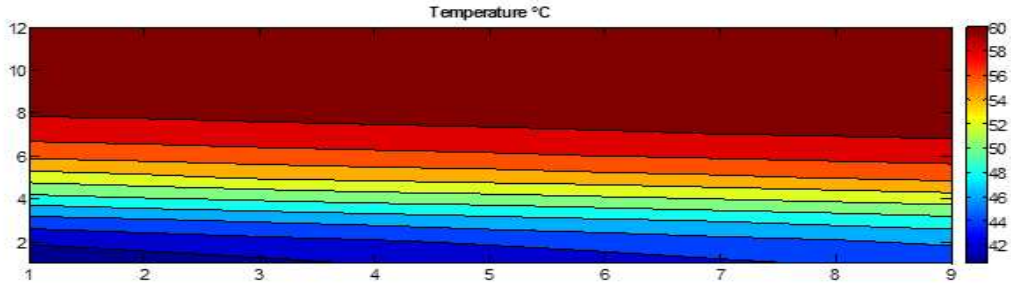


(a)Discharge Time=500 seconds (10mm PCM thickness)

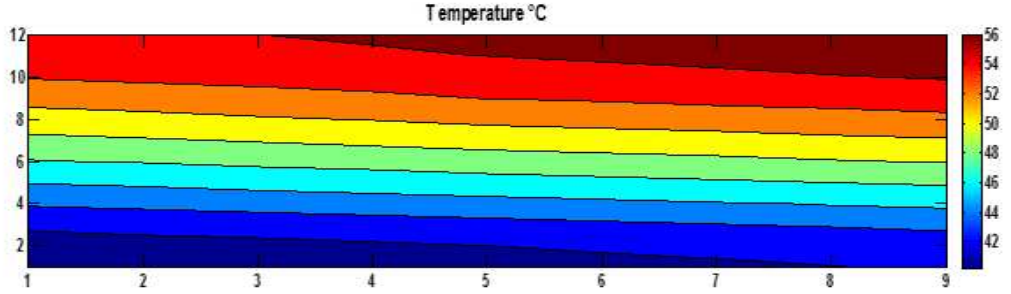


(b) Discharge Time=2000 seconds (10mm PCM thickness)

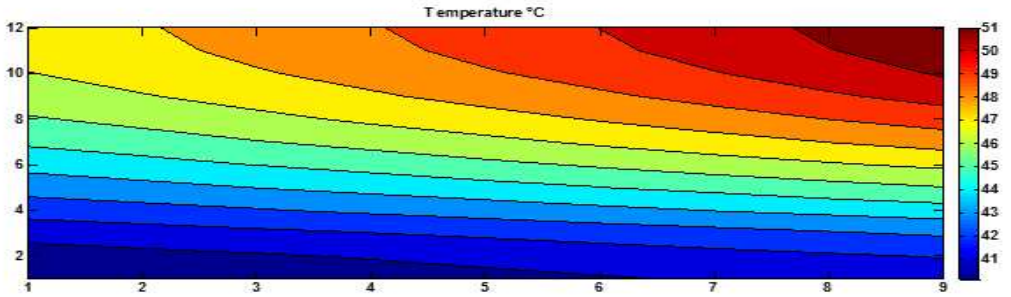


(c)Discharge Time=2800 seconds (10mm PCM thickness)

Figure 10:26: Temperature contour map showing the discharging process (from initial store temperature of 65°C).

The same analysis done for the charge process is carried out for the discharge process. Figure 10:27 and Figure 10:28 shows the result obtained using the properties of RT 58 during the simulation for energy stored and charge rate respectively. The charge rate and energy obtained from the discharging process at different thickness (10, 20 and 40mm) shows the thicker PCM possess more energy when compared to the thinner PCM (10 and 20mm). However, the problem with this is that it takes a longer time to discharge the store at thicker PCMs. Based on the objective of this research to study the behaviour of PCMs in a thermal energy storage and optimize the parameters with integration of domestic heat pump, it is vital to be able to charge and discharge the store quickly within the off peak periods using economy 7 tariffs.

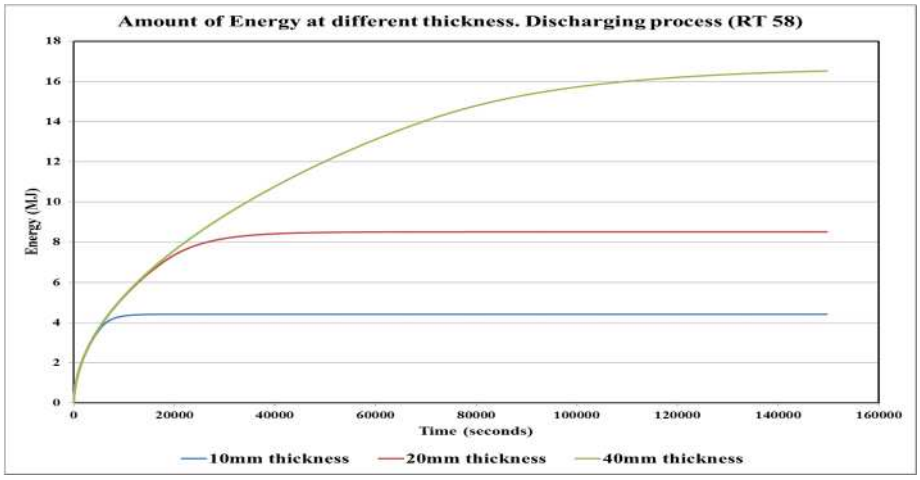


Figure 10:27: Energy at different thickness using RT 58.

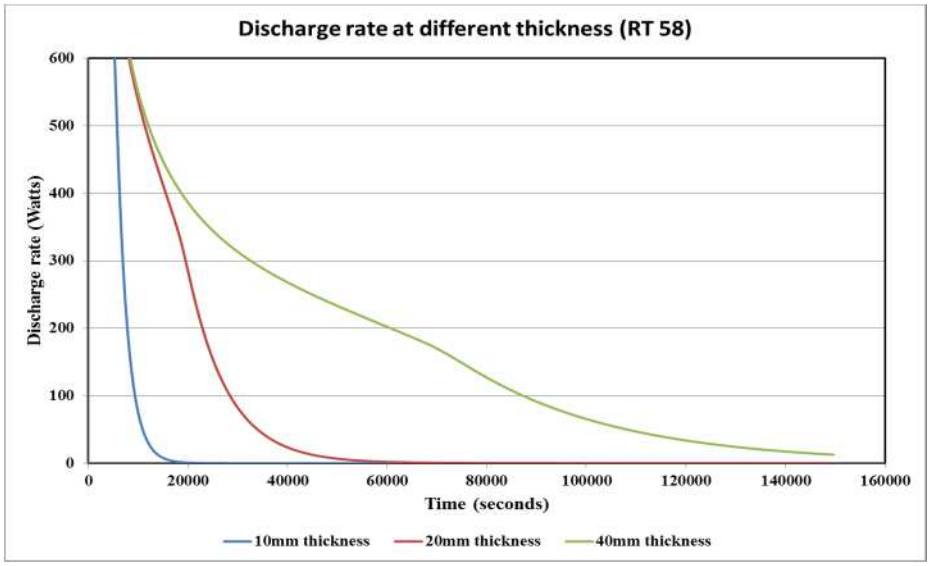


Figure 10:28: Discharge rate at different thickness using RT 58.

### 10.4.4 Discharge process using RT 52.

Figure 10:29 and Figure 10:30 show the result for discharging the store at different thickness using the properties of RT 52. This is done for six (6) different thicknesses (10, 20,30,40,50 and 60mm). The results show that the energy from the store is higher than when the store is charged. The results show a similar trend to when the store was charged; the higher the PCM thickness, the higher the amount of energy. Also the rate of melting reduces as the PCM thickness increases. It takes a longer time to discharge the store as the PCM thickness increases.

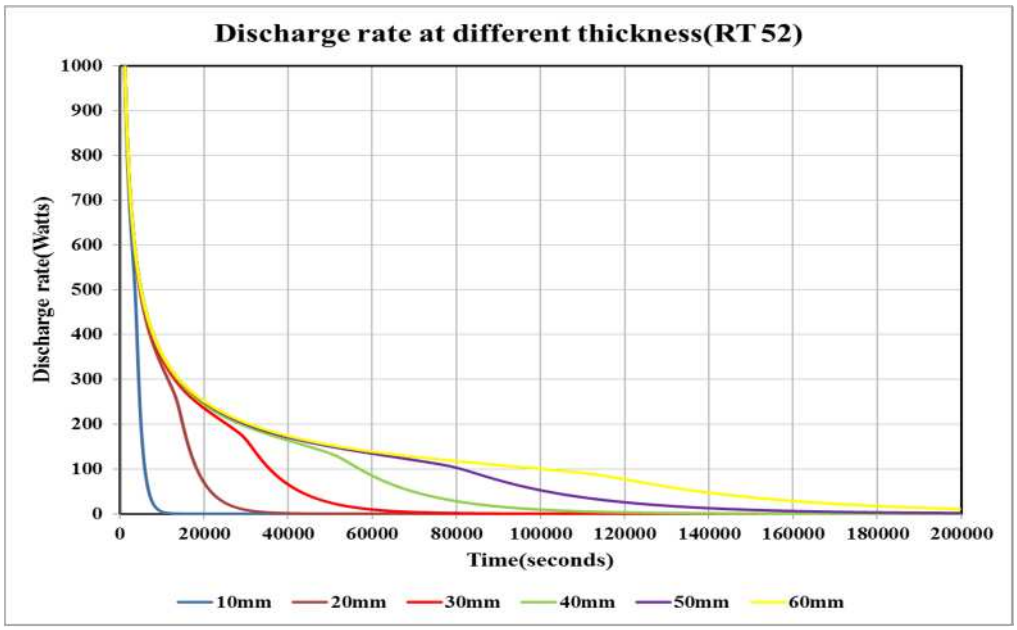


Figure 10:29: Discharge rate at different thickness using RT 52.

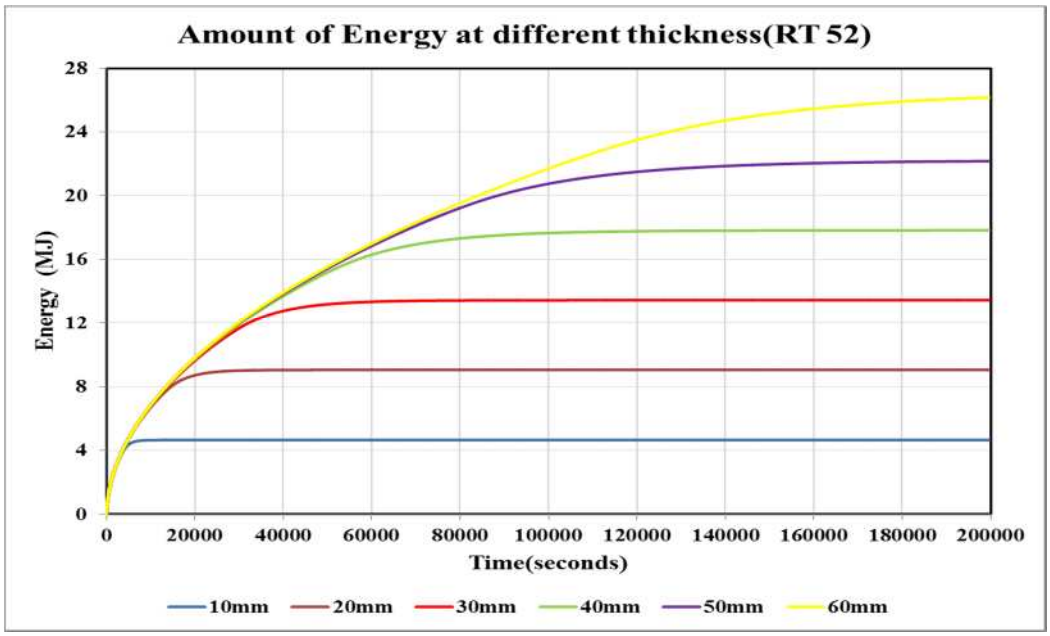


Figure 10:30: Energy stored at different thickness using RT 52(Discharging).

Table 10:7 and Table 10:8 give the details of the discharge rate of the store when it is half charged and fully charged for both RT 52 and RT 58.

Table 10:7: Discharge rate for RT 58.

| Thickness (mm) | Full discharge (MJ) | Half discharge (MJ) | Discharge rate (W) |
|---|---|---|---|
| 10 | 4.40 | 2.20 | 1244 |
| 20 | 8.50 | 4.25 | 673 |
| 40 | 16.50 | 8.25 | 355 |

Table 10:8: Discharge rate for RT 52.

| Thickness (mm) | Full discharge (MJ) | Half discharge (MJ) | Discharge rate (W) |
|---|---|---|---|
| 10 | 4.64 | 2.32 | 941 |
| 20 | 9.03 | 4.52 | 512 |
| 30 | 13.42 | 6.71 | 353 |
| 40 | 17.63 | 8.82 | 272 |
| 50 | 22.10 | 11.05 | 218 |
| 60 | 26.15 | 13.08 | 185 |

Table 10:8 shows the discharge rate and energy using RT 52 is greater than the result obtained using RT 58 at the same thicknesses (10, 20 and 40mm) on Table 10:7. The thickness of the PCM used results in an increase in energy stored in the store during the charging process. However, the thicker the PCM, the longer it takes for the PCM to melt (melting time). Thus for applications in homes, the melting time and amount of energy required from the store when it is fully or half charged is vital.

Keeping the same number of sheet as the charge cycle, the same analysis done for the charging process using RT 52 was done for the discharging process. This is presented using Figure 10:31 to Figure 10:34. Table 10:9 gives an overview of the thickness of the PCM, sheet discharge rate and total store discharge rate based on calculations done using Equation 10.40 to Equation 10.43.

Table 10:9: Overview of the result(Discharging)

| Thickness(mm) | Thickness ($m^{-1}$) | Sheet discharge rate(W) | Total Store discharge rate(kW) |
|---|---|---|---|
| 10 | 100 | 941 | 46.73 |
| 20 | 50 | 512 | 13.05 |
| 30 | 33.33 | 353 | 6.06 |
| 40 | 25 | 272 | 3.55 |
| 50 | 20 | 218 | 2.27 |
| 60 | 16.67 | 185 | 1.63 |

The relationship between the discharge rate and thickness of PCM was ascertained by plotting the results from the simulation based against the PCM thickness. Results obtained from Figure 10:29 and Figure 10:30 were used to acquire this relationship as shown in Figure 10:31. The results show that as the thickness of the PCM increases, the discharge rate reduces. This indicates that the discharge rate is inversely proportional to the PCM thickness. A power fit was applied to the result for the six different points. Based on this relationship, a further plot of the charge rate and inverse

of the thickness was used to get a linear relationship between both parameters. Figure 10:32 shows this linear relationship with a $R^2$ of 1. The graph can be used to obtain the required thickness or discharge rate for the thermal store. R-squared is a statistical measure of how near the data points are to the fitted regression line.

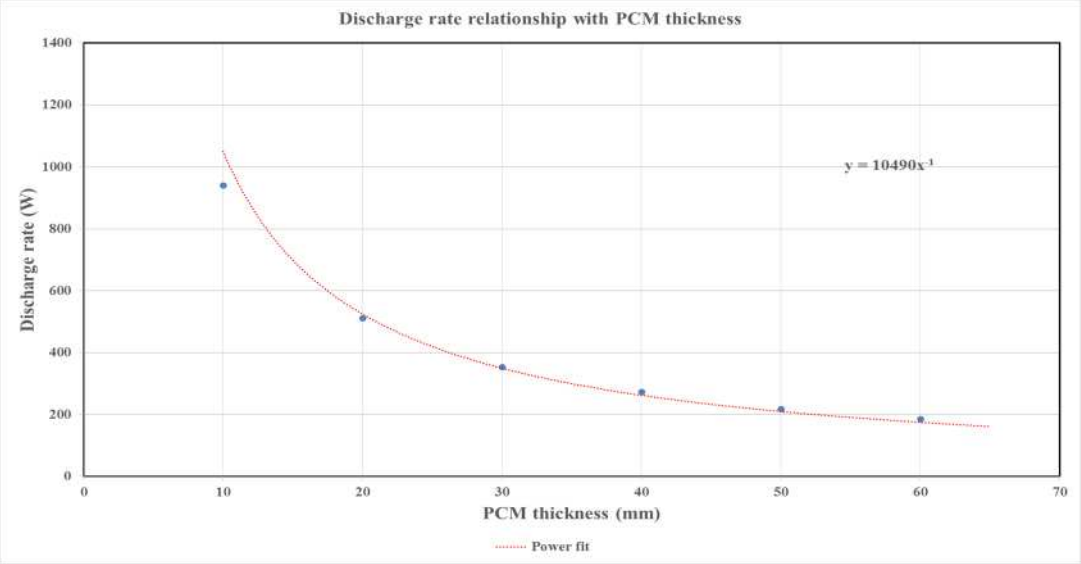


Figure 10:31: Relationship of discharge rate and thickness of PCM (RT 52).

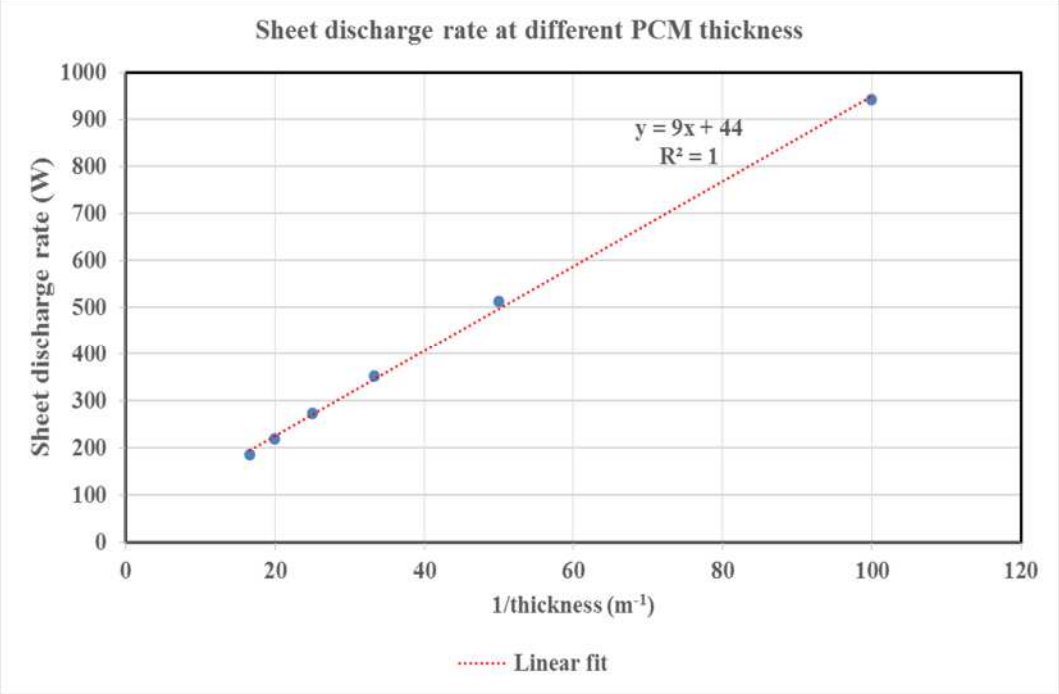


Figure 10:32: Single sheet charge rate at different thickness ($m^{-1}$).

The total store discharge rate is a multiplication of the sheet discharge rate and the number of sheets (N). Figure 10:33 shows the relationship between the total store discharge rate and thickness ($m^{-1}$) of the PHE thermal store.

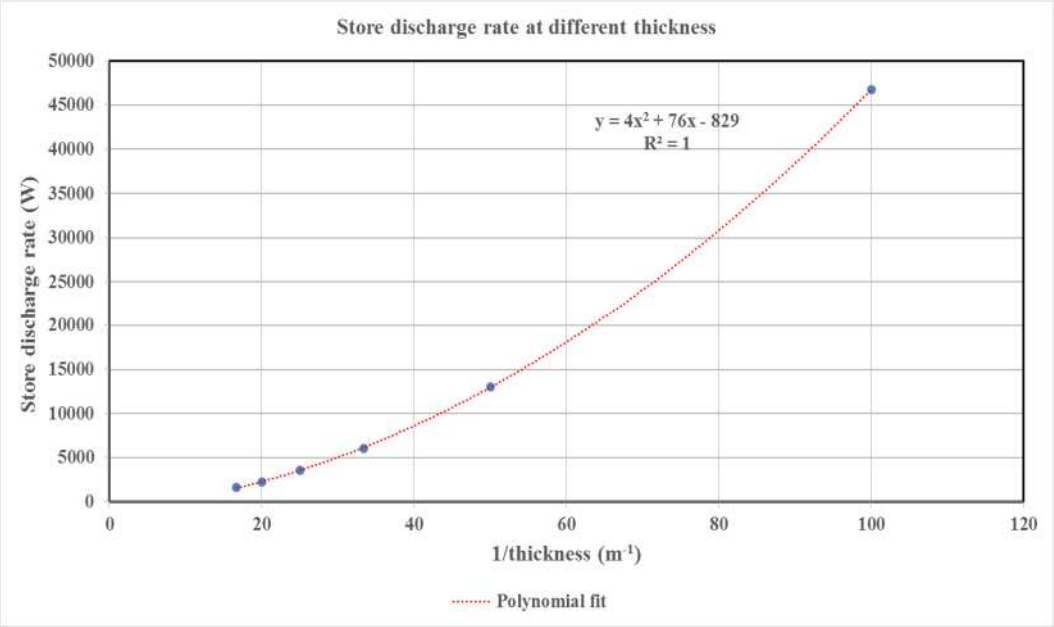


Figure 10:33: Store charge rate at different thickness ($m^{-1}$).

Figure 10:34 shows how long is required to discharge the store at a given discharge rate for different thicknesses. The greater the thickness of the store, the lower the discharge rate. From the graph, to discharge the store for four hours, you require a period of 0.18 per hour. The time it takes to charge the store and thickness required can be obtained from Figure 10:34.

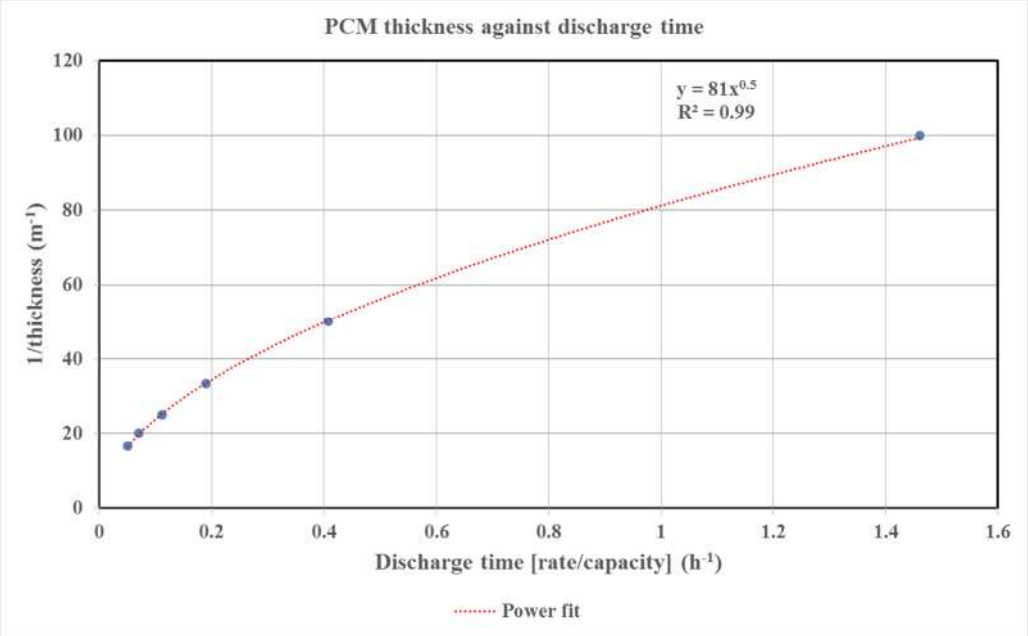


Figure 10:34: Plot of thickness against ratio of discharge rate and store capacity.

Based on the economy 7, it is vital that the heat pump is operating during the periods of cheap electricity. Having a thermal store that can charge quickly within these periods will be of great advantage. PHE charges under three hours, which makes it suitable to be used for any of the economy tariffs for cheap electricity. The PCM thickness of 30mm was chosen as the optimal thickness to be used. Based on the optimal thickness of 30mm, the sheet charge rate is 8.89kW, and at the same thickness, sheet discharge rate is 6.06kW. Based on the chosen PCM thickness, the size of the thermal store with the PCM at the top and bottom for a single sheet, taking into consideration the height of the sheet is 64mm. Thus for twenty sheets (22), the overall height is (64mm*22=1408mm).

The size of the PHE made from polypropylene sheet store can be incorporated into walls for domestic applications, thus eliminating worries of space for the thermal energy storage within the house. The dimensions of the PP sheet (1.9mx0.4m) used in this research are suitable for use in domestic applications. The sheet could be mounted in the following locations within domestic homes;

- In ceilings, between joints.
- In walls, between studworks.
- Underneath kitchen units (600mm deep, plight height=100mm).
- In corner units (600mm x 600mm x900mm).

The sheets could be positioned horizontally or vertically depending on the space available within the home. To increase the amount of energy required from the storage and utilise the capacity of the heat pump used for the storage, the number of PP sheets can be increased to meet up to this demand. The sheets can be stacked or positioned vertically within the walls. The pipe connections can go through the ceiling of the home for pipes coming from the top of the sheet. The outlet pipe of one sheet would be the inlet of the corresponding sheet.

### 10.5 Summary.

This chapter describes the numerical model used to validate the PHE experiment. The Matlab model validates both experimental results using two different phase change material (RT 52 and RT 58). Experimental results using RT 58 was done at a single flow only, however experimental result using RT 52 was done at three different flow rates (35, 47 and 65 g/s). The simulation results agree with experimental data for both charging and discharging process. The model was updated and a constant inlet HTF temperature of 60°C and 65°C for RT 52 and RT 58 respectively was used to simulate the behaviour of the thermal store at different PCM thickness. It was observed that the thickness of the PCM affects the charge rate and energy. The greater the PCM thickness, the longer the time it takes to charge or discharge.

Based on the research done in this thesis, I would recommend a PCM thickness of 30mm, based on the amount of energy required from the store using an 8kW heat pump for four hours using the economy 7 (32kWh). Economy 7 provides cheaper electricity rate, mostly at night (12a.m to 7a.m). This is dependent on the energy providers, for the time for off peak periods could vary.

The sheet capacity, number of sheets required for a store of 32kWh was determined for six different PCM thickness using RT 52. A plot that could be used to determine the thickness, charge rate and discharge rate was presented. The size of the plate heat exchanger makes it suitable for use in domestic homes. It is not bulky and fits in different locations within the home.

# 11 Conclusion and further work

## 11.1 Conclusion

The thermal behaviour of the PCMs; RT 52 and RT 58 used on the experimental rig shows promise on its suitability as a thermal energy storage. An advantage of this plate heat exchanger design using polypropylene sheet is a low fluid volume, ensuring a higher proportion of PCM thus maximising the storage potential. Heat exchange between the heat transfer fluid and the phase change material was investigated and found to give satisfactory performance. There is an effective heat transfer between the plate heat exchanger using the polypropylene sheet and the PCM, based on the large contact surface area which makes it easy for the store to be charged and discharged with a short period of time. The plate heat exchanger concept used, enables us to have higher ratio of PCM to water within the store. The PCM thickness can be optimized for the anticipated charge/discharge rate and required storage density.

The work has demonstrated that an effective thermal store can be constructed from polymer (polypropylene). The plate heat exchanger design and heat transfer characteristics of the mini channels allow the store to be charged with only a small ($<5^{o}C$) temperature difference. The Matlab model developed using the experimental data was used to solve the heat transfer problem between the HTF, wall and PCM. The analysis compared the experimental outlet HTF temperature with the simulated outlet HTF temperature. The performance of the bench top test rig was compared with a model written in MATLAB, considering conduction only in the PCM and validated. The validated model is used to study the effects of variation of relevant parameters during charging and discharging. This shows that the Matlab model is reliable in studying the behaviour of the thermal store using different PCMs, experiments at different flow rates etc. HTF flow rate does not significantly affect the performance of the thermal store. Varying the inlet HTF temperature could be used to increase or reduce the melting time and solidification time of the thermal store. It can also be used to increase the energy desirable from the thermal store.

Polypropylene (PP) sheet used for this research is lightweight and resistant to corrosion, when compared to metals. PP sheet is chemically resistant to attack from PCMs and due to the thin walls, it would be useful as an effective PHE due to its small conduction path length. Based on the results from this research, PP sheet exhibited

good heat transfer and due to their compatibility with PCMs, it can be used as a PCM heat exchanger. The wall of the sheet are thin walled, which facilitates an effective heat transfer between the HTF, wall and PCM on top of the PP sheet during charging and discharging process. The polypropylene sheet can easily be integrated in structures in buildings and with the concerns of space, it provides a good advantage over other types of geometries used as heat exchangers. Also, due to the modular nature of the sheets, it is possible to arrange the sheets in parallel or in series based on the kind of space available and energy desired.

The challenges faced using polypropylene as a PCM plate heat exchanger include the following; deformation of the plastic after several cycles of charging and discharging and blockage of the channels due to the adhesive used during construction.

Thermo physical properties of four different PCMs, paraffin (RT 52 and RT58) and two salt hydrates (61.5% Magnesium nitrate hexahydrate + 38.5% Ammonium Nitrate and Climsel C58) were tested using a differential scanning calorimeter (DSC) and hot disk instrument. The results from the DSC and hot disk were comparable to data obtained from manufacturers and other researchers. The result highlighted the problem of using inorganic PCM aforementioned for the thermal energy storage. However, despite the low thermal conductivity of both organic PCMs, they show good promise as potential PCMs to be used for this application. RT 52 and RT 58 were used for the experiment because of its availability, melting temperature range similar or within domestic application, cost and thermal stability. The salt hydrates showed a degree of hysteresis from the DSC result. The advantage of identifying the thermo physical properties of the PCM was vital in order to determine the PCM used. The thermal behaviour of RT 52 and RT 58 in the experimental rig demonstrates the potential for a plastic heat exchanger to be used for thermal energy storage.

The modular design of a thermal store using the polypropylene sheet based on a plate heat exchanger design is more suitable for integration with domestic heat pump compared to the serpentine heat exchanger. There exists an effective heat transfer within the PHE, as the store can be charged and discharged quickly. The polymer (polypropylene) material is compatible with the PCM used. The store can be half or fully charged within the off-peak period, where cheap electricity is available. The SHE requires a longer charging time because of the arrangement of the copper pipes within

the aluminum tray, spacing between the pipes and diameter of the pipe. At same flow rate, the higher the HTF inlet temperature, the faster the store is charged (higher temperature difference). At the same HTF inlet temperature, higher flow rate yields faster charging. This is due to lower temperature drop in HTF temperature, which yields a higher temperature difference between the HTF and the PCM. Compared to the polypropylene sheet; the serpentine heat exchanger takes a longer time to charge and discharge. Varying the mass flow rate can influence heat transfer to the store with the serpentine heat exchanger arrangement.

The PCM storage can be used to shift the bulk of the heating loads to off-peak period, where the cost of electricity is cheaper and stored latent heat in the PCM can be released during peak time. The selected PCMs were selected for this research to match the operation of the heat pump and domestic home application. This allows the store to charge/discharge within the phase change temperature range of the PCM.

The charge rate and energy stored during charge and discharge process for different thickness of PCM; shows that the higher the PCM thickness, the higher the amount of energy obtainable from the store and the slower it is for the store to charge or discharge. Based on the model, the performance for when the store was full charged and half charged was studied and result presented. To increase the capacity of the store for effective use with domestic heat pump for a specified period of charging during off-peak tariff periods, the thermal store design using 30mm PCM thickness is proposed. Using the aforementioned thickness, the thermal store would require about twenty-two PP sheets (22). At half charge, the thermal store can be charged for four(4) hours, which is within the off-peak period using economy 7. This can be installed in suitable location in the home; such as kitchen cabinet, ceiling which would accommodate the dimensions of the plate heat exchanger. The sheet capacity, number of sheets required for a store of 32kWh was determined for six different PCM thickness using RT 52.

A plot of sheet charge rate or store charge rate against the reciprocal of the thickness was produced that could be used to determine the thickness or charge rate was presented. This will enable the number of sheets to be used to be configured from the chart or plot.

## 11.2 Further Work

Cascading thermal storage store can be looked into where different PCM can be used to enhance the thermal performance of the PHE thermal store. The PCM should be arranged in order of decreasing melting temperature range for the charging process and reverse order or the discharge process. This may produce a more energy efficient thermal energy storage. Installing the thermal store in conjunction with a heat pump in a domestic home to test the performance of the thermal store and study how it helps provide cheap electricity using economy 7 or 10 tariff. The store can be charged during the off peak periods, thus reducing energy cost. Various sheet length, width and channel dimensions can be studied using the polypropylene sheet (PHE) and different type of plastic material or other suitable heat exchanger material can be used to check the behaviour of the TES. Based on the challenges faced in bonding the PP sheet, applying the technology of 3D printing could overcome such challenges.

For the serpentine heat exchanger, fins could be introduced to enhance the conduction from the HTF to the PCM. The spacing between the copper pipe and diameter of the copper pie could be increased to promote a more effective heat transfer. Perspex can be used to cover the length of the tank, so the PCM melt process can be visible and monitored. A numerical model written in MATLAB or use of COMSOL or ANSYS can be used to validate the experiment result obtained using the serpentine heat exchanger. This will allow the store to be optimized by varying the diameter of the pipe, pitch between the pipes, introduction of fins etc.

Further calorimetric test could be carried out on different phase change material (PCM) that could be suitable for the thermal store. Enhancing the properties of PCM used in the TES could also be investigated by using metal matrices, graphite etc.

# 12 References

ABHAT, A. 1980. Short term thermal energy storage. Revue de Physique Appliquee, 15, 477-501.

ABHAT, A. 1983. Low temperature latent heat thermal energy storage - Heat storage materials. 313-332.

ACT. 2018. PCM Heat Sink Design Consideration [Online]. LANCASTER, PENNSYLVANIA 17601, USA: Advanced Cooling Technologies(ACT). Available: https://www.1-act.com/innovations/thermal-storage/pcm-heat-sink-design-considerations/ [Accessed 3 January 2018].

AGYENIM, F. & HEWITT, N. 2010. The development of a finned phase change material (PCM) storage system to take advantage of off-peak electricity tariff for improvement in cost of heat pump operation. Energy and Buildings, 42, 1552-1560.

AGYENIM, F. & HEWITT, N. 2012. Experimental investigation and improvement in heat transfer of paraffin PCM RT58 storage system to take advantage of low peak tariff rates for heat pump applications. International Journal of Low-Carbon Technologies.

AIGBOTSUA, C. O. 2011. Thermal Energy Storage Using Phase Change Materials in Corrugated Copper Panels. Texas A&M University.

AL-ABIDI, A. A., BIN MAT, S., SOPIAN, K., SULAIMAN, M. Y. & MOHAMMED, A. T. 2013. CFD applications for latent heat thermal energy storage: a review. Renewable and Sustainable Energy Reviews, 20, 353-363.

AL-HALLAJ, S. & KIZILEL, R. 2012. Applications of Phase Change Materials for Sustainable Energy. In: THESIS, T. & TOMKIN, J. (eds.) Sustainability: A Comprehensive Foundation Illinois.

ALEXIADES, V. 1993. Mathematical Modeling of Melting and Freezing Processes. Mathematical Modeling of Melting and Freezing Processes.Washington,USA: Hemisphere Publishing Corporation.

ANTONY AROUL RAJ, V. & VELRAJ, R. 2011. Heat transfer and pressure drop studies on a PCM-heat exchanger module for free cooling applications. International Journal of Thermal Sciences, 50, 1573-1582.

ARASU, A. V. & MUJUMDAR, A. S. 2012. Numerical study on melting of paraffin wax with Al2O3 in a square enclosure. International Communications in Heat and Mass Transfer, 39, 8-16.

ARAÚJO, A. A. S., BEZERRA, M. D. S., STORPIRTIS, S. & MATOS, J. D. R. 2010. Determination of the melting temperature, heat of fusion, and purity analysis of different samples of zidovudine (AZT) using DSC. Brazilian Journal of Pharmaceutical Sciences, 46, 37-43.

ASHRAE 2003. ASHRAE Handbook-Heating,Ventilation,and Air-Conditioning System and Applications. Atlanta: American Society of Heating,Refrigeration and Air Conditioning Engineers,Inc.

ATAER, O. E. 2006. ENERGY STORAGE SYSTEMS,in Storage of Thermal Energy, [Ed. Yalcin Abdullah Gogus], in Encyclopedia of Life Support Systems (EOLSS), Developed under the Auspices of the UNESCO, Eolss Publishers, Oxford ,UK, [http://www.eolss.net].

BEDECARRATS, J. P. 2009. Study of a Phase Change Energy Storage System Using Spherical Capsules. Numerical Modelling, Energy Conversion and Management, 50, 2537-2546.

BONY, J. & CITHERLET, S. 2007. Numerical model and experimental validation of heat storage with phase change materials. Energy and Buildings, 39, 1065-1072.

CAMPOS-CELADOR, Á., DIARCE, G., ZUBIAGA, J. T., BANDOS, T. V., GARCÍA-ROMERO, A. M., LÓPEZ, L. M. & SALA, J. M. 2014. Design of a Finned Plate Latent Heat Thermal Energy Storage System for Domestic Applications. Energy Procedia, 48, 300-308.

CELADOR, Á., DIARCE, G., GONZÁLEZ-PINO, I. & SALA, J. M. 2013. Development and comparative analysis of the modeling of an innovative finned-plate latent heat thermal energy storage system.

CENGEL, Y. & GHAJAR, A. 2011. Heat and Mass Transfer Fundamentals and Applications, New York, McGraw-Hill.

CHIU, J. N. 2011. Heat transfer aspects of using phase change material in thermal energy storage applications. Tek. Lic., KTH,School of Industrial Engineering and Management.

CLIMATOR 2016. Climator.

CLIMATOR. 2017. ClimSel C58 product specification sheet [Online]. Sweden: Climator.Available:http://climator.com/wpcontent/pdf/Prodblad_Climsel_C58_4.1.pdf [Accessed 19 February 2018].

COLELLA, F., SCIACOVELLI, A. & VERDA, V. 2012. Numerical analysis of a medium scale latent energy storage unit for district heating systems. Energy, 45, 397-406.

COLEPALMER 2016. ColePalmer.

D.A, N. Potential benefits of distributed PCM thermal storage. In: Coleman MJ, Proceedings of 14th National Passive Solar Conference, 1989 Denver, Colorado. American Solar Energy Society,, 283-288.

D'AVIGNON , K. 2015. Modeling and Experimental validation of the performance of Phase change material storage tanks in buildings. Ph.D., École Polytechnique de Montreal.

DINCER, I. & ROSEN, M. A. 2002. Thermal Energy Storage, England, John Wiley & Sons,Ltd.

DINCER, I. & ROSEN, M. A. 2011. Thermal Energy Storage Systems and Applications, Wiley&Sons.

DINKER, A., AGARWAL, M. & AGARWAL, G. D. 2017. Heat storage materials, geometry and applications: A review. Journal of the Energy Institute, 90, 1-11.

DRISSI, S., EDDHAHAK, A., CARÉ, S. & NEJI, J. 2015. Thermal analysis by DSC of Phase Change Materials, study of the damage effect. Journal of Building Engineering, 1, 13-19.

DUTIL, Y., ROUSSE, D. R., SALAH, N. B., LASSUE, S. & ZALEWSKI, L. 2011. A review on phase-change materials: Mathematical modeling and simulations. Renewable and Sustainable Energy Reviews, 15, 112-130.

ELGAFY , A. & LAFDI, K. 2005. Effect of carbon nanofiber additives on thermal behavior of phase change materials. Carbon, 3067–3074.

EMERSON. 2017. Principles of Coriolis Technology [Online]. Available: http://www.emerson.com/en-us/automation/measurement-instrumentation/flow-measurement/coriolis-flow-meters [Accessed 10th September 2017].

EMERSON 2018. Micro Motion Elite Coriolis Flow and Density Meters. In: EMERSON (ed.).

ESEN, M., DURMUŞ, A. & DURMUŞ, A. 1998. Geometric design of solar-aided latent heat store depending on various parameters and phase change materials. Solar Energy, 62, 19-28.

FARID, M. M. 1990. An electrical storage heater using phase change method of heat storage. Energy Convers. Manage. , 219-230.

FARID, M. M., KHUDHAIR, A. M., RAZACK, S. A. K. & AL-HALLAJ, S. 2004. A review on phase change energy storage: materials and applications. Energy Conversion and Management, 45, 1597-1615.

FRAZZICA, A., PALOMBA, V., ROSA, D. L. & BRANCATO, V. 2017. Experimental comparison of two heat exchanger concepts for latent heat storage applications. Energy Procedia, 135, 183-192.

G.A.LANE 1980. Low temperature heat storage with phase change materials. Int.J.Ambient Energy 1, 155-168.

GANG LI, X. Z. 2016. Thermal energy storage system integration forms for a sustainable future. Science direct, 736-757.

GÜNTHER, E., HIEBLER, S. & MEHLING , H. 2005. Measurement of the enthalpy of PCM. Bavarian Center for Applied Energy Research (ZAE Bayern e. V.), 8.

GÜNTHER, E., HIEBLER, S., MEHLING, H. & REDLICH, R. 2009. Enthalpy of Phase Change Materials as a Function of Temperature: Required Accuracy and Suitable Measurement Methods. Int J Thermophys, 30, 12.

HALALWA, E. 2005. Numerical analysis of a PCM thermal storage system with varying wall temperature. Energy Convers. Manage. , 2592-2604.

HASSAN, H. M. A. 2014. Development and Evaluation of a CFD Model to Simulate Thermal Performance of Phase Change Material (PCM) Based Energy Storage Systems. Masters, KTH School of Industrial Engineering and Management

HORST MICHELS & PITZ-PAAL, R. 2006. Cascaded latent heat storage for parabolic trough solar power plants.

HSE PUBLICATIONS 2013. Legionnaires' disease. The control of legionella bacteria in water systems: Approved Code of Practice and Guidance L8. UK Health and Safety Executive.

HU, H. & ARGYROPOULOS, S. 1996. Mathematical modelling of solidification and melting:a review. Modelling Simul.mater. Sci.Eng. 4, 371-394.

HUANG, M. J., EAMES, P. C. & NORTON, B. 2004. Thermal regulation of building-integrated photovoltaics using phase change materials. International J.of Heat and Mass Transfer 47, 2715-2733.

HUANG, M. J. & HEWITT, N. J. 2011. Prediction of phase change material heat storage for air-source heat pump application. ICR. Prague,Czech Republic.

ITEN, M. & LIU, S. 2014. A work procedure of utilising PCMs as thermal storage systems based on air-TES systems. Energy Conversion and Management, 77, 608-627.

JEGADHEESWARAN, S. & POHEKAR, S. D. 2009. Performance enhancement in latent heat thermal storage system: A review. Renewable and Sustainable Energy Reviews, 13, 2225-2244.

KAKAÇ, S., SHAH, R. K. & AUNG, W. 1987. Handbook of single-phase convective heat transfer, New York, Wiley.

KAYS, W. M. & CRAWFORD, M. E. 1993. Convection Heat and Mass Transfer, New York, McGraw Hill.

KLIMES, L., CHARVAT, P. & OSTRY, M. 2012. Challenges in the computer modeling of phase change materials. Materials and technology 46, 4.

KOTZÉ, J. P. 2014. Thermal energy storage in metallic phase change materials. Ph.D., Stellenbosch University.

KRAGBAEK, J. & REINHOLDT, N. P. 2011. Heat Storage based on PCM for concentrated solar applications. Masters, University of Aalborg, Denmark.

KRANE, R. J. 2009. Energy Storage Systems, Oxford, United Kingdom, Eolss.

KTH 2010. SOP for TPS 2500 thermal conductivity. In: KTH, D. O. E. T. (ed.). Sweden.

KÜRKLÜ, A., WHELDON, A. & HADLEY, P. 1996. Mathematical modelling of the thermal performance of a phase-change material (PCM) store: Cooling cycle. Applied Thermal Engineering, 16, 613-623.

KURNIA, J. C., SASMITO, A. P., JANGAM, S. V. & MUJUMDAR, A. S. 2013. Improved design for heat transfer performance of a novel phase change material (PCM) thermal energy storage (TES). Applied Thermal Engineering, 50, 896-907.

LAMBERG, P., LEHTINIEMI, R. & HENELL, A.-M. 2004. Numerical and experimental investigation of melting and freezing processes in phase change material storage. International Journal of Thermal Sciences, 43, 277-287.

LANE, G. A. 1989. Handbook of applied thermal design, New York, McGraw-Hill Book Company.

LAWRENCE, J. C. & BULL, J. P. 1976. THERMAL CONDITIONS WHICH CAUSE SKIN BURNS. Engineering in Medicine, 5, 61-63.

LEONHARDT C, M. D. 2009. Modelling of Residential Heating Systems using a Phase change Material Storage System. Proceedings 7th Modelica Conference Como,Italy, 507-512.

LIN QIU & MIN YAN 2012. Numerical Simulation and Analysis Of PCM on Phase Change Process Consider Natural Convection Influence The 2nd International Conference on Computer Application and System Modeling. Bejing, China.

LIU, C. 2012. Phase Change behaviour of lauric acid in a horizontal cylindrical latent heat energy storage system. MASc, Dalhousie University.

LIU, C., YUAN, Y., ZHANG, N., CAO, X. & YANG, X. 2014. A novel PCM of lauric–myristic–stearic acid/expanded graphite composite for thermal energy storage. Materials Letters, 120, 43-46.

MANZELLO S, P. S., MIZUKAMI T,DALE P 2008. Measurement of thermal properties of Gypsum board at elevated temperatures. Proceedings of the Fifth International Conference on Structures in Fire (SiF'08), 657-665.

MAO, Q. 2016. Recent developments in geometrical configurations of thermal energy storage for concentrating solar power plant. Renewable and Sustainable Energy Reviews, 59, 320-327.

MCCDAQ 2016. mccdaq.

MEHLING, H. & CABEZA, L. 2008. Design of latent heat storages. Heat and cold storage with PCM. Springer Berlin Heidelberg.

MOHAMED, A. S. 2011. Simulation and Optimization of Solar Thermal System Integrated with PCM Thermal Energy Storage for Seawater Desalination. Msc., Kassel University.

MORENO, P., CASTELL, A., SOLÉ, C., ZSEMBINSZKI, G. & CABEZA, L. F. 2014. PCM thermal energy storage tanks in heat pump system for space cooling. Energy and Buildings, 82, 399-405.

NALLUSAMY 2016. Study on performance of a packed bed latent heat thermal energy storage unit integrated with solar water heating system.

ORÓ, E., BARRENECHE, C., FARID, M. M. & CABEZA, L. F. 2013. Experimental study on the selection of phase change materials for low temperature applications. Renewable Energy, 57, 130-136.

PÄR JOHANSSON, A. S. K., HELÉN JANSSON 2015. Investigating PCM activation using transient plane source method Energy Procedia 6th International Building Physics Conference, IBPC Energy Procedia 78 800 – 805

PICOTECH. 2014. USB TC-08 Thermocouple Data Logger [Online]. Picotech. Available: http://www.picotech.com/thermocouple.html [Accessed 23/06/2014 2014].

PIELICHOWSKA, K. & PIELICHOWSKI, K. 2014. Phase change materials for thermal energy storage. Progress in Materials Science, 65, 67-123.

QIANJUN, M. 2016. Recent development in geometrical configuration of thermal energy storage for concentrating solar power. Science direct.

RATHGEBER, C., MIRÓ, L., CABEZA, L. F. & HIEBLER, S. 2014a. Measurement of enthalpy curves of phase change materials via DSC and T-History: When are both methods needed to estimate the behaviour of the bulk material in applications? Thermochimica Acta, 596, 79-88.

RATHGEBER, C., SCHMIT, H., HENNEMANN, P. & HIEBLER, S. 2014b. Investigation of pinacone hexahydrate as phase change material for thermal energy storage around 45°C. Applied Energy, 136, 7-13.

REDDY, K. S. 2007. Thermal modeling of PCM-based solar integrated collector storage water heating system. Journal of Solar Energy Engineering129, 458.

RUBITHERM 2013. Rubitherrm. Rubitherm.

RUBITHERM. 2017. Remarks on subcooling, hysteresis and other properties of the SPproducts[Online].Available:https://www.rubitherm.eu/media/products/datasheets/Remarks-on-subcooling-hysteresis-and-other-properties-of-the-SP-products.pdf [Accessed 30 July 2017].

SAMAN, W., BRUNO, F. & HALAWA, E. 2005. Thermal performance of PCM thermal storage unit for a roof integrated solar heating system. Solar Energy, 78, 341-349.

SCRINIVAS, V. Analysis and Topology Optimization of Heat Sinks with a Phase Change Material on COMSOL Multiphysics Platform. Proceedings of the COMSOL Users Conference, 2006 Banglore. 1-7.

SETARAM, I. 2005. Sensys DSC and TG DSC, France, Setaram Instrumentation KEP Technologies.

SHARMA, A., TYAGI, V. V., CHEN, C. R. & BUDDHI, D. 2009. Review on thermal energy storage with phase change materials and applications. Renewable and Sustainable Energy Reviews, 13, 318-345.

SHARMA, A., WON, L. D., BUDDHI, D. & PARK, J. U. 2005. Numerical heat transfer studies of the fatty acids for different heat exchanger materials on the performance of a latent heat storage system. Renewable Energy, 30, 2179-2187.

SHATIKIAN, V., ZISKIND, G. & LETAN, R. 2005. Numerical investigation of a PCM-based heat sink with internal fins. International Journal of Heat and Mass Transfer, 48, 3689-3706.

SHIN, D. H., KIM, K., SHIN, Y. & KARNG, S. W. 2017. Thermal characteristics of phase change materials in a latent heat storage system Proceedings of the Asian Conference on Thermal Sciences 2017, 1st ACTS, 4.

TIAN, Y., ZHAO, C.-Y. & LAPKIN, A. 2012. Exergy optimisation for cascaded thermal storage. Proceedings of 12th International Conference on Energy Storage (Innostock 2012), INNO-SP-78.

TIAN, Y. & ZHAO, C. Y. 2009. Heat transfer analysis for phase change materials. Effstock Conference Proceedings Stockholm, Sweden: Richard Stockton College of New Jersey.

TRP, A. 2005. An experimental and numerical investigation of heat transfer during technical grade paraffin melting and solidification in a shell-and-tube latent thermal energy storage unit. Solar Energy, 79, 648-660.

VELRAJ , R., SEENIRAJ, R. V., HAFNER, B., FABER, C. & SCHWARZER, K. 1999. Heat Transfer Enhancement in a Latent Heat Storage System. Solar Energy, 65, 171–180.

VERMA, P., VARUN & SINGAL, S. K. 2008. Review of mathematical modeling on latent heat thermal energy storage systems using phase-change material. Renewable and Sustainable Energy Reviews, 12, 999-1031.

VOLLER, V. R. 1997. An overview of numerical methods for solving phase change problems. Advances in Numerical Heat Transfer. New York: Taylor& Francis.

WANG, P., WANG, X., HUANG, Y., LI, C., PENG, Z. & DING, Y. 2015a. Thermal energy charging behaviour of a heat exchange device with a zigzag plate configuration containing multi-phase-change-materials (m-PCMs). Applied Energy, 142, 328-336.

WANG, Y., WANG, L., CHEN, H., XIE, N., YANG, Z. & CHAI, L. 2015b. Numerical study on thermal performance characteristics of a cascaded latent heat storage unit. Proceedings of the Institution of Mechanical Engineers, Part A: Journal of Power and Energy.

WEINSTEIN, R., KOPEC, T., FLEISCHER, A., D′ADDIO, E. & BESSEL, C. 2008. The experimental exploration of embedding phase change materials with graphite nanofibers for the thermal management of electronics. Journal of Heat Transfer, 130.

WHIFFEN, T. R. & RIFFAT, S. B. 2012. A review of PCM technology for thermal energy storage in the built environment: Part I. International Journal of Low-Carbon Technologies, 12.

ZALBA, B., MARíN, J. M., CABEZA, L. F. & MEHLING, H. 2003. Review on thermal energy storage with phase change: materials, heat transfer analysis and applications. Applied Thermal Engineering, 23, 251-283.

ZALBA B, M. J., CABEZA LF, MEHLING H. 2003. Review on thermal energy storage with phase change material,heat transfer analysis and application. Appl Therm Eng, 251-283.

ZHOU, D., ZHAO, C. Y. & TIAN, Y. 2012. Review on thermal energy storage with phase change materials (PCMs) in building applications. Applied Energy, 92, 593-605.

## Appendix A: Hot disk procedure to carry out thermal conductivity test.

**Sequence of test on the hot disk device:**

1. Double Click on the hot disk icon to activate software
2. Click on ‘New Experiment’ on the File
3. Enter Parameters for the PCM to be tested. (name of material)
4. Choose an appropriate value of power output and time. A software wizard is available to do this. The values should not be too high to avoid convection.
5. Press the single measurement or scheduled measurement to run the measurement. The scheduled measured runs the experiment at specified time intervals.
6. Click on start measurement.
7. Select the analysis tab>Select points from graph.
8. A graph of temperature increase against time curve is plotted. Having a smooth curve indicates a successful measurement; else the experiment needs to be repeated.
9. Select “Calculations from the analysis menu. This gives a plot of temperature difference against square root of time. A successful plot should show a good random scatter without presence of a curvature.
10. The software of the HOT disk thermal constant analyser also provides checks to indicate if data obtained from the measurement can be accepted or not. Total characteristic time should be in the region of 0.3 to 1.0. Also Total temperature increase should be less than 2°C.
11. For a higher accuracy, there is an option in the software to input the value of known specific heat for a sample. This has a higher accuracy when compared to a standard calculation.
12. Disassemble the sensor from the stainless plate and accessories when the measurement has been completed. Proper housekeeping is essential on the TPS sensor and environs to ensure accurate result.

## Appendix B: USB TC-08 Thermocouple data logger specifications

| USB TC-08 Thermocouple Data Logger General Specifications | |
|---|---|
| **Number of channels (per TC-08)** | 8 |
| **Maximum number of channels (using multiple TC-08s)** | 160 |
| **Conversion time** | 100 ms (thermocouple and cold junction compensation) |
| **Temperature accuracy** | Sum of ±0.2% of reading and ±0.5 °C |
| **Voltage accuracy** | Sum of ±0.2% of reading and ±10 µV |
| **Input range (voltage)** | ±70 mV |
| **Resolution** | 20 bits |
| **Noise free resolution** | 16.25 bits |
| **Thermocouple types supported** | B, E, J, K, N, R, S, T |
| **Input connectors** | Miniature thermocouple |

## Appendix C: PCM & HTF Thermocouple positions on the PP sheet

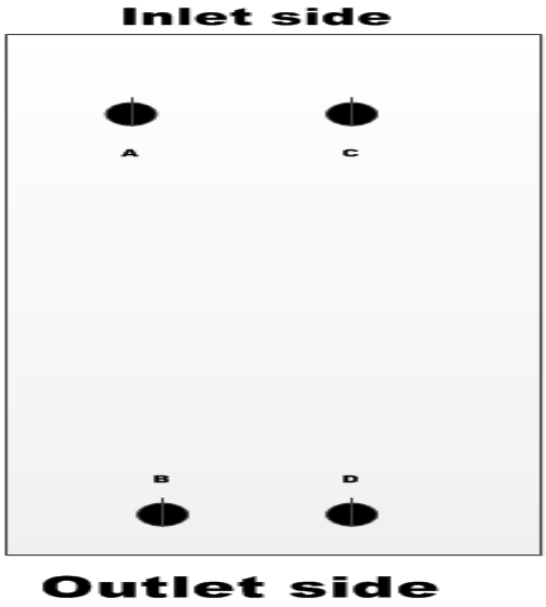


A=PROBE thermocouple (10mm)

B=PROBE thermocouple (5mm)

C=SHIM thermocouple

D=SHIM thermocouple

**EIGHT THERMOCOUPLES WERE USED ON THE POLYPROPYLENE RIG**

| THERMOCOUPLE (K-TYPE) | POSITION |
|---|---|
| 1. PROBE THERMOCOUPLE(10MM DEPTH) | PCM (RT 58 & RT 52) |
| 2. PROBE THERMOCOUPLE(5MM DEPTH) | |
| 3. SHIM THERMOCOUPLE(INLET) | |
| 4. SHIM THERMOCOUPLE(OUTLET) | |
| 5. PROBE THERMOCOUPLE (INLET) | HTF |
| 6. PROBE THERMOCOUPLE(OUTLET) | |
| 7. SHIM THERMOCOUPLE TEMPERATURE | POLYPROPYLENE WALL |
| 8. PROBE THERMOCOUPLE | ROOM TEMPERATURE |

## Appendix D: Performance specification for POLYSTAT R6L (Water bath)

| Model | | R6L | |
|---|---|---|---|
| Description | | 6-liter cooling/heating circulating bath | |
| Reservoir volume | | 6 liters (1.5 gallons) | |
| Temperature range[1,2] | Digital | –20 to 150°C | |
| | Advanced digital | –20 to 200°C | |
| | Programmable | –20 to 200°C | |
| Stability[3] | Digital | ±0.05°C | |
| | Advanced digital | ±0.01°C | |
| | Programmable | ±0.01°C | |
| Work area dimensions | | 8"W x 6"H x 5¼" D (20 x 15 x 13 cm) | |
| Overall dimensions | | 10"W x 21½"H x 15¾"D (25 x 55 x 40 cm) | |
| Shipping weight[4] | | 79 lb (36 kg) | |
| Heater | | 800 W | 1000 W |
| Cooling capacity[5] | At +20°C | 350 W | 290 W |
| | At 0°C | 120 W | 100 W |
| | At –10°C | 90 W | 75 W |
| | At –20°C | — | — |
| Refrigerant | | R134A | |
| Pumping capacity[6] | | 15 L/min at 0 psig | 12 L/min at 0 psig |
| Drain valve | | No | |
| Electrical requirements | | 115 VAC, 60 Hz<br>15 amps | 230 VAC, 50 Hz<br>10 amps |
| Digital controller | Catalog number | MK-12122-00 | MK-12122-05 |
| Advanced digital controller | Catalog number | MK-12122-10 | MK-12122-15 |
| Programmable controller | Catalog number | MK-12122-20 | MK-12122-25 |

## Appendix E: Experiment result for charging the serpentine thermal store.

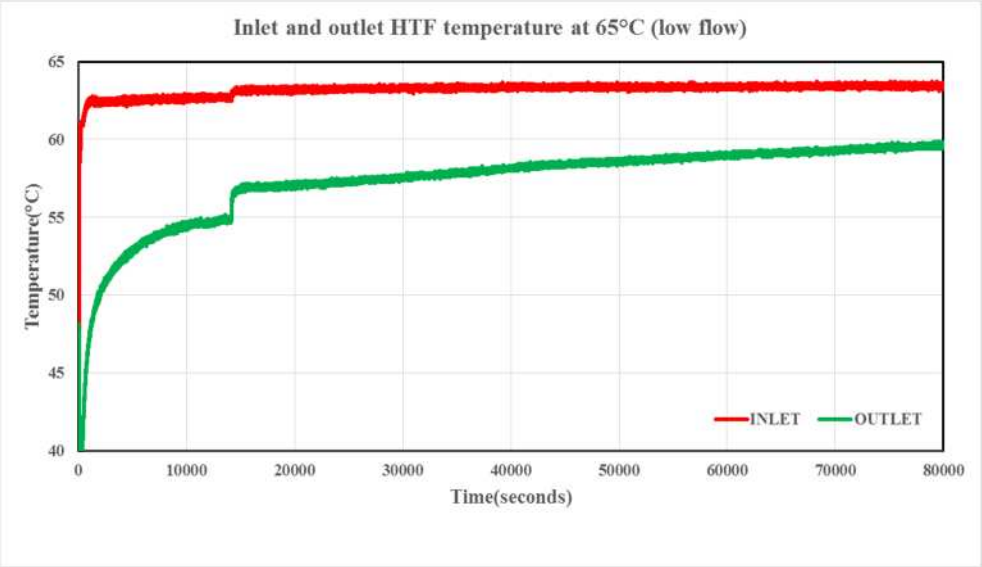


Figure E 1: HTF outlet at inlet HTF temperature of 65°C (7g/s).

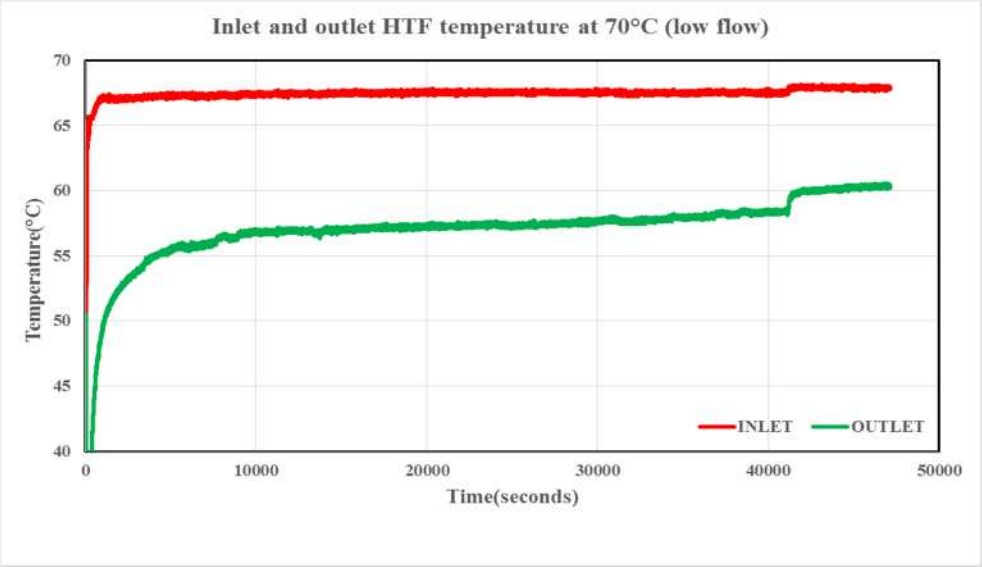


Figure E 2: HTF outlet at inlet HTF temperature of 70°C (7g/s).

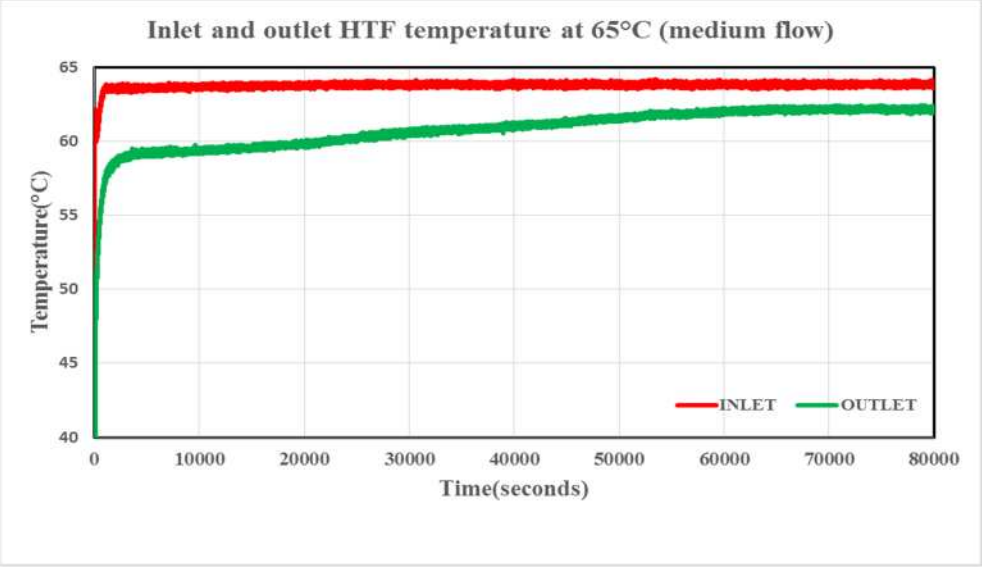


Figure E3:HTF outlet at inlet HTF temperature of 65°C (15g/s).

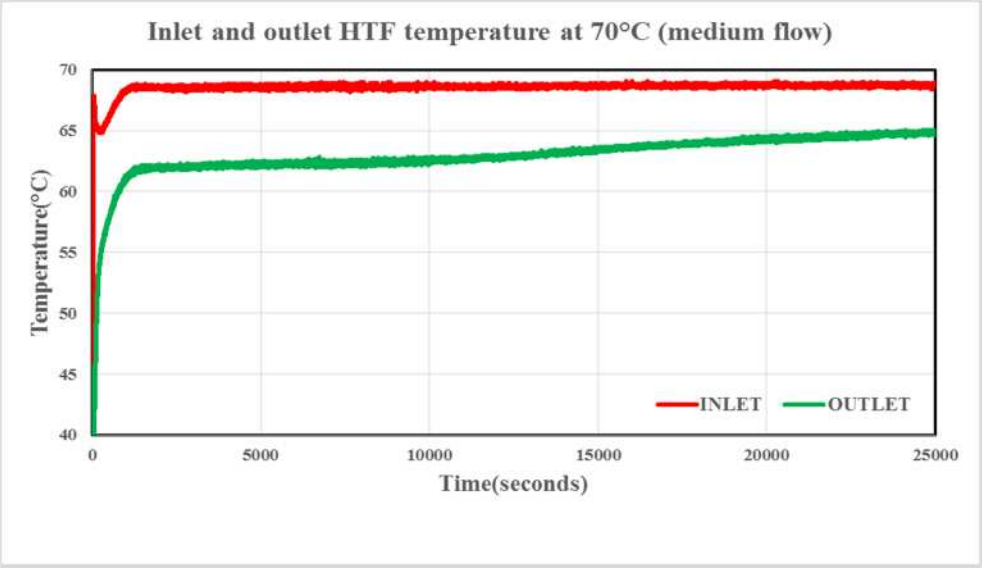


Figure E4: HTF outlet at inlet HTF temperature of 70°C (15g/s).

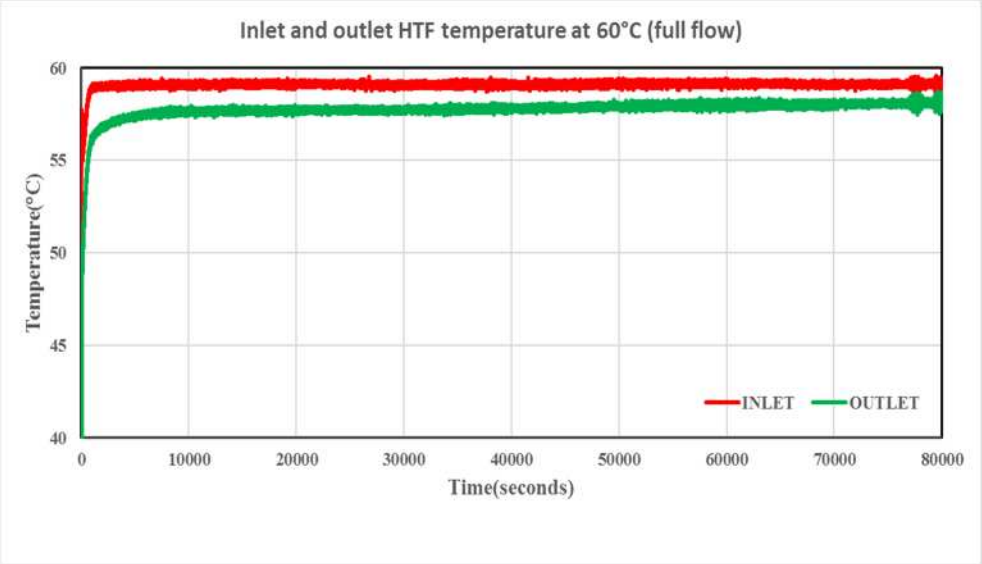


Figure E5: HTF outlet at inlet HTF temperature of 60°C (30g/s).

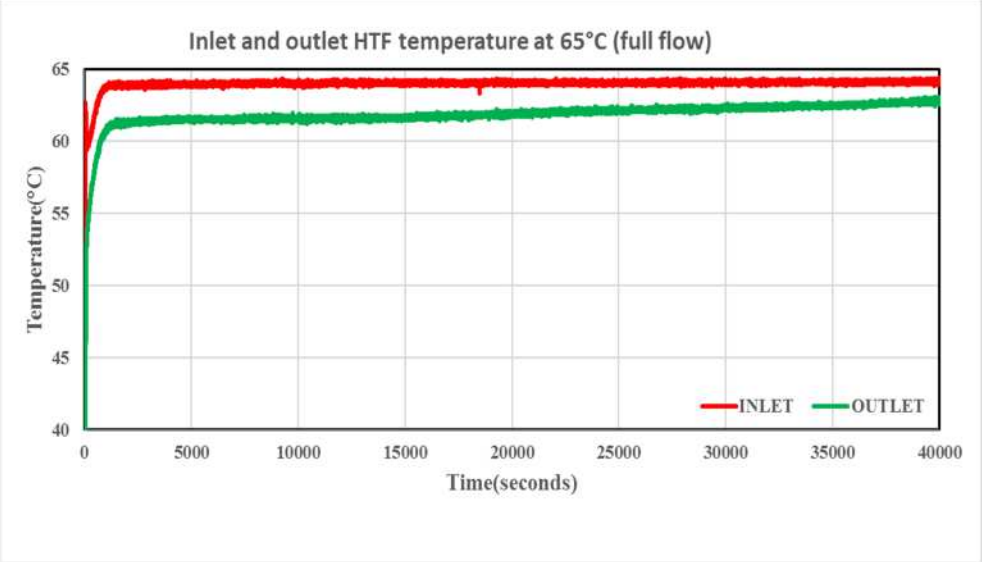


Figure E6: HTF outlet at inlet HTF temperature of 65°C (30g/s).

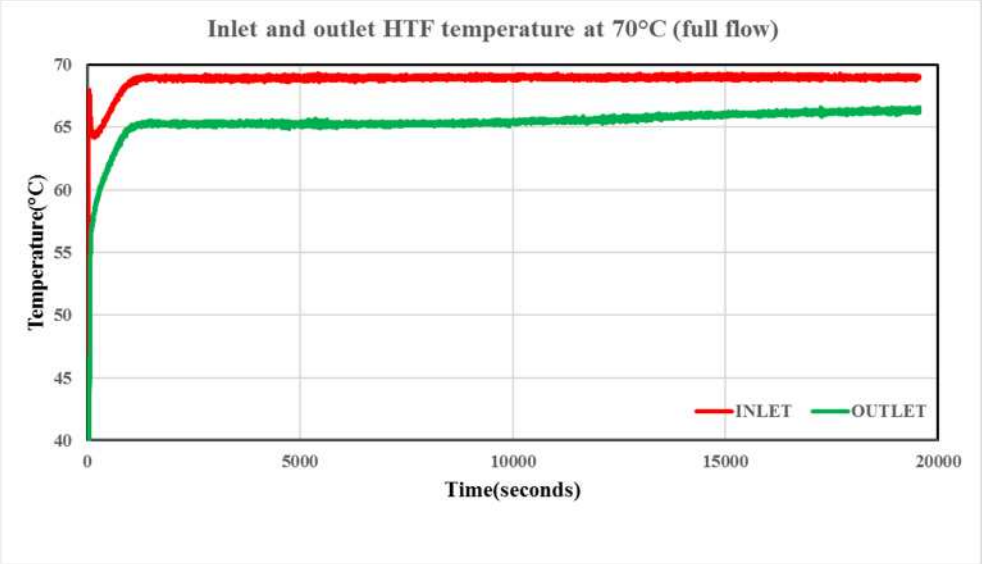


Figure E7: HTF outlet at inlet HTF temperature of 70°C (30g/s).

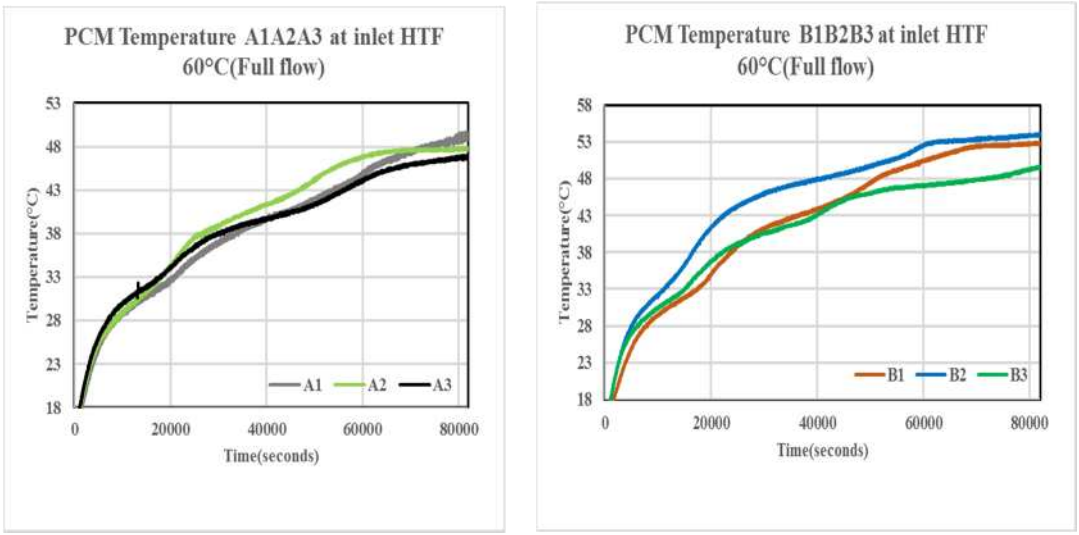


Figure E8: PCM temperature at radial points (A1A2A3) and (B1B2B3) at inlet HTF temperature of 60°C (high flow).

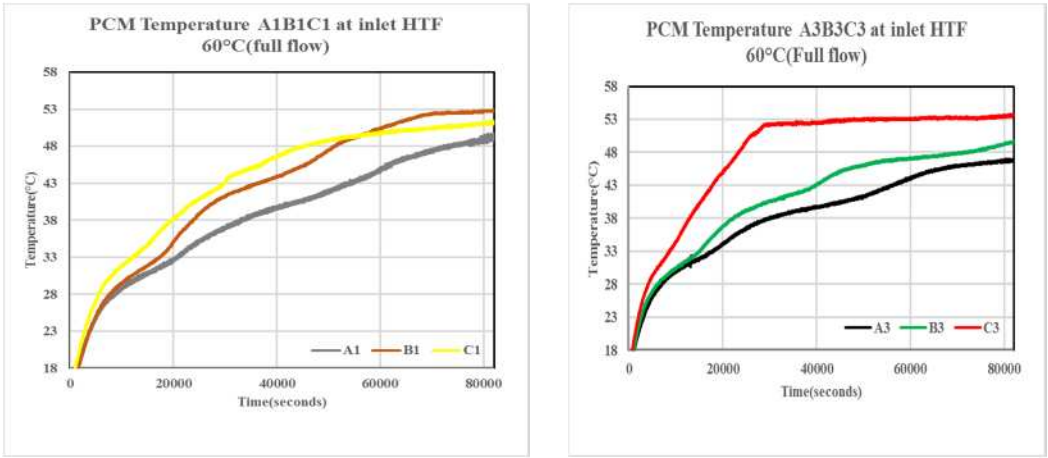


Figure E9: PCM temperature at axial points (A1B1C1) and (A3B3C3) at inlet HTF temperature of 60°C (high flow).

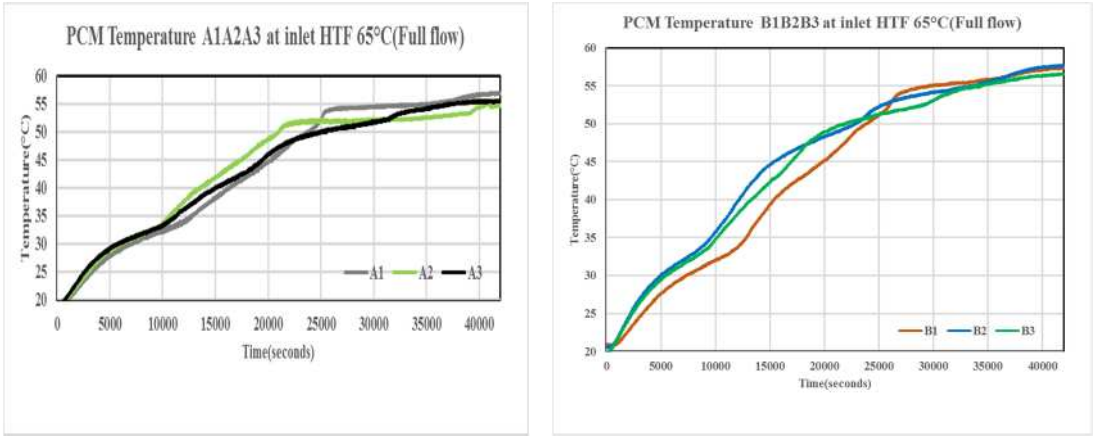


Figure E10: PCM temperature at radial points (A1A2A3) and (B1B2B3) at inlet HTF temperature of 65°C (high flow).

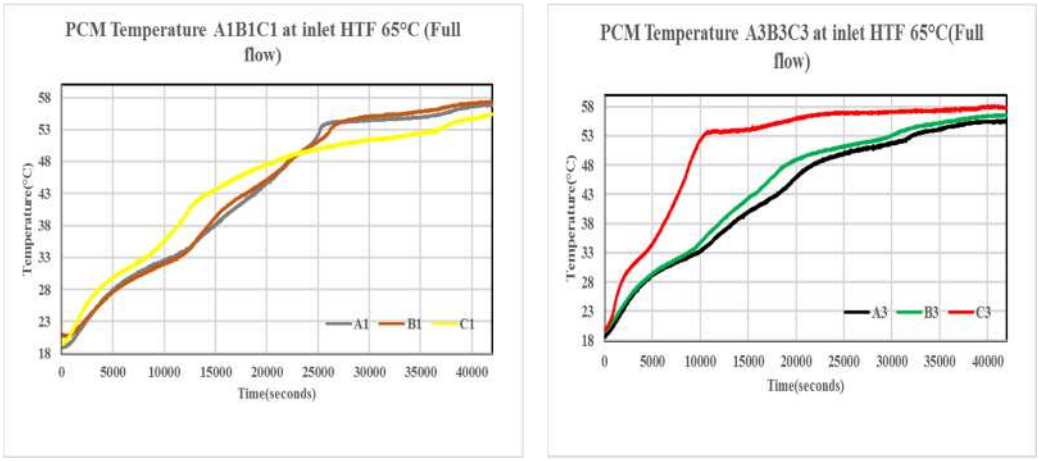


Figure E11: PCM temperature at axial points (A1B1C1) and (A3B3C3) at inlet HTF temperature of 65°C (high flow).

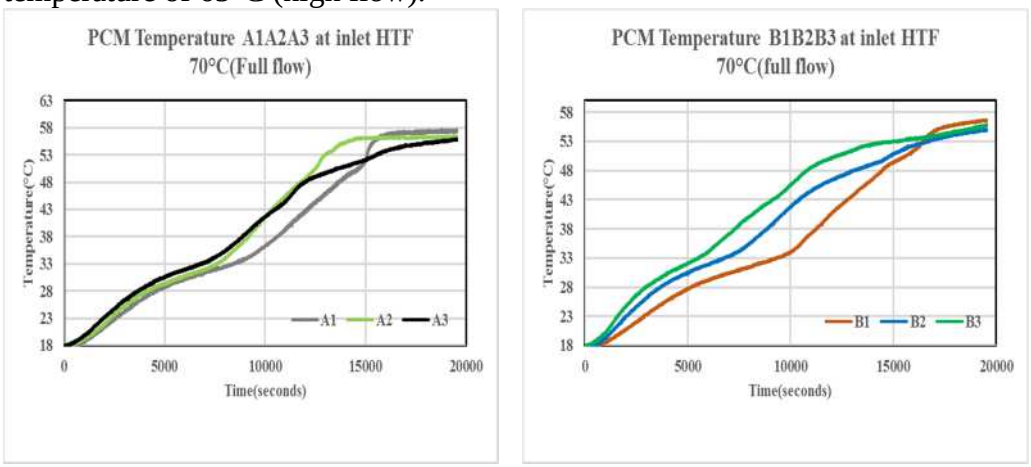


Figure E12: PCM temperature at radial points (A1A2A3) and (B1B2B3) at inlet HTF temperature of 70°C (high flow).

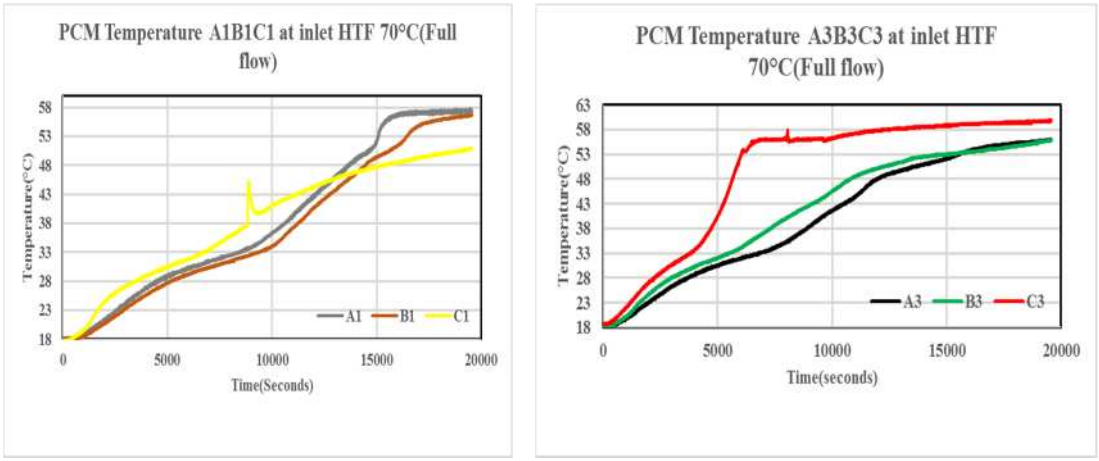


Figure E13: PCM temperature at axial points (A1B1C1) and axial (A3B3C3) at inlet HTF temperature of 70°C (high flow).

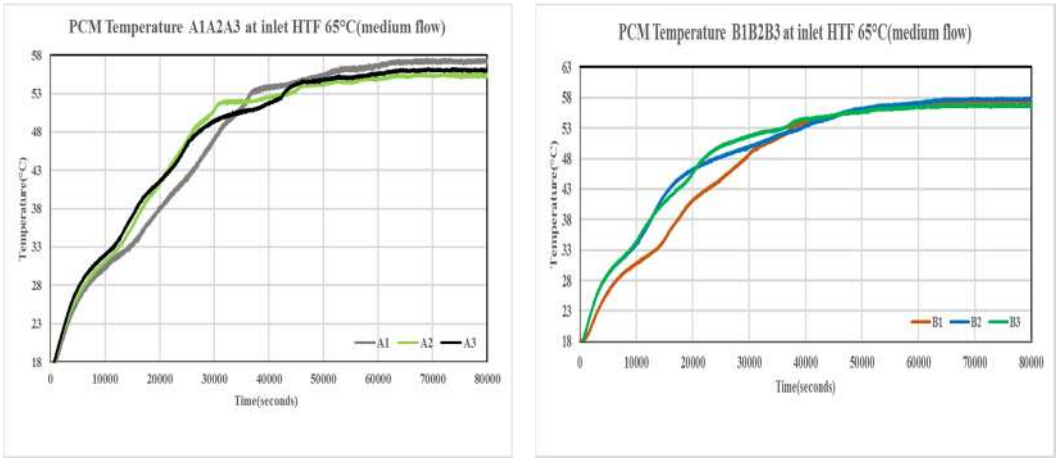


Figure E14: PCM temperature at radial points (A1A2A3) and (B1B2B3) at inlet HTF temperature of 65°C (medium flow).

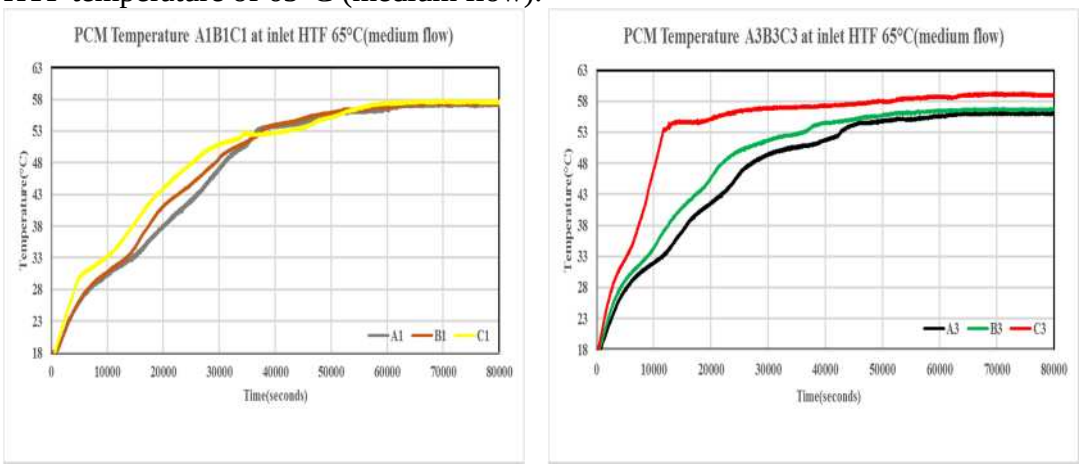


Figure E15: PCM temperature at axial points (A1B1C1) and (A3B3C3) at inlet HTF temperature of 65°C (medium flow).

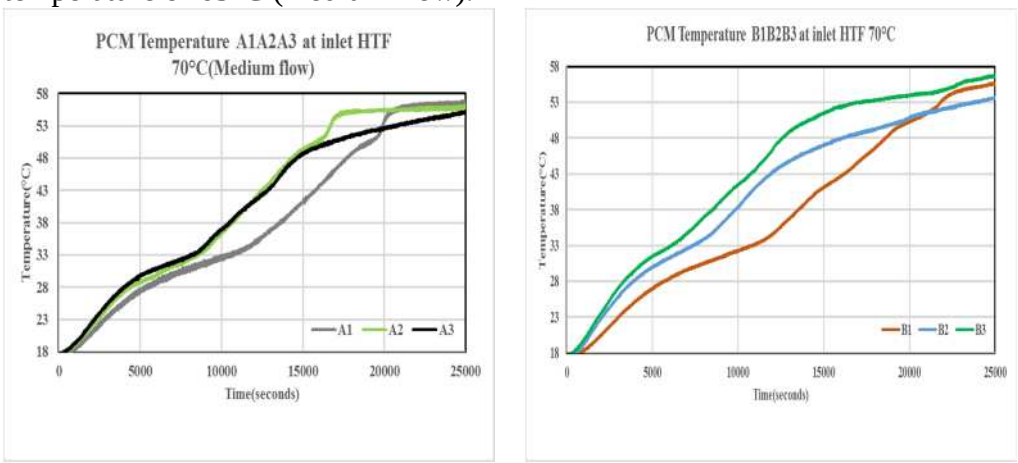


Figure E16: PCM temperature at radial points (A1A2A3) and (B1B2B3) at inlet HTF temperature of 70°C (medium flow).

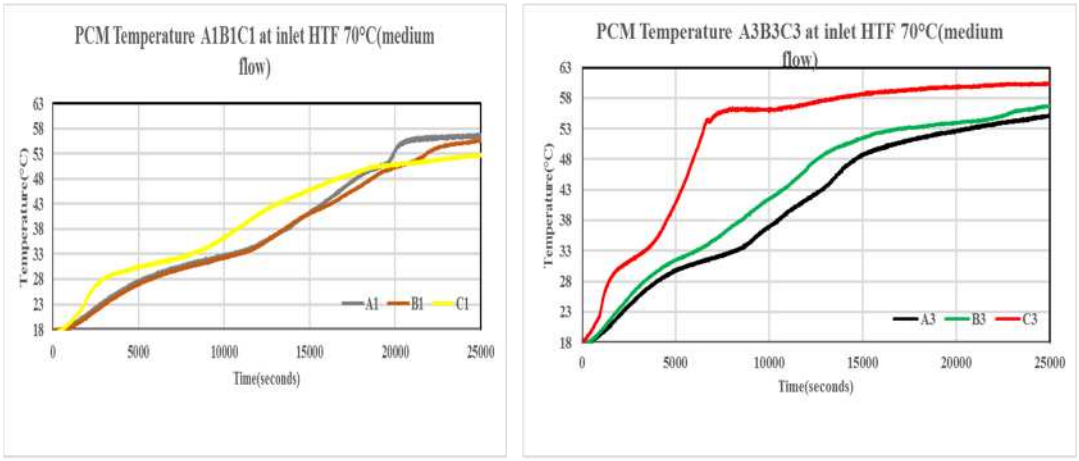


Figure E17: PCM temperature at axial points (A1B1C1) and (A3B3C3) at inlet HTF temperature of 70°C (medium flow).

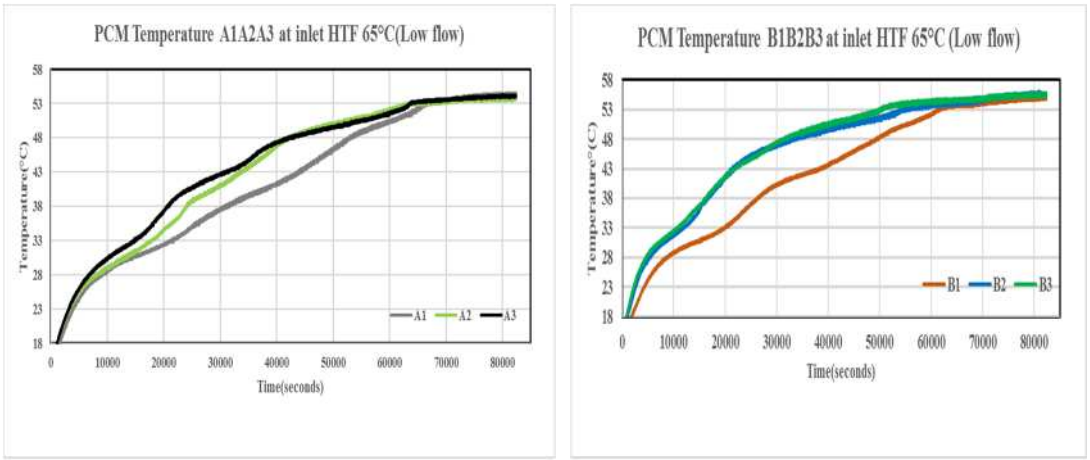


Figure E18: PCM temperature at radial points (A1A2A3) and (B1B2B3) at inlet HTF temperature of 65°C (low flow).

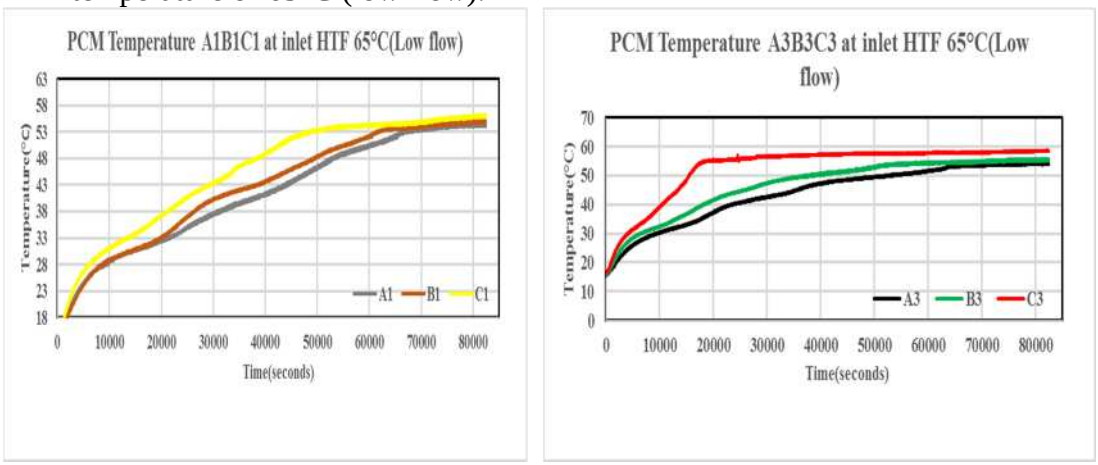


Figure E19: PCM temperature at axial points (A1B1C1) and (A3B3C3) at inlet HTF temperature of 65°C (low flow).

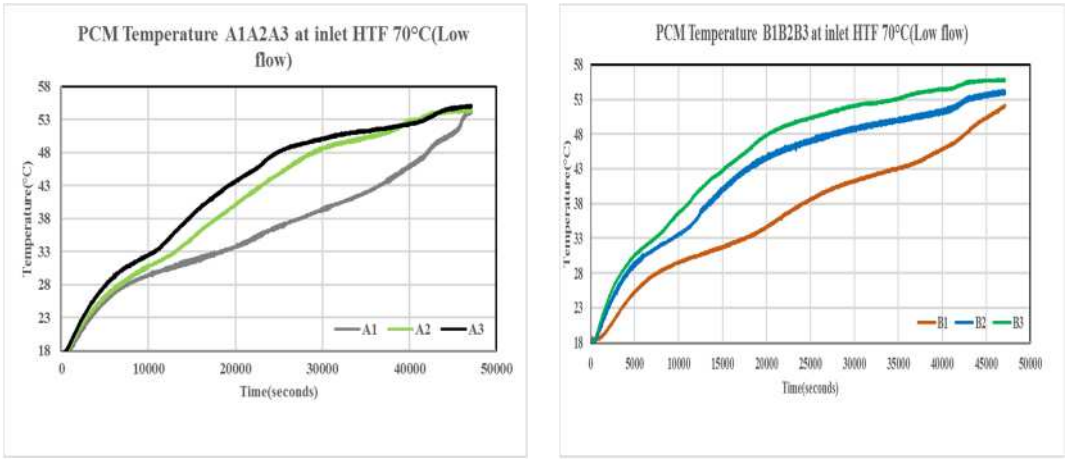


Figure E20: PCM temperature at radial points (A1A2A3) and (B1B2B3) at inlet HTF temperature of 70°C (low flow).

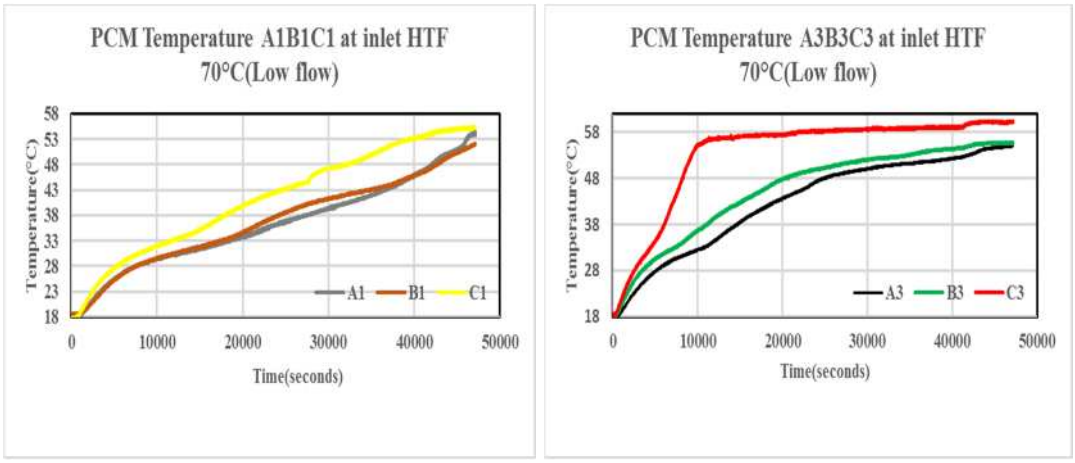


Figure E21: PCM temperature at axial points (A1B1C1) and (A3B3C3) at inlet HTF temperature of 70°C (low flow).

## Appendix F: Experiment result for discharging the serpentine thermal store.

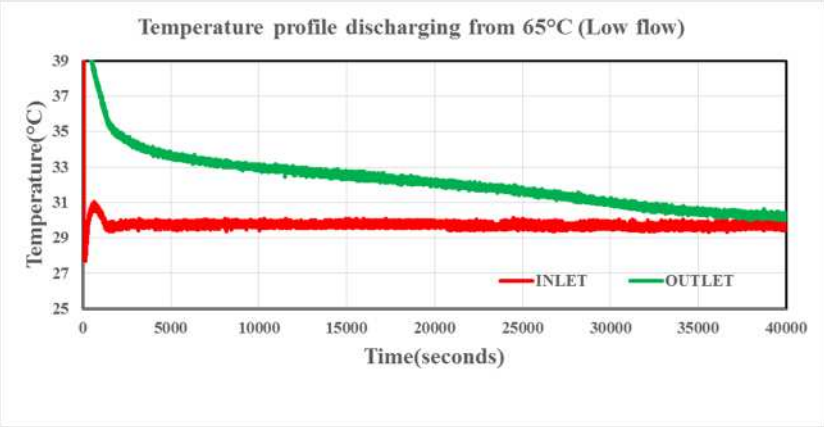


Figure F1: Temp. profile; discharging from 65°C (Low flow)

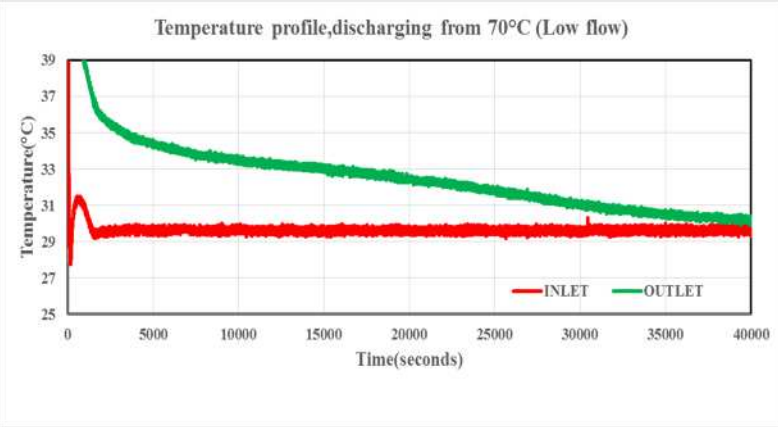


Figure F2: Temp. profile; discharging from 70°C (Low flow)

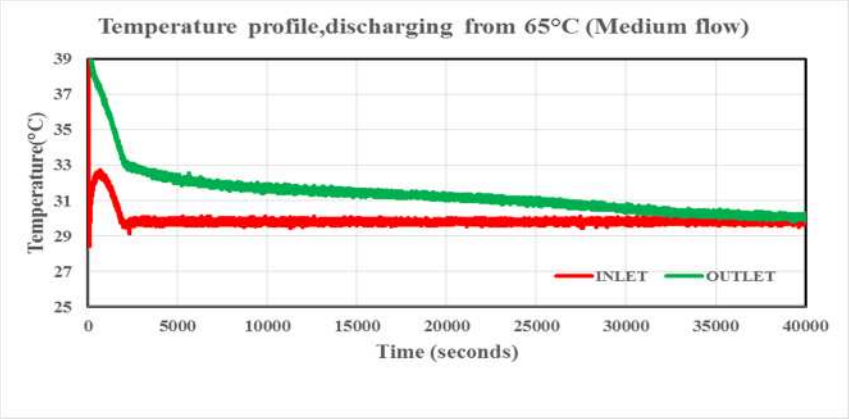


Figure F3: Temp. profile; discharging from 65°C (Medium flow)

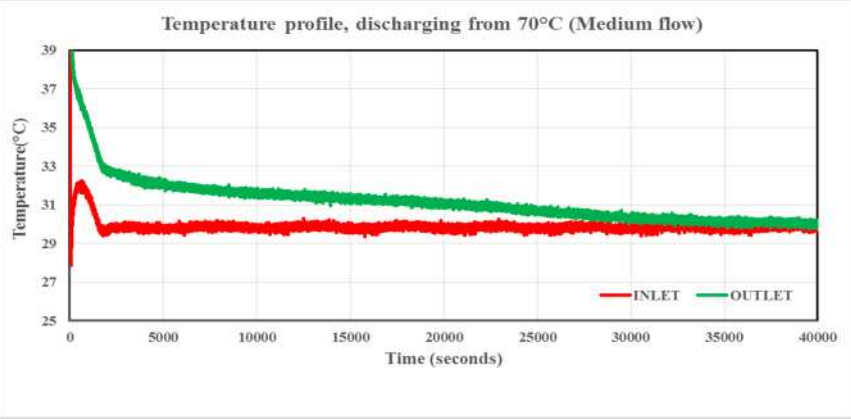


Figure F4: Temp.  profile; discharging from 70°C (medium flow).

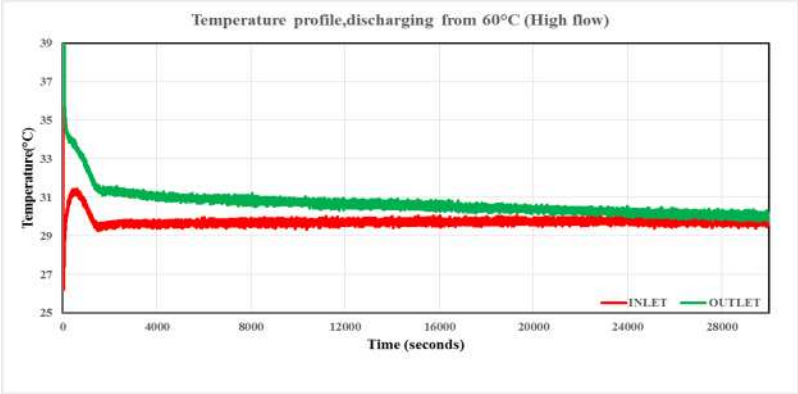


Figure F5: Temp. profile; discharging from 60°C (High flow)

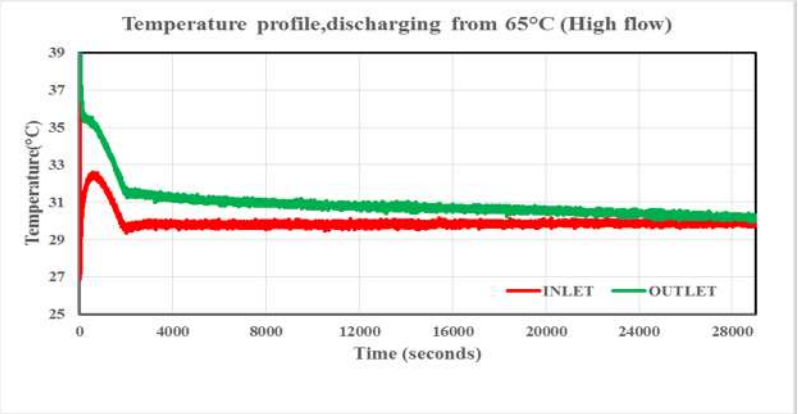


Figure F6: Temp. profile; discharging from 65°C (High flow)

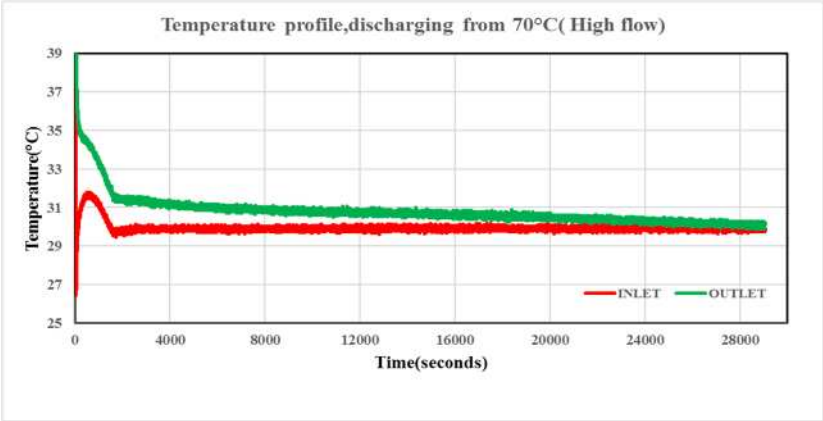


Figure F7: Temp. profile; discharging from 70°C (High flow)

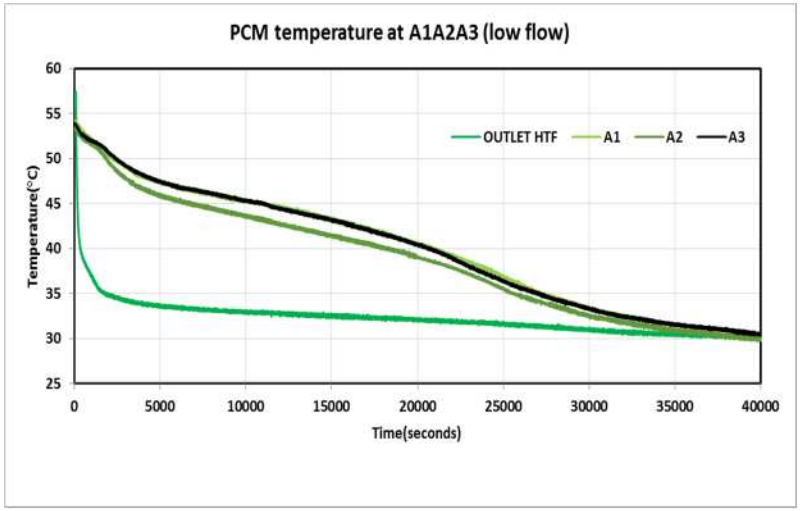


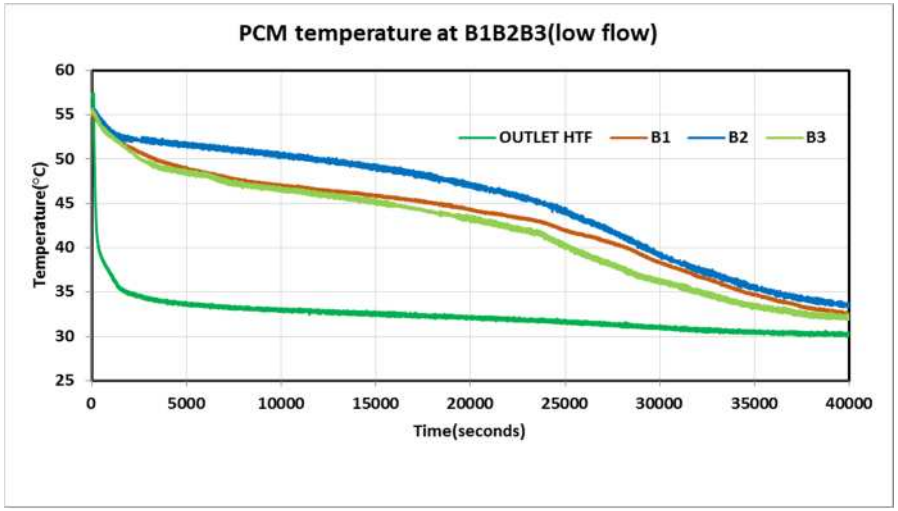


Figure F8: PCM temperature at radial points (A1A2A3) and (B1B2B3) discharging from inlet HTF temperature of 65°C (low flow).

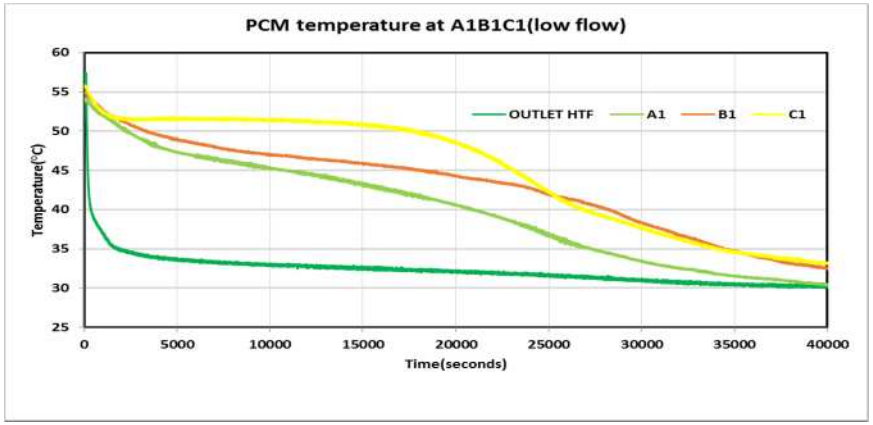


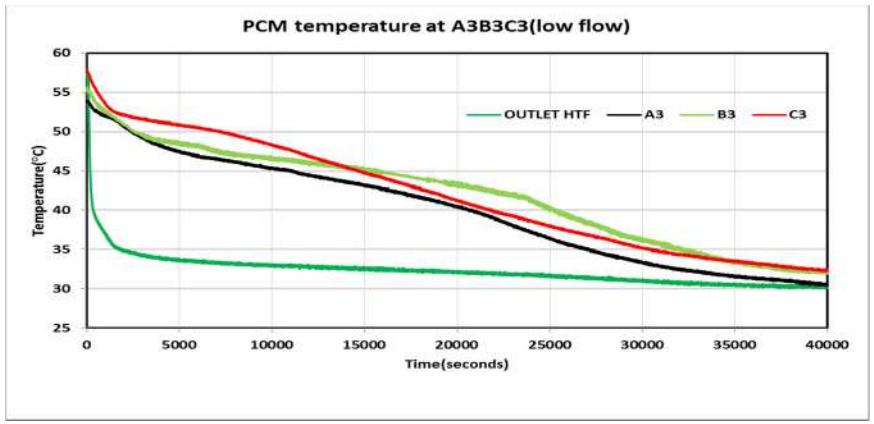


Figure F9: PCM temperature at axial points (A1B1C1) and (A3B3C3) discharging from inlet HTF temperature of 65°C (low flow).

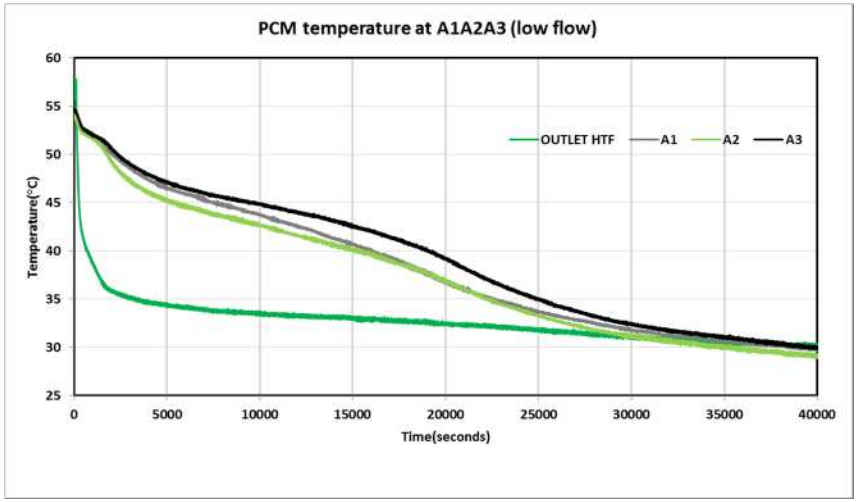


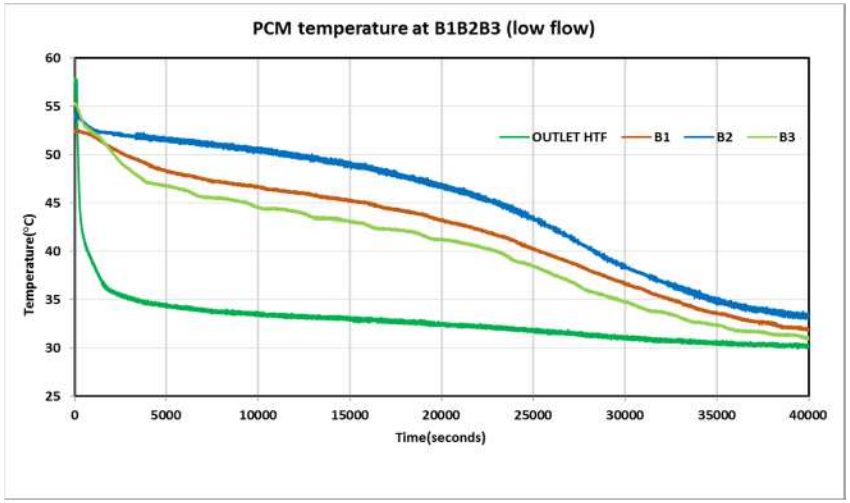


Figure F10: PCM temperature at radial points (A1A2A3) and (B1B2B3) discharging from inlet HTF temperature of 70°C (low flow).

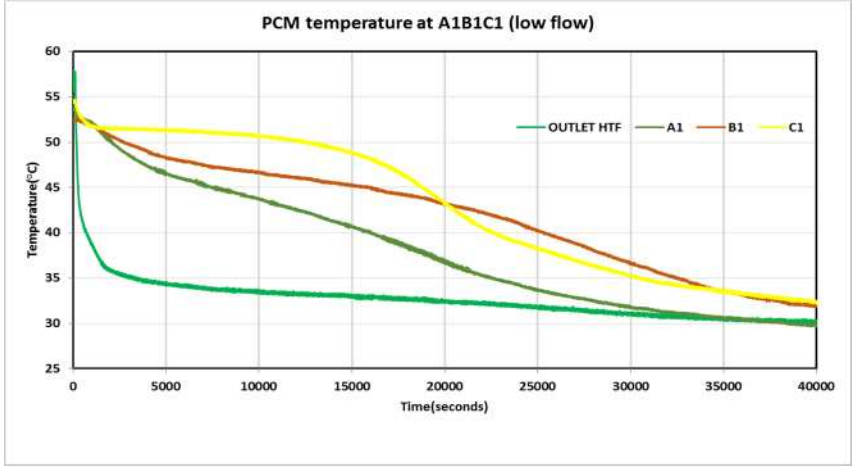


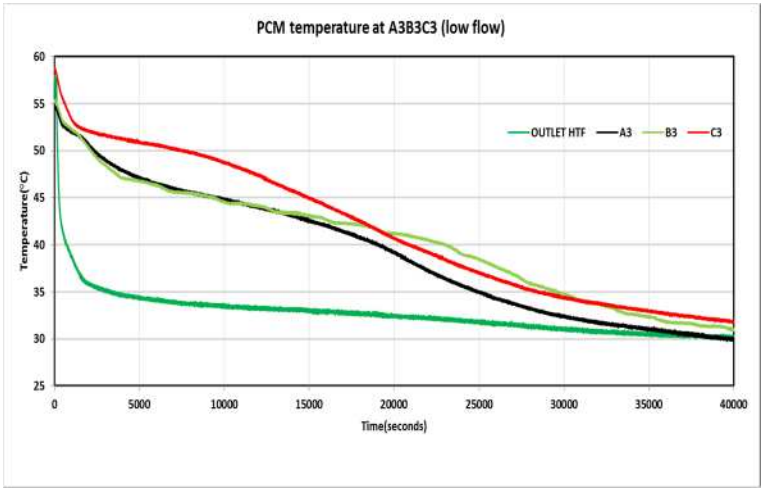


Figure F11: PCM temperature at axial points (A1B1C1) and (A3B3C3) discharging from inlet HTF temperature of 70°C (low flow).

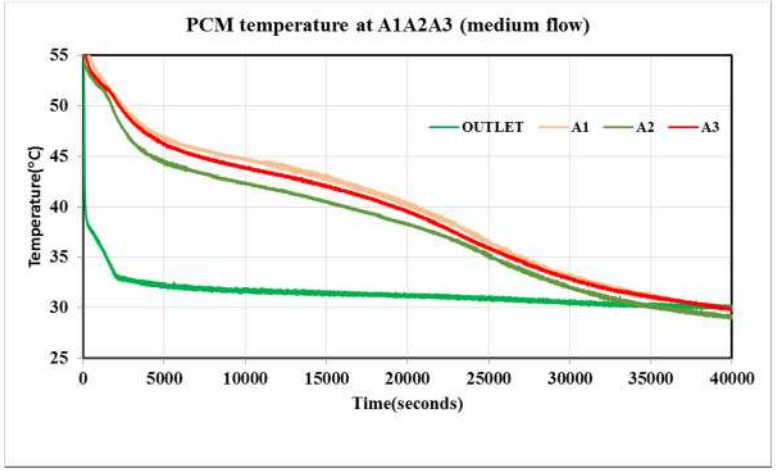


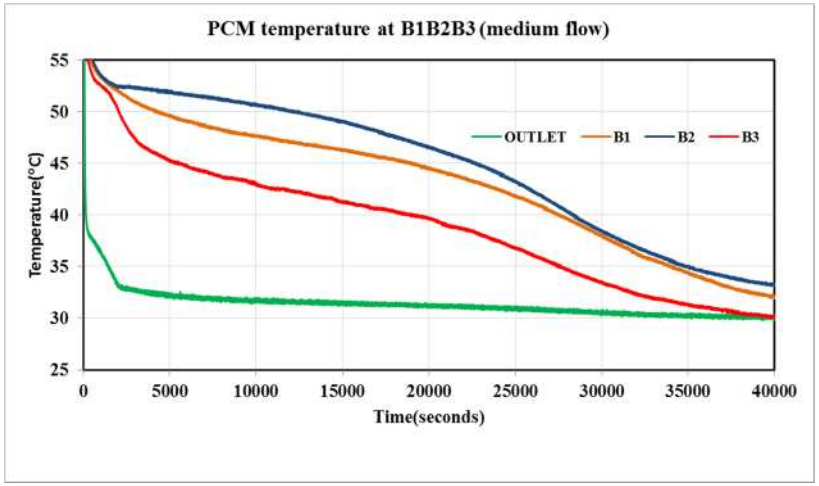


Figure F12: PCM temperature at radial points (A1A2A3) and (B1B2B3) discharging from inlet HTF temperature of 65°C (medium flow).

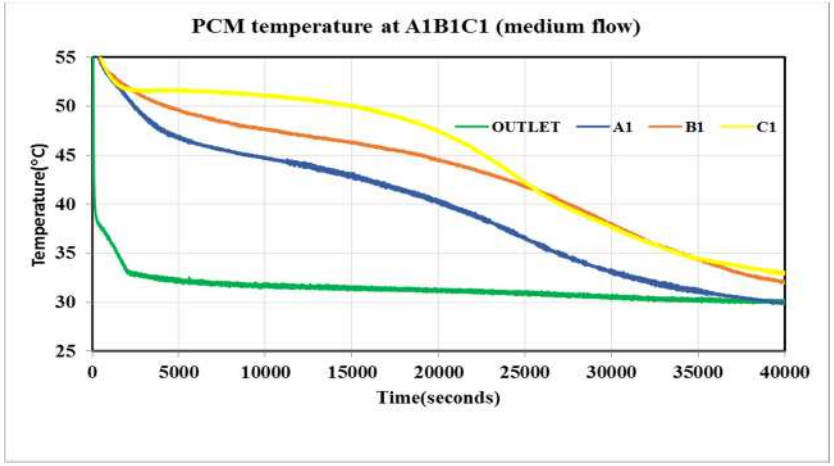


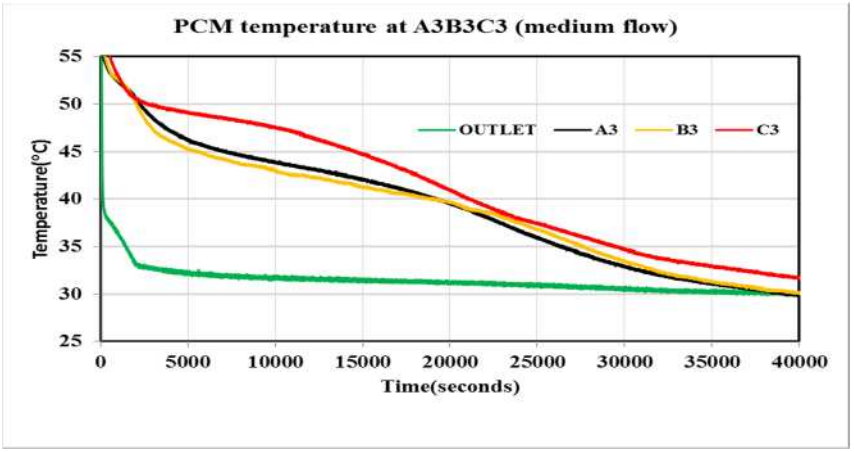


Figure F13: PCM temperature at axial points (A1B1C1) and (A3B3C3) discharging from inlet HTF temperature of 65°C (medium flow).

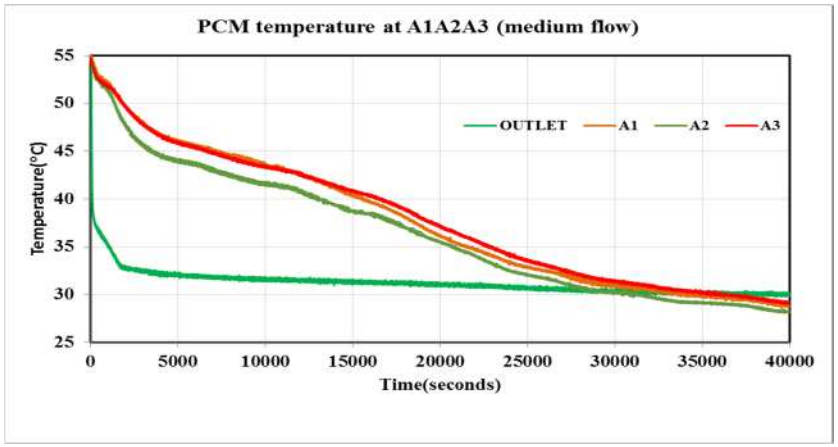


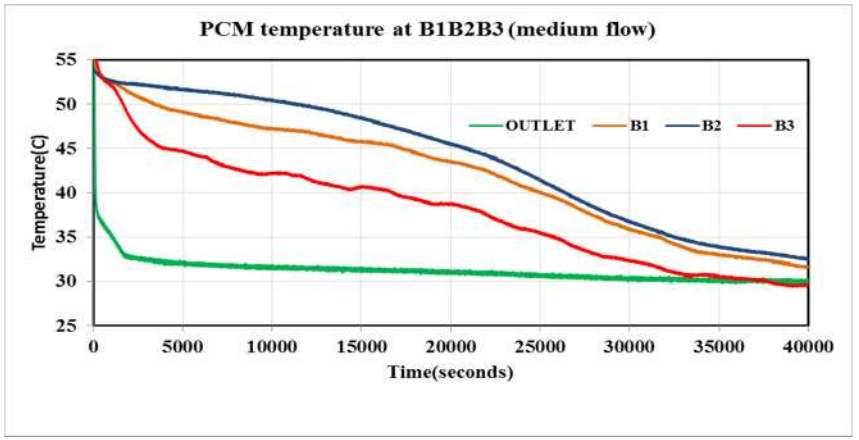


Figure F14: PCM temperature at radial points (A1A2A3) and (B1B2B3) discharging from inlet HTF temperature of 70°C (medium flow).

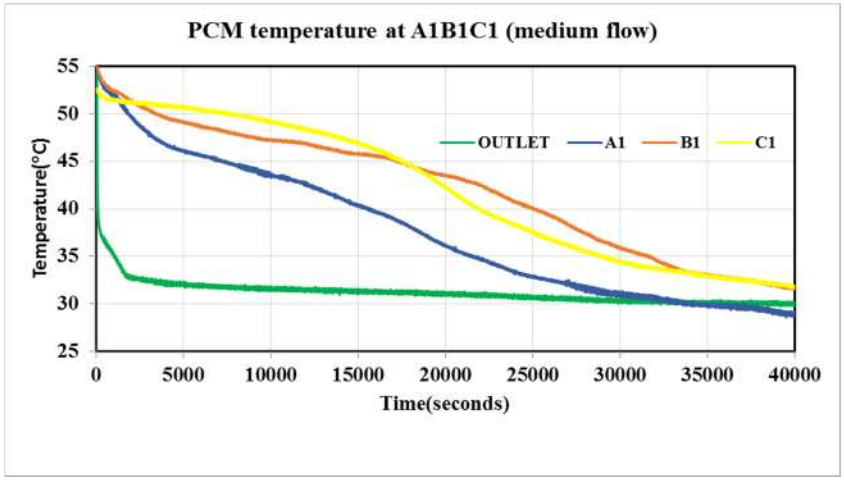


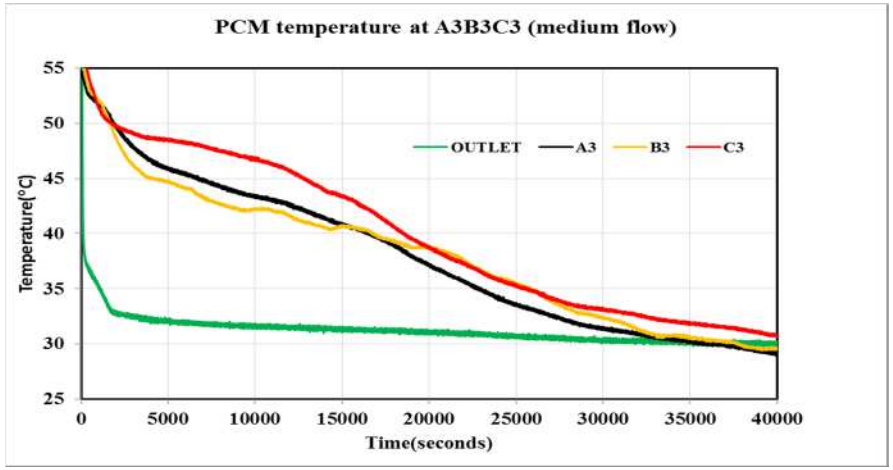


Figure F15: PCM temperature at axial points (A1B1C1) and (A3B3C3) discharging from inlet HTF temperature of 70°C (medium flow).

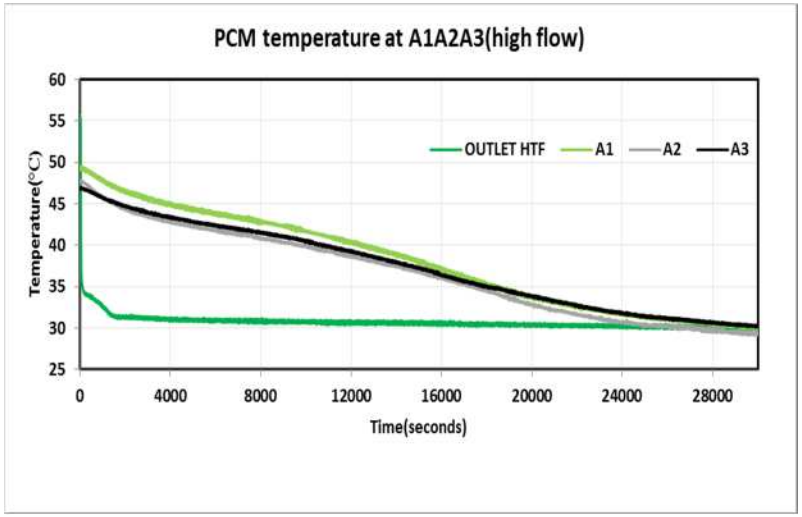


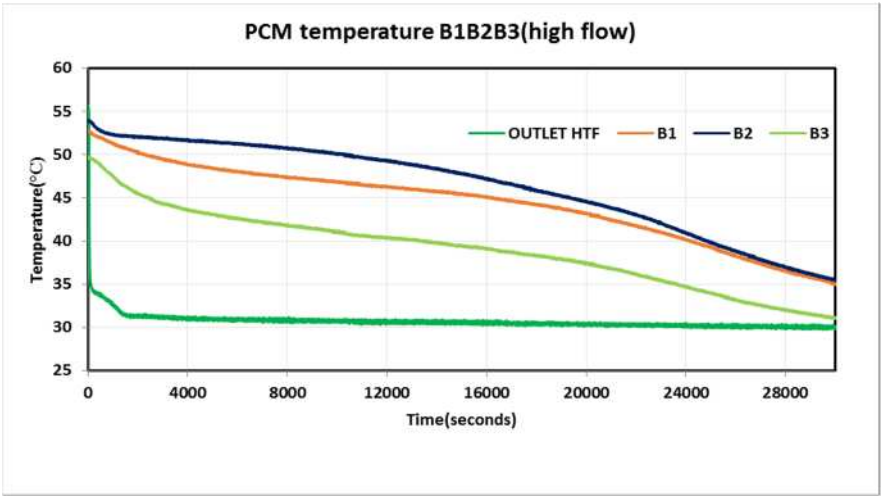


Figure F16: PCM temperature at radial points (A1A2A3) and (B1B2B3) discharging from inlet HTF temperature of 60°C (high flow).

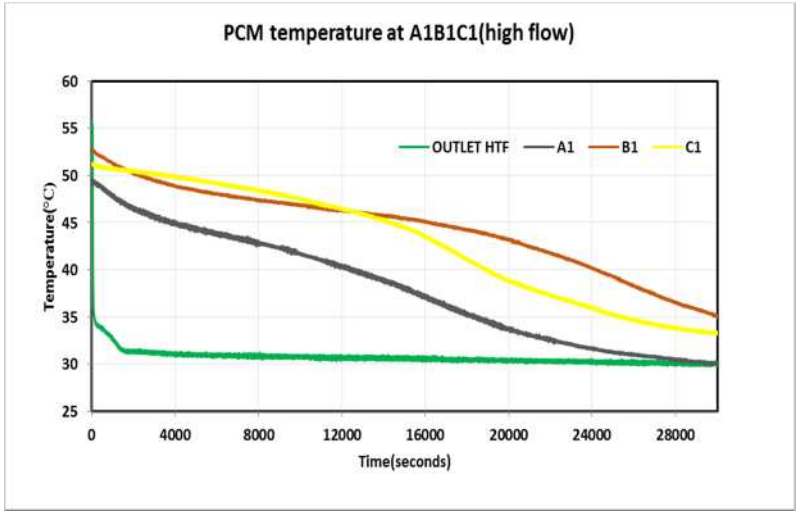


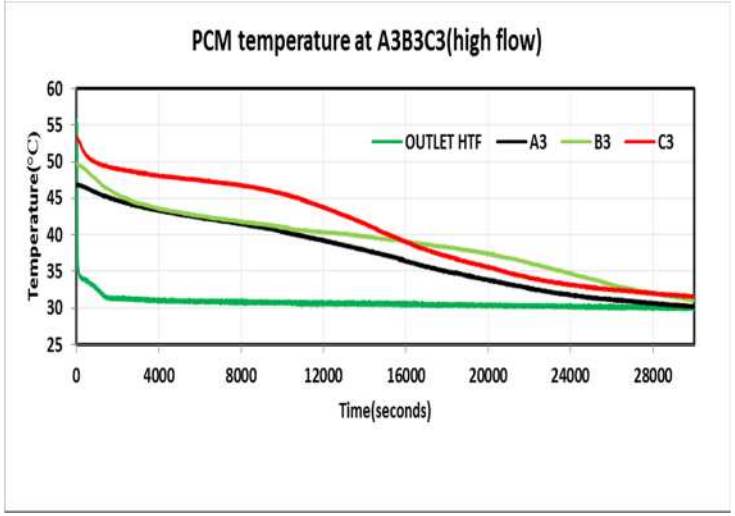


Figure F17: PCM temperature at axial points (A1B1C1) and (A3B3C3) discharging from inlet HTF temperature of 60°C (high flow).

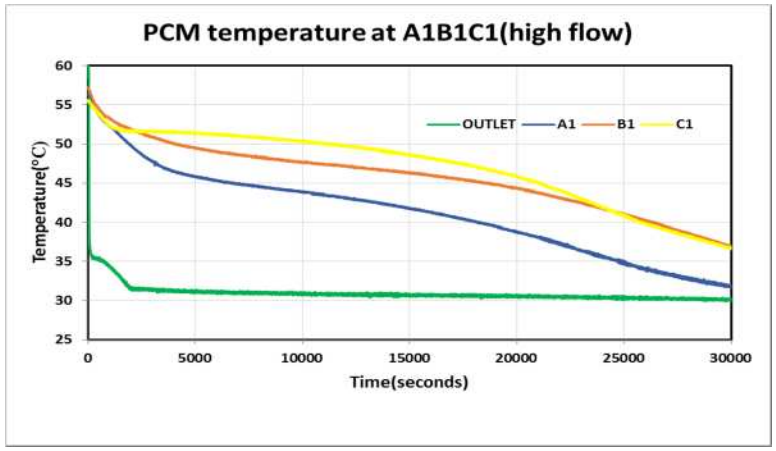


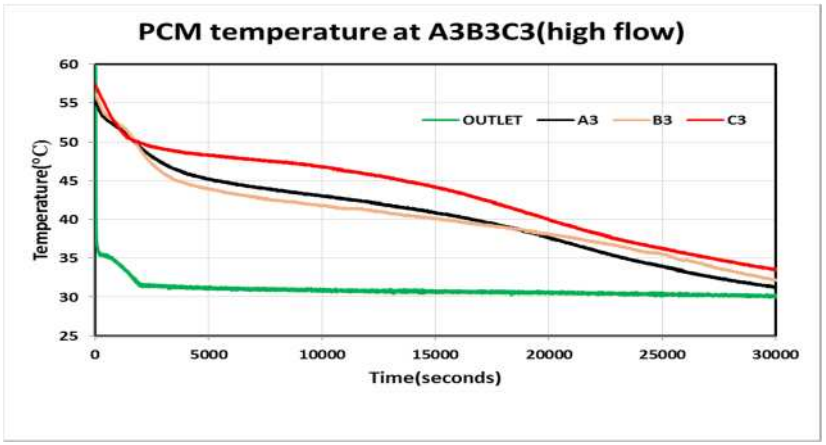


Figure F18: PCM temperature at axial points (A1B1C1) and (A3B3C3) discharging from inlet HTF temperature of 65°C (high flow).

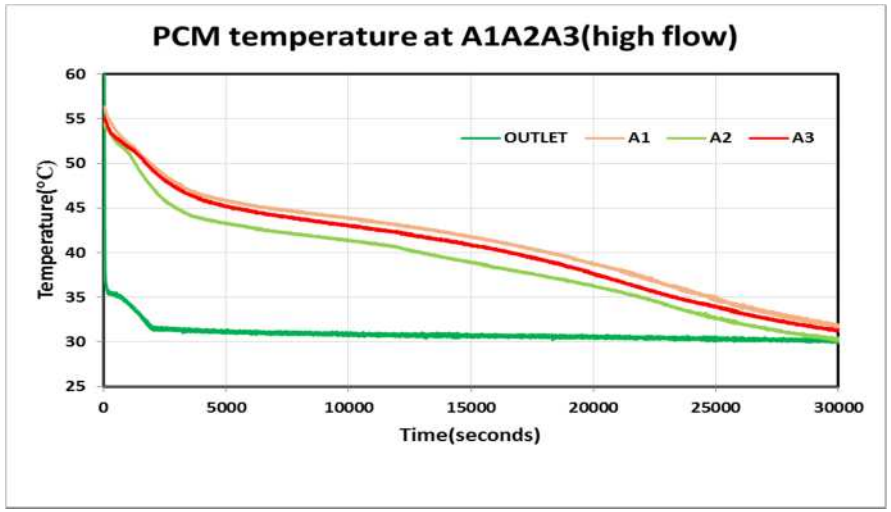


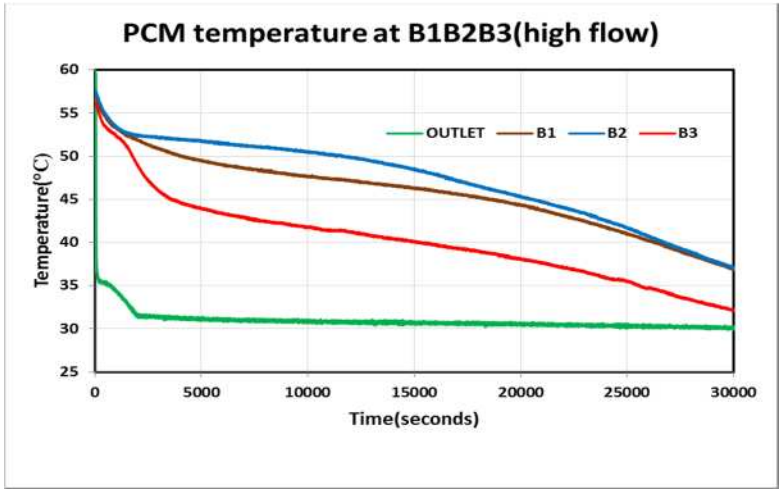


Figure F19: PCM temperature at radial points (A1A2A3) and (B1B2B3) discharging from inlet HTF temperature of 65°C (high flow).

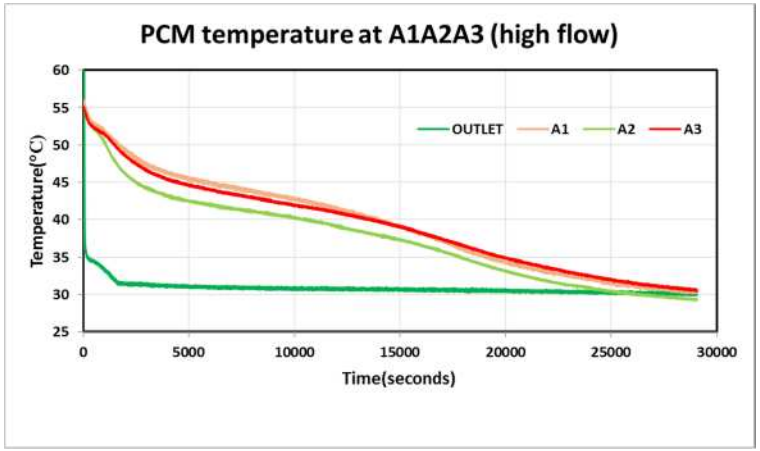


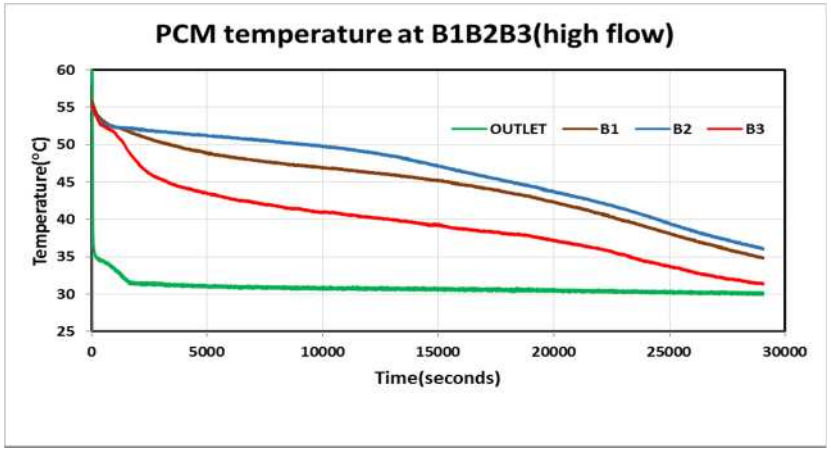


Figure F20: PCM temperature at radial points (A1A2A3) and (B1B2B3) discharging from inlet HTF temperature of 70°C (high flow).

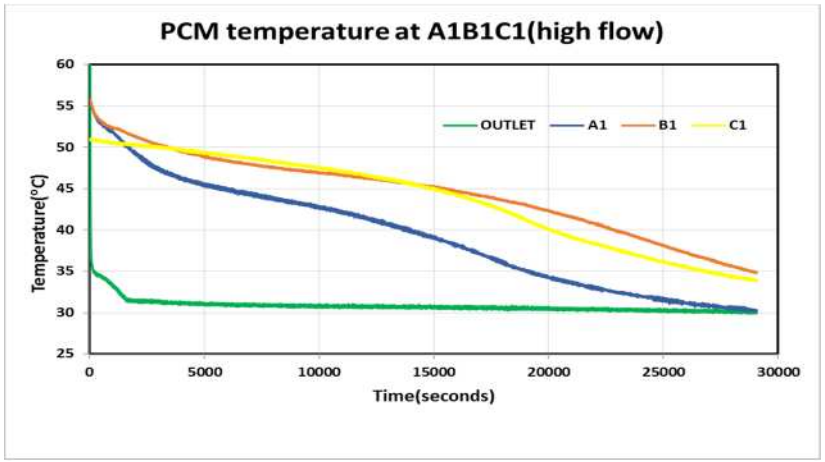


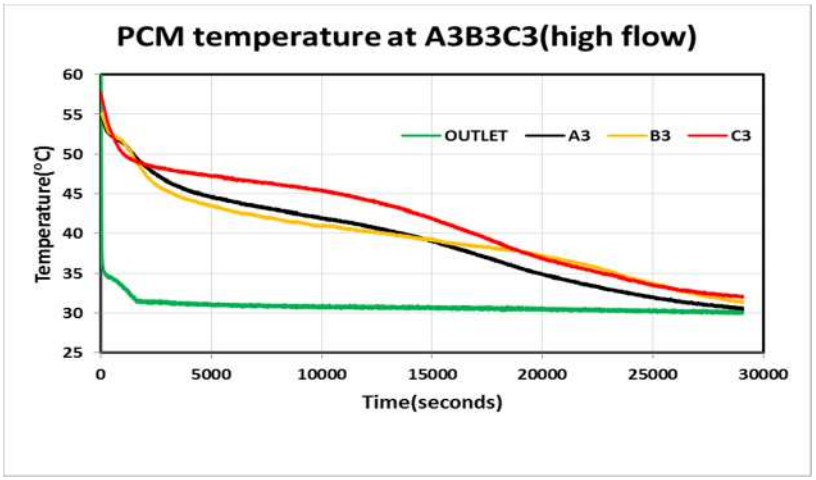


Figure F21: PCM temperature at axial points (A1B1C1) and (A3B3C3) discharging from inlet HTF temperature of 70°C (high flow).

**Appendix G: Room temperature during the experiment using SHE.**

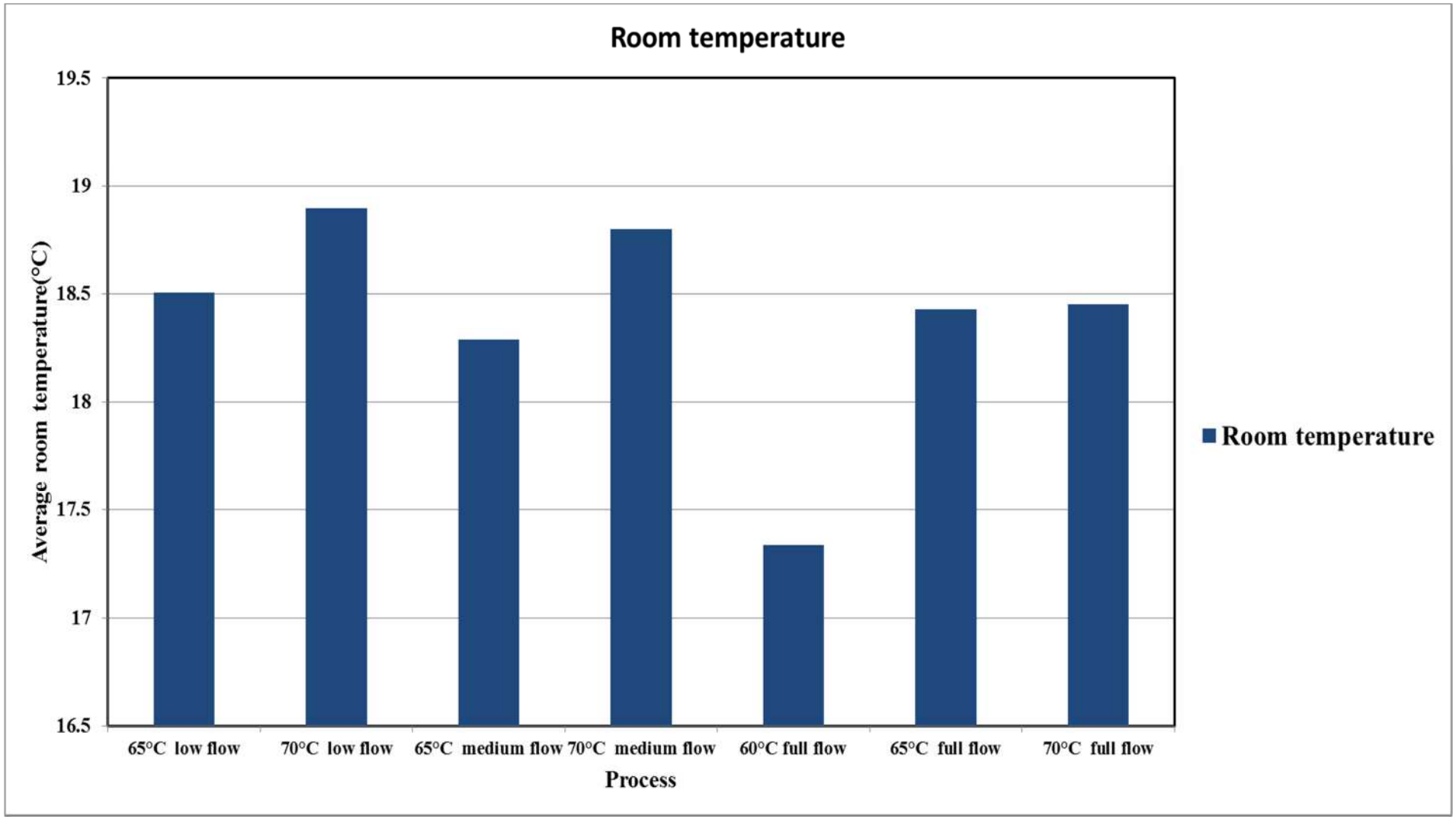

**Appendix H: Image of the SHE thermal store during Charge Process.**

**a)Image of store during charge process.**

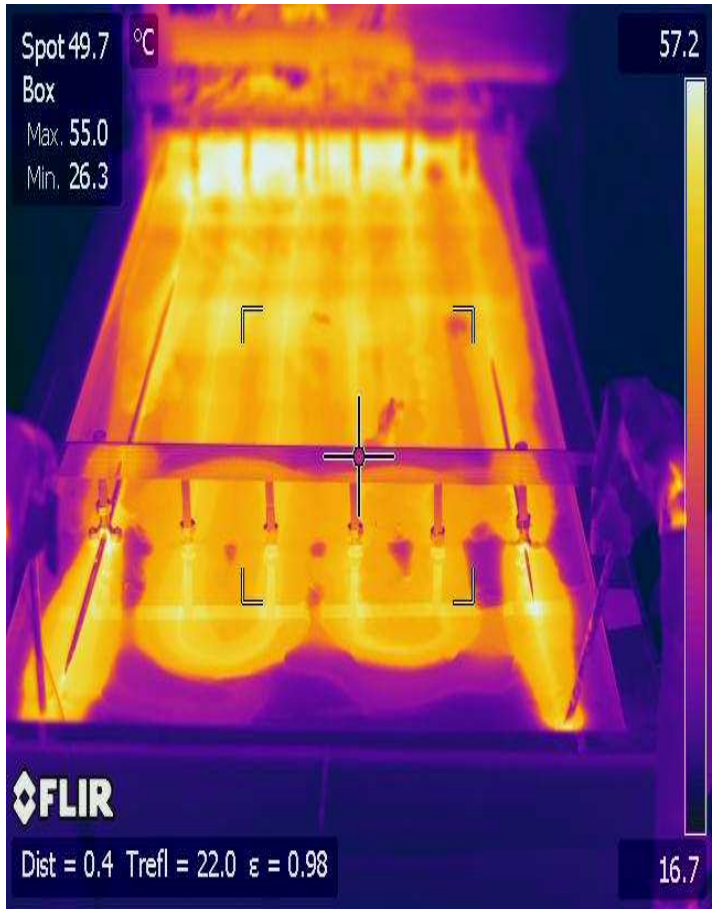


**b) Thermal image of store during charge process.**

**Appendix I: Solid works drawing of the SHE.**

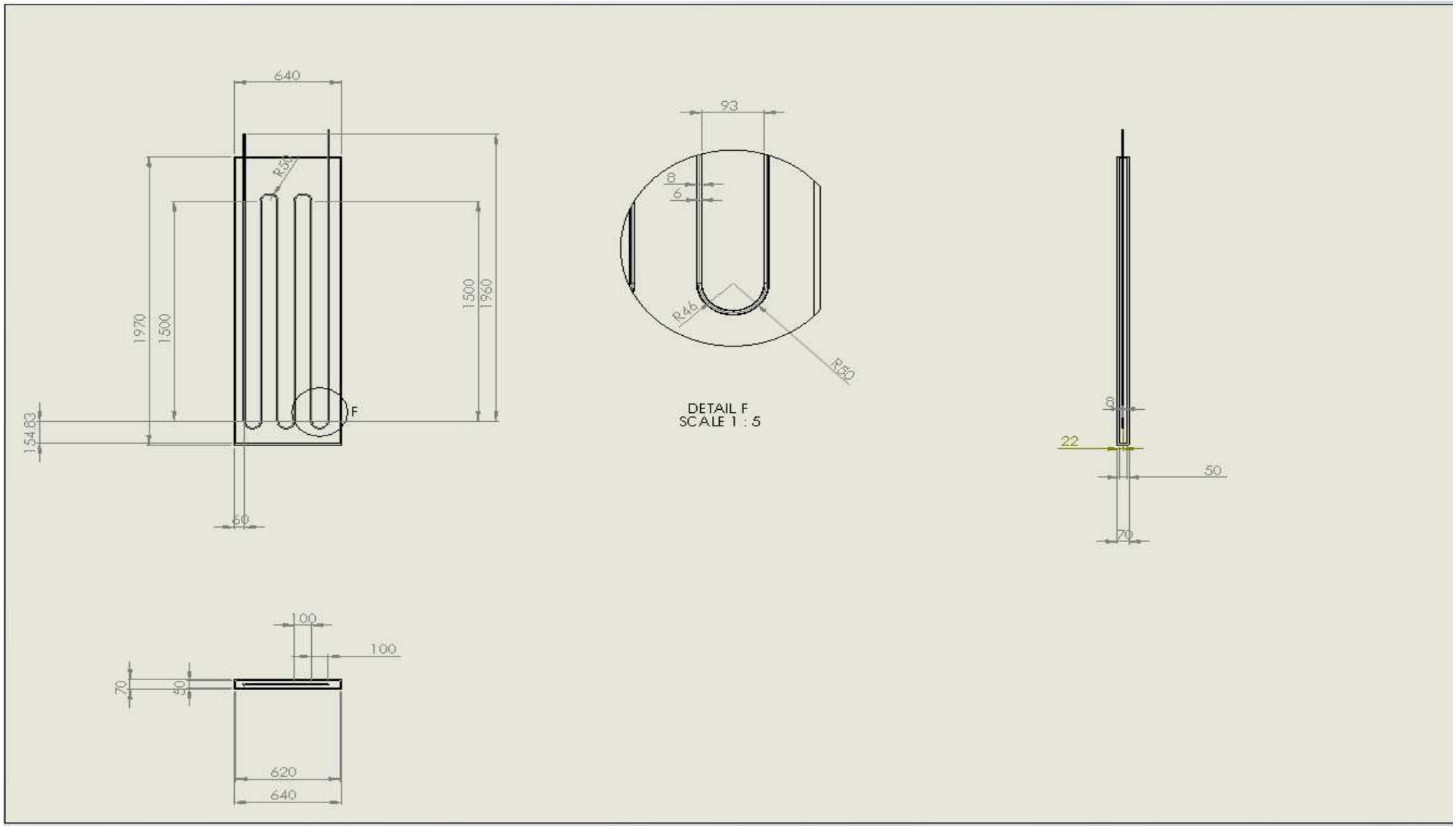

## Appendix J: Matlab model for Plate heat exchanger thermal store (PHE).

```
Main script
% Definitions of variables
clear
load('PCMdata.mat')
Tinitial = HeatingTt(1,2) % Initial temperature of store (C)
mdotw=0.065*1000/368; % Mass flow of water per HALF channel (kg/s)
Cpwater=4182; % Specific heat of water at mean temperature (J/kg/K)
dt= 0.01;% Time step (s);to make the simulation faster,
totalthot=(length(HeatingTt)-1)*20%1800;% Total time for heat input
half cycle simulation
totaltcold=0%1800;% Total time for heat discharge half cycle
simulation
numthot=totalthot/dt;
numtcold=totaltcold/dt;
dx=0.2; % Distance step in water flow direction (m)
dy=0.001; % Distance step in PCM (m)
Lx=1.9; % Channel length (m)
numx=round(Lx/dx); % number of elements in flow direction
tPCM=0.01; % half thickness of PCM(m)
numy=tPCM/dy+2; % number of elements in y direction
Tinhot=70%55; % Hot inlet temp (C) make f(t) later
Tincold=40;% Cold inlet temperature - can be made f(t) later
T=Tinitial*ones(numx,numy); % Temperature array
Tnew=T; % New temperatures
B11=0.0036; % Channel width(m)
B12=0.0033; % Channel height (m)
aoverb=B12/B11; % A guess at the moment. Must be 0 to 1.
Nu=9.4406*(aoverb^4)-28.322*(aoverb^3)+33.537*(aoverb^2)-
19.209*aoverb+...
    7.5569;% Laminar flow Nu quartic in channel width ratio 0 to 1.
dh=4*B11*B12/(2*B12+2*B11);% Hydraulic diameter (m)
kwater=0.643; % conductivity of water at 50C (W/mK)
h=Nu*kwater/dh % heat transfer coefficient from water to wall W/m^2
/K
Re=mdotw*2/(B11+B12)/(544e-6) % Reynolds number using viscosity at
50 C.
dywater=B12; % half thickness of water channel
M=982*dx*dywater; % Mass of water in element (kg)
rhos=946;% Polypropylene wall density (kg/m^3)
Cps=1900; % Polypropylene wall Cp (J/kg/K)
ksteel=0.158; % polypropylene wall conductivity (W/m/K)
Ms=rhos*dx*wt; % Mass of wall element
%*****************************************************************
*******
% PCM properties etc.
Ts=54; % Solidus (?) temperature (C)    for RT 58
Tl=62; % Liquidus (?) temperature (C)   for RT 58
% Ts=51; % Solidus (?) temperature (C)      for RT 52
% Tl=55; % Liquidus (?) temperature (C)     for RT 52
ks=0.23; % Solid conductivity (W/mK)
kl=0.23; % Liquid conductivity (W/mK)
% CpPCMs=6837; % Solid specific heat (J/kg K)     for RT 52
% CpPCMl=5037; % Liquid specific heat (J/kg K)    for RT 52
CpPCMs=5700; % Solid specific heat (J/kg K)   for RT 58
CpPCMl=2300; % Liquid specific heat (J/kg K)  for RT 58
L=1.4e5; % Latent heat (J/kg)RT 58
L=1.53e5; % Latent heat (J/kg)RT 52
rho=880; % Nominal PCM density
```

```
Mpcm=dx*dy*rho; % mass of PCM in element (kg/m depth)
Cpmelt=L/(Tl-Ts); % 'Additional specific heat' in melting
%*****************************************************************
******
X=zeros(numx,numy); % zero = solid, 1 = liquid. First two rows not
used.
k=X; % Conductivities. First row not used.
k(:,2)=ksteel*ones(numx,1);
Cp=X; % Specific heats. First two rows not used.
Qcum=0;% Cumulative heat in store (J). Zero datum at time zero.
Qcumarray=zeros(round((totalthot+totaltcold)/10)+1,1);
Qinarray=zeros(round((totalthot+totaltcold)/10)+1,1);
Tarray=zeros(round((totalthot+totaltcold)/10)+1,numx,numy);
Twateroutex=Qcumarray;
Twateroutsim=Qcumarray;
Tpcmtemp=Qcumarray;
Tin10=Qcumarray;
%Hold=zeros(numx,numy);
%Hnew=zeros(numx,numy);
%Hinc=zeros(numx,numy);
%H=0;
% Calculations
%CHARGING*******************************************************
******


for t=0:dt:totalthot; % time in seconds
    t10=t/10; % time/10 for saving data every 10 seconds.
    %Find Tin
    row1=floor(t/20)+1; %lower row
    row2=ceil(t/20)+1; %upper row
    Tin= HeatingTt(row1,2)+(HeatingTt(row2,2)-HeatingTt(row1,2))...
        *(t/20-row1+1);
    %Holdtot=H;
     % old Enthalpy array calculation from temperatures
              % Calculate total enthalpy H
     %     for i=1:numx;%Add water and wall values
     %         Hold(i,1)=M*Cpwater*Tnew(i,1);
     %         Hold(i,2)=Ms*Cps*Tnew(i,2);
     %     end
     %
     %     for i=1:numx
     %         for j=3:numy;    % Add PCM
     %              if X(i,j)==0; Hpcm=Mpcm*Tnew(i,j)*CpPCMs ;
     %              end
     %              if(X(i,j)>0 && X(i,j)<1);
     %                 hpcm=(Tnew(i,j)-Ts)*(CpPCMs+...
     %                (CpPCMl-CpPCMs)/2/(Tl-Ts)*(Tnew(i,j)-
Ts))+X(i,j)*L...
     %                +CpPCMs*Ts;
     %                 Hpcm=hpcm*Mpcm;
     %              end
     %              if X(i,j)>=1;
     %                hpcm=(Tl-Ts)*(CpPCMs+CpPCMl)/2+...
     %                L+(Tnew(i,j)-Tl)*CpPCMl+Ts*CpPCMs;
     %                Hpcm=hpcm*Mpcm;
     %              end
     %              Hold(i,j)=Hpcm;
     %         end
     %     end% of old enthalpies

    T=Tnew;
```

```
    % calculate properties
    for i=1:numx
        for j=3:numy
            X(i,j)= (T(i,j)-Ts)/(Tl-Ts);
            X(i,j)
            if(X(i,j)>1.);X(i,j)=1. ;end
            if(X(i,j)<0.);X(i,j)=0. ;end
            k(i,j)=X(i,j)*(kl-ks)+ks;
            Cp(i,j)=X(i,j)*(CpPCMl-CpPCMs)+CpPCMs;
            if(X(i,j)>0 && X(i,j)<1); Cp(i,j)=Cp(i,j)+Cpmelt;end
        end
    end
    if t==0;% Calculate initial enthalpy, zero at 0C datum
        Hw=M*numx*Cpwater*Tinitial;
        Hs=Ms*numx*Cps*Tinitial;
       if X(3,3)==0; Hpcm=Mpcm*numx*(numy-2)*Tinitial*CpPCMs;end
        if(X(3,3)>0 && X(3,3)<1);
            hpcm=(T(3,3)-Ts)*(CpPCMs+...
                (CpPCMl-CpPCMs)/2/(Tl-Ts)*(T(3,3)-Ts))+X(3,3)*L...
                +CpPCMs*Ts;
            Hpcm=hpcm*Mpcm*numx*(numy-2);
        end
        if X(3,3)>=1;
            hpcm=(Tl-Ts)*(CpPCMs+CpPCMl)/2+...
                     L+(T(3,3)-Tl)*CpPCMl+Ts*CpPCMs;
            Hpcm=hpcm*Mpcm*numx*(numy-2);
        end
        Hinitial=Hw+Hs+Hpcm;
    end

    % WATER
    Tnew(1,1)=T(1,1)+dt/M*mdotw*(Tin-T(1,1))...
        +dt/M/Cpwater*h*dx*(T(1,2)-T(1,1));% first element
    for i=2:numx-1;
        Tnew(i,1)=T(i,1)+dt/M*mdotw*(-T(i,1)+T(i-1,1)) ...
        + dt/M/Cpwater*h*dx*(T(i,2)-T(i,1) )...
        +dt/M/Cpwater*2*dx*(20-T(1,1)); %heat loss to ambient
h=2W/m2K
    end
        Tnew(numx,1)=T(numx,1)+dt/M/Cpwater*(mdotw*Cpwater* ...
            (T(numx-1,1)-T(numx,1))+h*dx*(T(numx,2)-T(numx,1)));
        % last element

     % WALL
      Tnew(1,2)=T(1,2)+dt/Ms/Cps*(h*dx*(T(1,1)-T(1,2))...
             +ksteel*wt/dx*(T(2,2)-T(1,2))...
             +dx*(T(1,3)-T(1,2))*2/(wt/ksteel+dy/k(1,3)));
     for i=2:numx-1;
         Tnew(i,2)=T(i,2)+dt/Ms/Cps*(h*dx*(T(i,1)-T(i,2))...
             +ksteel*wt/dx*(T(i-1,2)+T(i+1,2)-2*T(i,2))...
             +dx*(T(i,3)-T(i,2))*2/(wt/ksteel+dy/k(i,3)));
     end
      Tnew(numx,2)=T(numx,2)+dt/Ms/Cps*(h*dx*(T(numx,1)-
T(numx,2))...
             +ksteel*wt/dx*(T(numx-1,2)-T(numx,2))...
             +dx*(T(numx,3)-T(numx,2))*2/(wt/ksteel+dy/k(numx,3)));
```

```
%*****************************************************************
****
      % PCM
      for i=1:numx;
          for j=3:numy;

              % North resistance always defined:
              if j==3;
                  RN=wt/2/k(i,j-1)+dy/2/k(i,j);
              else
                  RN=dy/2/k(i,j-1)+dy/2/k(i,j);
              end

              % South resistance infinity on adiabatic line of
symmetry:
              if j==numy;
                  RS=0.5; %Heat loss from top of plate
                  TS=20.;
              else
                  RS=dy/2/k(i,j+1)+dy/2/k(i,j);
                  TS=T(i,j+1);
              end

              % West resistance infinity at left wall:
              if i==1;
                  RW=inf;
                  TW=1;
              else
                  RW=dx/2/k(i-1,j)+dx/2/k(i,j);
                  TW=T(i-1,j);
              end

              % East resistance infinity at right wall:
              if i==numx;
                  RE=inf;
                  TE=1.;
              else
                  RE=dx/2/k(i+1,j)+dx/2/k(i,j);
                  TE=T(i+1,j);
              end
              Tnew(i,j)=Tnew(i,j)+dt/Mpcm/Cp(i,j)*...
                  (dx/RN*T(i,j-1)+dx/RS*TS...
                  +dy/RE*TE+dy/RW*TW...
                  -T(i,j)*(dx/RN+dx/RS+dy/RE+dy/RW));
          end % of j=3:numy
      end % of i=1:numx
%*****************************************************************
*****
      % New Enthalpy array calculation from temperatures
              % Calculate total enthalpy H

        %  for i=1:numx;%Add water and wall values
        %      Hnew(i,1)=M*Cpwater*Tnew(i,1);
        %      Hnew(i,2)=Ms*Cps*Tnew(i,2);
        %  end
       %
       %   for i=1:numx
       %       for j=3:numy;    % Add PCM
       %            if X(i,j)==0; Hpcm=Mpcm*Tnew(i,j)*CpPCMs ;
```

```
        %            end
        %            if(X(i,j)>0 && X(i,j)<1);
        %               hpcm=(Tnew(i,j)-Ts)*(CpPCMs+...
        %              (CpPCMl-CpPCMs)/2/(Tl-Ts)*(Tnew(i,j)-
Ts))+X(i,j)*L...
        %              +CpPCMs*Ts;
        %               Hpcm=hpcm*Mpcm;
        %            end
        %            if X(i,j)>=1;
        %              hpcm=(Tl-Ts)*(CpPCMs+CpPCMl)/2+...
        %              L+(Tnew(i,j)-Tl)*CpPCMl+Ts*CpPCMs;
        %              Hpcm=hpcm*Mpcm;
        %            end
        %            Hnew(i,j)=Hpcm;
        %       end
        %   end% of new enthalpies

       %Hinc=Hnew-Hold;
       Qin=mdotw*Cpwater*(Tin-T(numx,1))*dt;
       %sumHinc=sum(sum(Hinc));
       %sumHnew=sum(sum(Hnew));
       Qcum=Qcum+Qin;
       if floor(t10)==t10; % condition to save all temperature data
           H=0;% Calculate total enthalpy H
           for i=1:numx;%Add water and wall values
               H=H+M*Cpwater*Tnew(i,1)+Ms*Cps*Tnew(i,2);
           end

           for i=1:numx
               for j=3:numy;    % Add PCM
                    if X(i,j)==0; Hpcm=Mpcm*Tnew(i,j)*CpPCMs ;
                    end
                    if(X(i,j)>0 && X(i,j)<1);
                       hpcm=(Tnew(i,j)-Ts)*(CpPCMs+...
                      (CpPCMl-CpPCMs)/2/(Tl-Ts)*(Tnew(i,j)-
Ts))+X(i,j)*L...
                      +CpPCMs*Ts;
                       Hpcm=hpcm*Mpcm;
                    end
                    if X(i,j)>=1;
                      hpcm=(Tl-Ts)*(CpPCMs+CpPCMl)/2+...
                      L+(Tnew(i,j)-Tl)*CpPCMl+Ts*CpPCMs;
                      Hpcm=hpcm*Mpcm;
                    end
                    H=H+Hpcm;
               end
           end
           t
           H
         %  sumHnew
           Hinitial
           Qcum
           Hstore=H-Hinitial
           Qin
         %  sumHinc

           %Find Tout actual value

Twateroutex(t10+1)= HeatingTt(row1,3)+(HeatingTt(row2,3)-
HeatingTt(row1,3))...
```

```
        *(t/20-row1+1);
    Twateroutsim(t10+1)=Tnew(numx,1);
    Tin10(t10+1)=Tnew(1,1);
          Qcumarray(t10+1)=Qcum;
          Qinarray(t10+1)=Qin;
          Tarray(t10+1,:,:)=Tnew;
      end
end% of time step

%Reverse bed temperatures to simulate flow in reverse direction
Tnew=Tnew(numx:-1:1,1:numy);

%
DISCHARGING************************************************************
**
for t=totalthot+dt:dt:totaltcold+totalthot; % time in seconds
    t10=t/10; % time/10 for saving data every 10 seconds.
    Tin=Tincold;
    %Holdtot=H;
     % old Enthalpy array calculation from temperatures
              % Calculate total enthalpy H
     %     for i=1:numx;%Add water and wall values
     %         Hold(i,1)=M*Cpwater*Tnew(i,1);
     %         Hold(i,2)=Ms*Cps*Tnew(i,2);
     %     end
     %
     %     for i=1:numx
     %         for j=3:numy;    % Add PCM
     %              if X(i,j)==0; Hpcm=Mpcm*Tnew(i,j)*CpPCMs ;
     %              end
     %              if(X(i,j)>0 && X(i,j)<1);
     %                 hpcm=(Tnew(i,j)-Ts)*(CpPCMs+...
     %                (CpPCMl-CpPCMs)/2/(Tl-Ts)*(Tnew(i,j)-
Ts))+X(i,j)*L...
     %                 +CpPCMs*Ts;
     %                  Hpcm=hpcm*Mpcm;
     %              end
     %              if X(i,j)>=1;
     %                hpcm=(Tl-Ts)*(CpPCMs+CpPCMl)/2+...
     %                L+(Tnew(i,j)-Tl)*CpPCMl+Ts*CpPCMs;
     %                Hpcm=hpcm*Mpcm;
     %              end
     %              Hold(i,j)=Hpcm;
     %         end
     %     end% of old enthalpies

    T=Tnew;

    % calculate properties
    for i=1:numx
        for j=3:numy
            X(i,j)= (T(i,j)-Ts)/(Tl-Ts);
            if(X(i,j)>1.);X(i,j)=1. ;end
            if(X(i,j)<0.);X(i,j)=0. ;end
            k(i,j)=X(i,j)*(kl-ks)+ks;
            Cp(i,j)=X(i,j)*(CpPCMl-CpPCMs)+CpPCMs;
            if(X(i,j)>0 && X(i,j)<1); Cp(i,j)=Cp(i,j)+Cpmelt;end
        end
    end
    if t==0;% Calculate initial enthalpy, zero at 0C datum
```

```
        Hw=M*numx*Cpwater*Tinitial;
        Hs=Ms*numx*Cps*Tinitial;
       if X(3,3)==0; Hpcm=Mpcm*numx*(numy-2)*Tinitial*CpPCMs;end
        if(X(3,3)>0 && X(3,3)<1);
            hpcm=(T(3,3)-Ts)*(CpPCMs+...
                (CpPCMl-CpPCMs)/2/(Tl-Ts)*(T(3,3)-Ts))+X(3,3)*L...
                +CpPCMs*Ts;
            Hpcm=hpcm*Mpcm*numx*(numy-2);
        end
        if X(3,3)>=1;
            hpcm=(Tl-Ts)*(CpPCMs+CpPCMl)/2+...
                     L+(T(3,3)-Tl)*CpPCMl+Ts*CpPCMs;
            Hpcm=hpcm*Mpcm*numx*(numy-2);
        end
        Hinitial=Hw+Hs+Hpcm;
    end

    % WATER
    Tnew(1,1)=T(1,1)+dt/M*mdotw*(Tin-T(1,1))...
        +dt/M/Cpwater*h*dx*(T(1,2)-T(1,1));% first element
    for i=2:numx-1;
        Tnew(i,1)=T(i,1)+dt/M*mdotw*(-T(i,1)+T(i-1,1)) ...
        + dt/M/Cpwater*h*dx*(T(i,2)-T(i,1) );
    end
        Tnew(numx,1)=T(numx,1)+dt/M/Cpwater*(mdotw*Cpwater* ...
            (T(numx-1,1)-T(numx,1))+h*dx*(T(numx,2)-T(numx,1)));
        % last element


     % WALL
      Tnew(1,2)=T(1,2)+dt/Ms/Cps*(h*dx*(T(1,1)-T(1,2))...
             +ksteel*wt/dx*(T(2,2)-T(1,2))...
             +dx*(T(1,3)-T(1,2))*2/(wt/ksteel+dy/k(1,3)));
     for i=2:numx-1;
         Tnew(i,2)=T(i,2)+dt/Ms/Cps*(h*dx*(T(i,1)-T(i,2))...
             +ksteel*wt/dx*(T(i-1,2)+T(i+1,2)-2*T(i,2))...
             +dx*(T(i,3)-T(i,2))*2/(wt/ksteel+dy/k(i,3)));
     end
      Tnew(numx,2)=T(numx,2)+dt/Ms/Cps*(h*dx*(T(numx,1)-
T(numx,2))...
             +ksteel*wt/dx*(T(numx-1,2)-T(numx,2))...
             +dx*(T(numx,3)-T(numx,2))*2/(wt/ksteel+dy/k(numx,3)));
      % PCM
      for i=1:numx;
          for j=3:numy;

              % North resistance always defined:
              if j==3;
                  RN=wt/2/k(i,j-1)+dy/2/k(i,j);
              else
                  RN=dy/2/k(i,j-1)+dy/2/k(i,j);
              end

              % South resistance infinity on adiabatic line of
symmetry:
              if j==numy;
                  RS=0.5; %heat loass from top of plate
                  TS=20.;
              else
                  RS=dy/2/k(i,j+1)+dy/2/k(i,j);
                  TS=T(i,j+1);
```

```
            end

            % West resistance infinity at left wall:
            if i==1;
                RW=inf;
                TW=1;
            else
                RW=dx/2/k(i-1,j)+dx/2/k(i,j);
                TW=T(i-1,j);
            end

            % East resistance infinity at right wall:
            if i==numx;
                RE=inf;
                TE=1.;
            else
                RE=dx/2/k(i+1,j)+dx/2/k(i,j);
                TE=T(i+1,j);
            end
            Tnew(i,j)=Tnew(i,j)+dt/Mpcm/Cp(i,j)*...
                (dx/RN*T(i,j-1)+dx/RS*TS...
                +dy/RE*TE+dy/RW*TW...
                -T(i,j)*(dx/RN+dx/RS+dy/RE+dy/RW));
        end % of j=3:numy
    end % of i=1:numx

    % New Enthalpy array calculation from temperatures
            % Calculate total enthalpy H

      %  for i=1:numx;%Add water and wall values
      %      Hnew(i,1)=M*Cpwater*Tnew(i,1);
      %      Hnew(i,2)=Ms*Cps*Tnew(i,2);
      %  end
     %
     %   for i=1:numx
     %       for j=3:numy;    % Add PCM
     %            if X(i,j)==0; Hpcm=Mpcm*Tnew(i,j)*CpPCMs ;
     %            end
     %            if(X(i,j)>0 && X(i,j)<1);
     %               hpcm=(Tnew(i,j)-Ts)*(CpPCMs+...
     %              (CpPCMl-CpPCMs)/2/(Tl-Ts)*(Tnew(i,j)-
Ts))+X(i,j)*L...
     %              +CpPCMs*Ts;
     %               Hpcm=hpcm*Mpcm;
     %            end
     %            if X(i,j)>=1;
     %              hpcm=(Tl-Ts)*(CpPCMs+CpPCMl)/2+...
     %              L+(Tnew(i,j)-Tl)*CpPCMl+Ts*CpPCMs;
     %              Hpcm=hpcm*Mpcm;
     %            end
     %            Hnew(i,j)=Hpcm;
     %       end
     %   end% of new enthalpies

    %Hinc=Hnew-Hold;
    Qin=mdotw*Cpwater*(Tin-T(numx,1))*dt;% negative
    %sumHinc=sum(sum(Hinc));
    %sumHnew=sum(sum(Hnew));
    Qcum=Qcum+Qin;
    if floor(t10)==t10; % condition to save all temperature data
```

```
          H=0;% Calculate total enthalpy H
          for i=1:numx;%Add water and wall values
              H=H+M*Cpwater*Tnew(i,1)+Ms*Cps*Tnew(i,2);
          end

          for i=1:numx
              for j=3:numy;    % Add PCM
                   if X(i,j)==0; Hpcm=Mpcm*Tnew(i,j)*CpPCMs ;
                   end
                   if(X(i,j)>0 && X(i,j)<1);
                      hpcm=(Tnew(i,j)-Ts)*(CpPCMs+...
                     (CpPCMl-CpPCMs)/2/(Tl-Ts)*(Tnew(i,j)-
Ts))+X(i,j)*L...
                     +CpPCMs*Ts;
                      Hpcm=hpcm*Mpcm;
                   end
                   if X(i,j)>=1;
                     hpcm=(Tl-Ts)*(CpPCMs+CpPCMl)/2+...
                     L+(Tnew(i,j)-Tl)*CpPCMl+Ts*CpPCMs;
                     Hpcm=hpcm*Mpcm;
                   end
                   H=H+Hpcm;
              end
          end
          t
          H
        %  sumHnew
          Hinitial
          Qcum
          Hstore=H-Hinitial
          Qin
        %  sumHinc
          Qcumarray(t10+1)=Qcum;
          Qinarray(t10+1)=Qin;
          Tarray(t10+1,numx:-1:1,:)=Tnew;
      end
end% of time step
hold off
plot(Twateroutex,'b')
ylabel('Temperature in centigrade')
xlabel('Time in tens of seconds')
hold on
plot(Tin10,'r')
%%%plot(Tpcmtemp,'k')
plot(Twateroutsim,'g')
legend('Outlet HTF experiment', 'Inlet HTF experiment', 'Outlet HTF
simulation')
figure(2)
plot(Qcumarray)%%%%%%%%%%%%Energy stored(J)
xlabel('Time in tens of seconds')
ylabel('Joules stored')
figure(3)
plot(Qinarray,('b'))%%%%%charge rate during charging(W)
xlabel('Time in tens of seconds')
ylabel('Charge rate stored')
figure(4)
contourf(T'); colorbar; title('Temperature °C')
```

## Appendix K: Plate heat exchanger design prior to construction

### PP sheet

The design of the plate heat exchanger thermal store was based on the desire to use a plastic (polypropylene) sheet to construct a PCM thermal store that could be retrofitted in domestic homes. The length and width of the store was based on suitability to mount the store in homes. In order to design the thermal store that would allow effective heat transfer along the store and a short conduction pat length. PP sheet with thin wall which would allow effective heat transfer between the HTF, wall and PCM was used.

For a mass flow rate of 65 g/s at high flow with an inlet HTF temperature of 60°C

$$\dot{Q} = \dot{m} Cp(T_{in} - T_{out})$$

$$(T_{in} - T_{out}) = 5^{o}C$$

$$\dot{Q} = 0.065x4.185x10^{3}x(5) = 1362\,\mathrm{W}$$

The hydraulic diameter is calculated based on the dimensions of the channels of the PP sheet (a=3.4mm; b=3.6mm)

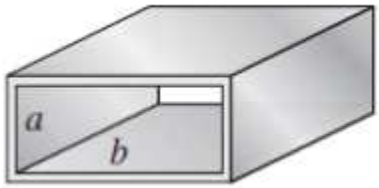


$$D_h = \frac{4A_c}{P}$$

$$A_c = a.b$$

$$P = 2(a+b)$$

$$D_h = \frac{2a.b}{(a+b)} = \frac{2(3.4x10^{-3})(3.6x10^{-3})}{(3.4x10^{-3} + 3.6x10^{-3})}$$

$$D_h = 0.0034m$$

Based on the channel width ratio, the Nusselt number at constant surface temperature was used. The internal convection for fully developed laminar flow at constant surface temperature for a channel width ratio of 1 has a Nusselt number of 2.98 (Nu=2.98) Kays and Crawford (1993).

The heat transfer coefficient of the HTF is calculated thus;

$$Nu = \frac{hD_h}{k}$$

$$h_f = \frac{Nu.k_f}{D_h} = \frac{2.98x0.6587}{0.0034} = 577.52$$

The temperature difference between the inlet HTF temperature for RT 52 and RT58 are 8°C and 7°C respectively. Considering the difference between the temperature of the HTF and PCM as the log mean temperature, the area of the store with a constant inlet HTF temperature (65°C) can be calculated as:

$$\dot{Q} = h_f A \Delta T$$
$$\Delta T = T_{HTF} - T_{PCM}$$
$$A = \frac{\dot{Q}}{h_f \Delta T}$$
$$A = \frac{1362}{577x8} = 0.3m^2$$

The area of the plate heat exchanger is calculated as $0.3m^2$. To increase the amount of energy obtainable from the store and to ensure a fully developed flow, the area of the PP sheet was increased to $0.76m^2$. Thus the length of the store was taken as 1.9m and the width; 0.4m. The PP sheet from the manufacturers are cut to match this dimensions. The dimensions of the channels results into a laminar flow within the channels as calculated in Table 6:4.

The number of channels of the PE sheet can be calculated thus;

$$Number \text{ of channel(N)} = \frac{Width \text{ of store}}{width \text{ of channel}}$$
$$\text{(N)} = \frac{400mm}{3.6mm} = 111 \text{ channels}$$

The total mass of PCM required to fill the PP sheet is determined based on the dimension of the store and the density of the PCM

$M_{PCM}$= Volume of PCM x density of PCM= 1.9x0.4x0.01 x 880 = 6.7kg

Estimate of the stored energy can be determined by multiplying the total mass of the PCM

E = $M_{PCM}$ x Latent heat = 6.7 x 140kJ/kg =0.938MJ for RT 58

E = $M_{PCM}$ x Latent heat = 6.7 x 153kJ/kg =1.03MJ for RT 52

## Appendix L: Serpentine heat exchanger design prior to construction

**SHE**

For the serpentine heat exchanger, the design was based on the desire to compare the thermal behaviour of the thermal store using a plastic (polypropylene) sheet and the serpentine heat exchanger. Similar length and width to the plate heat exchanger (PHE) was used to construct the serpentine heat exchanger (SHE) store. Copper pipe with internal diameter of 6.27mm was utilised for this construction, due to its availability.

For a mass flow rate of 30 g/s at high flow with an inlet HTF temperature of 70°C.

$$\dot{Q} = \dot{m} Cp(T_{in} - T_{out})$$

$$(T_{in} - T_{out}) = 10^{o}C$$

$$\dot{Q} = 0.03x4.19x10^{3}\,x(10) = 1257\,\mathrm{W}$$

Reynolds number is a measure of the ratio of the inertia force to the viscous force of the HTF. It can be expressed as a function of the mass flow rate and hydraulic diameter of the pipe.

$$\mathrm{Re} = \frac{4\dot{m}}{\mu \pi D_h}$$

$$\mathrm{Re} = \frac{4x0.03}{\pi(4.04\,\mathrm{x}10^{-4})(6.27x10^{-3})} = 15,042$$

Based on the calculated Reynolds number, the flow is turbulent. Thus to determine the Nusset number, Dittus-Boelter correlation is used.

$$\mathrm{Pr} = \frac{C_p \mu}{k}$$

Using Dittus-Boelter correlation, the Nusset number is estimated based on the Reynolds number and Prandtl number

$$Nu = 0.023\,\mathrm{Re}^{0.8}\,\mathrm{Pr}^{n^*} \quad (\mathrm{n}^*=0.4 \text{ for heating})$$

$$(n^* = 0.3 \text{ for cooling})$$

The Nusset number is calculated as 74. The heat transfer coefficient of the fluid can be determined using this relationship;

$$Nu = \frac{hD_h}{k}$$

The heat transfer coefficient of the HTF is calculated as 7788W/m$^2$K.

The overall heat transfer coefficient taking into consideration the convection in the HTF, wall and PCM, a value of 785W/m$^2$K is assumed. Based on this, the overall length of the copper pipe required for the SHE thermal store is determined.

Log mean temperature difference; $\Delta T_{LTMD}$ is the difference in temperature between the HTF and the surrounding surface (PCM in this case). The difference between the inlet HTF temperature and the melting temperature of the PCM (RT 52) is taken as the log mean temperature difference. The area and length of the pipe can be deduced.

$$\dot{Q} = UA\Delta T_{LTMD}$$

$$\Delta T_{LTMD} = T_{HTF} - T_{PCM} = 60 - 52 = 8^{o}C$$

$$A = \frac{\dot{Q}}{U\Delta T_{LTMD}}$$

$$A = \frac{1257}{785x8} = 0.2m^{2}$$

$$A = \pi DL$$

$$L = \frac{A}{\pi D} = \frac{0.2}{\pi(6.27x10^{-3})} = 10.16m$$

The total mass of PCM required to fill the SHE thermal store is determined based on the dimension of the store and the density of the PCM. The PCM only fills half of the height of the tank to allow for volume expansion of the PCM. The entire copper pipe is covered by the PCM

$M_{PCM}$= Volume of PCM x density of PCM= 1.97x0.62x0.025 x 880 = 26.8kg

Estimate of the stored energy can be determined by multiplying the total mass of the PCM

E = $M_{PCM}$ x Latent heat = 26.8 x 153kJ/kg =4.10MJ for RT 52.